TECHNISCHE UNIVERSITÄT MÜNCHEN
Lehrstuhl für Baumechanik

Augmented Beam Elements Using Unit Deflection Shapes Together with a Finite Element Discretisation of the Cross Section

Dipl.-Ing. Univ. Johannes Harald Gunnar Kreutz

Abstract

This thesis covers the field of augmented beam Finite Elements for geometrical and material linear, prismatic structures in the fields of static and dynamic excitations. An approach of superposed unit deflection shapes which are defined on a two dimensional Finite Element mesh of the cross section is used. This Finite Element mesh of the cross section is also used for the preparation of the unit deflection shapes by solving different differential equations such that unit deflection shapes emerge which most effectively cover the physical effects occurring on beam shaped structures with a three dimensional material law. The concept of unit deflection shapes is in analogy with the concept of warping torsion of beam elements. The method is validated and visualised with several numerical examples which are compared to the results of three dimensional standard Finite Element models.

Kurzfassung

Diese Arbeit behandelt erweiterte Finite Balkenelemente im materiell und geometrisch linearen Anwendungsbereich für prismatische Strukturen unter statischen und dynamischen Lasten. Dabei wird eine Superposition von Einheitsverformungszuständen eingesetzt, die auf einem zweidimensionalen Finite Elemente Netz des Querschnitts definiert sind. Dieses Finite Elemente Netz wird auch für die Erzeugung der Einheitsverformungszustände verwendet. Dabei werden auf diesem Netz verschiedene Differentialgleichungen gelöst, um Einheitsverformungen zu erhalten, mit denen das Verhalten einer balkenartigen Struktur mit dreidimensionalem Materialgesetz möglichst effektiv erfasst werden kann. Das Konzept der Einheitsverformungszustände steht dabei in Analogie zu dem der Wölbkrafttorsion. Die Methode wird in der Arbeit validiert und die Ergebnisse mit denen von dreidimensionalen Finite Elemente Berechnungen verglichen.

Acknowledgements

First of all, I would like to express my deep gratitude to and respect for my supervisor Prof. Gerhard Müller for giving me the opportunity to write this thesis at the Lehrstuhl für Baumechanik and for providing me with guidance and scientific freedom throughout this work.

I would like to thank Prof. Christoph Adam for the revision of the thesis and valuable hints and Prof. Kai-Uwe Bletzinger for chairing the board of examiners.

Special thanks go to Prof. Casimir Katz for the initial inspiration for this work and for all of the helpful hints.

It was a great pleasure for me to be part of the Lehrstuhl für Baumechanik of the Technische Universität München. I would like to express my sincere thanks to my colleagues for all of the fruitful discussions, helpful feedback, and a lot of fun.

I would also like to thank my parents and grandparents for giving me orientation, motivation, and support over the years.

My biggest gratitude goes to my beloved wife Julia for her love and patience, affectionately caring about me, supporting my decisions, and on top of it all making it possible to conduct many projects while balancing that with having children.

Contents

List of Symbols

The choice of symbols and notation was made according to popular text books and lecture notes on the topic of Finite Elements and Beam Theory. Different denominations for the same quantity were avoided as far as possible. Quantities which are used only once are declared by figures or text at the position of their use.

Greek Letters

$\boldsymbol{\psi}$	—	Unit deflection shapes
$[\boldsymbol{\Phi}]$	—	Matrix of unit deflection shapes
$\boldsymbol{\Psi}$		Eigenvector for a homogeneous problem
$\underline{\psi}$	—	Generalised amplitude of the primary torsional warp deflection
ν	—	*Poisson*[1] ratio
ρ	$\frac{\text{kg}}{\text{m}^3}$	density
$\boldsymbol{\varepsilon}, [\varepsilon]$	—	strain tensor and matrix of strain components (see section 2.2)
$\underline{\varphi}_x, \underline{\varphi}_y, \underline{\varphi}_z$	rad	(Generalised) rigid body rotations of the cross section
$\gamma_{ij}, \boldsymbol{\gamma}$	—	shear strain component, vector of shear strains
λ	m	Wave length
$\boldsymbol{\sigma}, [\sigma]$	$\frac{\text{N}}{\text{m}^2}$	Stress tensor and matrix of stress components (see section 2.3)
ω	m	Warp deflection field
ω_V	m	Primary torsional warp shape
Ω	$\frac{\text{rad}}{\text{s}}$	Angular frequency

---

[1]Siméon Denis Poisson (∗1781, †1840)

Latin Letters

$[0]$	—	Zero matrix
A	m^2	Area
$[B]$		Matrix of derived shape functions (FEM)
c	$\frac{\mathrm{m}}{\mathrm{s}}$	Wave speed (propagation)
$[D], [D_\omega], [D_{Mn}], [D_{Ms}]$	$\frac{\mathrm{N}}{\mathrm{m}^2}$	Material matrix (see section 2.3)
E	$\frac{\mathrm{N}}{\mathrm{m}^2}$	*Young*'s modulus
EA	N	Longitudinal stiffness
EI_y, EI_z, EI_{yz}	Nm^2	Bending stiffness (for composite beams)
EI_ω	Nm^4	Warping resistance (in literature also $EA_{\omega\omega}$ or EC_M)
f	$\frac{1}{\mathrm{s}}$	Frequency
G	$\frac{\mathrm{N}}{\mathrm{m}^2}$	Shear modulus
$GA_{Sy}, GA_{Sz}, GA_{Syz}$	$\frac{\mathrm{Nm}^2}{\mathrm{m}^2}$	Shear stiffness (see appendix A.5.2)
$GA_{S\omega}, GA_{Sy\omega}, GA_{Sz\omega}$	$\frac{\mathrm{Nm}^2}{\mathrm{m}^2}$	Stiffness against warping torsion shear deformation (see appendix A.5.2)
GI_t	Nm^2	Torsion constant (see appendix A.5.1.1)
i	—	Imaginary unit ($i = \sqrt{-1}$)
$[I]$	—	Identity matrix
ρI_ω	$\mathrm{kg\ m}^3$	Dynamic warping inertia
ρI_ϑ	$\mathrm{kg\ m}$	Dynamic rotational inertia
k_x	$\frac{\mathrm{rad}}{\mathrm{m}}$	Wave number
$[K]$		Stiffness matrix
$[M]$		Mass matrix
M_B	Nm^2	Bimoment
M_x	Nm	Torsional moment
M_{xV}	Nm	Primary torsional moment (*de St.-Venant* component)
M_{xS}	Nm	Secondary torsional moment (from warping torsion)
M_y, M_z	Nm	Bending moments
N	N	Normal force
$[N]$	—	Matrix of shape functions (FEM)
$p, \mathbf{p}, [p]$	N	Load, load vector, nodal load matrix
$q, \mathbf{q}, [q]$	N	General force, force vector, nodal force matrix
Q_y, Q_z	N	Transverse forces
t	s	Time
$u_x, u_y, u_z, \mathbf{u}, [u]$	m	Deflection components, deflection vector, nodal deflection matrix

$\underline{u}_x, \underline{u}_y, \underline{u}_z$	m	(Generalised) rigid body deflections of the cross section
$[U]$	$-$	Transmission matrix (see section 3.1.2)
V	m^3	Volume
W	Nm	Work
$\underline{v}$	$-$	Participation factor
$\breve{y}, \breve{z}$	m	Coordinates with reference to the centre of gravity $(y_S; z_S)$
$\acute{y}, \acute{z}$	m	Coordinates with reference to the shear centre/ centre of rotation $(y_M; z_M)$
x, y, z	m	(*Cartesian*) coordinates
y_M, z_M	m	Coordinates of the shear centre/ centre of rotation
y_S, z_S	m	Coordinates of the centre of stiffness
y_I, z_I	m	Coordinates of the centre of gravity/mass

Accents and Symbols

$\overset{\circ}{\square}$	Known value from a previous computation or state
$\underline{\square}$	Generalised quantity
$\bar{\square}$	Conjugate (complex) value
$\square_{,x}$	Partial derivative with respect to x
$[\square]$	Indicates a matrix
$[\square]^T$	Transpose of a matrix
$[\square]^{-1}$	Inverse of a matrix
$\dot{\square}$	Derivative with respect to time
$\ddot{\square}$	Second derivative with respect to time
$\hat{\square}$	Quantity in the *Fourier* domain
$\Re(\square)$	Real part of a complex quantity
$\Im(\square)$	Imaginary part of a complex quantity
$\boldsymbol{\tau}$	(bold face) Indicates a vector or tensor of higher order
$\delta\square$	Virtual quantity (principle of virtual work)
$f^{(n)}$	n^{th} Derivative of a function f

Abbreviations

BEM	Boundary Element Method
CAD	Computer aided design
DOF	Degree of freedom
FEM	Finite Element Method
FT	*Fourier*[2] transformation
GBT	Generalised beam theory
GEP	Generalised eigenvalue problem
IFT	Inverse *Fourier* transformation
ITM	Integral transformation method
QEP	Quadratic eigenvalue problem
SDOF	Single degree of freedom
SEA	Statistical energy analysis
SEP	Standard eigenvalue problem

---

[2]Jean Baptiste Joseph Fourier (∗1768, †1830)

1 Introduction

1.1 Problem statement

The Finite Element Method (FEM) became the most popular simulation tool in structural mechanics within the past decades. A huge variety of commercial tools is available for different types of problems with sometimes very comfortable graphic or text-based input or import from spatial computer aided design (CAD) models. In structural mechanics and especially in bridge design still beam elements play an important role. There are primarily two reasons for this [Katz 2008]: the basic results given in integral or generalised forces instead of stresses. This enables the engineer to check the results easily against the loading and gain a better feeling for the structure. The second is that not only the computer time for the solution is reduced but also the time spent on modeling a structural system is considerably smaller than for full 3D models. Furthermore, the data structure is well suitable for automated design or optimization either of reinforcement bars or parametric description of cross sections. Finally the ultimate limit design as formulated in the common design codes is based on integral resistances at least of a complete section, but in general of the whole structure. A non linear analysis is required which boosts the computational cost of the calculation for volume models.

As *Moore*'s law [Moore 1965] is still valid, but for the given subject only when parallel computing is made use of [Sutter 2005], it becomes obvious that the prospects of classically arranged analysis software is limited. In order to efficiently make use of many processors, new techniques are necessary. One that is well known is the substructure technique and the main advantage is that its benefits apply both for pre- and post processing. As stated in [Katz 2008], the sophisticated standard beam analysis procedure directly provides such a substructure: the cross section.

On the other hand, [G. Müller and Buchschmid 2011] show that especially for dynamic but also for static analysis beam models may quickly reach their limit of applicability if the lateral carrying action gains influence. Of course also for certain regions near supports,

snatch blocks, or loads in the so-called *de St.-Venant* zones, the classical beam theory is not applicable.

Furthermore academic examples are conceivable where the fact that the cross section of a beam cannot deform leads to severe inaccuracies:

- Composite beams with materials with a different *Poisson* ratio.

- Interaction of longitudinal and lateral direction due to the *Poisson* ratio. This may become of interest e.g. when the top plate of a girder is prestressed in the lateral direction.

- Beams of thin-walled troughed sheet close to their ultimate load.

The aim of augmented beam theories as presented in this thesis is to come up with the mentioned drawbacks without losing the advantages mentioned above.

1.2 Augmented Beam Theories: State of Knowledge

1.2.1 Thin-walled Sections

The development of the classical Beam Theory is connected with the names *Bernoulli*[1], *Timoshenko*[2], *Coulomb*[3], *de St.-Venant*[4], *Bredt*[5] and *Prandtl*[6]. It is understood to be the theory covering elongation, torsion with respect to the theory of *de St.-Venant* and the two bending deflections including the generalised shear deformation due to the transverse forces. The bending and shear deformations are coupled and such six degrees of freedom (three deflections and three rotations) occur which also arise in the general mechanics of three dimensional rigid bodies. The basic assumptions or restrictions are that plane sections remain plane to the axis of the beam and that the sections do not distort. [Cowper 1966] conducted further studies concerning the shear correction factor of *Timoshenko's* beam theory and provided a general procedure as to how to calculate it for an arbitrary cross section.

---

[1]Jakob I. Bernoulli (∗1655, †1705)
[2]Stepan Prokopowytsch Tymoschenko (∗1878, †1972)
[3]Charles Augustin de Coulomb (∗1736, †1806)
[4]Adhémar Jean Claude Barré de Saint-Venant (∗1797, †1886)
[5]Rudolf Bredt (∗1842, †1900)
[6]Ludwig Prandtl (∗1875, †1953)

At the beginning of the 20th century numerous authors developed the warping torsion or nonuniform torsion. *Vlasov*'s[7] textbooks [Wlassow 1964], [Wlassow 1965] and [Wlassow 1958] are probably the most relevant. Their terminology for this issue was adopted worldwide for the following decades until today. [Bornscheuer 1952] established a uniform notation for the surface integrals of the zeroth (F), first (F_y, F_z and F_ω) and second order (F_{yy}, F_{zz}, $F_{\omega\omega}$, F_{yz}, $F_{y\omega}$, and $F_{z\omega}$) and by that prepared the theory for practical use. The concept of warping torsion is basically to enable the beam to perform one additional out of plane deflection shape which is connected to the derivative of the rotation around the beam axis.

Parallel to these enhancements of beam theory a set of theories treating folded plates or strips was developed.

Wlassow's textbooks [Wlassow 1964], [Wlassow 1965] are German translations of Russian books from which the first edition was published in Russia in 1940. Beyond treating issues of torsional warping in traditional beam theory (only one additional degree of freedom and no deformation of the cross section) the mentioned books and [Wlassow 1958] contain further generalizations for thin-walled prismatic structures considering deformations of the cross section. One of them treats arbitrary (curved) open cross sections neglecting shear deformations. The other takes the shear deformations into account enabling the solution of closed (box-) girders with straight walls.

[Kreuzinger 1974] develops a formulation for thin-walled arbitrary (open unbranched, open branched and closed unbranched) cross sections allowing for distortions, warpings and shear deformation in the plane of the strips. Trigonometric ansatz functions are used. [Zienkiewicz and Taylor 2005, chapter 16] illustrates a rather similar approach making use of the orthogonality properties of sin and cos functions.

[Schardt 1989] concludes and illustrates the work done before by himself and others since 1966 in the area of enhanced beam theories. Shear deformations are neglected and by that a very schematic approach is obtained. The separation of variables is performed for so-called deformation processes. Each process includes both the warping and a corresponding deformation or displacement of the section in the $x - y$ plane. For each process a PDE of fourth order in the x-direction is to be solved. The methodology is called Generalised Beam Theory (GBT) or Verallgemeinerte Technische Biegetheorie (VTB) in German. This type of approach is still a matter of research. [Gonçalves and Camotim 2012] formulate a geometrically nonlinear GBT which also takes shear deformations into account. [Camotim and Basaglia 2012] uses the GBT for the distinction of local and global buckling shapes in

---

[7]Vasilii Zakharovich Vlasov (Wassili Sacharowitsch Wlassow) (∗1906, †1958)

shell Finite Element models. The theory is discussed in more detail in section 3.2.3 on page 26.

[Hofmann 1992] establishes an augmented beam theory by introducing a new warping degree of freedom for the warping from shear forces. The motivation is to quantify the error arising from inconsistencies due to the negligence of this effect in standard (*Timoshenko*) beam theory. His approach for the longitudinal direction is based on the complete separation of the deflection into the part arising from bending and the part from shear. The two differential equations appear to be completely decoupled inside the domain. They are nevertheless coupled by the boundary conditions since they affect the total deflections which consist of the sum of the two latter components. Couplings arising from the non-orthogonality of the shear- and torsional warp shapes are not covered. Hofmann analyses the arising differential equations and discusses the parallels to the PDE of torsional warping. The PDE is solved both analytically using hyperbolic functions and approximatively by a truncated *Taylor* series. Stiffness matrices for the end deformations of an element of finite length are derived using both principles. The method is additionally applied to the theory of second order and linear dynamics. The underlying warp shapes of the cross sections are derived from shear stresses which are gained by equilibrium at a cutout free end assuming a constant shear distribution in thickness direction which is applicable for thin-walled open cross sections. Theoretically this (secondary) warp shape can be taken as the basis for a further (tertiary) shape which itself could be a basis again. Since the gain of accuracy from these high order shapes is decaying very fast with the number of order only the secondary shapes are taken into account. The thesis ends saying that the newly introduced effects are of small importance and the gain of accuracy is only small even for dynamic and nonlinear problems.

1.2.2 General, thick-walled sections

For thick-walled sections only few extensions of the beam theory exist. A first "step" of extension can be seen in the improved numerical computation of section values (inertia of torsion, shear areas and warping resistance) for arbitrary sections. An overview of the literature on this topic can be found in section 4.2.1.1 on page 38.

There exist many extensions (high order versions) which enable enhanced computation of longitudinal stresses but apply only for a certain type of cross section (rectangle [Levinson 1985], [Bhimaraddi and Chandrashekhara 1993], [Bickford 1982] or circle or circular pipe): A comparison of various formulations is given in [Sayyad 2011].

[Zeller 1982] tried a very exciting way of extending beam theory for general thick-walled sections. He showed ways to compute generalised deflections using mixed plane finite elements. The scaling of the unit deflections is proportional to the high order derivatives of the beam variable (deflection or rotation).

[Ferradi et al. 2013] proposes a beam element for general thick walled sections enriched by high order warping deflections computed with the help of a Finite Element mesh of the cross section. The warp deformations are introduced as additional generalised deflection shapes. Other types of deformations of the cross section are not considered. The approach is thus similar to the one presented by [Hofmann 1992] but is applied to general sections and not only to rectangular ones.

[Gollwitzer 2007] formulates a method for wooden composite beams with a flexible compound. Therefore, a linear three dimensional Finite Element for open bundles of single beams is implemented. Each of the single beams conforms with the assumptions of *Euler-Bernoulli* for small deflections and the shape functions are straight forward. Non uniform torsion and the influence of the flexible compound on the position of the centre of rotation as well as distortions of the cross section are not considered. Theory of Second Order is considered for bending deformations. The work of [Roik and Sedlacek 1970] can also be classified into this group since the presented sections consist of several beam strips connected by joints either rigid or flexible with respect to shear. Each of the individual strips obeys the *Euler-Bernoulli* assumptions.

[Živković et al. 2001] presents a beam element based on the super-element technique. Only the rigid-body deflections of the cross-sections are part of the global system. The cross section is able to perform arbitrary relative deformations including both warping and distorions as local degrees of freedom. Elements can be grouped such that the continuity of the relative deflections between elements is adhered.

1.2.3 Linear Wave Guides

Wave guide in this context addresses a method for the numerical computation of systems of structural dynamics with one direction of primary extent. The systems may be of finite or infinite length. The method is also called semi-analytical FEM. It can be used to predict the behaviour infinite structures under moving loads or loads with a given wave number spectrum [e.g. Chen and Huang 2003; K. Müller 2007], or e.g. to analyse wave propagation in rib-stiffened plate structures typical of ship construction [Finnveden 2004]. Further applications

are the preprocessing of energy-transmission-properties for the statistical energy analysis [Orrenius and Finnveden 1996] or stiffness matrices for a super-element which can be used in larger beam or Finite Element systems [Friberg 1985].

By using a wave ansatz in the longitudinal direction every beam theory can be used as the basis for the formulation of a wave guide. [Friberg 1985] does this for the thin-walled *Vlassov* beam theory not considering shear deformations.

Additionally, more general methods exist which are based on a discretisation of the cross section of a continuous structure either with thin-walled strips [Finnveden 2004; Orrenius and Finnveden 1996] or area elements [Zienkiewicz and Taylor 2005, chapter 16].

[Hinke et al. 2004] enable for the computation of arbitrary (periodically repeating along x) waveguides. They use commercial Finite Element software to compute the dynamic stiffness matrix of a segment. Periodical boundary conditions are applied and an eigenvalue analysis is performed which is prone to numerical problems [Waki et al. 2009]. This approach is called the wave and finite element method (WFE).

1.3 Short Description of the Proposed Method

1.3.1 Separation of variables

All deflections $u_x(x,y,z)$, $u_y(x,y,z)$ and $u_z(x,y,z)$ of the beam structure are built by a linear combination of unit deflection shapes $\boldsymbol{\psi}_i(y,z)$ depending on the sectional coordinates (y, z) and their corresponding contribution factor $\underline{v}_i(x)$ depending on the longitudinal x-direction.

$$\mathbf{u}(x,y,z) = \begin{bmatrix} u_x(x,y,z) \\ u_y(x,y,z) \\ u_z(x,y,z) \end{bmatrix} = \sum_{i=1}^{n_{\text{shapes}}} \left[\boldsymbol{\psi}_i(y,z) \cdot \underline{v}_i(x) \right] = [\boldsymbol{\Phi}] [\underline{v}] \tag{1.1}$$

This separation of variables is especially appropriate for structures like beams, where the x-direction is of a greater extent than the other ones.

1.3.2 Unit Deflection Shapes

The unit deflection shapes or mode shapes $\boldsymbol{\psi}_i(y,z)$ in equation (1.1) are obtained from solving different problems on a plane Finite Element mesh of the cross section. In the following these problems are listed. It is important to mention that this list is not universally valid. Further types of deflection shapes are conceivable and might replace the presented. It is furthermore not a must to always apply all types of deflection shapes. In fact it depends on the type of problem and the properties of the structure which types of deflection shapes are more effective.

1.3.2.1 Eigenmodes of the section treated as a free plane plate in membrane action

The first three eigenmodes have the eigenvalue 0 and represent the rigid body modes of the plate. In the scope of the beam system they represent the two lateral deflections and the torsional rotation. Higher eigenmodes are distortion modes of the section. These unit deflection shapes are treated in section 4.1.1.

1.3.2.2 Eigenmodes of the section treated as a free plane plate in bending and transverse shear action

As above, the first three eigenmodes have the eigenvalue 0 and represent the rigid body modes. In the scope of the beam systems they represent the longitudinal deflection and the two rotations around the lateral axes. Higher eigenmodes are out of plane or warping shapes. These unit deflection shapes are treated in section 4.1.2.

1.3.2.3 Solution of the PDE of warping

The PDE of warping can be solved for the load cases primary torsion (rotation), shear force (two directions) and secondary torsion. It yields four out of plane deflection shapes. By this approach in standard beam-software the properties for non-uniform torsion and the shear correction factors for *Timoshenko* Elements are obtained. These unit deflection shapes are treated in section 4.2.1.

1.3.2.4 Derived plane and warping shapes

[Zeller 1979] shows that one can obtain warp shapes from in-plane shapes by using the PDE of warping (weak equilibrium in the longitudinal direction) again. He shows additionally that in-plane deflections can be derived from warping shapes. The underlying considerations are illustrated in section 3.2.4. The actual derivation of these unit deflection shapes can be found in the sections 4.2.3 and 4.3.2.

Also warping shapes themselves can be used to derive higher warping shapes (see section 4.2.2).

1.3.2.5 In Plane *Poisson* Shapes

If any warpshape changes its magnitude along x and the utilised material law shows a *Poisson* ratio $\nu \neq 0$, lateral strains occur. To some extent they are covered by the above mentioned in plane deflection shapes, but the convergence rate can be improved significantly if special unit deflection shapes are calculated here fore. This can be done utilising the PDE of a plate in membrane action with a prescribed strain in the x-direction.

1.3.2.6 Eigenmodes of the infinite beam for waves of a fixed frequency

The PDE is gained by a double *Fourier* transformation of the *Lamé*[8] equation in x and t. The Eigenvalues correspond to wave numbers k_x of waves travelling along the beam. The underlying Finite Element formulation is derived in section 4.4. and validated in appendix A.4. The numerical example in section 6.2.1 shows the potential capacity of this approach.

1.3.3 Beam Element Matrices and Load Vectors

The beam element stiffness matrices and load vectors are obtained by performing a volume integral for the virtual work inside the beam domain using the deflection shapes both as ansatz and test functions.
The inner virtual work integral is able to employ an arbitrary linear three dimensional material law.

---

[8]Gabriel Lamé (∗1795, †1870)

The volume integral is performed using standard non-conforming hexahedral Finite Elements with the *Wilson* extension [Bathe 2002; Wilson et al. 1973] (see appendix A.2) such that locking does not occur.

1.4 Content of the Thesis

In the present thesis, an approach for augmented beam Finite Elements is presented. It is based on the separation of variables aiming at unit deflections shapes and corresponding amplification factors. Arbitrary cross sections can be treated since the unit deflection shapes are defined on a two dimensional Finite Element mesh of the cross section.

The presented method allows for the use of a three dimensional material law. As results, three dimensional strain and stress tensors can be obtained. The underlying assumptions and sign conventions can be found in *chapter 2.*

Chapter 3 gives a brief overview of beam theories in literature and beam element techniques. Selected augmented beam theories are discussed more in detail.

Chapter 4 covers the computation of effective unit deflection shapes making use of the before mentioned Finite Element mesh of the cross section. Different differential equations are solved. In section 4.4 a Finite Element procedure for a *Fourier* transformed *Lamé* continuum is developed and a special eigenvalue problem for the wave number k_x is developed and illustrated. The Finite Element procedure itself is validated in appendix A.4.

Chapter 5 describes how the before calculated unit deflection shapes are arranged and processed to obtain an augmented beam Finite Element method. The element stiffness and mass matrices for the beam element are assembled. Different procedures for the application of boundary conditions and the post-processing of strains, stresses and sectional forces are introduced. Finally a method for the a posteriori error estimation is proposed.

Chapter 6 illustrates the capabilities, problems and the efficiency of the presented method with the help of different numerical examples. The results are compared against those from commercial Finite Element packages.

2 Basic relations

2.1 Sign Conventions
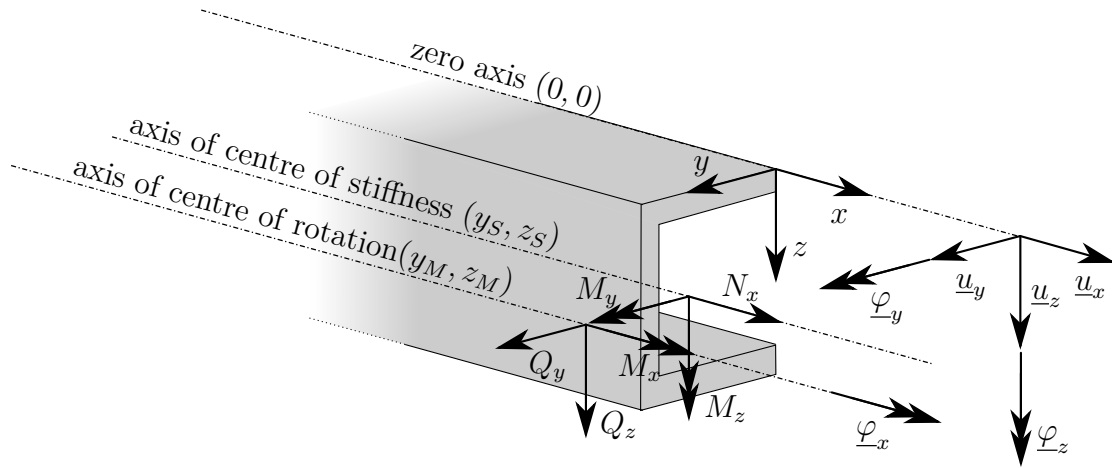
Figure 2.1: Sign- and direction conventions for forces and deflections.

2.2 Strains

The kinematics in this thesis shall be based on the *Green*[1]-*Lagrange*[2] strain formulation

$$\boldsymbol{\varepsilon} = \varepsilon_{ij}\, \mathbf{G}^i \otimes \mathbf{G}^j \tag{2.1}$$

$$\varepsilon_{ij} = \frac{1}{2}\left[u_i|_j + u_j|_i + u_l|_i\, u^l|_j\right]. \tag{2.2}$$

The last term of the latter formula is omitted when the strain tensor is linearised

$$\varepsilon_{ij\,\mathrm{lin}} = \frac{1}{2}\left[u_i|_j + u_j|_i\right]. \tag{2.3}$$

---

[1]George Green (∗1793, †1841)
[2]Joseph-Louis Lagrange (∗1736, †1813)

If, furthermore, a *Cartesian*[3] coordinate system is assumed the absolute derivatives $u_i|_j$ turn into partial derivatives $u_{i,j}$.

$$\varepsilon = \frac{1}{2} \begin{bmatrix} 2u_{x,x} & u_{x,y} + u_{y,x} & u_{x,z} + u_{z,x} \\ u_{y,x} + u_{x,y} & 2u_{y,y} & u_{y,z} + u_{z,y} \\ u_{z,x} + u_{x,z} & u_{z,y} + u_{y,z} & 2u_{z,z} \end{bmatrix} \tag{2.4}$$

Using the symmetry of this tensor

$$\begin{aligned} \gamma_{xy} &= \gamma_{yx} = \varepsilon_{xy} + \varepsilon_{yx} \\ \gamma_{xz} &= \gamma_{zx} = \varepsilon_{xz} + \varepsilon_{zx} \\ \gamma_{zy} &= \gamma_{yz} = \varepsilon_{zy} + \varepsilon_{yz} \end{aligned} \tag{2.5}$$

one can rewrite the remaining six independent values as a 6x1 matrix

$$[\varepsilon] = \begin{bmatrix} \varepsilon_x \\ \varepsilon_y \\ \varepsilon_z \\ \gamma_{xy} \\ \gamma_{xz} \\ \gamma_{yz} \end{bmatrix} = \begin{bmatrix} u_{x,x} \\ u_{y,y} \\ u_{z,z} \\ u_{x,y} + u_{y,x} \\ u_{x,z} + u_{z,x} \\ u_{y,z} + u_{z,y} \end{bmatrix} = \begin{bmatrix} \frac{\partial}{\partial x} & 0 & 0 \\ 0 & \frac{\partial}{\partial y} & 0 \\ 0 & 0 & \frac{\partial}{\partial z} \\ \frac{\partial}{\partial y} & \frac{\partial}{\partial x} & 0 \\ \frac{\partial}{\partial z} & 0 & \frac{\partial}{\partial x} \\ 0 & \frac{\partial}{\partial z} & \frac{\partial}{\partial y} \end{bmatrix} \begin{pmatrix} u_x(x,y,z) \\ u_y(x,y,z) \\ u_z(x,y,z) \end{pmatrix} = [G] \cdot \mathbf{u}\,. \tag{2.6}$$

2.3 Material Law

2.3.1 Three Dimensional Material Law

When a linear material behaviour is assumed it follows that stresses for the *Cauchy*[4] Stress Tensor $\boldsymbol{\sigma} = \sigma^{ij}\,\mathbf{G}_i \otimes \mathbf{G}_j$ can be obtained from strains by a simple multiplication

$$\sigma^{ij} = D^{ijkl}\varepsilon_{kl}. \tag{2.7}$$

Where $\mathbf{D} = D^{ijkl}\mathbf{G}_i \otimes \mathbf{G}_j \otimes \mathbf{G}_k \otimes \mathbf{G}_l$ is a tensor of 4th order.

---

[3]Cartesius, latin name of René Descartes (∗1596, †1650)
[4]Augustin-Louis Cauchy (∗1789, †1857)

For equilibrium reasons the stress tensor $\boldsymbol{\sigma}$ has to be symmetric. Just as with the strain tensor in equation (2.6) it is possible to collect the six independent values into a 6x1 matrix

$$[\sigma] = \begin{bmatrix} \sigma_{xx} & \sigma_{yy} & \sigma_{zz} & \sigma_{xy} & \sigma_{xz} & \sigma_{yz} \end{bmatrix}^T = \begin{bmatrix} \sigma_x & \sigma_y & \sigma_z & \tau_{xy} & \tau_{xz} & \tau_{yz} \end{bmatrix}^T . \tag{2.8}$$

By that, the relation in equation (2.7) can be represented as a simple matrix multiplication

$$[\sigma] = [D][\varepsilon] \tag{2.9}$$
$$[\varepsilon] = [D]^{-1}[\sigma] = [D]_{\text{inv}}[\sigma] . \tag{2.10}$$

For a linear elastic isotropic material with two free values E (elastic modulus) and ν (*Poisson* ratio) the matrix $[D]$ reads as follows

$$[D] = \frac{E}{(1+\nu)(1-2\nu)} \begin{bmatrix} 1-\nu & \nu & \nu & 0 & 0 & 0 \\ \nu & 1-\nu & \nu & 0 & 0 & 0 \\ \nu & \nu & 1-\nu & 0 & 0 & 0 \\ 0 & 0 & 0 & \frac{1-2\nu}{2} & 0 & 0 \\ 0 & 0 & 0 & 0 & \frac{1-2\nu}{2} & 0 \\ 0 & 0 & 0 & 0 & 0 & \frac{1-2\nu}{2} \end{bmatrix} . \tag{2.11}$$

In case of orthotropy, which means that three directions exist in which no coupling between longitudinal strains and shear strains occur, the material law has 9 free values

$$[D] = \begin{bmatrix} D_{11}^{11} & D_{22}^{11} & D_{33}^{11} & 0 & 0 & 0 \\ & D_{22}^{22} & D_{33}^{22} & 0 & 0 & 0 \\ & & D_{33}^{33} & 0 & 0 & 0 \\ & & & D_{12}^{12} & 0 & 0 \\ & \text{sym.} & & & D_{13}^{13} & 0 \\ & & & & & D_{23}^{23} \end{bmatrix} .$$

A general anisotropic linear material law can be covered by 21 free values. The matrix $[D]$

then has the form

$$[D] = \begin{bmatrix} D_{11}^{11} & D_{22}^{11} & D_{33}^{11} & D_{12}^{11} & D_{13}^{11} & D_{23}^{11} \\ & D_{22}^{22} & D_{33}^{22} & D_{12}^{22} & D_{13}^{22} & D_{23}^{22} \\ & & D_{33}^{33} & D_{12}^{33} & D_{13}^{33} & D_{23}^{33} \\ & & & D_{12}^{12} & D_{13}^{12} & D_{23}^{12} \\ & \text{sym.} & & & D_{13}^{13} & D_{23}^{13} \\ & & & & & D_{23}^{23} \end{bmatrix} \quad (2.12)$$

Still the existence of an elastic potential is a prerequesite for these material laws [G. Müller 2012].

In order to abbreviate and simplify references, the indices of $[D]$ are reduced and reordered

$$[D] = \begin{bmatrix} D_{11} & D_{12} & D_{13} & D_{14} & D_{15} & D_{16} \\ D_{21} & D_{22} & D_{23} & D_{24} & D_{25} & D_{26} \\ D_{31} & D_{32} & D_{33} & D_{34} & D_{35} & D_{36} \\ D_{41} & D_{42} & D_{43} & D_{44} & D_{45} & D_{46} \\ D_{51} & D_{52} & D_{53} & D_{54} & D_{55} & D_{56} \\ D_{61} & D_{62} & D_{63} & D_{64} & D_{65} & D_{66} \end{bmatrix}. \quad (2.13)$$

2.3.2 Deriving Two Dimensional Material Laws

2.3.2.1 Membrane Systems (plane strain)

Membrane systems in the y-z-plane with plane strain means that all strains except ε_y, ε_z and γ_{yz} are equal to zero. The corresponding material law can consequently be derived by picking the corresponding entries

$$[D_{Mn}] = \begin{bmatrix} D_{22} & D_{23} & D_{26} \\ D_{32} & D_{33} & D_{36} \\ D_{62} & D_{63} & D_{66} \end{bmatrix}. \quad (2.14)$$

2.3.2.2 Membrane Systems (plane stress)

Membrane systems in the y-z-plane with plane stress means that all stresses except σ_y, σ_z and τ_{yz} are equal to zero. This relation is introduced to equation (2.10) and thus the corresponding entries have to be picked from the inverse of the material matrix $[D]_{\text{inv}}$. The collected matrix has to be inverted finally

$$[D_{Ms}] = \begin{bmatrix} D_{\text{inv }22} & D_{\text{inv }23} & D_{\text{inv }26} \\ D_{\text{inv }32} & D_{\text{inv }33} & D_{\text{inv }36} \\ D_{\text{inv }62} & D_{\text{inv }63} & D_{\text{inv }66} \end{bmatrix}^{-1} . \tag{2.15}$$

2.3.2.3 Warping Problems

The material law for warping problems $[D_\omega]$ can be easily gained from each of the before presented matrices $[D]$ by picking the corresponding entries:

$$[D_\omega] = \begin{bmatrix} D_{44} & D_{45} \\ D_{54} & D_{55} \end{bmatrix} . \tag{2.16}$$

3 Beam Elements - Prior Art

This chapter shall give a slight overview of the traditional beam theories, on the one and extended beam theories, on the other hand.

3.1 Different Aspects of Traditional Beam Elements

The distinction between traditional and extended beam theories can never be done sharply. In the scope of this thesis traditional beam theories denote those with six or seven degrees of freedom. As the following sections will show, these traditional beam theories can also be enriched and refined as regards several details which are still a subject of research.

3.1.1 Key Issues of Traditional Beam Theories

Traditional beam theories can be distinguished and characterised as follows [see e.g. Wunderlich and Kiener 2004]:

1. The cross section of the beam remains undistorted. By that, the strains ε_y, ε_z and/or γ_{yz} and the corresponding stresses vanish. In some cases they can be resurrected by equilibrium considerations or using the material law but they in no case interact with the remaining strains or stresses.

2. Loads act as line or point loads and are defined with respect to the beam axis. This is an important prerequisite for item 1.

3. Shear deformations γ_{xy} and γ_{xz} are neglected (*Bernoulli* assumption) in the *Euler-Bernoulli* beam theory. As a consequence, plane cross sections remain plane and perpendicular to the longitudinal axis. In *Timoshenko* beam theory generalised shear strains $\underline{\gamma}_{xy}$ and $\underline{\gamma}_{xz}$ are taken into account. γ_{xy} and γ_{xz} are assumed to be constant over the cross section which violates equilibrium at the lateral surfaces. This fact

can be arrived at by calculating shear correction factors from exact shear warp deflections. This approach is then based on the assumption unrestricted thus constant warp deflections of the cross section (see section 4.2.1.3 and item 4a) here).

4. Concerning torsion and warping the following distinctions have to be made

   a) If warping effects are completely neglected and only *de St.-Venant* torsion is considered, it is assumed that the cross section can warp freely and no longitudinal stresses arise. The prerequisite is that the torsion moment is constant thus the drill (change of rotation) is constant.

   b) If warping effects are considered but shear deformations due to warping torsion are neglected (*Wagner*'s hypothesis), *Wlassow* Beam Theory [Wlassow 1964], [Wlassow 1965] is obtained.

5. The beam is prismatic (uniform along x). This important assumption underlies almost all derivations of all beam theories. Without this assumption especially item 1 does not hold. It can nevertheless be weakened in such a way that the sectional properties (sectional stiffnesses, position of the gravitational axis, position of the centre of rotation and excentricities) change along the longitudinal axis. It is noteworthy that this sort of extensions of theory may violate both equilibrium and compatibility and thus has to be handled with care.

6. The lateral dimensions are small compared to the longitudinal one.

7. Physical and geometrical relations are linear. The prerequisite is that rotations and especially strains remain small.

3.1.2 Method of Transmission Matrices (Reduction Method)

[see Bogensperger 2000; Kiener 1988; SOFiSTiK AG 2013b; Wunderlich and Kiener 2004]

The method of transmission matrices is very well suited for the differential equations occurring in beam calculations. It provides a replacement for the common "Finite Element toolbox" consisting of a set of mostly arbitrary advised shape functions plus a weightening scheme (virtual work, potential of inner forces, weighted residuals or variational calculus) and a numerical integration (*Gauss* [1] Points). It was commonly applied in hand calculations

---

[1]Johann Carl Friedrich Gauß (∗1777, †1855).

before the computer's triumph. It is still used in some commercial beam analysis software e.g. STAR [SOFiSTiK AG 2013b].

The basic idea is to see the beam as an initial value problem with both force and deflection values $[z_i]$ at the start point i. From there, the underlying differential relations are used and integrated along the whole beam or a part of it to the point $i + 1$. This integration can be performed either numerical using standard implicit or explicit integration schemes (*Gauss, Runge-Kutta, ...*) or in closed form (analytically) using e.g. a series expansion. This integration yields the matrix $[U]_i$ and a load term $[\bar{z}]_i$ such that

$$[z]_{i+1} = [U]_i \cdot [z]_i + [\bar{z}]_i \tag{3.1}$$

The following equation exemplifies the relations for a linear *Euler-Bernoulli* Beam with bending and normal force.

$$
\begin{bmatrix} u_x \\ u_z \\ \varphi_y \\ N \\ Q_z \\ M_y \end{bmatrix}_{i+1}
=
\begin{bmatrix}
1 & 0 & 0 & \frac{\Delta x}{EA_{yi}} & 0 & 0 \\
0 & 1 & -\Delta x & 0 & -\frac{\Delta x^3}{6EI_{yi}} & -\frac{\Delta x^2}{2EI_{yi}} \\
0 & 0 & 1 & 0 & \frac{\Delta x^2}{2EI_{yi}} & \frac{\Delta x}{EI_{yi}} \\
0 & 0 & 0 & 1 & 0 & 0 \\
0 & 0 & 0 & 0 & 1 & 0 \\
0 & 0 & 0 & 0 & \Delta x & 1
\end{bmatrix}
\cdot
\begin{bmatrix} u_x \\ u_z \\ \varphi_y \\ N \\ Q_z \\ M_y \end{bmatrix}_i
+ [\bar{z}]
\tag{3.2}
$$

The matrix $[\bar{z}]$ represents the loads (forces, curvatures, strains...): single loads and line loads with different functions depending on x.

$[U]$ can be decomposed into submatrices treating either only deflections $[u]$, only forces $[s]$ or the relation between them:

$$[z]_{i+1} = \begin{bmatrix} [u] \\ [s] \end{bmatrix}_{i+1} = \begin{bmatrix} [U]_{uu} & [U]_{us} \\ [U]_{su} & [U]_{ss} \end{bmatrix} \cdot \begin{bmatrix} [u] \\ [s] \end{bmatrix}_i + \begin{bmatrix} [\bar{u}] \\ [\bar{s}] \end{bmatrix} \tag{3.3}$$

Equation (3.1) can be applied repeatedly to obtain the variables $[z_b]$ at the end of a beam element depending on the start variables $[z_a]$. The following equation examplifies the process for three steps from a to b

$$[z_b] = \underbrace{[U]_3 [U]_2 [U]_1}_{[\hat{U}]} [z_a] + \underbrace{[U]_3 [U]_2 [\bar{z}]_1 + [U]_3 [\bar{z}]_2 + [\bar{z}]_3}_{[\hat{\bar{z}}]} . \tag{3.4}$$

The lines of equation (3.3) have to be solved for the force values $[s]_a$ and $[s]_b$

$$[u]_b = [\widehat{U}]_{uu} [u]_a + [\widehat{U}]_{us} [s]_a + [\widehat{\bar{u}}]$$
$$\Rightarrow [s]_a = [\widehat{U}]_{us}^{-1} [u]_b - [\widehat{U}]_{us}^{-1} [\widehat{U}]_{uu} [u]_a - [\widehat{U}]_{us}^{-1} [\widehat{\bar{u}}] \tag{3.5}$$

$$[s]_b = [\widehat{U}]_{su} [u]_a + [\widehat{U}]_{ss} [s]_a + [\widehat{\bar{s}}]$$
$$\Rightarrow [s]_b = [\widehat{U}]_{su} [u]_a + [\widehat{U}]_{ss} \left([\widehat{U}]_{us}^{-1} [u]_b - [\widehat{U}]_{us}^{-1} [\widehat{U}]_{uu} [u]_a - [\widehat{U}]_{us}^{-1} [\widehat{\bar{u}}] \right) + [\widehat{\bar{s}}]. \tag{3.6}$$

Equations (3.5) and (3.6) can be rearranged to separate terms depending on $[u]_a$ and $[u]_b$. Due to different sign conventions in the equilibrium conditions which underlie equation (3.2) and those of the edge forces $[q]$ in Finite Element derivations an intermediate step is necessary

$$[q]_a = -[s]_a$$
$$[q]_b = [s]_b. \tag{3.7}$$

before the stiffness relation can be written as

$$\begin{bmatrix} [q]_a \\ [q]_b \end{bmatrix} = \underbrace{\begin{bmatrix} [\widehat{U}]_{us}^{-1} [\widehat{U}]_{uu} & -[\widehat{U}]_{us}^{-1} \\ [\widehat{U}]_{su} - [\widehat{U}]_{ss} [\widehat{U}]_{us}^{-1} [\widehat{U}]_{uu} & [\widehat{U}]_{ss} [\widehat{U}]_{us}^{-1} \end{bmatrix}}_{[K]_e} \begin{bmatrix} [u]_a \\ [u]_b \end{bmatrix} + \underbrace{\begin{bmatrix} [\widehat{U}]_{us}^{-1} [\widehat{\bar{u}}] \\ [\widehat{\bar{s}}] - [\widehat{U}]_{ss} [\widehat{U}]_{us}^{-1} [\widehat{\bar{u}}] \end{bmatrix}}_{[p]_e}. \tag{3.8}$$

$$\begin{bmatrix} [q]_a \\ [q]_b \end{bmatrix} = \begin{bmatrix} [K]_{eaa} & [K]_{eab} \\ [K]_{eba} & [K]_{ebb} \end{bmatrix} \begin{bmatrix} [u]_a \\ [u]_b \end{bmatrix} + \begin{bmatrix} [p]_{ea} \\ [p]_{eb} \end{bmatrix} \tag{3.9}$$

$[K]_e$ represents the element stiffness matrix and $[p]_e$ the element load vector.

The presented process can be inverted to obtain a transmission matrix $[\widehat{U}]$ from an existing element stiffness matrix $[K]_e$

$$\begin{bmatrix} [\widehat{u}]_b \\ [\widehat{s}]_b \end{bmatrix} = \underbrace{\begin{bmatrix} -[K]_{eab}^{-1} + [K]_{eaa} & -[K]_{eab}^{-1} \\ [K]_{eba} - [K]_{ebb} [K]_{eab}^{-1} [K]_{eaa} & -[K]_{ebb} [K]_{eab}^{-1} \end{bmatrix}}_{[\widehat{U}]} \begin{bmatrix} [\widehat{u}]_a \\ [\widehat{s}]_a \end{bmatrix} + \underbrace{\begin{bmatrix} -[K]_{eab}^{-1} [p]_{ea} \\ -[K]_{ebb} [K]_{eab}^{-1} [p]_{ea} + [p]_{eb} \end{bmatrix}}_{[\widehat{z}]}.$$
$$\tag{3.10}$$

3.1.3 High-Order Finite Elements

This section addresses the ansatz functions in the x-direction. The underlying theory is not modified. The concept is to use not only linear and quadratic shape functions but functions of even higher polynomial order (p). It is also called the p-version of Finite Elements [Babuska et al. 1981]. It was shown by many authors, that for this class of problems the p-version is superior to the classical h-version approach. Combined with a proper mesh design, the p-version shows an exponential rate of convergence in energy norm in the preasymptotic range. In addition to high accuracy the p-version includes some further advantages. It was theoretically and numerically shown, that the p-version is free of locking effects, if the polynomial degree is chosen to be moderately high [Düster et al. 2001; Szabó et al. 2004].

The so-called p-refinement (order elevation of the ansatz functions) reaches very high convergence rates if the problem is sufficiently smooth [Sprague and Geers 2007]. Singularities such as load applications inside elements are covered much worse and thus should be treated with (additional) separate elements (hp-refinement). Error estimates and proofs of convergence of both refinement strategies for *Timoshenko* elements can be found e.g. in [Li 1990].

High order ansatz functions are also the prerequisite for modelling a curved beam element and the effects occurring from curvature.

3.1.3.1 h-Type Finite Elements

The first possibility to enrich the functional basis is to use a series of $p+1$ *Lagrangian* interpolants of polynomial order p

$$N_i(\xi) = \prod_{j=1,\ j \neq i}^{p+1} \frac{\xi - \xi_j}{\xi_i - \xi_j} \tag{3.11}$$

where the positions ξ_j are called nodes. Usually the nodes are evenly spaced [Düster 2007; Sprague and Geers 2007]. An attractive feature of *Lagrangian* interpolants is that they constitute a nodal basis, i.e.,

$$N_i(\xi_j) = \delta_{ij} \tag{3.12}$$

where δ_{ij} is the Kronecker delta. [Sprague and Geers 2007] call this approach h-type Finite Elements, [Düster et al. 2001] standard Finite Element basis.
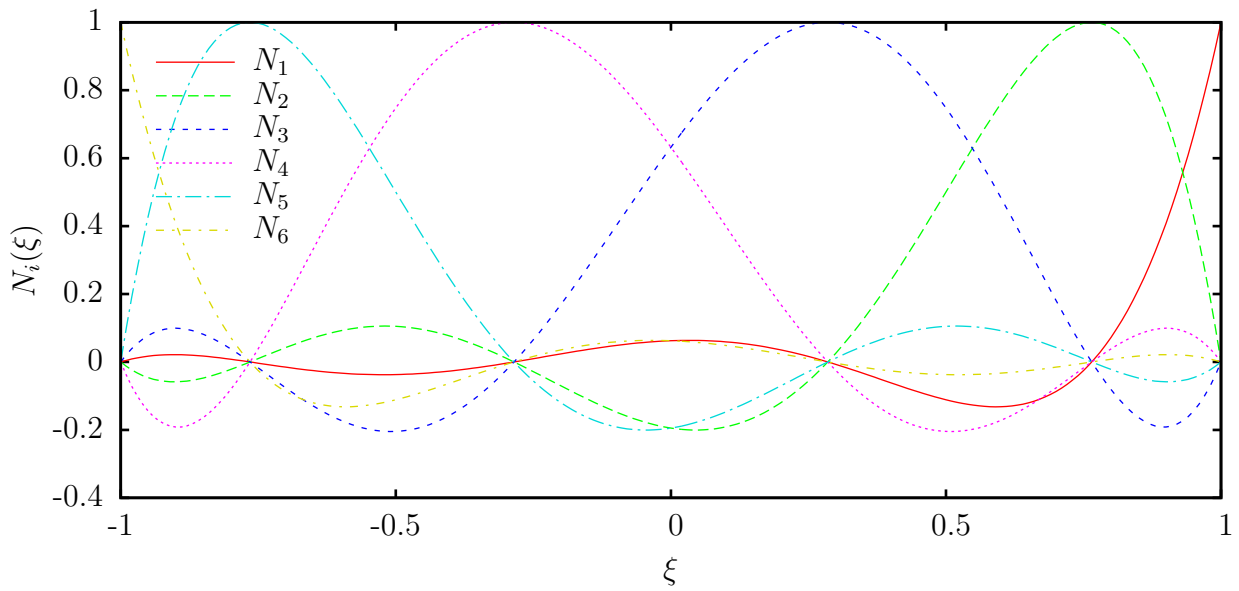
(a) Spectral shape functions for order $p = 5$.
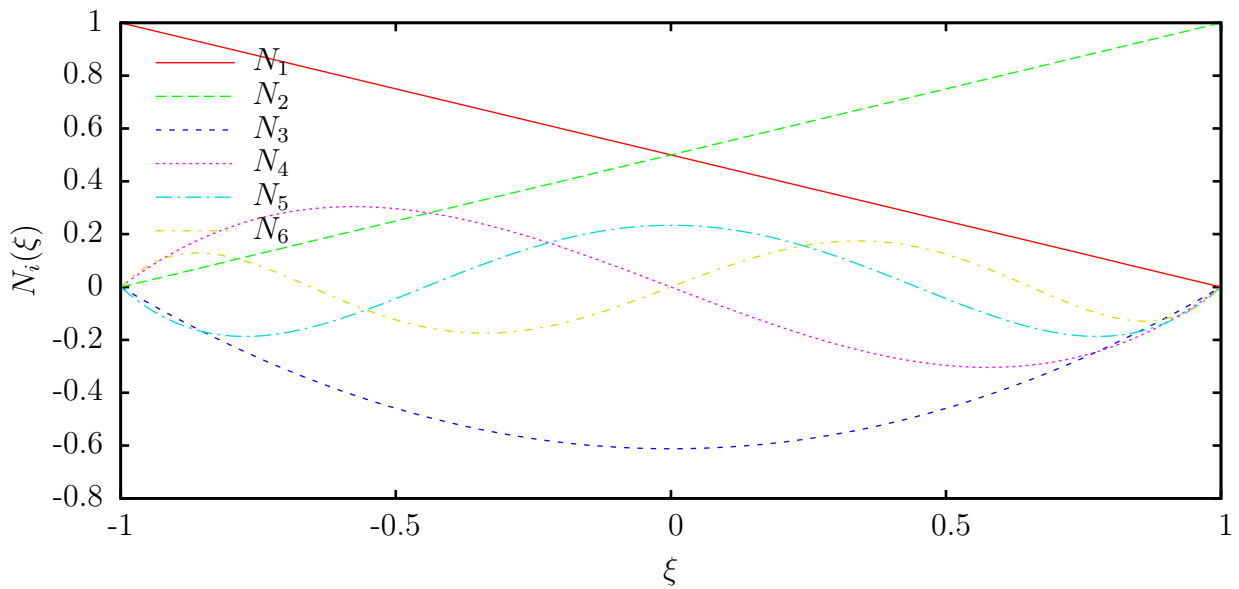
(b) Hierarchical shape functions until order $p = 5$.

Figure 3.1: Different shape functions for high order Finite Elements.

3.1.3.2 Spectral Finite Elements

The first possibility to improve this approach are the so-called spectral[2] Finite Elements. Their shape functions are *Lagrangian* interpolants with node locations either at the $(p + 1)$ *Gauss-Lobatto*[3]-*Chebyshev*[4] or *Gauss-Lobatto-Legendre*[5] points [Deville et al. 2002; Sprague and Geers 2007]. The latter are defined by.

$$\left(1 - \xi^2\right) L_{p,\xi} \overset{!}{=} 0 \tag{3.13}$$

where L_p represents a *Legendre* polynomial of degree p.

With this nodal distribution, the *Lagrangian* interpolant for the ith node can be written as

$$N_i(\xi) = -\frac{1 - \xi^2}{p(p+1)L_p(\xi_i)(\xi - \xi_i)} L_{p,\xi} \quad \forall i \in \{0; 1; \ldots; p\}. \tag{3.14}$$

Elements of this type differ from the before mentioned by the fact that the shape functions are attached to nodes which are not evenly spaced. They still form a nodal basis, thus equation (3.12) holds. Quadrature points and nodes coincide which leads to an optimally lumped mass matrix and little computational effort for the evaluation of integrals. A plot of this type of shape functions for order $p = 5$ can be seen in figure 3.1a.

3.1.3.3 Hierarchical Ansatz Functions

A different way of enrichment are the so-called hierarchical ansatz functions using the *Legendre* polynomials differently:

$$\begin{aligned} N_1(\xi) &= \frac{1 - \xi}{2}, \qquad N_2(\xi) = \frac{1 + \xi}{2} \\ N_i(\xi) &= \phi_{i-1}(\xi), \quad \forall i \in \{3; 4; \ldots; p + 1\} \end{aligned} \tag{3.15}$$

with

$$\phi_j(\xi) = \frac{1}{\sqrt{4j - 2}} \left(L_j(\xi) - L_{j-2}(\xi)\right), \quad \forall j \in \{2; 3; \ldots; p\} \tag{3.16}$$

---

[2]The term "spectral elements" is not uniquely defined and may also refer to elements utilising harmonic or exponential ansatz functions.
[3]Rehuel Lobatto (∗1797, †1866)
[4]Pafnuti Lwowitsch Tschebyschow (∗1821, †1894)
[5]Adrien-Marie Legendre (∗1752, †1833)

While such shape functions do not constitute a nodal basis like before, they are well suited to adaptive refinement (order elevation) [Düster et al. 2001; Hartmann and Katz 2007; Sprague and Geers 2007]. The prerequisite is that the new functions are orthogonal with respect to the strain energy product of the treated problem. For continuum problems, this product reads

$$\int\limits_{-1}^{1} N_{i,\xi} N_{j,\xi} \, d\xi = \delta_{ij}. \tag{3.17}$$

The functions defined in equations (3.15) and (3.16) fulfil this orthogonality condition. For beam elements this property is not sufficient to eliminate off-diagonal terms in stiffness matrices because the strain energy is not exclusively contained in the first order derivatives. This can be seen e.g. from equation (4.76) on page 70 for the *Timoshenko* beam theory.

Furthermore, the element mass matrix becomes fully populated [Sprague and Geers 2007] which may lead to stability problems of a transient analysis [Rank et al. 1983].

The hierarchical ansatz functions up to degree $p = 5$ can be seen in figure 3.1b.

3.1.4 Using Degenerate Hexahedral Continuum Elements

In [Düster et al. 2001] a hierarchic hexahedral element is presented which is able to vary the polynomial degree for the three different local directions and also to choose a different degree for each primary variable (e.g. u_x, u_y and u_z). This enables the element to be used in degenerate cases, e.g. to represent the volume of a plate with a comparable ansatz space as in e.g. *Reissner/Mindlin* plate theory. The authors state that the element is stable even if the aspect ratio of the elements becomes very large. By this, the element can also represent a beam with a cross section with 4 corners and curved edges. More elements can be combined to represent more difficult shapes. If the order of the shape function is sufficient the shape of the beam in longitudinal direction can be curved and the cross section may vary.

The different polynomial degrees for u_x, u_y and u_z in the different directions can be chosen such that deformations of higher order and also distortions of the cross section can be covered, thus this solution can go beyond the standard beam theories.

3.2 Selected Extended Beam Theories in the Literature

3.2.1 Attributes and Classifications of Extended Beam Theories

Theories which enrich the solution space of the traditional approaches are the subject of research at least since 1940 [Wlassow 1964]. Several approaches exist which are sometimes hard to distinguish. This section shall provide a possible set of criteria to classify different theories.

3.2.1.1 Thin or Thick Walled Cross Sections

Some extensions of beam theory apply only for rectangular cross sections [e.g. Bickford 1982; Hofmann 1992; Levinson 1985]. Most extensions for beam theories apply for thin-walled cross sections [e.g. Gonçalves and Camotim 2011, 2012; Gonçalves, Ritto-Corrêa, et al. 2010; Kreuzinger 1974; Möller 1982; Okur 1971; Orrenius and Finnveden 1996; Roik and Sedlacek 1970; Schardt 1989]. The cross section is then mostly subdivided into strips for which different shell theories are applied. If this reduction of dimensions is not done, thick walled cross sections are treated [e.g. Ferradi et al. 2013; Zeller 1979]. This approach is more general but further reductions and simplifications are harder to find. Few approaches such as [Zeller 1979] treat both mentioned types of cross sections.

3.2.1.2 Shape of the Beam

Most beam formulations apply for (straight) prismatic shapes. Commercial standard Finite Element software packages sometimes offer the possibility to consider changes of beam parameters in longitudinal direction which might be confused with the ability to calculate haunched beams. The latter requires a huge set of effects to be treated exactly which is explained and illustrated in [Hartmann and Katz 2007], [Bogensperger 2000] and [Unterweger 2001]. Besides the expectable effects like lateral stresses e.g. the haunched (tapered) box girder under torsional loading causes unexpected huge warping stress [Unterweger 2008]. Extended beam theories may cover this issue [Bogensperger 2000].

Curvature effects (plane or skew) on beams go beyond coupled stiffnesses which are covered either by high order Finite Beam Elements (see 3.1.3) or directly by special transmission matrices given e.g. in [Petersen 1966] which can be easily computed into stiffness matrices (see section 3.1.2). This does not cover e.g. the effects on the cross section from deviation

forces. This is only possible by allowing for lateral distortions of the cross section. To the knowledge of the author there is no extended beam formulation available covering both curved beams and lateral distortions.

3.2.1.3 Polynomial Degree or Type of Interpolation Functions

Almost all extended beam theories are based on deformation approaches using nodal deflections or rotations and shape functions to interpolate between nodes. The function type may vary for different types of deflections (longitudinal/lateral) or rotations. Most procedures use linear interpolation [e.g. Schardt 1989]. [Kreuzinger 1974] uses a series of trigonometric functions.

Theories which address a certain thick type of cross section like [Bickford 1982; Hofmann 1992; Levinson 1985] contain high order shapes for e.g. warping deflections $u_x(y,z)$. [Sayyad 2011] compares different shear stress distributions occurring in the literature.

Also the longitudinal interpolation functions may have different specifications. It also depends on the emerging type of PDE (see section 3.2.1.6) and the type of problem (static or dynamic) which approach is suitable.

3.2.1.4 Considering Additional Terms of Virtual Work

Standard beam theory neglects a lot of components of the stress- or strain tensor or of both. In some constrictive cases (homogeneous material, no compound material) either stresses or strains can be resurrected from the material law and an assumption about the other. For example, the assumption of zero stresses in the lateral direction can enable the calculation of lateral strains.

Extended beam theories can be distinguished and judged by the sorts of additional strains and stresses taken into account.

For thin-walled sections, the distinction becomes even more subtle since not only the tensor components but different types of plate degrees of freedom or also plate assumptions (*Reissner-Mindlin* or *Kirchhoff*) can occur.

The more terms are taken into account the more complex the computations get and the harder it gets to perform orthogonalisations or reductions of the bandwidth.

3.2.1.5 Orthogonalisation

Some beam formulations are based on local degrees of freedom with respect to the cross section. These may be deflections or rotations of single nodes or strips [e.g. Kreuzinger 1974; Wlassow 1958, 1965]. This approach is straight forward and allows for a simple application of arbitrary boundary conditions. The drawback is that the solution is not comprehensible without performing a post processing and obtaining stresses. Values such as moment and shear force have to be computed as resultants of stresses.

This precedure is not necessary if the degrees of freedom are global with respect to the cross section like they are in standard beam theories (rotation or deflection of the whole section, global deflection shapes like warping) [e.g. Möller 1982; Roik and Sedlacek 1970; Schardt 1989]. This approach additionally allows for the orthogonalisation of the degrees of freedom or at least a bandwidth reduction provided that some additional assumptions are made (see section 5.2 on page 77).

Orthogonalisation or the reduction of the bandwidth is of great importance for the numerical efficiency of a method. Different theories treat this problem with different priorities. Two approaches lead to the goal of decoupling the degrees of freedom

1. Neglecting off-diagonal terms or special underlying parts of the virtual work term. This approach may lead to a lack of accuracy (see section 3.2.1.4).

2. Transforming the problem to a new modal domain (rearranging of the unknowns) by solving one or more eigenvalue problems. This is done e.g. in the GBT [Schardt 1989] (see section 3.2.3 on page 26).

3.2.1.6 Emerging Type of PDE

Different augmented beam theories lead to different types and orders of differential equations. For the solution of higher order differential equations different approaches exist. The first refers to *Euler-Bernoulli* Beams and solves the equations "directly" leading to the need for ansatz functions with high continuity requirements. This strategy is chosen e.g. by the GBT [Schardt 1989]. The second approach is to develop the high order differential equation into a coupled system of linear differential equations. The derivatives (e.g. rotations or curvatures) are substituted to new unknowns. This strategy is chosen e.g. by [Zeller 1979].

For the integration in the longitudinal direction which is necessary to obtain the virtual work terms for the stiffness matrix various procedures can be applied. One option are the

"classical" numerical integration schemes which are familiar from standard Finite Element procedures. But also an exact or stepwise numerical integration of the PDE or the solution state, known as the reduction method (see section 3.1.2) comes into use e.g. in [Zeller 1979].

3.2.2 Beam Theory with Enhanced Warping

This type of extension was published in the most general form by [Roik and Sedlacek 1970] (German: Stabtheorie mit Zusatzverwölbungen, SZW). It employs additional warping degrees of freedom for thin walled cross sections to capture shear-lag effects (effective width) and effects in the vicinity of load applications. The cross section remains undeformed.

The biggest advantage of this method is that only few further information needs to be provided with respect to a standard beam calculation. The new DOFs are coupled to the standard beam DOFs via the shear stiffness of the membrane members.

Numerous considerations exist which treat thin walled cross sections and presume generalised shapes (e.g. quadratic parabolas). They are listed e.g. in [Bogensperger 2000].

3.2.3 Generalised Bending Theory (GBT)

This theory was founded by Schardt in the 1960s. The intention was to collect and unify developments in the area of prismatic (thin-walled) folded plate structures. It allows for distortions of the cross section and makes a huge (also computational) effort to obtain stiffness matrices which are strongly decoupled or even orthogonal. To achieve that, some restrictions in the solution set are introduced and some effects are neglected. There exist different flavours of the theory which differ in their capabilities and orthogonality properties.

The theory was used to evaluate the buckling behaviour of thin-walled metal structures [Okur 1971].

[Schardt 1989] collects and illustrates research work done on beams with thin-walled cross sections allowing for distortions (linear theory). The second volume announced to cover the nonlinear theory is not yet published.

The first version described in [Schardt 1989] presumes strict assumptions such as the absense of shear deformations and lateral normal strains ε_{yy} and ε_{zz} in the mid-planes of the plates. The assumptions are equivalent to those of *Euler-Bernoulli*, *Kirchhoff* and *Wagner* (no shear

deformation). The basic principle is to combine a couple of one warping deflection shape and one corresponding in-plane deflection shape to something called a "deformation process" for which a separation of variables with respect to the longitudinal direction x is applied. The in-plane deflections are classified into uniform deflections (global modes)

$$u(x,y,z) = {}^k u(y,z) \cdot {}^k V(x)_{,x}$$
$$\begin{bmatrix} v \\ w \end{bmatrix}(x,y,z) = \begin{bmatrix} {}^k v \\ {}^k w \end{bmatrix}(y,z) \cdot {}^k V(x) \tag{3.18}$$

The unit warping deflections are chosen by engineering experience such that they are orthogonal. From those the corresponding in-plane deflections are obtained from a geometrical procedure which only works for open unbranched sections (see figure 3.2 a)). The usual deformations (processes) occurring at a *Euler-Bernoulli* beam are fitted into that concept where each of the processes (numbered by k) is described by a PDE of fourth order:

$$E\,{}^k C\,{}^k V_{,xxxx} = {}^k q. \tag{3.19}$$

Where E is the elastic modulus, ${}^k C$ a sectional value, ${}^k V$ a participation factor and ${}^k q$ the load. Like in *Euler-Bernoulli* Beam Theory shear forces are recovered afterwards from an equilibrium consideration. At this stage, all processes are orthogonal to each other and thus can be considered separately without the need to solve a system of equations.

If in addition the influence of plate bending moments with stresses in the y-z-plane is considered an additional term occurs

$$E\,{}^k C\,{}^k V_{,xxxx} + {}^k B\,{}^k V = {}^k q. \tag{3.20}$$

The effect of this term can be compared with an elastic bedding for the process k.
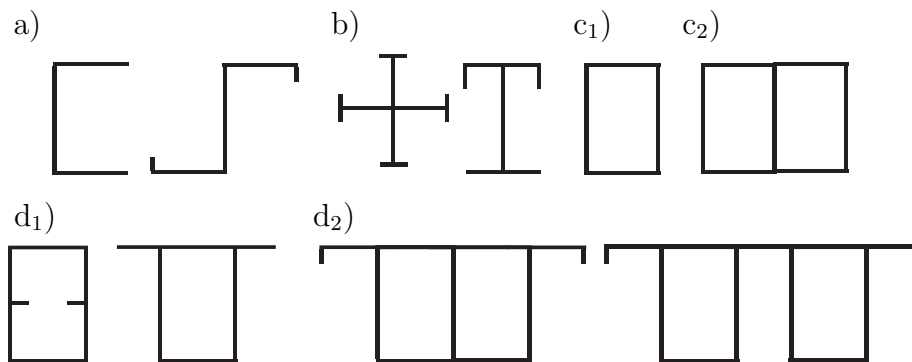
Figure 3.2: Cross-section types in GBT: a) open, unbranched, b) open, branched, c) closed, single and multi-cell, d) closed cells with open branches [Gonçalves, Dinis, et al. 2009]
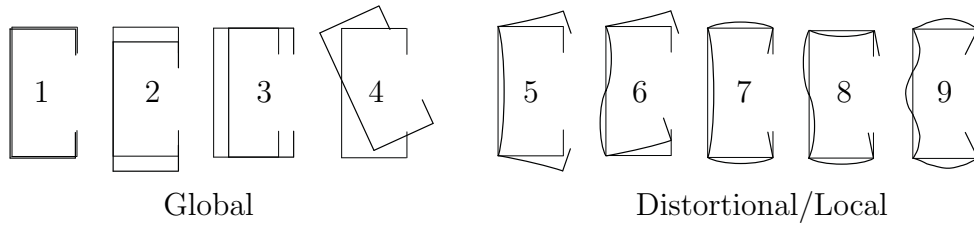
Figure 3.3: Different types of deformation shapes of the conventional GBT each belonging to one deformation process [Camotim and Basaglia 2012]

If in addition the longitudinal bending and drilling moments are taken into account, the differential equation is extended further and becomes coupled such that one process cannot be treated separately any more:

$$E\left[C\right]\left[V\right]_{,xxxx} - G\left[D\right]\left[V\right]'' + \left[B\right]\left[V\right] = \left[q\right].$$

(3.21)

Still an orthogonalisation with respect to the matrices $[C]$ and $[B]$ is done to keep the bandwidth small and thus reduce the computational effort. At the same time the remaining off diagonal elements of the matrix $[D]$ may be neglected.

In later chapters of [Schardt 1989], the assumption of the absense of shear deformations is dropped to allow for the solution of a single-cell closed cross section (see figure 3.2 c)). Still the restriction to unbranched sections prohibits the applicability to multi-cell sections.

[Möller 1982] extended the theory by the ability to cover shear deformations and Theory of II. Order. His concept is more based on the one presented by [Wlassow 1964] which means it is rather a theory of folded plates or finite strip theory. The first line of the equation (3.18) is changed to

$$u(x,y,z) = {}^{k}u(y,z) \cdot {}^{k}V(x).$$

(3.22)

This fundamentally modifies the structure and leads to the fact that considerably more deflection shapes have to be taken into account which are moreover coupled to a greater extent. The gain is the fact, that arbitrary cross sections can be handled. The theory is applied to dynamic problems (eigenvalue problem) and stability analysis.

The development of GBT is still alive since for example Camotim et al. recovered and extended the theory. [Gonçalves, Dinis, et al. 2009] extend the theory for arbitrary, thin-walled prismatic beams keeping the key properties of the theory. They introduce the theory of second order such that a linearized buckling analysis can be performed. [Gonçalves and

Camotim 2011] enrich the GBT by an elastoplastic material law and [Gonçalves and Camotim 2012] enable for geometrically non-linear effects such that the post buckling behaviour and collapse loads of elastoplastic members can be determined. [Camotim and Basaglia 2012] deal with the behaviour and influence of joints and shows opportunities to use the theory as part of a general, three dimensional beam finite element program.

3.2.4 Cross-Sectional Distortions of Bars by Zeller

A way of enhancing or refining beam theory which is very similar to the one presented in this work can be found in [Zeller 1979] and [Zeller 1982]. It is formulated both for thin and thick walled sections. The general approach is a stepwise correction of non-equilibrated states of stress which result from the assumptions of the *Bernoulli* bending and *de St.- Venant* torsion theory. The correction is done by introducing additional unit displacement and stress states of the cross section computed from previous non-equilibrated states. This is done by introducing two types of problems based on a 2D Finite Element representation of the cross section: warping and distortion. Thin-walled cross sections are just derived from the genreal ones as a special case. Zeller derives and uses a huge variety of general variational formulations for all the problems which subsequently lead to a 2D mixed Finite Element discretisation of the cross section. As in this thesis, warping describes only out of plane deflections distortion only in-plane deflections.

In the end, a coupled linear differential equation system depending on the longitudinal coordinate is obtained. This is integrated in the longitudinal direction in order to obtain a linear beam element stiffness matrix with additional degrees of freedom.

3.2.4.1 Warping Problem
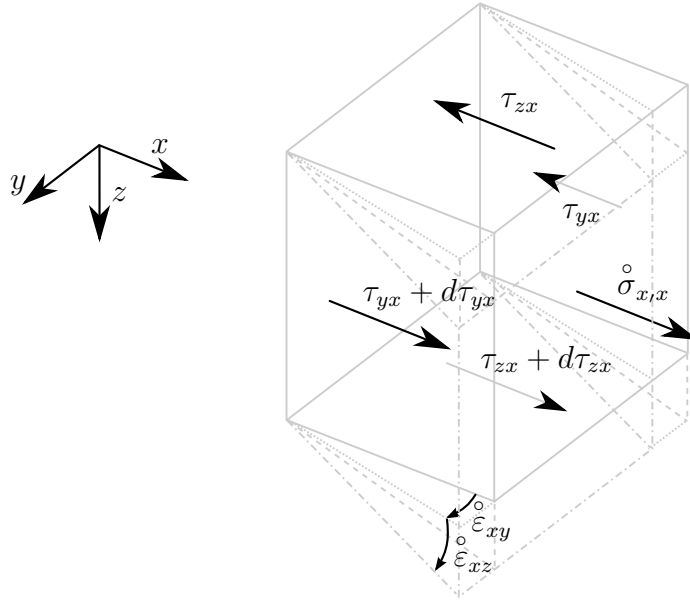
Figure 3.4: Quantities of the Warping Problem

Zeller formulates a general warping problem similar to the ones chapter 4.2.1 of this work. The problems are enumerated with i. The PDE is based on equilibrium in longitudinal direction

$$\tau_{zx,z} + \tau_{yx,y} + \overset{\circ}{\sigma}_{x,x} \overset{!}{=} 0. \tag{3.23}$$

Additionally, the equilibrium at the surface is considered

$$\tau_{zx} n_z + \tau_{yx} n_y \overset{!}{=} 0. \tag{3.24}$$

Quantities with a $\overset{\circ}{\square}$ indicate a type of load which here is assumed to be known.

Shear strains can arise both from warping and distortion deflections

$$\begin{aligned}
\gamma_{xy} &= \varepsilon_{yx} + \overset{\circ}{\varepsilon}_{xy} = u_{x,y} + \overset{\circ}{u}_{y,x} \\
\gamma_{xz} &= \varepsilon_{zx} + \overset{\circ}{\varepsilon}_{xz} = u_{x,z} + \overset{\circ}{u}_{z,x} \; .
\end{aligned} \tag{3.25}$$

In an arbitrary i^{th} warping problem, a deflection u_x and shear stress state (τ_{zx}, τ_{yx}) is wanted for satisfying the known longitudinal stresses $\overset{\circ}{\sigma}_x$ and shear strains $\overset{\circ}{\varepsilon}_{xy}$ and $\overset{\circ}{\varepsilon}_{xz}$. The longitu-
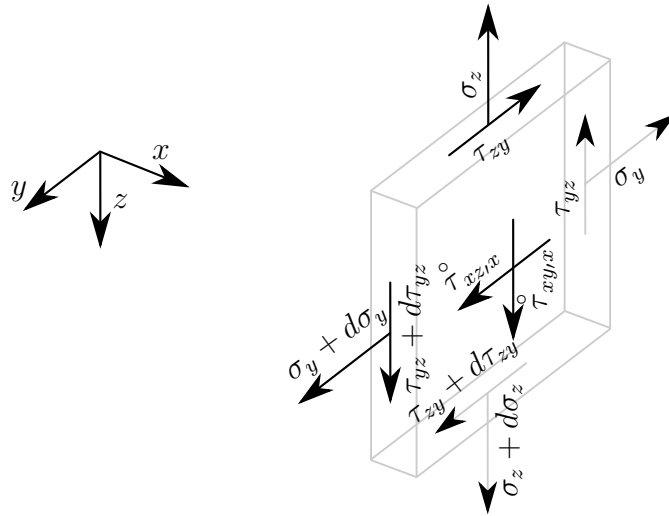
Figure 3.5: Quantities of the Distortion Problem

dinal stresses $\mathring{\sigma}_x$ result from the $i-1^{\text{th}}$ warping problem, the shear strains $\mathring{\varepsilon}_{xy}$ and $\mathring{\varepsilon}_{xz}$ from the $i-1^{\text{th}}$ distortion problem.

3.2.4.2 Distortion Problem

As a second type of problem, Zeller introduces the distortion problem. He points out the analogy to a plate problem. As the latter, it is based on the equilibrium in the u_y and u_z direction

$$\sigma_{y,y} + \tau_{zy,z} + \mathring{\tau}_{xy,x} \overset{!}{=} 0$$
$$\sigma_{z,z} + \tau_{zy,y} + \mathring{\tau}_{xz,x} \overset{!}{=} 0. \tag{3.26}$$

At the bounding surfaces of the section the stresses are in equilibrium with the components of the load

$$\sigma_y n_y + \tau_{zy} n_z + \bar{p}_y = 0$$
$$\sigma_z n_z + \tau_{zy} n_y + \bar{p}_z = 0. \tag{3.27}$$

Quantities with a $\mathring{\square}$ indicate a type of in-plane load which results from the ith warping problem.

External
Load

p_y, p_z p_y, p_z p_y, p_z

Distortion

$\boxed{0}$ $\boxed{1}$ $\boxed{2}$

$\overset{\circ}{\varepsilon}_{xy}, \overset{\circ}{\varepsilon}_{xz}$ $\overset{\circ}{\tau}_{xy}$ $\overset{\circ}{\varepsilon}_{xy}, \overset{\circ}{\varepsilon}_{xz}$ $\overset{\circ}{\tau}_{xy}$
$\overset{\circ}{\tau}_{xz}$ $\overset{\circ}{\tau}_{xz}$

Warping

$\boxed{0}$ $\overset{\overset{\circ}{\sigma}_x}{\longrightarrow}$ $\boxed{1}$ $\overset{\overset{\circ}{\sigma}_x}{\longrightarrow}$ $\boxed{2}$
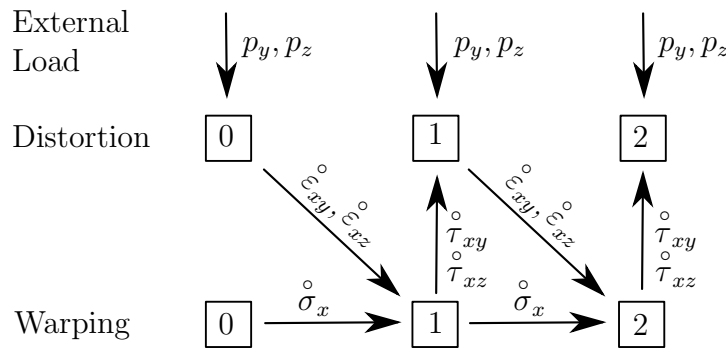
Figure 3.6: Relation between the different types and orders of problems

3.2.4.3 Setting up and Solving the Problem in the Longitudinal Direction

The method follows the scheme that free or unconsidered forces of the already covered problems are taken as input to generate new deflection shapes (see Figure 3.6). The procedure can theoretically be continued infinitely often, but the gain of accuracy will decay with rising order. Due to that and due to limitations of the size of computational problems those days Zeller stopped the enhancements at order two. Thus, he considered four problems:

- the primary warping problem

- the primary distortion problem

- the secondary warping problem

- the secondary distortion problem.

This set of extensions is applied to three types of load impacts: bending with respect to the y-axis, bending with respect to the z-axis and torsion.

By the fact that he uses mixed elements, Zeller obtains both unit deflection shapes and the corresponding strains and stresses at the same time. These are used to calculate by integration sectional values which are then used in the integration in longitudinal direction which yields the element stiffness matrix.

To solve the actual beam problem, several of these element stiffness matrices are assembled to a global stiffness matrix into which the boundary conditions (supports) are implemented. Different new types of supports are possible since the additional degrees of freedom like the warpings and the distortions of the section at a beam node can independently be either fixed or not.

3.2.4.4 Remarks About the Method

The fact that the integration is done in two steps, first lateral to obtain sectional values, and then longitudinal opens the gate for applying the sectional values multiple times even for elements of different lengths which can be an advantage in the computational effort.

The fact that the series of problems is truncated at order 2 is an arbitrary choice which should be evaluated e.g. by a reference calculation using a volume model.

The unit distortions are determined taking into account the external load and its position which certainly improves the accuracy and thus the efficiency of the method. On the other hand, forces induced by supports are not considered which is acceptable as long as the supports are defined such that they prevent any distortion which is not the case in general.

$$
\begin{bmatrix}
\sigma_x \\
\tau_{xy} \\
\tau_{xz} \\
\sigma_y \\
\sigma_z \\
\tau_{yz}
\end{bmatrix}
=
\begin{bmatrix}
e_{11} & 0 & 0 & & & \\
0 & e_{22} & e_{23} & & 0 & \\
0 & e_{32} & e_{33} & & & \\
& & & e_{44} & e_{45} & e_{46} \\
& 0 & & e_{54} & e_{55} & e_{56} \\
& & & e_{64} & e_{65} & e_{66}
\end{bmatrix}
\cdot
\begin{bmatrix}
\varepsilon_x \\
\gamma_{xy} \\
\gamma_{xz} \\
\varepsilon_y \\
\varepsilon_z \\
\gamma_{yz}
\end{bmatrix}
\tag{3.28}
$$

Equation (3.28) shows the material law as utilised by Zeller. The two types of problems do not interact at all on the basis of the material law. It can be observed that the coupling of the longitudinal and lateral direction due to the *Poisson* ratio is not covered.

4 Gaining Effective Unit Deflections Shapes with a 2D Finite Element Mesh

As indicated in the overview of the method (see section 1.3) one of the first steps of the solution process of a beam problem as presented here is to gain a set of unit deflection shapes which form a solution basis as effective as possible. Different possible types of unit deflection shapes are derived and presented in this chapter.

4.1 Using Dynamic Eigenmodes of Plane Systems

This type of shapes is gained by solving the homogeneous dynamic problem of the cross section

$$\left([K] - \Omega^2\,[M]\right)\boldsymbol{\Psi} = [0]\,. \tag{4.1}$$

It is a generalised eigenvalue problem with respect to the eigenvalue Ω^2. $[K]$ represents the stiffness matrix, $[M]$ the mass matrix and Ω the angular frequency. Equation (4.1) here refers to two differential equations: the one of a plate in membrane action (see following section 4.1.1) and the one of a plate in bending action (see following section 4.1.2).

Though the PDEs underlying plane systems do not represent the behaviour of the structure exactly (or not at all, see section 4.1.2), it is still possible to use the computed eigenmodes as ansatz functions. Eigenmodes are particularly suitable because of their arrangement where the most smooth shapes come first and the more curved ones later. The shapes are applicable as ansatz functions even if the system is not calculated for dynamic loads. Furthermore, the fact that eigenmode shapes fulfil certain orthogonality conditions implies their linear independency which is indispensable for using them as ansatz functions. The eigenvalues obtained by equation (4.1) are not of interest.

The mass and stiffness distribution can be adopted from the 3D model. In each case, the first three eigenmodes have the eigenvalue 0 and can only be computed using a shifted configuration as illustrated in appendix A.1. They represent an arbitrary linear combination of the three rigid body modes.

4.1.1 Eigenmodes of a Plate in Membrane Action

Shapes of this type are gained by solving the homogeneous dynamic problem of a slice of the beam regarding only the lateral deflections. The underlying PDE is depicted later in section 4.3.

In the scope of the beam system the rigid body modes represent an arbitrary mix of the two lateral deflections and the torsional rotation. In order to obtain pure deflections and the pure rotation about the shear centre they are generated manually. Higher eigenmodes can be seen as distortion shapes of the section (see **4.** in figure 4.1).

The Finite Element system of the section is set up using bilinear quadrilateral elements with the *Wilson* extension (see appendix A.2).

4.1.2 Eigenmodes of a Plate in Bending Action

Analogously to the previous section, the cross section can be treated as a plate in bending action with "arbitrary" thickness. The mass and stiffness distribution can be adopted from the 3D model. The first three eigenmodes with eigenvalue 0 represent an arbitrary linear combination of the three rigid body modes. Here, they are generated manually assuring that they represent the longitudinal deflection and the two rotations around the lateral axes which intersect with the centre of stiffness. Higher eigenmodes, from eigenmode 4 on, extend the standard beam theory by further longitudinal deflection shapes. Since the *Reissner-Mindlin* plate formulation was used, the actual shape of the higher eigenmodes depends on the chosen thickness of the plate. The thicker the plate is the more dominated by shear deformation they get. The underlying PDE is straight forward such that it will not be derived or illustrated here.

1.

Rigid body

2.

Rigid body

3.

Rigid body

4.
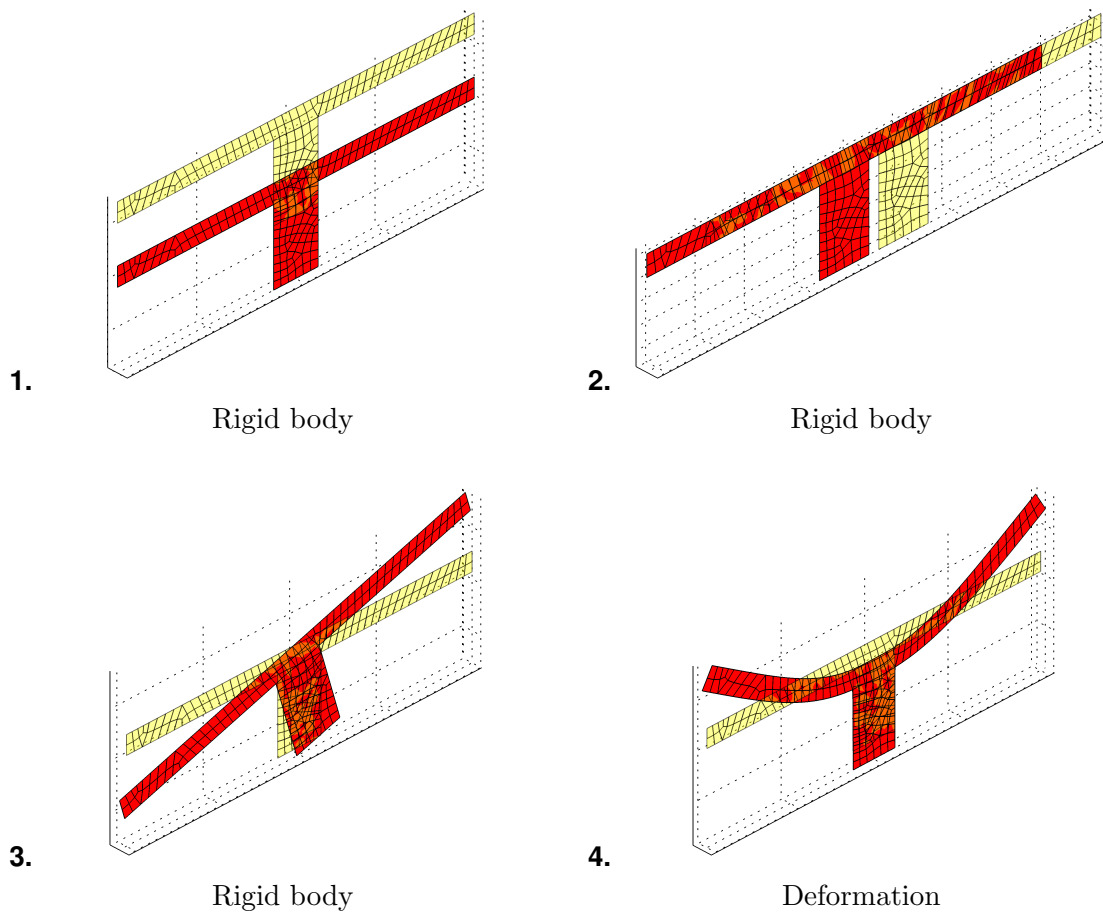
Deformation

Figure 4.1: Eigenmodes one to four of the cross section (in-plane).

Remark 1

Concerning its physical behaviour the utilised PDE is far away from the actual deformation processes happening in a continuous beam structure. Nevertheless, this type of shape functions can be used and because of their smoothness the shapes are effective compared to arbitrary deflection shapes like e.g. setting step by step one nodal deflection equal to 1.0 and all remaining equal to 0. Nevertheless the deflection shapes computed here are not as effective as the shapes derived in the following sections.

The Finite Element system of the cross section is set up using bilinear quadrilateral elements which is an element type prone to shear locking [Bathe 2002; Bathe and Dvorkin 1985]. For the above mentioned reason, that this type of deflection shape does not represent the behaviour of the structure at all the element formulation was not refined further.
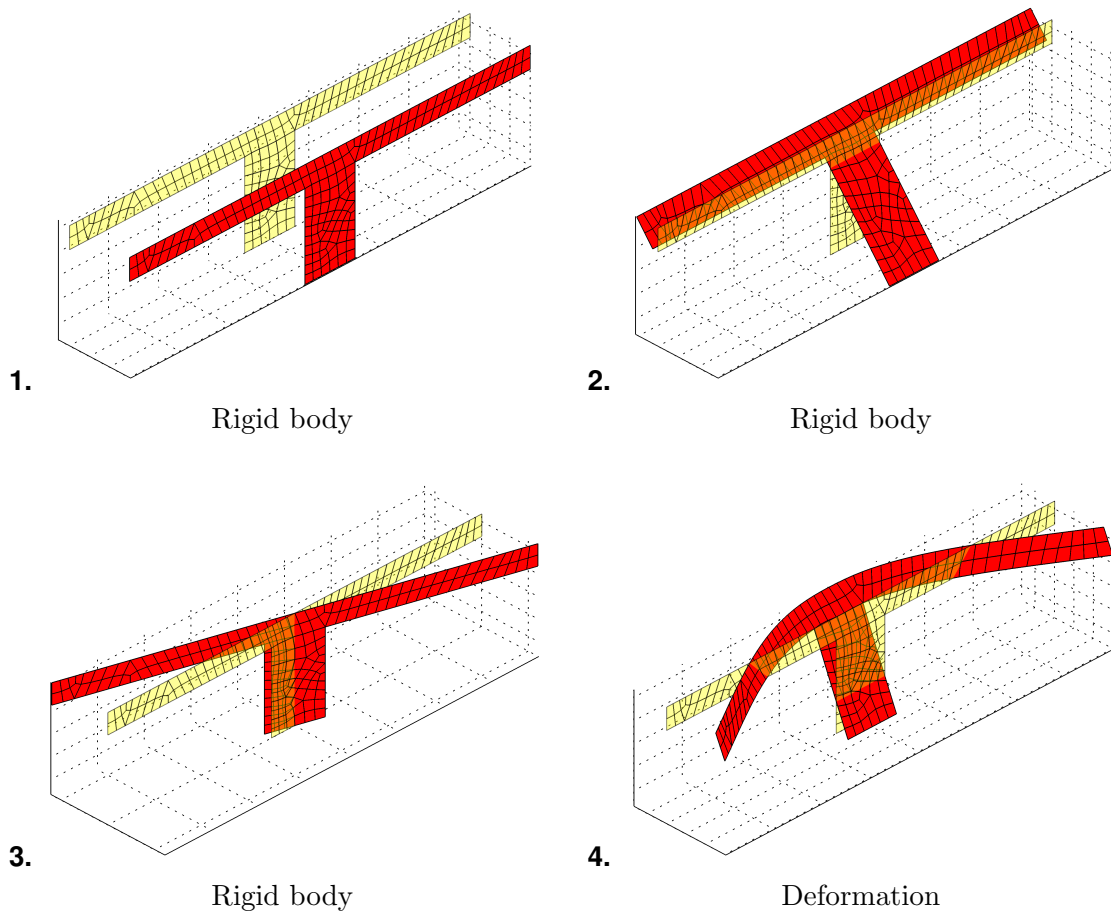
Figure 4.2: Eigenmodes one to four of the cross section (out of plane).

Remark 2

The desired unit deflection shapes contain only deformation degrees of freedom u_x. The solution of the procedure explained here contains both a deflection and two rotations per node. For the further usage the rotations are simply neglected which induces the need for caution concerning the linear independency of the generated shapes. At most one third of the producible modeshapes can be used for further computation.

4.2 Deriving Further Shapes from Existing Shapes Using the PDE of Shear Warping

4.2.1 Calculation of Shear Warp Shapes with the FEM

The differential equations for the determination of all types of shear warp figures are based on equilibrium in the longitudinal direction.

4.2.1.1 Literature

Computing shear warp shapes with the help of Finite Elements published in German can be found in [Gruttmann et al. 1998a,b], [Gruttmann and Wagner 2001], [Wunderlich and Kiener 2004], [Kraus 2005] and [Kraus 2007a,b]. Early works on this topic are e.g. [Herrmann 1965], [Krahula and Lauterbach 1969] and [Haberl and Och 1974]. [Gruttmann and Wagner 2001] extend the procedure to a nonlinear material law such that plastic torsions resistances and shear stress distributions can be obtained.

Procedures to compute shear warp shapes and section values for nonuniform torsion with Boundary Elements can be found for example in [Katz 1986] and [Athanasiadis 1982]. The warping resistance cannot be determined with boundary integrals [SOFiSTiK AG 2013a] because the applicability of the divergence theorem is limited.

4.2.1.2 Primary or uniform torsion

[Wunderlich and Kiener 2004]

The warp ordinate or warp shape for uniform torsion is derived under the following preliminaries (assuming a *Cartesian* coordinate system where the x-direction is pointing in the direction of the beam axis):

1. The beam exhibits a prismatic shape and the x-axis is parallel to the central axis.

2. The lateral surface of the beam is free of external forces.

3. The self weight of the beam is neglected.

4. The torque at the ends is applied as shearing stress only.
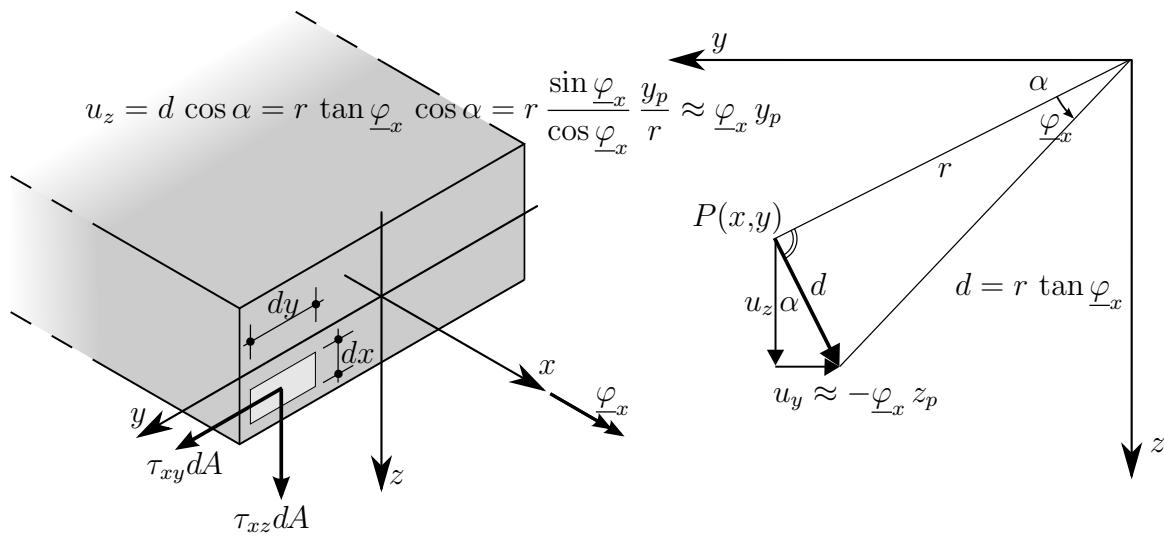
Figure 4.3: Prismatic beam, torqued around the x-axis and deflection of an arbitrary point P on the cross section

5. The stresses and through that the strains are independent of the coordinate x. Thus, the torque $\underline{\varphi}_{x,x}$ remains constant along x.

6. The shape of the cross section in the y-z-plane does not distort.

The assumptions from above lead to the fact that the normal stresses σ_x are zero. σ_y and σ_z as well as τ_{yz} are equal to zero due to the assumptions of beam theory. The shear stresses τ_{xy} and τ_{xz} can be computed as follows.

Starting from the shear strains

$$\boldsymbol{\gamma} = \begin{bmatrix} \gamma_{xy} \\ \gamma_{xz} \end{bmatrix} = \begin{bmatrix} u_{x,y} + u_{y,x} \\ u_{x,z} + u_{z,x} \end{bmatrix}. \tag{4.2}$$

The lateral deformations u_y and u_z in this respect according to figure 4.3 singularily have one origin - the rotation $\underline{\varphi}_x$. Thus, the shear strains can be rewritten

$$\boldsymbol{\gamma} = \begin{bmatrix} u_{x,y} - z\underline{\varphi}_{x,x} \\ u_{x,z} + y\underline{\varphi}_{x,x} \end{bmatrix}. \tag{4.3}$$

A warping function $\omega_V(y,z)$ is defined on the cross section such that the deformation u_x can
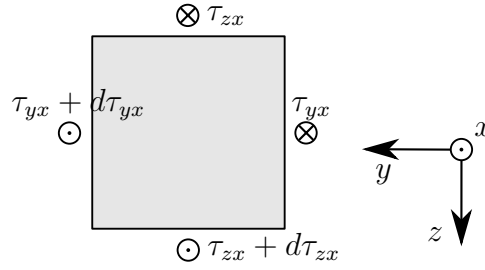
Figure 4.4: Infinitesimal element of a beam with shear stresses.

be written with a separation of variables:

$$u_x(x,y,z) = \underline{\psi}(x) \cdot \omega_V(y,z). \tag{4.4}$$

$\underline{\psi}(x)$ represents the scaling factor for the deflection field $\omega_V(y,z)$. Equation (4.4) together with the material law yields the shear stresses

$$\boldsymbol{\tau} = \begin{bmatrix} \tau_{xy} \\ \tau_{xz} \end{bmatrix} = [D_\omega] \cdot \boldsymbol{\gamma} = [D_\omega] \cdot \begin{bmatrix} \omega_{V,y} - z\underline{\varphi}_{x,x} \\ \omega_{V,z} + y\underline{\varphi}_{x,x} \end{bmatrix}. \tag{4.5}$$

where the material matrix $[D_\omega]$ is allocated as illustrated in section 2.3 on page 11.

Strong formulation

Using figure (4.4) to set up the equilibrium in the axial direction gives

$$\tau_{xz,z} + \tau_{xy,y} \overset{!}{=} 0. \tag{4.6}$$

Equation 4.5 can be introduced to obtain an equation containing the unknown deflection field $\omega_V(y,z)$.

According to assumption 2 on page 38 the shear stresses parallel to the lateral surface must vanish

$$\mathbf{n} \cdot \boldsymbol{\tau} = 0. \tag{4.7}$$

This relation is also visualised in figure 4.5.

The strong formulation is based on equilibrium and thus not suitable for a computer calcula-tion of a statically overdeterminate system (which always applies for continuum calculations). Therefore in the next section a weak formulation is derived. On that basis a FEM formulation can be formulated.
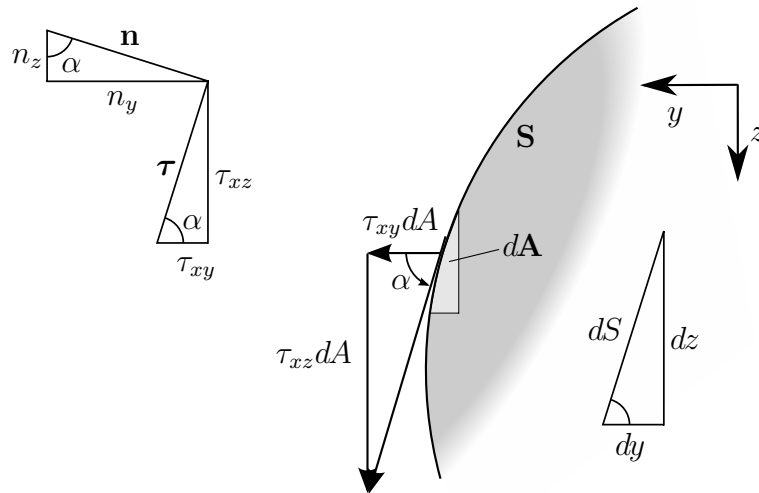
Figure 4.5: Shear strain at lateral surfaces. Normal stresses are assumed not to occur. The stress vector τ needs to be parallel to the surface and perpendicular to the normal vector $\mathbf{n}$.

Weak formulation

The weak formulation can be obtained by applying the principle of virtual work.

$$\delta W_i = -\int_{(A)} \boldsymbol{\delta\gamma} \cdot \boldsymbol{\tau} \; dA \qquad \text{with} \qquad \boldsymbol{\delta\gamma} = \begin{bmatrix} \delta\omega_{,y} \\ \delta\omega_{,z} \end{bmatrix}. \tag{4.8}$$

Since a linear system behaviour is presumed it is possible to decompose $\boldsymbol{\tau}$ from equation (4.5) into a part depending on ω_V and one on $\underline{\varphi}_{x,x}$. Additionally, $\underline{\varphi}_{x,x} = 1.0$ is introduced because $\underline{\psi}$ in equation (4.4) shall be equal to 1.0 for a unit of torque $\underline{\varphi}_{x,x} = 1$ (*Wagner*'s hypothesis).

$$\boldsymbol{\tau} = \boldsymbol{\tau}_\omega + \boldsymbol{\tau}_\varphi = [D_\omega] \cdot \begin{bmatrix} \omega_{V,y} \\ \omega_{V,z} \end{bmatrix} + [D_\omega] \cdot \begin{bmatrix} -z \\ y \end{bmatrix}. \tag{4.9}$$

This can be used to set up two separate parts of the virtual work

$$\delta W_i = -\int\limits_{(A)} \boldsymbol{\delta\gamma} \cdot \boldsymbol{\tau}_\omega \, dA - \int\limits_{(A)} \boldsymbol{\delta\gamma} \cdot \boldsymbol{\tau}_\varphi \, dA \overset{!}{=} 0. \tag{4.10}$$

This expression can be formulated using the FEM approach

$$\int\limits_{(A)} [\delta\omega]^T \cdot [B]^T \cdot [D_\omega] \cdot [B] \cdot [\omega_V] \; dA = \int\limits_{(A)} [\delta\omega]^T \cdot [B]^T \cdot [D_\omega] \cdot \begin{bmatrix} z \\ -y \end{bmatrix} [N] \; dA \tag{4.11}$$

with the following matrices:

$$[\delta\omega] = \begin{bmatrix} \delta\omega_1 & \delta\omega_2 & \delta\omega_3 & \delta\omega_4 & \dots \end{bmatrix}^T \qquad \text{(arbitrary) discrete virtual deflections}$$

$$[\omega_V] = \begin{bmatrix} \omega_{V1} & \omega_{V2} & \omega_{V3} & \omega_{V4} & \dots \end{bmatrix}^T \qquad \text{(unknown) discrete deflections}$$

$$[N] = \begin{bmatrix} N_1 & N_2 & N_3 & N_4 & \dots \end{bmatrix} \qquad \text{shape functions}$$

$$[B] = \begin{bmatrix} N_{1,y} & N_{2,y} & N_{3,y} & N_{4,y} & \dots \\ N_{1,z} & N_{2,z} & N_{3,z} & N_{4,z} & \dots \end{bmatrix} \qquad \text{derived shape fuctions}$$

The left hand side of equation (4.11) ends up to be a stiffness matrix since it contains the wanted nodal values ω_V. The right hand side can be seen as a load vector. The resulting system of equations is at this stage singular since there is no "support". This can be solved by fixing ω_V at one node e.g. to 0. This procedure is numerically stable and the resulting wrong rigid body motion can be determined and subtracted afterwards.

Normalisation of the Results

The result of the linear system of equations is the warp shape ω_V for a drill $\underline{\varphi}_{x,x} = 1$ about the origin of the coordinate system y-z. For further computation, the warp shape should be normalised. First the rigid body motion which was mentioned above has to be eliminated. The result is the unit warp shape $\bar{\omega}_V$

$$\bar{\omega}_V = \omega_V - \frac{1}{EA} \int\limits_{(A)} E\omega_V \, dA = \omega_V - \frac{EA_\omega}{EA}. \tag{4.12}$$

The next step is to determine the "real" centre of rotation - the shear centre. The coordinates of the shear centre y_M and z_M can be found from the demand that the torque shall not cause any bending moment. The corresponding warp shape is the principal warp shape $\tilde{\omega}_V$.

$$\int\limits_{(A)} E\tilde{\omega}_V \breve{y}\, dA \stackrel{!}{=} 0 \qquad (4.13\text{a}) \qquad \int\limits_{(A)} E\tilde{\omega}_V \breve{z}\, dA \stackrel{!}{=} 0 \qquad (4.13\text{b})$$

where $\breve{y} = y - y_S$ and $\breve{z} = z - z_S$ are the coordinates with reference to the centre of stiffness $(y_S; z_S)$. These coordinates are also needed for any type of shift of the axis of rotation by $(\Delta y; \Delta z)$ [1]:

$$\omega_{V\text{new}} = \omega_{V\text{old}} + \Delta y \breve{z} - \Delta z \breve{y} \qquad (4.14)$$

The difference between $\bar{\omega}_V$ and $\tilde{\omega}_V$ is also just a shift of the centre of rotation from the coordinate origin to $(y_M; z_M)$ which is expressed through

$$\tilde{\omega}_V = \bar{\omega}_V + y_M \breve{z} - z_M \breve{y}. \qquad (4.15)$$

If this condition is introduced into the equations (4.13a) and (4.13b) two equations for the unknown coordinates $(y_M; z_M)$ are obtained:

$$\int\limits_{(A)} E\left(\bar{\omega}_V \breve{y} + y_M \breve{z}\breve{y} - z_M \breve{y}^2\right) dA \stackrel{!}{=} 0 \quad (4.16\text{a}) \qquad \int\limits_{(A)} E\left(\bar{\omega}_V \breve{z} + y_M \breve{z}^2 - z_M \breve{y}\breve{z}\right) dA \stackrel{!}{=} 0 \quad (4.16\text{b})$$

Solving this system of equations and using the abbreviation $EA_{ab} = \int\limits_{(A)} Eab\, dA$ leads to

$$y_M = \frac{-EA_{\bar{\omega}_V \breve{z}}EA_{\breve{y}\breve{y}} + EA_{\bar{\omega}_V \breve{y}}EA_{\breve{y}\breve{z}}}{EA_{\breve{y}\breve{y}}EA_{\breve{z}\breve{z}} - EA_{\breve{y}\breve{z}}{}^2} \quad (4.17\text{a}) \qquad z_M = \frac{EA_{\bar{\omega}_V \breve{y}}EA_{\breve{z}\breve{z}} - EA_{\bar{\omega}_V \breve{z}}EA_{\breve{y}\breve{z}}}{EA_{\breve{y}\breve{y}}EA_{\breve{z}\breve{z}} - EA_{\breve{y}\breve{z}}{}^2} \quad (4.17\text{b})$$

With this information equation (4.15) can be solved and the principal warp shape $\tilde{\omega}_V$ is obtained. It is corresponding to a change of rotation around the shear centre.

---

[1]Remark: Also other coordinate systems can be used for shifting the centre of rotation but then a new rigid body component in the longitudinal direction is reintroduced and the substraction step (equation (4.12)) has to be performed again.
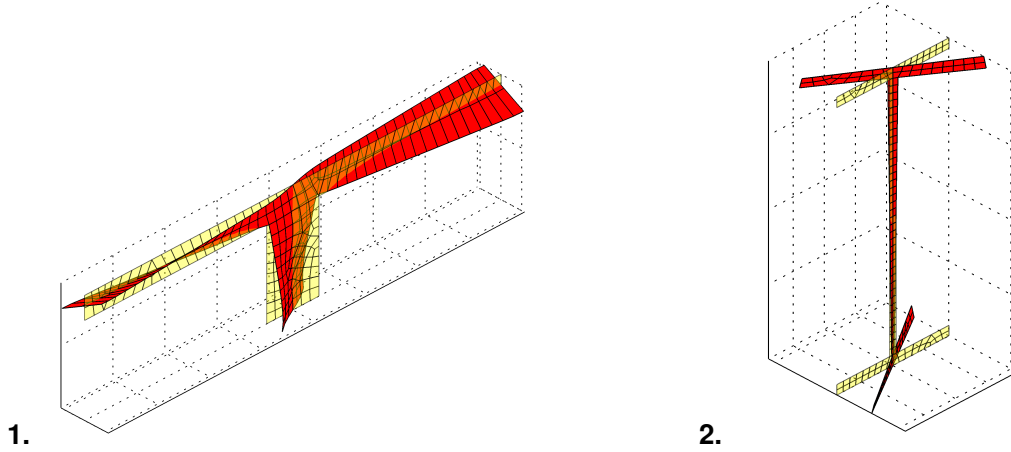
Figure 4.6: Torsional warp shapes ω_V.

4.2.1.3 Shear force and non-uniform (secondary) torsion

In equation (4.6) it was assumed that no change of stresses in the longitudinal direction occurs. In fact, longitudinal normal stresses σ_x occur as well as their derivatives $\sigma_{x,x}$. They can be computed as

$$\sigma_x = \sigma_x(M_y) + \sigma_x(M_z) + \sigma_x(M_\omega) \tag{4.18}$$

with

$$\sigma_x(M_y) = M_y \left(E \cdot \frac{EI_z}{EI_y EI_z - EI_{yz}^2} \cdot z - E \cdot \frac{EI_{yz}}{EI_y EI_z - EI_{yz}^2} \cdot y \right) \tag{4.19a}$$

$$\sigma_x(M_z) = M_z \left(-E \cdot \frac{EI_y}{EI_y EI_z - EI_{yz}^2} \cdot y + E \cdot \frac{EI_{yz}}{EI_y EI_z - EI_{yz}^2} \cdot z \right) \tag{4.19b}$$

$$\sigma_x(M_\omega) = E \cdot \frac{M_B}{EI_\omega} \omega_V . \tag{4.19c}$$

If the stiffness properties EI_i are assumed to be constant over x the differential relations of the sectional forces can be made use of

$$\sigma_{x,x} = \sigma_{x,x}(Q_z) + \sigma_{x,x}(-Q_y) + \sigma_{x,x}(M_{xS}) \tag{4.20}$$

with

$$\sigma_{x,x}(Q_z) = Q_z \left(E \cdot \frac{EI_z}{EI_yEI_z - EI_{yz}{}^2} \cdot z - E \cdot \frac{EI_{yz}}{EI_yEI_z - EI_{yz}{}^2} \cdot y \right) \tag{4.21a}$$

$$\sigma_{x,x}(Q_y) = -Q_y \left(-E \cdot \frac{EI_y}{EI_yEI_z - EI_{yz}{}^2} \cdot y + E \cdot \frac{EI_{yz}}{EI_yEI_z - EI_{yz}{}^2} \cdot z \right) \tag{4.21b}$$

$$\sigma_{x,x}(M_{xS}) = E \cdot \frac{M_{xS}}{EI_\omega}\omega_V. \tag{4.21c}$$

For composite sections the different *Young*'s moduli E have to be taken into account.

The derivatives or changes of the longitudinal normal stress $\sigma_{x,x}$ in equations (4.21a) through (4.21c) due to equilibrium cause shear stresses τ_{yx} and τ_{zx}.
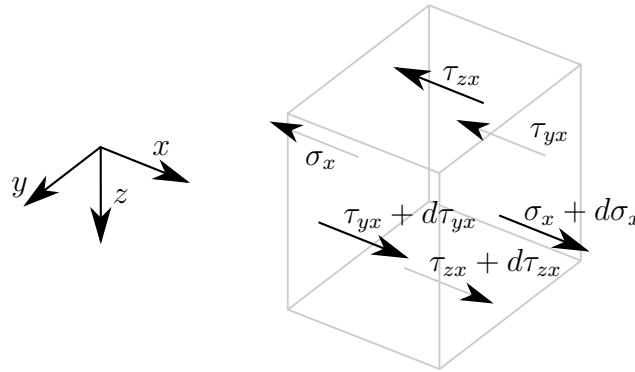
Figure 4.7: Shear stresses caused by the change of longitudinal stress on an infinitesimal element.

For each of the stress states (Q_y, Q_z and M_{xS}) the following virtual work formulation can be set up:

$$\delta W = \int_{(A)} \left(\sigma_{x,x}\delta\omega - \tau_{yx}\delta\omega_{,y} - \tau_{zx}\delta\omega_{,z} \right) dA \overset{!}{=} 0. \tag{4.22}$$

Using a general material law this can be transformed to

$$\delta W = \int_{(A)} \left(\delta\omega \cdot \sigma_{x,x\,\mathrm{i}} - \boldsymbol{\delta\gamma} \cdot \boldsymbol{\tau}_{\omega\mathrm{Si}} \right) dA \overset{!}{=} 0 \tag{4.23}$$

where $\sigma_{x,x\,\mathrm{i}}$ is one of the normal stress states caused by M_y, M_z and M_B as depicted in equations (4.21a) to (4.21c) and $\omega_{S\mathrm{i}}$ is the corresponding warp ordinate.

This leads to the following representation in FEM notation:

$$\int\limits_{(A)} [\delta\omega]^T \cdot [B]^T \cdot [D_\omega] \cdot [B] \cdot [\omega_{Si}] \ dA = \int\limits_{(A)} [\delta\omega]^T \cdot [N]^T \cdot [N] \cdot [\sigma_{x'x \ i}] \ dA. \qquad (4.24)$$

$[\sigma_{x'x \ i}]$ represents a vector of discrete nodal values of $\sigma_{x'x \ i}$. The other matrices are explained near equation (4.11) on page 42.

Figure 4.8 shows the shear deformation caused by transverse forces (first and second term in equation (4.20)). Figure 4.9 shows the shear deformation caused by the secondary torsional moment (third term in equation (4.20)).

1.

Shear force in the y-direction

2.

Shear force in the z-direction
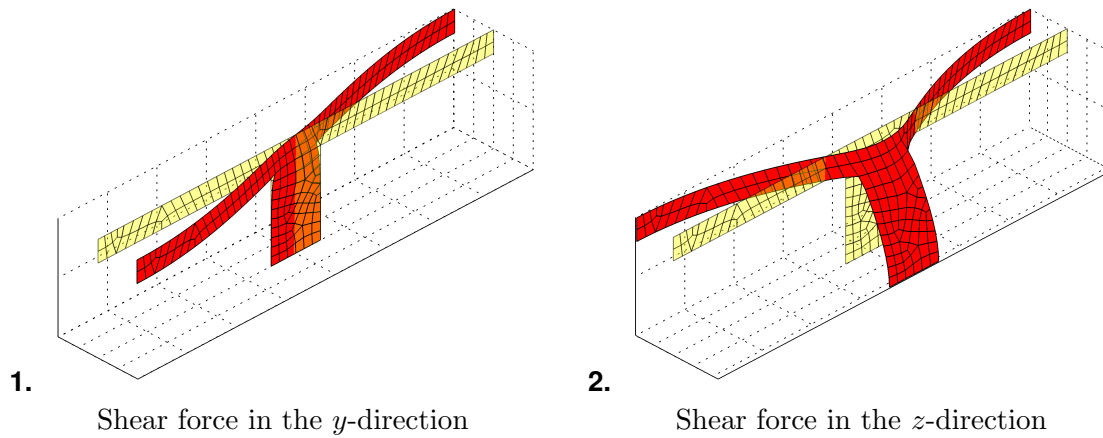
Figure 4.8: Shear deformation due to transverse forces.

1.

Concrete section

2.

Steel section
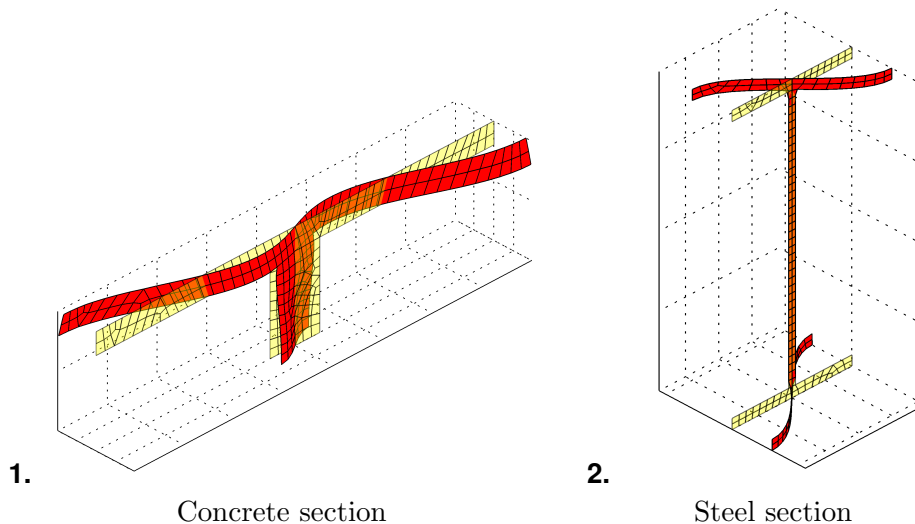
Figure 4.9: Shear deformations due to the secondary torsional moment.

4.2.2 Calculation of Derived Warp Shapes from Warp Shapes

The concept of the previous section (4.2.1.3) works for any kind of warping deflection shape. The procedure is that every warp shape when it is blocked or changes along the x-axis causes normal stress distributions which are affine to itself with respect to y and z. If these normal stresses change along the x-axis shear stresses are caused to fulfil the equilibrium (see figure 4.7 on page 45). Analogously to section 4.2.1.3 every calculated warp figure can be taken as another loadcase to calculate another, high order warp figure.

As a matter of fact, for usual load situations and compact sections of beam structures, the participation of these warp shapes on the solution decreases fast with increasing order. So introducing them as additional degrees of freedom will not result in a big gain of accuracy [see e.g. Ferradi et al. 2013; Hofmann 1992]. Nevertheless, for beams where the distortions of the sections are of considerable importance also this type of warp shape may gain influence and improve the accuracy of the beam solution.

4.2.3 Calculation of Derived Warp Shapes from Distortions

4.2.3.1 Basic considerations and equilibrium

[Zeller 1979] shows that one can compute a warp field from every distortion or in-plane deflection field $\boldsymbol{\psi}_{\mathrm{plane}}(y,z) \cdot \underline{v}(x)$. Under the supposition that the derivative of the amplitude of the in-plane field in the x-direction $\boldsymbol{\psi}_{\mathrm{plane}}\,\underline{v}_{,x}$ is constant and all the other preconditions from section 4.2.1.2 one can assume that there is a warp deflection field which is free of normal stresses σ_x as claimed in equation (4.6) (see also figure 4.4 on page 40).

$$\tau_{zx,z} + \tau_{yx,y} \overset{!}{=} 0 \qquad\qquad \text{(see equation 4.6)}$$

where

$$\boldsymbol{\tau} = \begin{bmatrix} \tau_{xy} \\ \tau_{xz} \end{bmatrix} = [D_\omega] \cdot \begin{bmatrix} \varepsilon_{xy} + \varepsilon_{yx} \\ \varepsilon_{xz} + \varepsilon_{zx} \end{bmatrix}. \qquad\qquad (4.25)$$

As the shear strains result from the different derivatives of the different deflections one can separate

$$\varepsilon_{xy} = u_{x,y} = \omega_{,y} \qquad \text{and} \qquad \varepsilon_{xz} = u_{x,z} = \omega_{,z} \qquad\qquad (4.26)$$

which arise from the warp deflections ω from ε_{yx} and ε_{zx} which result from the in-plane distortions $\boldsymbol{\psi}_{\text{plane}}$

$$
\begin{aligned}
\varepsilon_{yx} &= u_{y,x} = \psi_{\text{plane}\,y}\,\underline{v}_{,x} \\
\varepsilon_{zx} &= u_{z,x} = \psi_{\text{plane}\,z}\,\underline{v}_{,x}.
\end{aligned}
\tag{4.27}
$$

$\underline{v}$ represents the participation factor as introduced in equation (1.1) on page 6.

4.2.3.2 Virtual work and weak form

The weak form of the problem can be found by applying virtual work

$$
\delta W_i = \int\limits_{(A)} \boldsymbol{\delta\gamma} \cdot \boldsymbol{\tau}\ dA \qquad \text{with} \qquad \boldsymbol{\delta\gamma} = \begin{bmatrix} \delta\omega_{,y} \\ \delta\omega_{,z} \end{bmatrix}. \qquad\qquad \text{(see equation 4.8)}
$$

Introducing equation (4.25) leads to

$$
\delta W = -\int\limits_{(A)} [\delta\gamma] \cdot [D_\omega] \begin{bmatrix} \omega_{,y} + u_{y,x} \\ \omega_{,z} + u_{z,x} \end{bmatrix}\ dA.
\tag{4.28}
$$

which can be rearranged to

$$
\delta W = -\int\limits_{(A)} \underbrace{[\delta\gamma] \cdot [D_\omega] \cdot \begin{bmatrix} \omega_{,y} \\ \omega_{,z} \end{bmatrix}}_{\delta W \text{ from } \omega} + \underbrace{[\delta\gamma] \cdot [D_\omega] \cdot \begin{bmatrix} u_{y,x} \\ u_{z,x} \end{bmatrix}}_{\delta W \text{ from } \boldsymbol{\psi}_{\text{plane}}\,\underline{v}_{,x}} \overset{!}{=} 0.
\tag{4.29}
$$

The first part represents the virtual work performed by warp deflections and analogously to equation (4.23) it turns out to be the very same stiffness term of the shear PDE. Consequently the second term represents the load. Equation (4.29) can be written in FEM notation

$$
\int\limits_{(A)} [\delta\omega]^T \cdot [B]^T \cdot [D_\omega] \cdot [B] \cdot [\omega]\ dA = -\int\limits_{(A)} [\delta\omega]^T \cdot [B]^T \cdot [D_\omega] \cdot \begin{bmatrix} u_{y,x} \\ u_{z,x} \end{bmatrix} \cdot [N]\ dA. \tag{4.30}
$$

Since the aim of this procedure is to find unit deflection shapes it is not necessary to care about the actual size of $\underline{v}_{,x}$. It can be replaced by 1.0 when equations (4.27) are introduced.

1.

Distortion shape ("input")

2.

Derived warp shape

3.

Distortion shape ("input")

4.
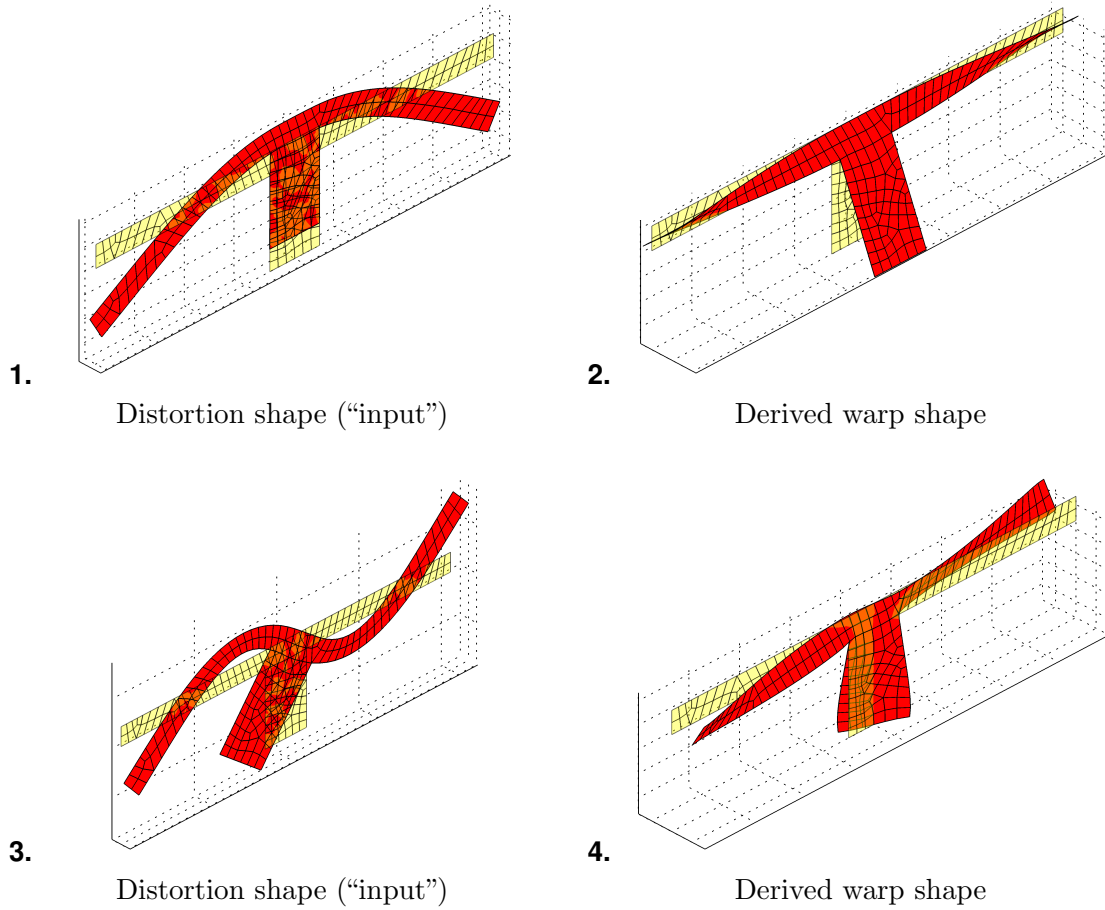
Derived warp shape

Figure 4.10: In-plane shapes (left) and corresponding derived warp shapes (right).
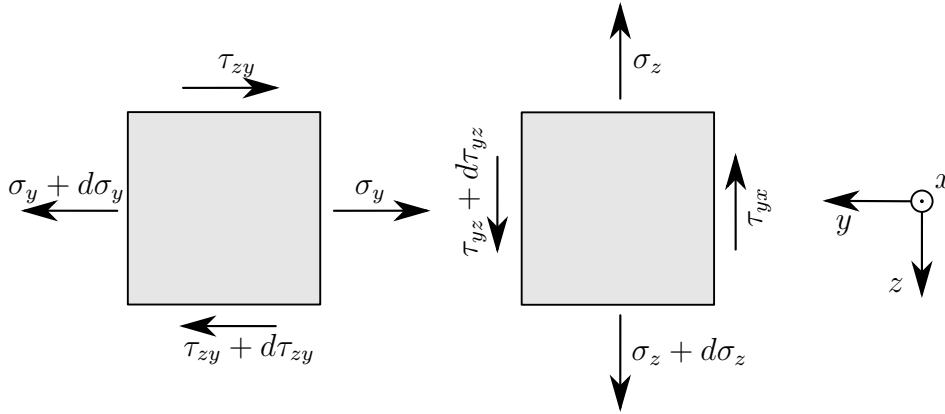
Figure 4.11: Infinitesimal element with occurring stresses in the y and the z-direction.

4.3 Deriving Further Shapes from Existing Shapes Using the PDE of a Membrane Plate

The previous section showed how to compute unit deflection shapes from other shapes using the PDE of shear warping. The obtained shapes are all warp shapes. In the present section, the goal is to compute in-plane unit deflection shapes in a similar way by using previously calculated shapes to derive a load function for a PDE, namely the PDE of a plate in membrane action (membrane plate).

Strong Formulation

The strong formulation is based on equilibrium equations

$$
\begin{aligned}
\sigma_{y,y} + \tau_{zy,z} &\overset{!}{=} 0 \\
\sigma_{z,z} + \tau_{zy,y} &\overset{!}{=} 0.
\end{aligned}
\tag{4.31}
$$

The occurring stresses for each direction are visualised in figure 4.11.

At the free edges the following boundary conditions apply

$$
\begin{aligned}
\sigma_y n_y + \tau_{zy} n_z &= 0 \\
\sigma_z n_z + \tau_{zy} n_y &= 0.
\end{aligned}
\tag{4.32}
$$

Weak Formulation

The weak equilibrium can be stated on the basis of the principle of virtual work

$$\int\limits_{(A)} -\boldsymbol{\delta\varepsilon} \cdot [D] \cdot \boldsymbol{\varepsilon}_{\text{tot}} + \boldsymbol{\delta u} \cdot \mathbf{p} \, dA \overset{!}{=} 0. \tag{4.33}$$

The vector $\boldsymbol{\varepsilon}_{\text{tot}}$ contains strains both from the unknown displacement field $\boldsymbol{\varepsilon}$ and from "prescribed strains" $\overset{\circ}{\boldsymbol{\varepsilon}}$ which might either come from e.g. a temperature load or a prescribed deflection shape.

$$\boldsymbol{\varepsilon}_{\text{tot}} = \boldsymbol{\varepsilon} + \overset{\circ}{\boldsymbol{\varepsilon}} . \tag{4.34}$$

The material matrix $[D]$ is here written in the general form. It has to be noted that the vector $\boldsymbol{\delta\varepsilon}$ here only contains the components $\delta\varepsilon_y, \delta\varepsilon_z$ and $\delta\gamma_{yz}$ unequal to zero. If plane strain is assumed this holds analogously for $\boldsymbol{\varepsilon}$. It then contains only components $\varepsilon_y, \varepsilon_z$ and γ_{yz} unequal to zero. For plane stress, the material matrix can be transformed such that the strains adept and stresses in the x-direction vanish (see chapter 2.3.2).

However, the prescribed stresses $\overset{\circ}{\boldsymbol{\varepsilon}}$ may contain arbitrary components

$$\overset{\circ}{\boldsymbol{\varepsilon}} = \begin{bmatrix} \overset{\circ}{\varepsilon}_x & \overset{\circ}{\varepsilon}_y & \overset{\circ}{\varepsilon}_z & \overset{\circ}{\gamma}_{xy} & \overset{\circ}{\gamma}_{xz} & \overset{\circ}{\gamma}_{yz} \end{bmatrix}^T . \tag{4.35}$$

Equation (4.33) can be rewritten in terms of finite element formulation and the part containig known forces or prescribed stresses is interpreted as a load matrix.

$$\int\limits_{(A)} \left(-[\delta u]^T [B]^T [D] [B] [u] - [\delta u]^T [B]^T [D] [N] \begin{bmatrix} \overset{\circ}{\varepsilon} \end{bmatrix} + [\delta u]^T [p] \right) \, dA \overset{!}{=} 0 \tag{4.36}$$

with the following matrices

$$[\delta u] = \begin{bmatrix} \delta u_{y1} & \delta u_{z1} & \delta u_{y2} & \delta u_{z3} & \dots \end{bmatrix}^T \qquad \text{(arbitrary) discrete virtual deflections}$$

$$[u] = \begin{bmatrix} u_{y1} & u_{z1} & u_{y2} & u_{z2} & \dots \end{bmatrix}^T \qquad \text{(unknown) discrete deflections}$$

$$[p] = \begin{bmatrix} p_{y1} & p_{z1} & p_{y2} & p_{z2} & \dots \end{bmatrix}^T \qquad \text{(nodal) force vector}$$

$$[N] = \begin{bmatrix} N_1 & N_2 & N_3 & N_4 & \dots \end{bmatrix} \qquad \text{shape functions}$$

$$[B] = \begin{bmatrix} N_{1,y} & N_{1,y} & N_{2,y} & N_{2,y} & \dots \\ N_{1,z} & N_{1,z} & N_{2,z} & N_{2,z} & \dots \end{bmatrix} \qquad \text{derived shape functions.}$$

The second and the third part in equation (4.36) represent the right hand side and form the nodal load vector.

In contrast to section 4.1.1 where eigenmodes of the section were calculated it is now necessary to introduce supports to make the system solvable. This can be done in two ways: either support every node with a very soft spring in each direction or introduce a statically determined support: lock two deflections at a node and one at another node such the direction of the latter deflection does not intersect with the first node.

Depending on how the support conditions are set up this may lead to implausible shapes because rigid body deflections can be contained to a considerable extent. This is removed later by the orthogonalisation (see chapter 5.2.1).

4.3.1 Unit deflection shapes for Transverse Strain

The underlying three dimensional material law with a *Poisson* ratio $\nu \neq 0$ leads to the fact that longitudinal stresses lead to lateral stresses if the cross section is not enabled to deform. Actually all previously presented deformation shapes only very poorly cope with that and thus the stresses are not in equilibrium at the edges (see figure 4.12a). Consequently, deflection shapes are needed which enable for the lateral distortion caused by strains emerging from the *Poisson* ratio.

The derivation of these shapes starts with prescribed strains in the x-direction $\overset{\circ}{\varepsilon}_x$ as the only
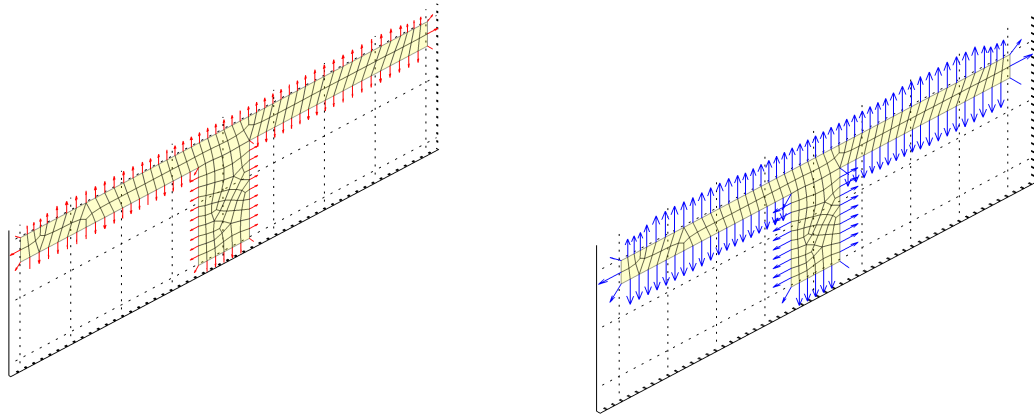
(a) Error force[2] for a structure under normal force with a material with $\nu \neq 0$ and no *Poisson* shapes enabled.

(b) Nodal load vector for uniform compression in the x-direction (right hand side of equation (4.38)).

Figure 4.12: Comparison of error force[2] and nodal load vector of a system under uniform compression.

load. Thus, equation (4.33) can be modified as follows

$$\int\limits_{(A)} \boldsymbol{\delta \varepsilon} \cdot [D] \cdot \boldsymbol{\varepsilon} \; dA = - \int\limits_{(A)} \boldsymbol{\delta \varepsilon} \cdot [D] \cdot \overset{\circ}{\boldsymbol{\varepsilon}} \; dA. \tag{4.37}$$

The corresponding Finite Element formulation reads

$$\int\limits_{(A)} [\delta u]^T [B]^T [D] [B] [u] \; dA = - \int\limits_{(A)} [\delta u]^T [B]^T [D] [N] \, [\overset{\circ}{\varepsilon}] \; dA. \tag{4.38}$$

with

$$[\overset{\circ}{\varepsilon}] = \begin{bmatrix} \overset{\circ}{\varepsilon}_x & 0 & 0 & 0 & 0 & 0 \end{bmatrix}^T. \tag{4.39}$$

$\overset{\circ}{\varepsilon}_x$ is obtained from a previously computed out of plane deflection shape $\boldsymbol{\psi}_{\text{warp}}(y,z)$ by

$$\overset{\circ}{\varepsilon}_x (y,z) = u_{x,x}(y,z) = \sum_{i=1}^{n_{\text{modes}}} \left[\boldsymbol{\psi}_{\text{warp}i}(y,z) \cdot \underline{v}_{i,x}(x) \right]. \tag{4.40}$$

The separation of variables is again made use of. One can see that $\overset{\circ}{\varepsilon}_x (y,z)$ is affine to $\overset{\circ}{u}_x (y,z)$ which is the longitudinal component of a previously computed warp shape $\boldsymbol{\psi}_{\text{warp}}(y,z)$. Thus,

---

[2]For the derivation of the error forces printed here, refer to section 5.6.

$$\overset{\circ}{\varepsilon}_x\,(y,z) \sim \boldsymbol{\psi}_{\mathrm{warp}}(y,z). \tag{4.41}$$

Since the purpose is to compute unit deflection shapes, the absolute amplitude of $\overset{\circ}{\varepsilon}_x\,(y,z)$ is not of interest and one can set $\overset{\circ}{\varepsilon}_x\,(y,z) = \boldsymbol{\psi}_{\mathrm{warp}}(y,z)$.

1.	**2.**
Warp shape ("input")	Derived distortion shape
1.	**4.**
Warp shape ("input")	Derived distortion shape
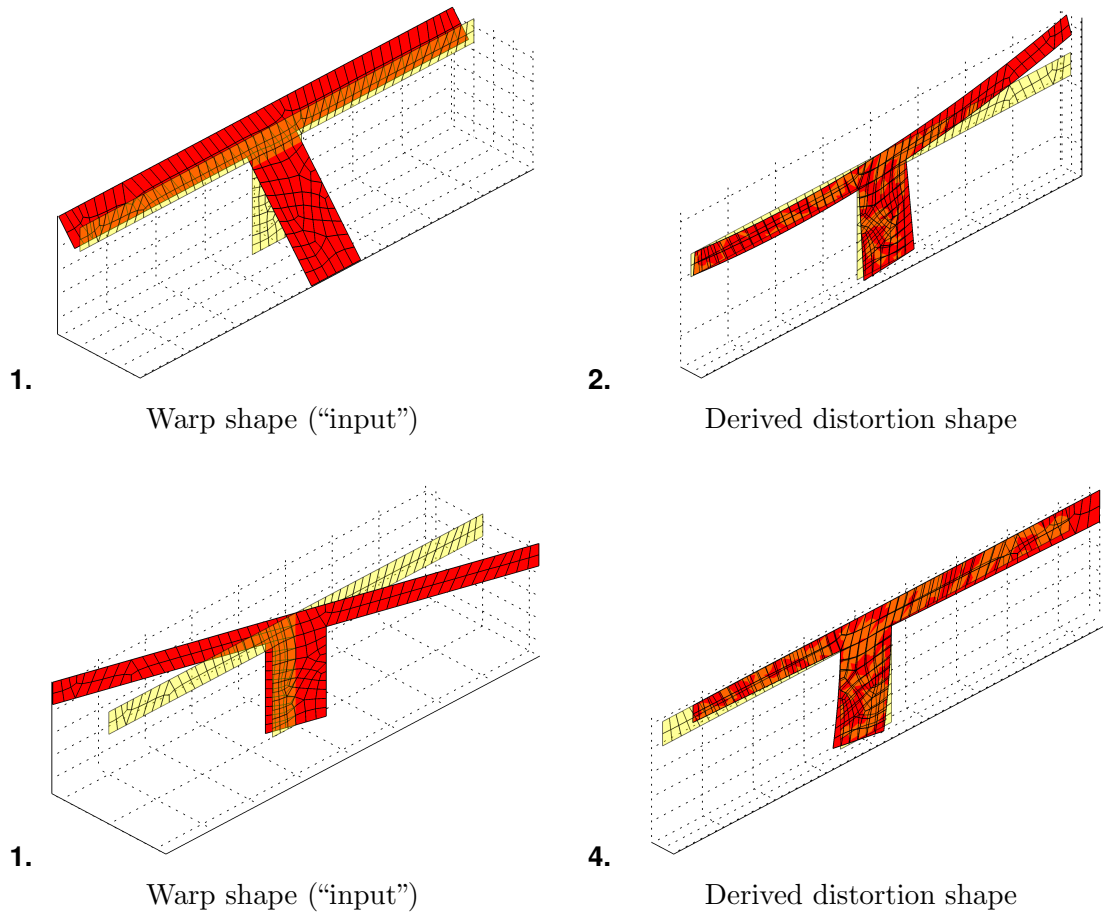
Figure 4.13: Derived *Poisson* shapes (right) from warp shapes (left).

4.3.2 Derived Distortion Shapes from Warp Shapes

Analogously to section 4.2.3 where warp shapes were calculated from distortion shapes the inverse procedure to calculate distortion shapes from warp shapes is possible as well [Zeller 1979, 1982] (see also chapter 3.2.4 and figure 3.5 on page 31). The PDE (4.31) is extended

(a) Warp shape from force in z-direction ("input")

(b) Derived in-plane loading
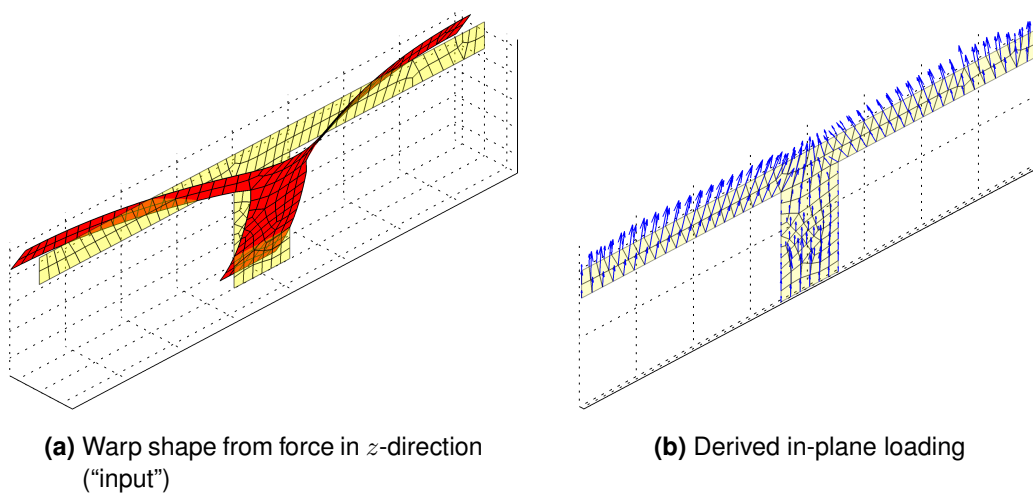
Figure 4.14: Input for the calculation of derived distortion shapes.

by a load term $\left[\overset{\circ}{\tau}\right]_{,x}$

$$
\begin{aligned}
\sigma_{y,y} + \tau_{zy,z} + \overset{\circ}{\tau}_{xy,x} &\overset{!}{=} 0 \\
\sigma_{z,z} + \tau_{zy,y} + \overset{\circ}{\tau}_{xz,x} &\overset{!}{=} 0.
\end{aligned}
\tag{4.42}
$$

The load terms $\left[\overset{\circ}{\tau}\right]_{,x}$ are computed from a previously determined warp shape and the material law. The components $\left[\overset{\circ}{\gamma}\right]$ occurring in a warp shape $\boldsymbol{\psi}_{\text{warp}}(y,z)$ can be computed as

$$
\begin{aligned}
\overset{\circ}{\gamma}_{xy} &= \psi_{\text{warp } x,y} \\
\overset{\circ}{\gamma}_{xz} &= \psi_{\text{warp } x,z}.
\end{aligned}
\tag{4.43}
$$

These strains can be used to form a prescribed strain vector $\left[\overset{\circ}{\varepsilon}\right]$ which can be introduced to equation (4.36)

$$
\left[\overset{\circ}{\varepsilon}\right] = \begin{bmatrix} 0 & 0 & 0 & \overset{\circ}{\gamma}_{xy} & \overset{\circ}{\gamma}_{xz} & 0 \end{bmatrix}^{T}.
\tag{4.44}
$$

Figure 4.14b shows the nodal forces calculated from a sample warp shape in figure 4.14a.

As it can be seen in figure 4.14b these forces do not necessarily form an equilibrium group. In [Zeller 1979] they are in equilibrium with the part of the load carried by the prior warping problem. The approach presented here does not allow for this type of information (amount

(a) Distortion shape

(b) Distortion shape after orthogonalisation (see section 5.2)
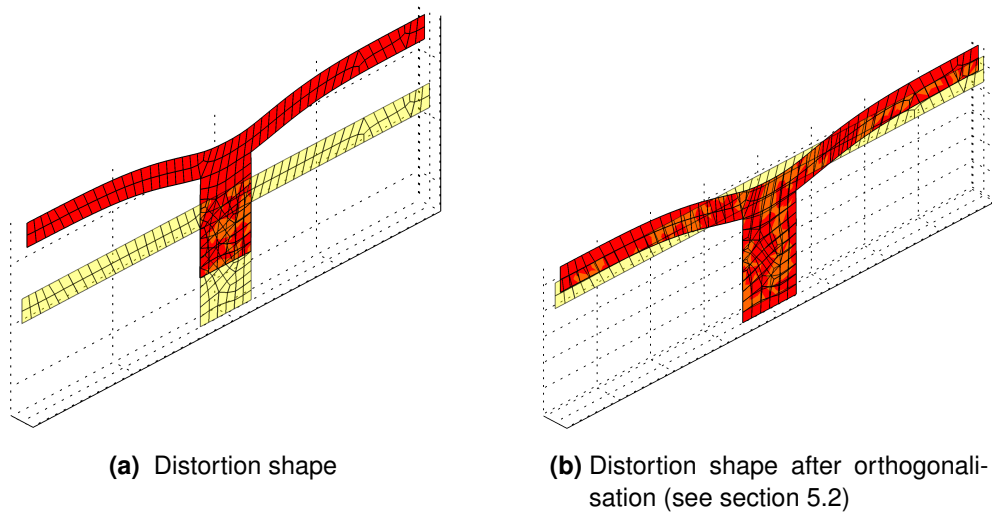
Figure 4.15: Distortion shape derived from the warp shape in 4.14a.

and location of load carried by another shape) in this stage of the process (preprocessing). Therefore, another solution has to be found to bring the forces to equilibrium.

The first possibility would be to introduce rigid supports as in the previous section 4.3.1. Their location has to be chosen arbitrarily and has a big influence on the out-coming shape. Furthermore, this approach in neither way refers to the actual behaviour of the structure.

The chosen solution is to apply a constant elastic spring bed to the plate. Thereby, the ratio of the stiffnesses of the plate and springs influences the outcoming deformation shapes. The best approach seems to be to choose a very soft springbed. Possibly occurring large rigid body displacements will be eliminated later when the set of unit deflection shapes is orthogonalised (see section 5.2).

Figure 4.15 shows the distortion corresponding to the warp shape and the therefrom derived load from figure 4.14 before (4.15a) and after (4.15b) orthogonalisation.

4.4 Using Eigenmodes of an Infinite Waveguide Structure

4.4.1 Formulation of a Finite-Element Procedure in the Wave Number Domain

In this chapter, a Finite Element Formulation shall be derived for a problem domain which is infinitely extended in the x-direction. The procedure was published in [Hackenberg 2010] and [K. Müller 2007] with plane 2D constant strain triangle (CST) elements. [Finnveden 2004] performs similar steps to 1D line elements of high order.

Both in the x- and the time direction a *Fourier* transformation is applied to an arbitrary function f

$$f(t) \circ\!\!\!-\!\!\!-\!\!\!\bullet \hat{f}(\Omega) \tag{4.45}$$

$$f(x) \circ\!\!\!-\!\!\!-\!\!\!\bullet \hat{f}(k_x). \tag{4.46}$$

The transformation rules read as follows [Brigham 1987]:

$$\hat{f}(\Omega) = \int\limits_{-\infty}^{\infty} f(t)\, e^{-i\Omega t}\, dt \qquad \textit{Fourier integral} \tag{4.47}$$

$$f(t) = \frac{1}{2\pi} \int\limits_{-\infty}^{\infty} \hat{f}(\Omega)\, e^{i\Omega t}\, d\Omega \qquad \text{inversion formula} \tag{4.48}$$

And for the x-direction, the functions are transformed to the wave number domain k_x:

$$\hat{f}(k_x) = \int\limits_{-\infty}^{\infty} f(x)\, e^{-ik_x x}\, dx \qquad \textit{Fourier integral} \tag{4.49}$$

$$f(x) = \frac{1}{2\pi} \int\limits_{-\infty}^{\infty} \hat{f}(k_x)\, e^{ik_x x}\, dk_x \qquad \text{inversion formula} \tag{4.50}$$

The transformed domain yields an advantage concerning the nth derivatives $f^{(n)}$ in the

transformed direction. They turn out to be a simple multiplication [Bronstein et al. 2005]

$$f^{(n)}(t) \circ\!\!-\!\!\bullet (i\Omega)^n \cdot \hat{f}(\Omega) \tag{4.51}$$

$$f^{(n)}(x) \circ\!\!-\!\!\bullet (ik_x)^n \cdot \hat{f}(k_x). \tag{4.52}$$

This can be applied to the operator matrix $[G]$ which is used to compute strains $[\varepsilon]$ from deflections $[u]$

$$\begin{pmatrix} \varepsilon_x \\ \varepsilon_y \\ \varepsilon_z \\ \gamma_{xy} \\ \gamma_{xz} \\ \gamma_{yz} \end{pmatrix} = \begin{bmatrix} \frac{\partial}{\partial x} & 0 & 0 \\ 0 & \frac{\partial}{\partial y} & 0 \\ 0 & 0 & \frac{\partial}{\partial z} \\ \frac{\partial}{\partial y} & \frac{\partial}{\partial x} & 0 \\ \frac{\partial}{\partial z} & 0 & \frac{\partial}{\partial x} \\ 0 & \frac{\partial}{\partial z} & \frac{\partial}{\partial y} \end{bmatrix} \begin{pmatrix} u_x(x,y,z) \\ u_y(x,y,z) \\ u_z(x,y,z) \end{pmatrix} \qquad \text{(see equation 2.6)}$$

$$[\varepsilon] = [G] \cdot [u]$$

and yields the following form

$$\begin{pmatrix} \hat{\varepsilon}_x \\ \hat{\varepsilon}_y \\ \hat{\varepsilon}_z \\ \hat{\gamma}_{xy} \\ \hat{\gamma}_{xz} \\ \hat{\gamma}_{yz} \end{pmatrix} = \begin{bmatrix} ik_x & 0 & 0 \\ 0 & \frac{\partial}{\partial y} & 0 \\ 0 & 0 & \frac{\partial}{\partial z} \\ \frac{\partial}{\partial y} & ik_x & 0 \\ \frac{\partial}{\partial z} & 0 & ik_x \\ 0 & \frac{\partial}{\partial z} & \frac{\partial}{\partial y} \end{bmatrix} \begin{pmatrix} \hat{u}_x(k_x,y,z) \\ \hat{u}_y(k_x,y,z) \\ \hat{u}_z(k_x,y,z) \end{pmatrix} \tag{4.53}$$

$$[\hat{\varepsilon}] = \left[\hat{G}\right] \cdot [\hat{u}] \ .$$

4.4.1.1 Virtual Work of Stresses

Equation (4.53) together with the linear material law (see equation (2.9)) enables for the formulation of the inner virtual work

$$
\delta W_{\mathrm{i}} = -\int\limits_{(V)} \boldsymbol{\delta\varepsilon}(x,t) \cdot \boldsymbol{\sigma}(x,t)\, dV = -\int\limits_{(V)} [\delta\varepsilon]^T \cdot [D] \cdot [\varepsilon]\, dV
$$
$$
= -\int\limits_{(V)} [\delta u]^T \cdot [B]^T \cdot [D] \cdot [B] \cdot [u]\, dV. \tag{4.54}
$$

where $[B] = [N] \cdot [G]$ and $[N]$ is the matrix containing the finite element shape functions.

This statement can be reformulated as follows by *Parseval's*[3] theorem [K. Müller 2007]

$$
\int\limits_{-\infty}^{+\infty} \boldsymbol{\delta\varepsilon}(x) \cdot \boldsymbol{\sigma}(x)\, dx = \int\limits_{-\infty}^{+\infty} \boldsymbol{\delta\varepsilon}(x) \cdot \left[\frac{1}{2\pi} \int\limits_{-\infty}^{+\infty} \hat{\boldsymbol{\sigma}}(k_x) e^{ik_x x}\, dk_x \right] dx
$$
$$
= \frac{1}{2\pi} \int\limits_{-\infty}^{+\infty} \left[\int\limits_{-\infty}^{+\infty} \boldsymbol{\delta\varepsilon}(x) e^{ik_x x}\, dx \right] \cdot \hat{\boldsymbol{\sigma}}(k_x) dk_x
$$
$$
= \frac{1}{2\pi} \int\limits_{-\infty}^{+\infty} \left[\int\limits_{-\infty}^{+\infty} \boldsymbol{\delta\varepsilon}(x) e^{-i(-k_x)x}\, dx \right] \cdot \hat{\boldsymbol{\sigma}}(k_x) dk_x
$$
$$
= \frac{1}{2\pi} \int\limits_{-\infty}^{+\infty} \boldsymbol{\delta\hat{\varepsilon}}(-k_x)^T \cdot \hat{\boldsymbol{\sigma}}(k_x) dk_x = \frac{1}{2\pi} \int\limits_{-\infty}^{+\infty} \boldsymbol{\delta\hat{\varepsilon}}(k_x)^T \cdot \hat{\boldsymbol{\sigma}}(-k_x) dk_x. \tag{4.55}
$$

Where $\left[\hat{B}\right] = \left[\hat{G}\right] \cdot \left[\hat{N}\right]$ and $\left[\hat{N}\right]$ is the matrix containing the finite element shape functions which depend on the lateral coordinates y and z.

With the help of equation (4.55), the expressions from equation (4.54) can now be transformed into the k_x domain without the need for a convolution

$$
\delta W_i = -\frac{1}{2\pi} \int\limits_{(k_x)} \int\limits_{(z)} \int\limits_{(y)} [\delta\hat{u}(-k_x)]^T \cdot \left[\hat{B}(-k_x,y,z)\right]^T \cdot [D] \cdot \left[\hat{B}(k_x,y,z)\right] \cdot [\hat{u}(k_x)]\, dy\, dz\, dk_x. \tag{4.56}
$$

---

[3]Marc-Antoine Parseval (∗1755, †1836)

4.4.1.2 Virtual Work of Inertia Forces

In the original (x, y, z)-domain, the virtual work of the inertia forces reads

$$\delta W_T = - \int\limits_{(V)} \boldsymbol{\delta u}(x,t) \cdot \rho \cdot \ddot{\mathbf{u}}(x,t) \, dV = - \int\limits_{(V)} [\delta u]^T \cdot [N]^T \cdot \rho \cdot [N] \cdot [\ddot{u}] \, dV. \tag{4.57}$$

It can be transformed to the wave number/frequency domain by applying equation (4.55)

$$\delta W_T = \frac{1}{2\pi} \int\limits_{(k_x)} \int\limits_{(z)} \int\limits_{(y)} [\delta\hat{u}(-k_x)]^T \cdot [N]^T \rho \, [N] \cdot \Omega^2 \, [\hat{u}(k_x)] \, dy \, dz \, dk_x \tag{4.58}$$

4.4.1.3 Virtual Work of the External Forces

In the original domain the virtual work of the external forces reads

$$\delta W_e = \int\limits_{(V)} \boldsymbol{\delta u}(x,t) \cdot \mathbf{p}(x,t) \, dV. \tag{4.59}$$

This can just as before be transformed into the wave number/frequency domain by applying equation (4.55)

$$\delta W_e = \frac{1}{2\pi} \int\limits_{(k_x)} \int\limits_{(z)} \int\limits_{(y)} [\delta\hat{u}(-k_x)]^T \cdot [p(k_x,\Omega)] \, dy \, dz \, dk_x. \tag{4.60}$$

4.4.1.4 System Matrices and Solution

The solution is obtained for setting the total virtual work equal to zero. The virtual displacements δu can be chosen arbitrarily but at least one of them has to be unequal to zero. The most useful procedure is to stepwise choose one of them equal to one and all others equal to zero. By that the symmetric system matrices and the load vector are obtained line by line.

$$\delta W = \delta W_i + \delta W_T + \delta W_e \overset{!}{=} 0 \tag{4.61}$$

It can be rearranged such that

$$\left[\hat{K}(k_x) \right] [\hat{u}] - \Omega^2 \left[\hat{M} \right] [\hat{u}] = [\hat{p}(k_x,\Omega)] \,. \tag{4.62}$$

This system of equations can be solved for the nodal deflections $\hat{u}$ (in all three directions of space) presuming a discrete tuple of (k_x,Ω).

The obtained deflections $\hat{u}$ are then used to compute the strains $\hat{\varepsilon}$ and stresses $\hat{\sigma}$ by

$$[\hat{\varepsilon}] = \left[\hat{B}(k_x) \right] [\hat{u}] \tag{4.63}$$

$$[\hat{\sigma}] = [D] [\hat{\varepsilon}] \,. \tag{4.64}$$

Remark 1

As shown in appendix A.3, an arbitrary sinusoidal function in the real domain leads to both positive and negative wave numbers/frequencies simultaneously. The usual approach is to skip the negative tuple since the function values are simply conjugate to those from the positive tuple and thus can be determined directly. This saves computational effort and simplifies the understanding of the problem. As shown in appendix A.3 this procedure is applicable for cases where a complex stiffness term is used to cover frequency constant viscous damping effects as long as the positive and negative frequency are treated equally. This is for example not the case for moving loads (which are approximated by a frequency shift) and negative frequencies have to be treated differently than positive and thus separately.

Remark 2

All three terms in equation (4.62) contain a $\frac{1}{2\pi}$ which can be skipped consequently.

Secondly, for example the *Fourier* transformed representation of a cos function is

$$A \cos(\Omega_0 t) \circ\!\!-\!\!\!-\!\!\bullet A\pi \big(\delta(\Omega - \Omega_0) + \delta(\Omega + \Omega_0) \big). \tag{4.65}$$

It has become common practice to "not think" about the π which occurs as a factor of the *Dirac*[4]-δ terms since they skip with the $\frac{1}{2\pi}$ of the inverse *Fourier* transformation (equations (4.48) and (4.50)). The actual quantity of interest, the amplitude A, is not affected.

---

[4]Paul Dirac (*1902, †1984)

4.4.1.5 Transformation Back to the Real Domain

The procedure of the latter section provides a solution set $\hat{u}$, $\hat{\varepsilon}$ and $\hat{\sigma}$ for each wave number and angular frequency. They can be transformed back to the time/x-domain by equations (4.48) and (4.50). Since linearised materials and deflections are presumed the results of various frequencies and wave numbers can be superposed to form the total solution.

4.4.1.6 Validation

The solution procedure presented in this section is validated in appendix A.4. The results show that the procedure is prone to shear locking when bilinear elements are used as done within the scope of this thesis. The *Wilson* extension as presented in section A.2 can resolve this issue. It is nevertheless not applied since the element matrix has to be inverted partially. By that the element matrix is not suited for the procedure of formulating an eigenvalue problem as illustrated in the following section.

4.4.2 Eigenvalue Problem for the Waveguide

4.4.2.1 Setup of the Problem

As $\left[\hat{B}(k_x)\right]$ in equation (4.64) contains terms with different polynomial degrees of k_x ($k_x{}^0 = 1$ and $k_x{}^1 = k_x$) it is obvious that $\left[\hat{K}(k_x)\right]$ contains terms with $k_x{}^0$, $k_x{}^1$ and $k_x{}^2$. On that basis equation (4.62) can be transformed into a homogeneous problem depending on both the wave number k_x and the angular frequency of excitation Ω:

$$\left[\hat{K}(k_x)\right]\left[\hat{\psi}\right] - \Omega^2 \left[\hat{M}\right]\left[\hat{\psi}\right] = [0] \tag{4.66}$$

$$\left(\left[\hat{K}_0\right] - \Omega^2 \left[\hat{M}\right] + k_x \left[\hat{K}_1\right] + k_x{}^2 \left[\hat{K}_2\right]\right)\left[\hat{\psi}\right] = [0] \tag{4.67}$$

with

$$\left[\hat{K}(k_x)\right] = \left[\hat{K}_0\right] + k_x \left[\hat{K}_1\right] + k_x{}^2 \left[\hat{K}_2\right]. \tag{4.68}$$

Equation (4.66) can be solved by fixing k_x and solving a generalised eigenvalue problem (GEP) for Ω. Secondly, it is possible to treat it in the configuration of equation (4.67) by

fixing the value for Ω and solve a polynomial eigenvalue problem (PEP) of order 2 which is also called a quadratic eigenvalue problem (QEP) depending on k_x. The first approach is numerically much less expensive and more stable but in some cases (like here) not suitable. The QEP in the second approach can be transformed GEP as explained in [Orrenius and Finnveden 1996, Appendix A]. This process is also called linearisation. [Tisseur and Meerbergen 2001] states that such linearised Polynomial Eigenvalue Problems can be numerically ill-conditioned which was not encountered during the investigations presented in this work.

4.4.2.2 Properties of the Problem

In the following section the properties of the involved matrices are listed since the characteristics of the solution can be determined or checked on that basis.

1. Real Material Properties

   For real valued material properties E and ν the following conditions apply for the matrices:

   - $\left[\hat{K}_0\right] - \Omega^2 \left[\hat{M}\right]$ is real and symmetric thus *Hermitian*[5], depending on Ω mostly non-singular but indefinite.

   - $\left[\hat{K}_1\right]$ is imaginary, skew symmetric and equal to 0 on the diagonal thus *Hermitian*. It is indefinite.

   - $\left[\hat{K}_2\right]$ is real, symmetric thus *Hermitian*. Additionally it is positive definite.

   - $\left[\hat{K}(k_x)\right] - \Omega^2 \left[\hat{M}\right]$ is real and symmetric thus *Hermitian* depending on Ω mostly non-singular.

   - All matrices are sparse.

   Given that $\left[\hat{K}_2\right]$ is non-singular $2n$ finite eigenvalues occur, none of the eigenvalues is infinite.

2. Complex Material Properties

   For complex valued material properties E and ν (considering viscous damping) the follwing conditions apply for the matrices:

---

[5]Charles Hermite ($*$1822, $\dagger$1901)

- $\left[\hat{K}_0\right] - \Omega^2 \left[\hat{M}\right]$ is complex, symmetric and, depending on Ω mostly non-singular but indefinite.

- $\left[\hat{K}_1\right]$ is complex, skew symmetric and equal to 0 on the diagonal.

- $\left[\hat{K}_2\right]$ is real, symmetric and positive definite.

- All matrices are sparse.

4.4.2.3 Solution

This special arrangement of the QEP is rarely discussed in the literature [Tisseur and Meerbergen 2001]. It has $2n$ eigenvalues where n is the size of the matrices. It can be solved either directly e.g. using the `xGGEV` algorithm from LAPACK [Anderson et al. 1999] which underlies the `polyeig` function in MATLAB and yields all the eigenvalues of the problem. Effective iterative approaches like [Benner et al. 2007] have to be checked for their applicability before they come to use. [Benner et al. 2007] requires real matrices. [Meerbergen 2001] gives an overview of applicable iterative methods. Applicable methods are e.g. the Quadratic Arnoldi Method [Meerbergen 2008] or the Second Order Arnoldi Method (SOAR) [Bai and Su 2005].

Alternatively, the problem can be solved iteratively using a linearisation like the first companion form

$$\left(\begin{bmatrix} [0] & [I] \\ -\left[\left[\hat{K}_0\right] - \Omega^2 \left[\hat{M}\right]\right] & \left[\hat{K}_1\right] \end{bmatrix} - k_x \begin{bmatrix} [I] & [0] \\ [0] & \left[\hat{K}_2\right] \end{bmatrix} \right) \begin{bmatrix} \left[\hat{\psi}\right] \\ \left[\hat{\psi}_{ks}\right] \end{bmatrix} = [0] . \tag{4.69}$$

It is obtained by substituting $\left[\hat{\psi}_{ks}\right] = k_x \left[\hat{\psi}\right]$ into equation (4.67)

$$\left(\left[\hat{K}_0\right] - \Omega^2 \left[\hat{M}\right] \right) [\hat{u}] + \left[\hat{K}_1\right] [\hat{u}_s] + k_x \left[\hat{K}_2\right] [\hat{u}_s] = [0] . \tag{4.70}$$

[Afolabi 1987] notes that the matrix $[I]$ can be replaced by any non-singular matrix. Further types of linearisation are possible [see e.g. Tisseur and Meerbergen 2001].

Equation (4.69) represents a complex generalised eigenvalue problem (GEP) and can be solved by the corresponding algorithms. In the scope of this thesis, the MATLAB function

`eigs` is used. It is capable of searching a specified number of eigenvectors/-values iteratively. One can specify a value in the vicinity of which the eigenvalue search starts. Since in a modal superposition the lowest wave numbers have to be included to describe the system behaviour correctly, this value is chosen as 0.

4.4.2.4 Results

The results show that for real material properties the eigenvalues are either pure real, pure imaginary or complex. Complex eigenvalues are appear to be dominated by the imaginary part. The eigenvalues occur to be symmetric to both the real and the imaginary axis in the complex plane. This means that the eigenvalues occur in pairs k_x^+/k_x^- where $k_x^+ = -k_x^-$ if they are either purely imaginary or real. Complex eigenvalues occur in quadruples $k_x^{++} = -k_x^{--} = \bar{k}_x^{+-} = -\bar{k}_x^{-+}$.

For complex material parameters, all occurring eigenvalues are complex. The size relation of real and imaginary part cannot be predicted. The eigenvalues occur either in pairs with $k_x^+ = -k_x^-$ or in quadruples $k_x^{++} = -k_x^{--} = \bar{k}_x^{+-} = -\bar{k}_x^{-+}$.

The eigenvectors $[\psi]$ are complex and occur in an arbitrary phase position. The vectors of an eigenvalue pair k_x^+/k_x^- are conjugate to each other

$$\left[\psi(k_x^+)\right] = \left[\bar{\psi}(k_x^-)\right]. \tag{4.71}$$

Still the phase position of both vectors is arbitrary.

All results discussed here are obtained for a positive angular frequency Ω^+. To obtain a complete solution basis for arbitrary load cases (including e.g. moving loads) the procedure has to be repeated for the corresponding negative angular frequency $\Omega^- = -\Omega^+$.

4.4.2.5 Mechanical Interpretation

The eigenvectors can be transformed back to the original domain by applying the inversion formulae (4.48) and (4.50)

$$\mathbf{u}(x,y,z) = \boldsymbol{\psi} e^{ik_x x} e^{i\Omega t}. \tag{4.72}$$

Real eigenvalues represent harmonic waves along x, the far field. Complex eigenvalues represent waves which decay or grow in the x-direction. Pure imaginary eigenvalues describe waves which follow a real e-function either with a positive exponent (decaying) or negative (growing) amplitude. The latter two represent the near field

- in the positive x-direction if decaying with positive x

- in the negative x-direction if decaying with positive x or growing with negative x respectively.

The general relations are as follows:

- If the real part of k_x is positive, the wave travels in the positive x-direction for a positive Ω and vice versa.

- If the imaginary part of k_x is positive, the amplitude of the wave decays in the positive x-direction and vice versa.

To illustrate the properties, some numerical examples will follow.

4.4.2.6 Numerical Example 1

This example treats a rectangular cross section with a height of 0.6 m and a width of 0.4 m. The material properties are chosen as follows:

$$E = 28300 \cdot 10^6 \, \tfrac{\text{N}}{\text{m}^2}$$
$$\nu = 0.2$$
$$\rho = 2500 \, \tfrac{\text{kg}}{\text{m}^3}$$

The frequency of excitation is chosen to be $f = 10$ Hz or $\Omega = 62.83 \, \tfrac{\text{rad}}{\text{s}}$.

The eigenvalues and eigenvectors are given in figures 4.16 and 4.17. For low frequencies the real eigenvalues occur for the waves of a classical beam: longitudinal compression, torsion bending in y- and z-direction. *Euler-Bernoulli* beam theory yields the following analytical
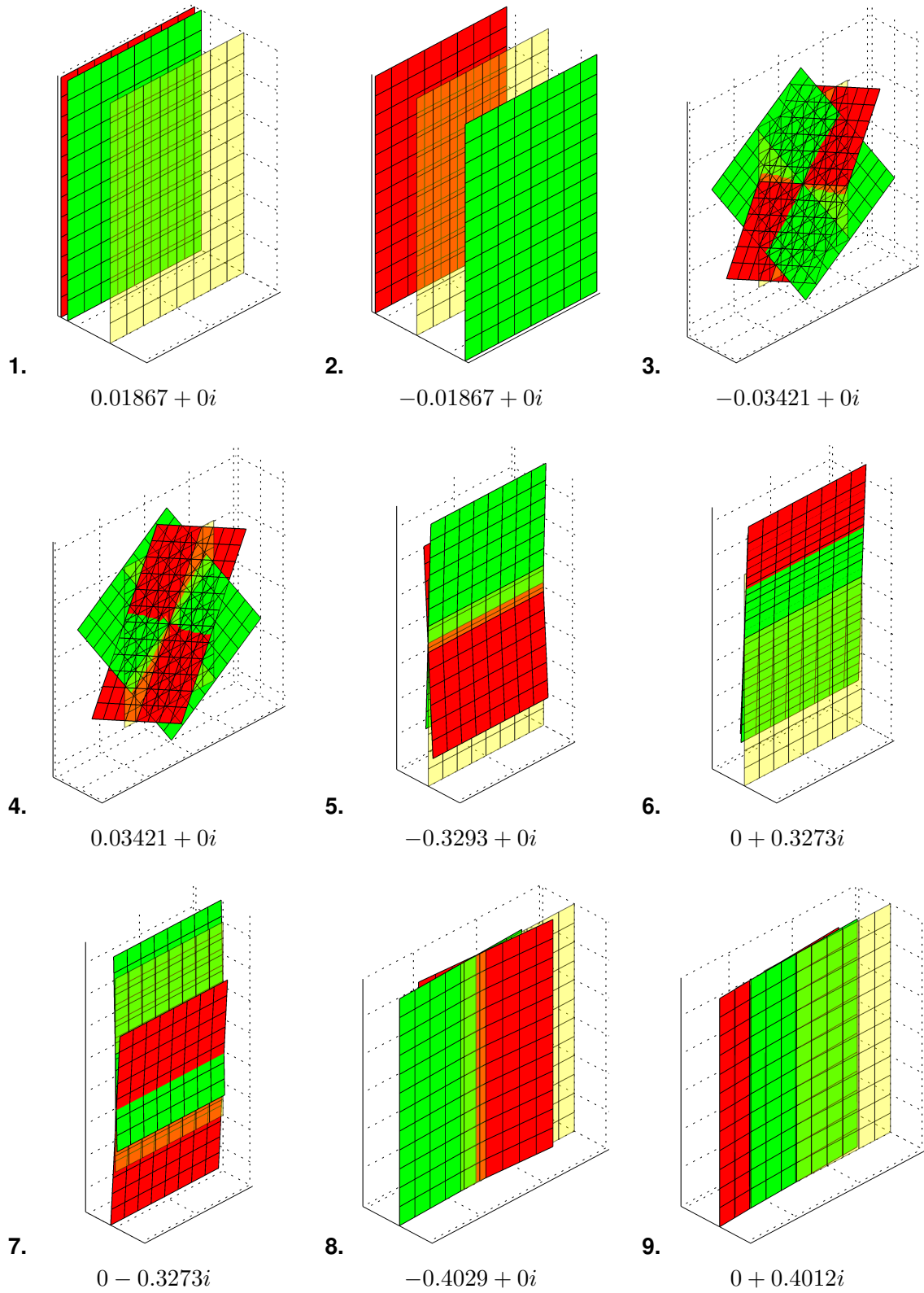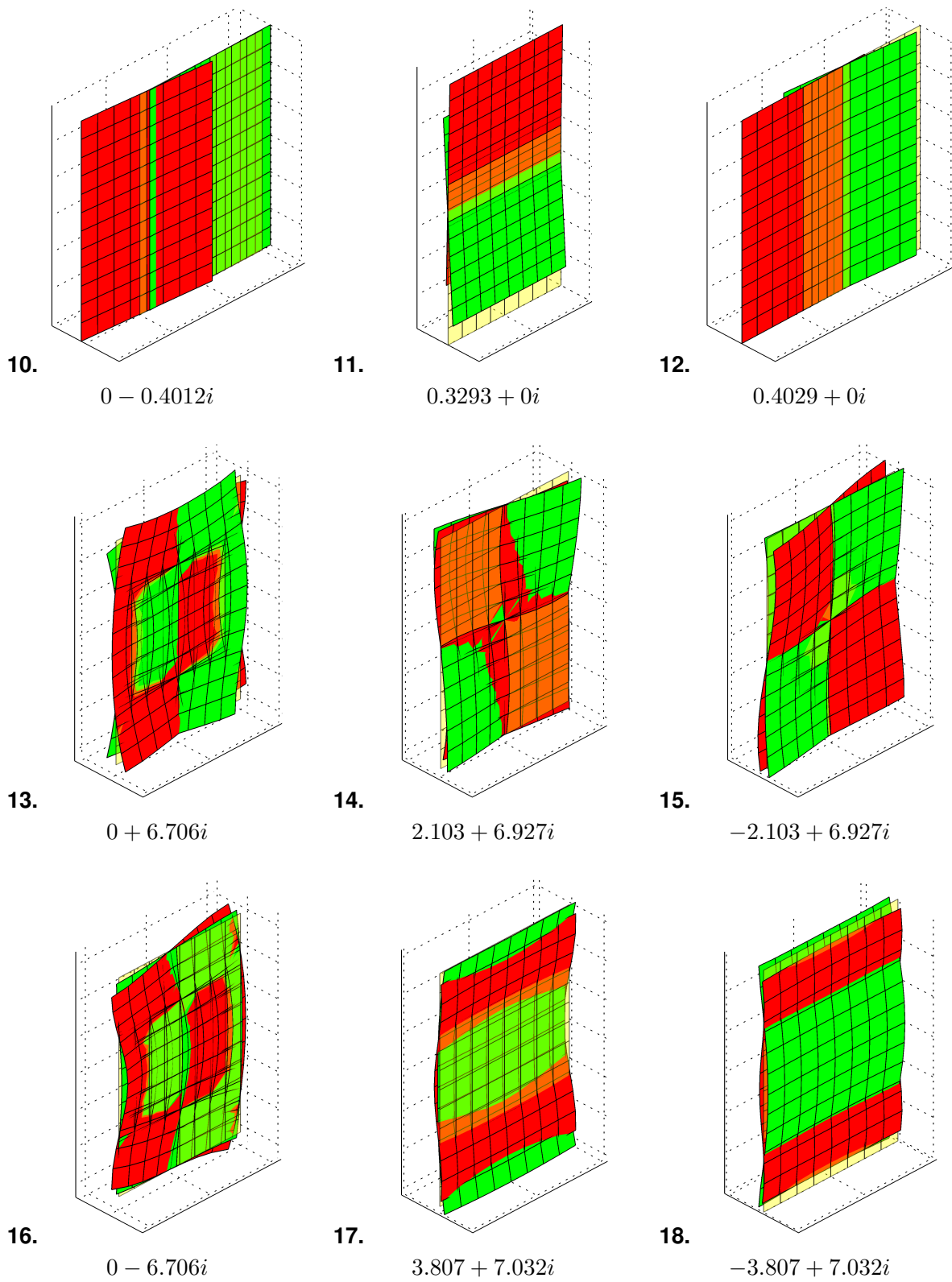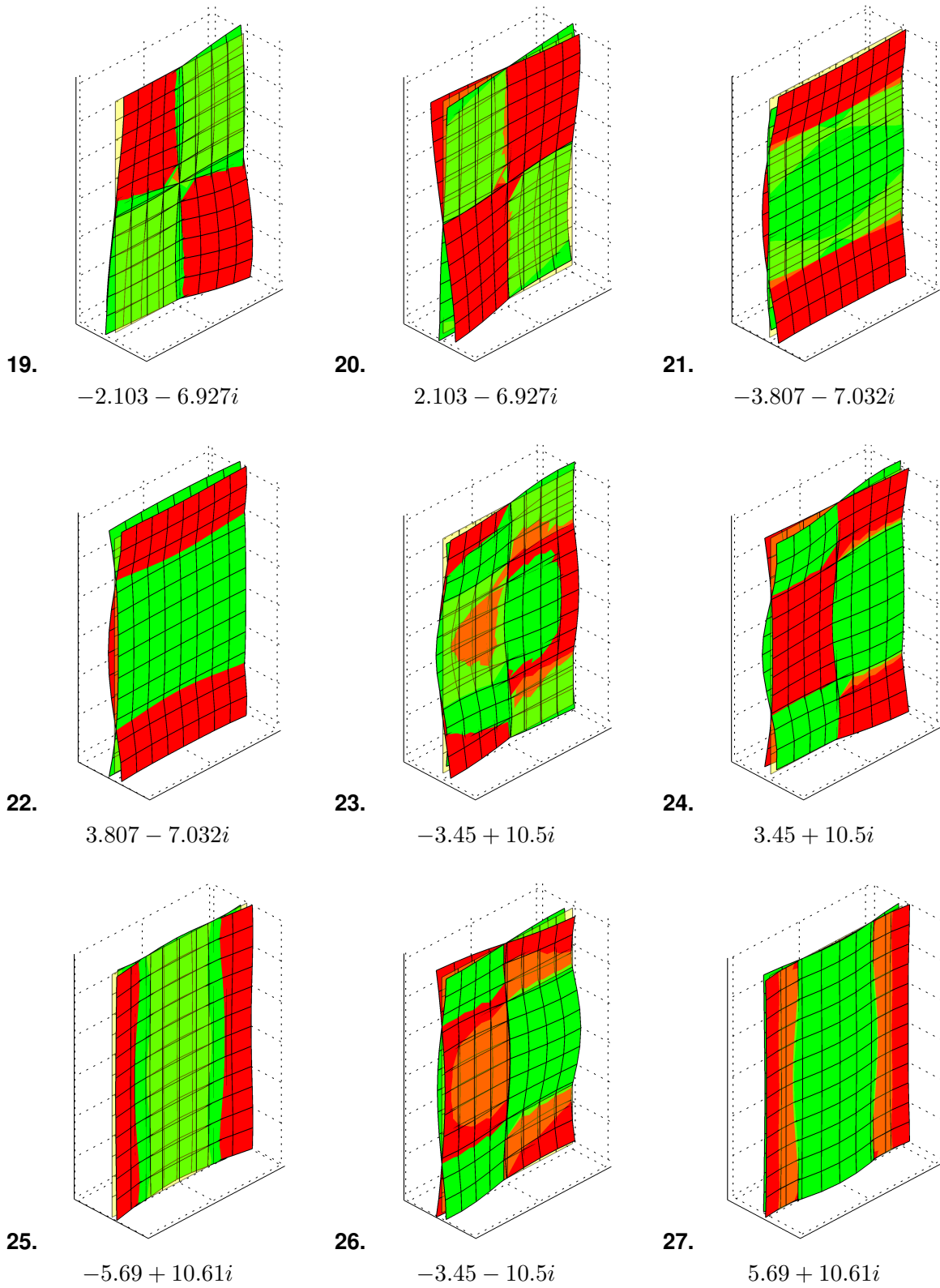
Figure 4.16: Eigenvectors and eigenvalues (k_x) 1 to 9 for a rectangular section at $f = 10$Hz.

10.

$0 - 0.4012i$

11.

$0.3293 + 0i$

12.

$0.4029 + 0i$

13.

$0 + 6.706i$

14.

$2.103 + 6.927i$

15.

$-2.103 + 6.927i$

16.

$0 - 6.706i$

17.

$3.807 + 7.032i$

18.

$-3.807 + 7.032i$

Figure 4.17: Eigenvectors and eigenvalues (k_x) 10 to 18 for a rectangular section at $f = 10$Hz.

19.
$-2.103 - 6.927i$

20.
$2.103 - 6.927i$

21.
$-3.807 - 7.032i$

22.
$3.807 - 7.032i$

23.
$-3.45 + 10.5i$

24.
$3.45 + 10.5i$

25.
$-5.69 + 10.61i$

26.
$-3.45 - 10.5i$

27.
$5.69 + 10.61i$

Figure 4.18: Eigenvectors and eigenvalues (k_x) 19 to 27 for a rectangular section at $f = 10$Hz.

solutions for the wave numbers of these processes depending on the frequency of excitation

Compression:
$$k_{xc} = \frac{\Omega}{c_c} = \Omega\sqrt{\frac{\rho}{E}} \tag{4.73}$$

Torsion:
$$k_{xt} = \frac{\Omega}{c_t} = \Omega\sqrt{\frac{\rho I_\vartheta}{GI_t}} \tag{4.74}$$

with $\quad I_t = 0.196 b^3 h$ [6] $\qquad$ and $\quad I_\vartheta = \dfrac{bh^3 + hb^3}{12}$

Bending:
$$k_{xb} = \frac{\Omega}{c_b(\Omega)} = \sqrt{\Omega}\sqrt[4]{\frac{A\rho}{EI}}. \tag{4.75}$$

Equations (4.73) through (4.75) yield the following numerical results for $\Omega = 62.83 \frac{\text{rad}}{\text{s}}$:

$$k_{xc} = 0.0187 \tfrac{\text{rad}}{\text{m}} \qquad\qquad\qquad k_{xt} = 0.0340 \tfrac{\text{rad}}{\text{m}}$$
$$k_{xby} = 0.3284 \tfrac{\text{rad}}{\text{m}} \qquad\qquad\qquad k_{xbz} = 0.4022 \tfrac{\text{rad}}{\text{m}}.$$

4.4.2.7 Numerical Example 2

This example treats the same setup as the latter. The difference is that the frequency is changed in terms of a frequency sweep. The results are compared against various available beam formulations including those from the latter section.

The graph in figure 4.19 shows that for lower frequencies all occurring eigenvalues fit well with the beam equations. *Euler-Bernoulli* beam theory quite quickly leaves its range of validity. Therefore, the curves for the *Timoshenko* beam theory are computed in addition starting from the following set of equations e.g. from [Petersen 1996]

$$\rho A \ddot{u}_z = \left(GA_{Sz}\left(u_{z,x} - \varphi_y\right)\right)_{,x}$$
$$\rho I \ddot{\varphi}_y = \left(EI_y \varphi_{y,x}\right)_{,x} + GA_{Sz}\left(u_{z,x} - \varphi_y\right). \tag{4.76}$$

Assuming constant sectional values and applying the *Fourier* transformations according to equations (4.47) and (4.49) yields

$$-\rho A \hat{u}_z \Omega^2 + GA_{Sz}\hat{u}_z k_x{}^2 + GA_{Sz}\hat{\varphi}_y i k_x = 0$$
$$-\rho I \hat{\varphi}_y \Omega^2 + EI_y \hat{\varphi}_y k_x{}^2 - GA_{Sz}\hat{u}_z i k_x + GA_{Sz}\hat{\varphi}_y = 0. \tag{4.77}$$

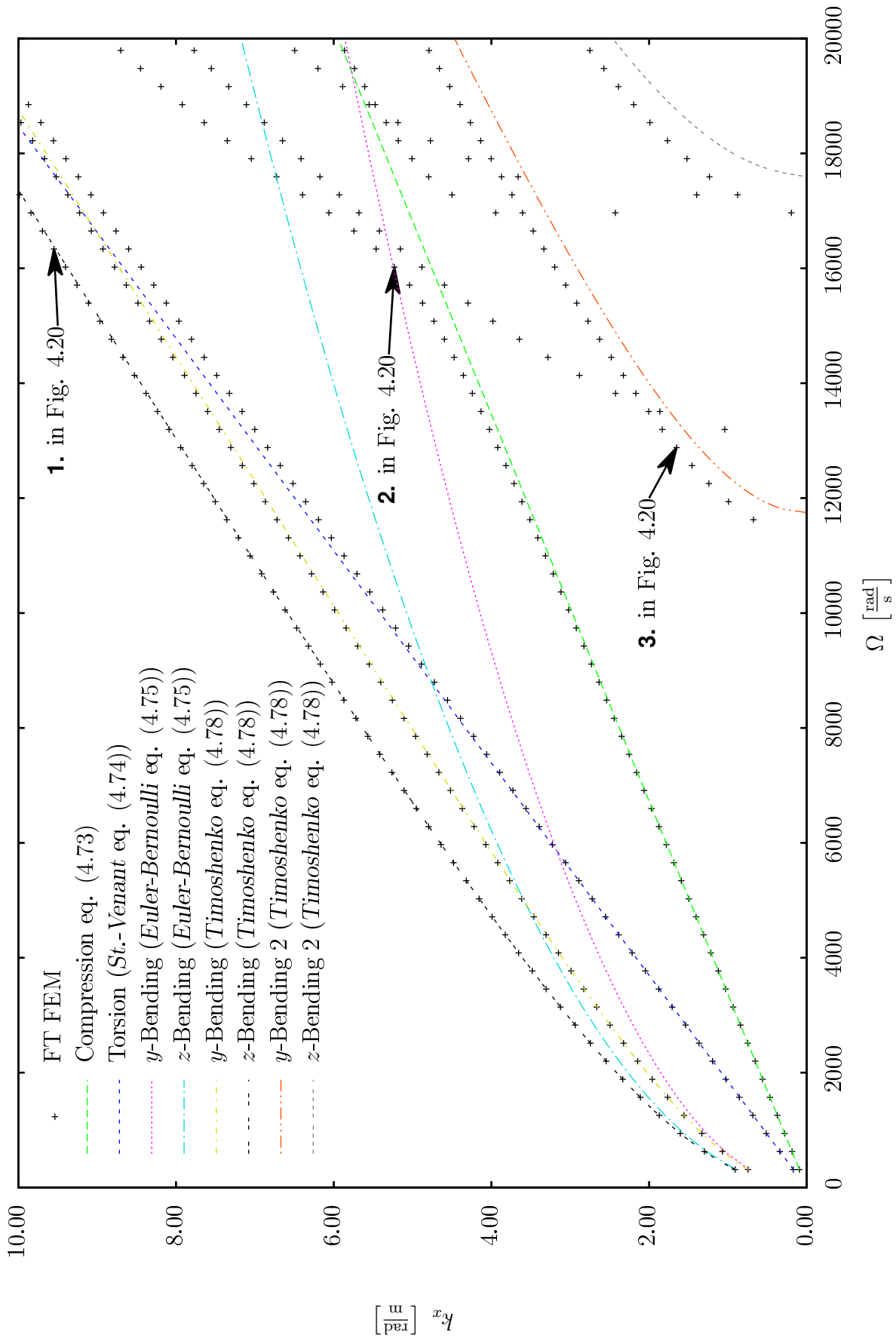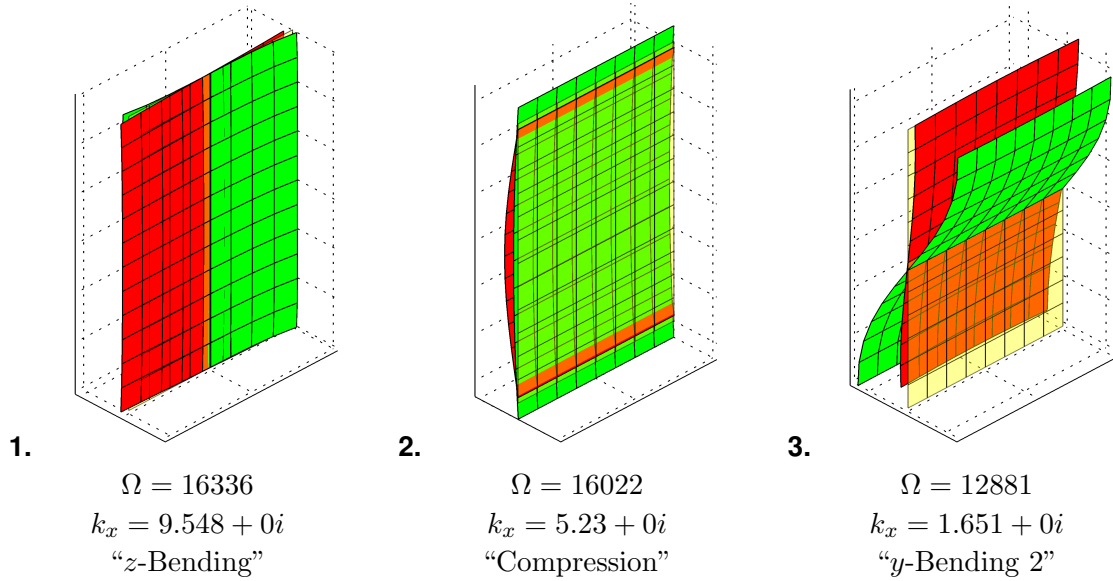[6]Value taken from [Schneider 2008], only valid for $h/b = 1.5$.

Figure 4.19: Different k_x eigenvalues for the rectangular cross-section together with results from different beam governing equations.

This system of equations in analogy to equation (4.67) can be interpreted as a QEP with respect to k_x

$$\left(\begin{bmatrix} -\rho A \Omega^2 & 0 \\ 0 & GA_{Sz} - \rho I\Omega \end{bmatrix} + ik_x \begin{bmatrix} 0 & GA_{Sz} \\ -GA_{Sz} & 0 \end{bmatrix} + k_x{}^2 \begin{bmatrix} GA_{Sz} & 0 \\ 0 & EI_y \end{bmatrix} \right) \begin{bmatrix} \hat{u}_z \\ \hat{\varphi}_y \end{bmatrix} = \begin{bmatrix} 0 \\ 0 \end{bmatrix}.$$

$$(4.78)$$

The solution sets $(k_x, \hat{u}_z, \hat{\varphi}_y)$ can be obtained e.g. by applying MATLAB's `polyeig` function. Four eigenvalues can be computed. As in section 4.4.2.3 the eigenvalues occur in pairs k_x^+/k_x^- and are potentially complex. Figure 4.19 only contains real eigenvalues. It can be seen that wave numbers from this theory fit far better with the results from the FT FEM than those from *Euler-Bernoulli*. This even holds in frequencies where the wave of compression already left its range of validity. Additionally, even some of the wave patterns which occur beyond $12000 \frac{\text{rad}}{\text{s}}$ are covered quite well by the second occurring eigenvalue ("*Timoshenko 2*").

1.

$\Omega = 16336$
$k_x = 9.548 + 0i$
"z-Bending"

2.

$\Omega = 16022$
$k_x = 5.23 + 0i$
"Compression"

3.

$\Omega = 12881$
$k_x = 1.651 + 0i$
"y-Bending 2"

Figure 4.20: Eigenvectors and eigenvalues (k_x) as indicated in figure 4.19.

In a medium, no mechanical wave is faster than the compression wave. Nevertheless, the fact that wave numbers occur which are smaller than the compression wave numbers is neither unrealistic nor wrong. The problem treated here is the steady state part of the solution. Wave numbers lower than the compression wave numbers do not represent a fast wave but a wave pattern with a very long wavelength.

4.4.2.8 Numerical Example 3

The third example shows that for structured sections the widely used beam theories do not keep their validity as long as in the previous example. The investigated section is a steel I-beam as illustrated in figure 4.22. The material properties are those of steel:

$$E = 210000 \cdot 10^6 \tfrac{\text{N}}{\text{m}^2}$$
$$\nu = 0.3$$
$$\rho = 7850 \tfrac{\text{kg}}{\text{m}^3}.$$

Figure 4.21 shows the results in an analogous way to figure 4.19. One can see that *de St.-Venant* torsion is a bad estimate of the torsional behaviour of this cross section. Therefore in addition the PDE of warping torsion is evaluated

$$GI_t \varphi_{x,xx} - EI_\omega \varphi_{x,xxxx} - \rho I_\vartheta \ddot{\varphi}_x + \rho I_\omega \ddot{\varphi}_{x,xx} = 0. \tag{4.79}$$

This equation can be transformed to the wave number/frequency domain analogously to equations (4.76) and wave numbers for each frequency of excitation. The results are plotted in figure 4.21. Note that the displayed frequency range is much smaller than in figure 4.19.

Additional terms which couple to bending equations (4.76) to the torsion equation (4.79) would be necessary if the shear and mass centre didn't coincide [see e.g. Friberg 1985]. The system can be refined further by considering the fact that the shear correction factors are not orthogonal.

While the bending waves about the y-axis are covered well by the *Timoshenko* equations this does not hold true for bending about the z-axis. **1.** in figure 4.23 shows why: the deformation of the cross section becomes so severe that the assumption of their absense is not valid. Figure 4.23 **3.** shows that from $\Omega = 2500\tfrac{\text{rad}}{\text{m}}$ also the torsion wave contains severe deformations of the cross section leading to deviations from the curve beloning to warping torsion in figure 4.21.
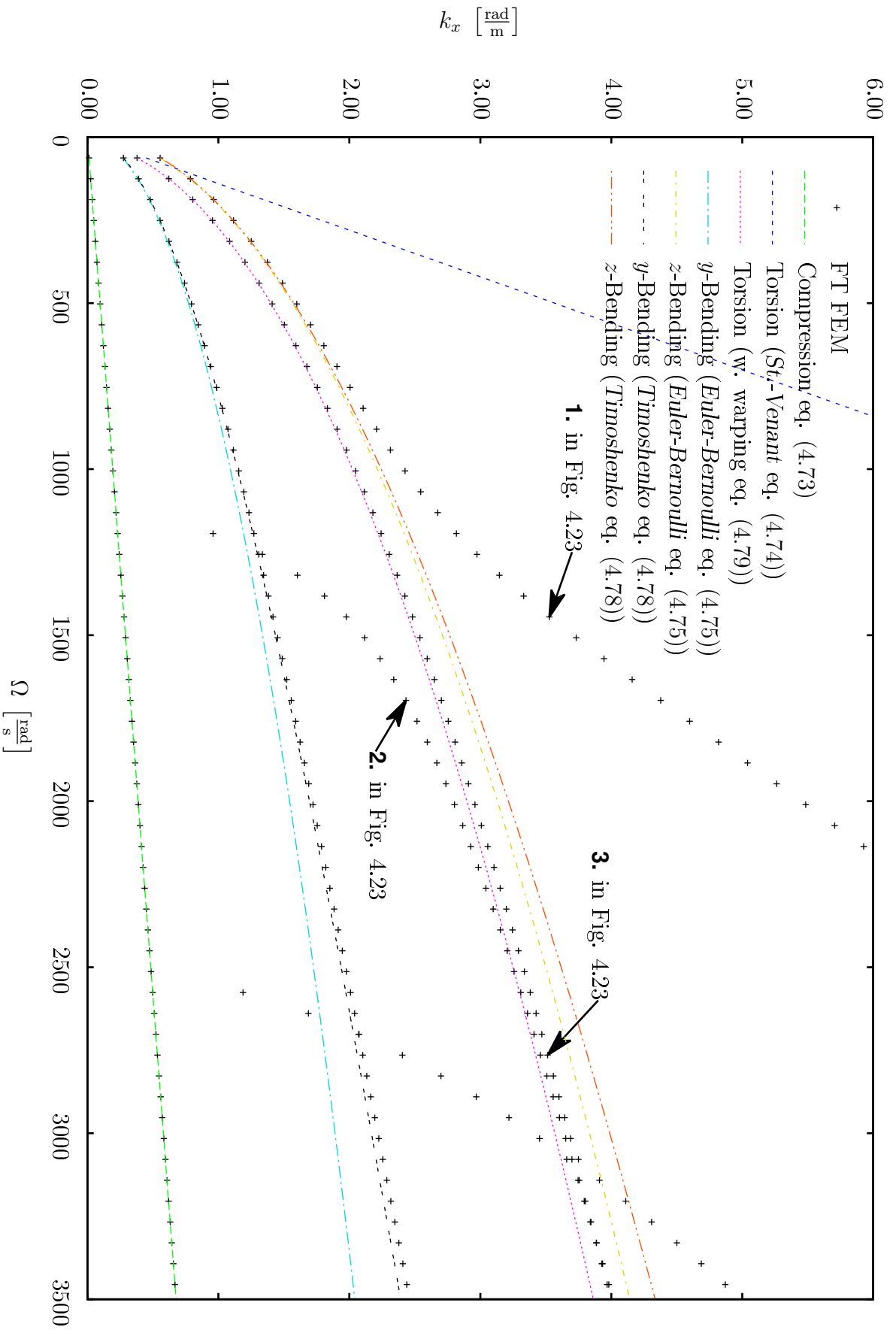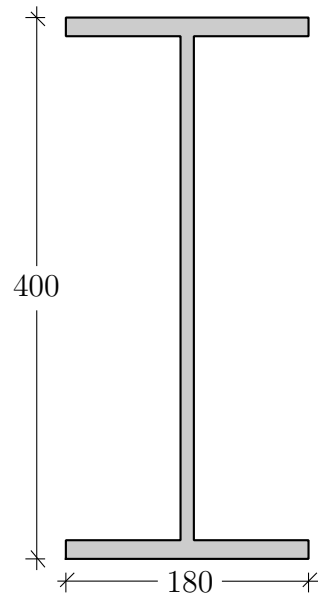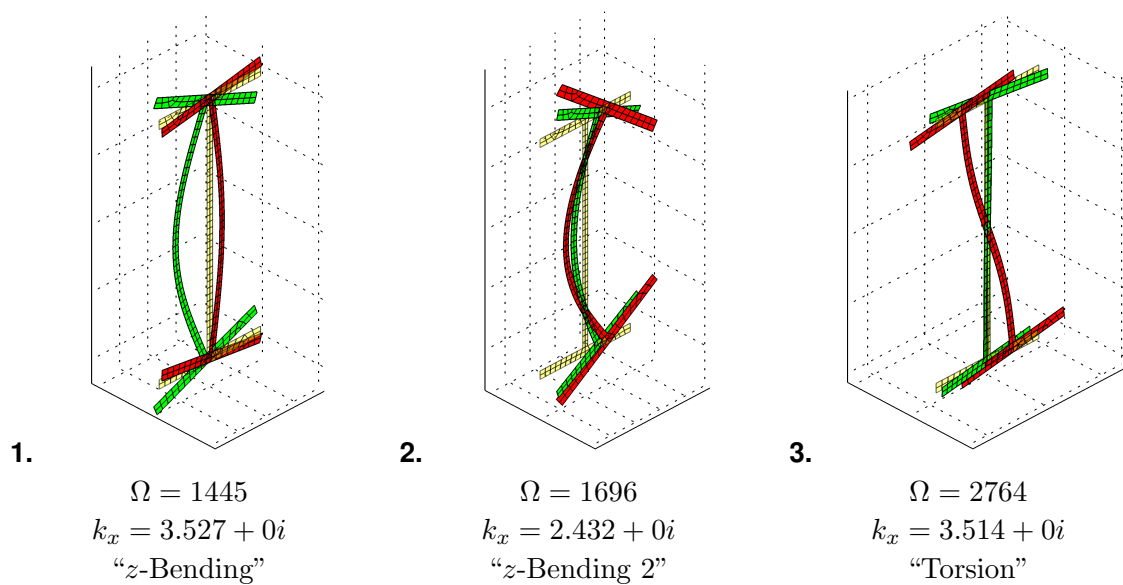
Figure 4.21: Different k_x eigenvalues for the I cross-section together with results from different beam governing equations.

Figure 4.22: Cross section for example 3. Dimensions in mm. The thickness of the flanges is 14 mm, the thickness of the web is 10 mm.

1.	**2.**	**3.**
$\Omega = 1445$	$\Omega = 1696$	$\Omega = 2764$
$k_x = 3.527 + 0i$	$k_x = 2.432 + 0i$	$k_x = 3.514 + 0i$
"z-Bending"	"z-Bending 2"	"Torsion"

Figure 4.23: Eigenvectors and eigenvalues (k_x) as indicated in figure 4.21.

5 Processing of the Beam System

5.1 Choice of Unit Deflection Shapes

Table 5.1 shows an overview of different types of unit deflection shapes presented in the previous chapter together with a short name each which will be used in the following.

Table 5.1: Short names for different unit deflection shapes.

Long name	Short name	see section
Eigenmodes of a Plate in Membrane Action	Eigenmodes membrane	4.1.1
Eigenmodes of a Plate in Bending Action	Eigenmodes bending	4.1.2
Calculation of Shear Warp Shapes with the FEM	Shear warp shapes	4.2.1
Calculation of Derived Warp Shapes from Distortions	High order shear warp shapes	4.2.3
Derived Distortion Shapes from Warp Shapes	High order deformation shapes	4.3.2
Unit deflection shapes for Transverse Strain	*Poisson* shape	4.3.1
Using Eigenmodes of an Infinite Waveguide Structure	FT modes	4.4

In order to conduct a beam calculation one has to choose a set of unit deflection shapes from the types listed in table 5.1. Some remarks about the choice are given in the following:

1. The FT modes cannot be combined with the other, "conventional" unit deflection shapes. The reason is that the FT modes must not be orthogonalised (see section 5.2.4) which is a prerequisite for an arbitrary combination. All following points address the combination of "conventional" unit deflection shapes.

2. The rigid body modes of the cross section (eigenmodes membrane 1 to 3 and eigenmodes bending 1 to 3) have to be part of every set of unit deflection shapes. Exceptions

are systems of reduced dimension like plane frames with plane loading or grids with perpendicular loading.

3. The calculation in [Paolini 2012] showed that it is generally a good strategy to employ many different types of deflection shapes.

4. The calculation in [Paolini 2012] also showd that the shear warp shapes 1 to 3 (torsional warping and warping due to transverse forces) are very effective and thus should be part of the set.

5. If a material law with *Poisson* ratio $\nu \neq 0$ is used, there should be a *Poisson* shape for each out of plane shape since otherwise the stiffness of the warp shapes is not considered correctly.

6. The high order deformation shapes at the current state appear to behave poorly and should not be used. Their calculation procedure might be enhanced by information about the load application analogously to [Zeller 1979].

7. The bending eigenmodes do not cover the physical behaviour of a beam structure. Their only purpose is to generate arbitrary, smooth deflection shapes which get curved more and more the higher the number gets. The calculations in [Paolini 2012] approved, that high order warp shapes should be used instead.

5.2 Orthogonalisation of the Unit Deflection Shapes

5.2.1 Orthogonalisation of Conventional Unit Deflection Shapes[1]

Provided that the unit deflection shapes are linearly independent further orthogonalisation is not mandatory from a computational or numerical point of view [see e.g. Bogensperger 2000].

Nevertheless, orthogonalisation is necessary to allow that comprehensive values like moment, shear force or normal force can be computed from participation factors $\underline{v}$. Furthermore, it enables to apply comprehensive boundary conditions like for example a simple support. Additionally, it allows for comprehensive loading like transverse loads or line moments.

---

[1]Conventional unit deflection shapes in this chapter addresses the shapes gained with the procedures presented in the sections 4.1 to 4.3. The mode shapes gained in section 4.4 have to be treated differently (see section 5.2.4).

The orthogonalisation is organised hierarchically. From every further deflection shape the contained components of all preceding deflection shapes are subtracted by the following scheme:

$$\boldsymbol{\psi}_{i,\text{ortho}} = \boldsymbol{\psi}_i - \sum_{k=1}^{i-1} \frac{\boldsymbol{\psi}_i^T \cdot [A] \cdot \boldsymbol{\psi}_k}{\boldsymbol{\psi}_i^T \cdot [A] \cdot \boldsymbol{\psi}_i} \cdot \boldsymbol{\psi}_k. \tag{5.1}$$

Listing 5.1: MATLAB-Code for the orthogonalisation loop equation (5.1).

```
1  for i=2:size(modeset,2)
2    cont = modeset'*A*modeset;
3    for j=1:i-1
4      modeset(:,i) = modeset(:,i)-cont(j,i)/cont(j,j)*modeset(:,j);
5    end
6  end
```

Warp shapes and in-plane shapes are treated separately since both groups are orthogonal to each other by definition. For warp shapess the matrix $[A]$ contains the longitudinal stiffness (elasticity) weighted with the influence area of the section node. For the in-plane shapes the matrix $[A]$ contains the transverse stiffness (shear modulus) weighted with the influence area of the section node.

Figure 5.1 illustrates how by the process of orthogonalisation the deflection shapes change. However, as this orthogonalisation is just referred to the deformation patterns of the cross section it will not lead to diagonal mass and stiffness matrices.

5.2.2 Remarks to the Orthogonalisation of Warp Shapes

Orthogonalisation and Three Dimensional Material Laws

The main goal of the orthogonalisation is the preservation of comprehensive values like bending moment and normal force from standard beam theories. This means that it would be desirable to make e.g. the bending moment depend on only one participation factor $\underline{v}_i(x)$ or its derivative $\underline{v}_{i,x}(x)$.

(a) Before orthogonalisation (see figure 4.13)   **(b)** After orthogonalisation
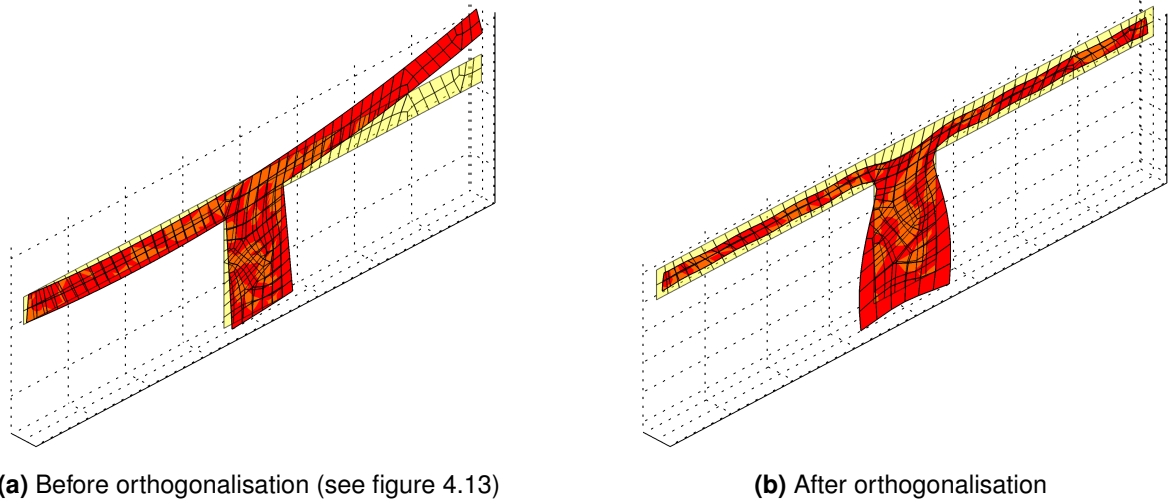
Figure 5.1: *Poisson* shape before (left) and after (right) orthogonalisation.

The bending moment M_y is defined as

$$M_y(x) = \int\limits_{(A)} \sigma_x(x,y,z) \cdot z \, dA. \tag{5.2}$$

For the case of an isotropic linear material it can be itemised as follows

$$M_y(x) = \int\limits_{(A)} E \frac{(1-\nu)\varepsilon_x(y,z,\underline{v}_{i,x}(x)) + \nu\varepsilon_y(y,z,\underline{v}_i(x)) + \nu\varepsilon_z(y,z,\underline{v}_i(x))}{(1+\nu)(1-2\nu)} \cdot z \, dA. \tag{5.3}$$

It can be seen that for the general, non-orthogonalised case it depends on all participation factors $\underline{v}_i(x)$. The structure of equation (5.3) makes it obvious that the demand to make M_y depend on only one $\underline{v}_i(x)$ cannot be fulfilled exactly for $\nu \neq 0$. It would entail requirements to different degrees of derivation of the primary variables $\underline{v}_{i,x}(x)$ which cannot be involved in the calculation of the shape functions $\boldsymbol{\psi}_i(y,z)$.

The next best option is to fulfil this demand for the special case "plane stress". For a linear elastic isotropic material this means

$$\varepsilon_y = \varepsilon_z = -\nu\varepsilon_x. \tag{5.4}$$

Introducing that into equation (5.3) leads to the well known formula

$$M_y(x) = \int\limits_{(A)} E\varepsilon_x(x,y,\underline{v}_{i,x}(x)) \cdot z \, dA. \tag{5.5}$$

Now only one degree of derivation occurs: $\underline{v}_{i,x}(x)$.

The gained insight is that warp shapes can be approximatively orthogonalised with respect to the longitudinal stiffness E. This means that for warp shapes the matrix $[A]$ in equation (5.1) is a stiffness matrix of a spring bed in longitudinal direction for which the stiffness corresponds to the longitudinal stiffness $E(y,z)$. For sections with a homogeneous material the mass matrix can be used instead since the absolute values of $[A]$ are not of importance but only the relative ones. The latter is eqivalent to using a weightening corresponding to the nodal area which is used (in analytical integrals over the section area) in [Roik and Sedlacek 1970].

Sequence of Orthogonalisation

The sequence in which the unit deflection shapes are arranged for the orthogonalisation procedure is of importance since the first shape is not modified at all. From the second its contents affine to the first are subtracted and so on. That's why shapes which shall not be modified have to come first. The following order was found to be an appropriate one:

1. Rigid body shapes from the plate in bending problem (Rotation about the y- and z-axis and the elongation).

2. Shear warp shapes (torsional warping, shear warping in y- and z-direction and the secondary warp torsion shape).

3. Plate in bending modes with index greater that 3.

4. Warp shapes derived from in-plane shapes 4.2.3

5.2.3 Remarks to the Orthogonalisation of In-plane Shapes

The orthogonalisation of the transverse deflection is even more ambiguous. Even for the standard *Timoshenko* beam theory the shear force depends on at least two generalised variables

$\underline{\varphi}_y$ and $\underline{u}_z$:

$$Q_z(x) = \int_{(A)} \tau_{zx}(x,y,z)\, dA = \int_{(A)} G \cdot (\varepsilon_{xz} + \varepsilon_{zx})\, dA$$

$$= \int_{(A)} G \cdot \left(\underline{u}_{z\prime x} - \underline{\varphi}_y + \sum (\omega_{i\prime z} \cdot \underline{v}_i(x)) - (y - y_M)\underline{\varphi}_{x\prime x} \right)\, dA.^2 \tag{5.6}$$

with

$\underline{u}_z$: uniform deflection in the y-direction

$\underline{\varphi}_{x\prime}, \underline{\varphi}_{y\prime}$: rotation about the x- and y-axis with respect to the shear centre

y_M : y-coordinate of the shear centre

ω_i : warp shapes as computed in section 4.2.1 [3]

Actually every warp figure and every distortion or deflection shape (excluding some exceptions occurring on symmetric cross sections) affects the shear stress state $\boldsymbol{\tau}(y,z)$. Consequently, an exact orthogonalisation of in-plane shapes with respect to the shear stiffness is not achievable.

Performing a "mixed orthogonalisation" including both distortion and warp shapes is not feasable because to many specifications would have to be addressed.

5.2.4 Orthogonalisation of Dynamic Mode Shapes

The mode shapes gained in section 4.4 typically contain both in and out of plane deflections within the same shape. The relation between the amplitudes of these two components is part of the wave character and must not be changed. Actually a modification within a hierarchic orthogonalisation as presented in section 5.2.1 would do exactly that. Therefore, this type of shapes cannot be mixed with others and orthogonalised.

On the other hand, the set of modeshapes provided by the procedure presented in section 4.4 is highly redundant when the real and imaginary part of each eigenmode are used as a

---

[2] Additional terms would occur in case of tapered beams with changes of the coordinates of the shear centre and the centre of gravity [see e.g. Hartmann and Katz 2007].

[3] When shear correction factors are used, the participation factor of the shear warping figures are assumed to be affine to the generalised shear strain $\underline{\theta}_y = \underline{\varphi}_y - \underline{u}_{z\prime x}$.
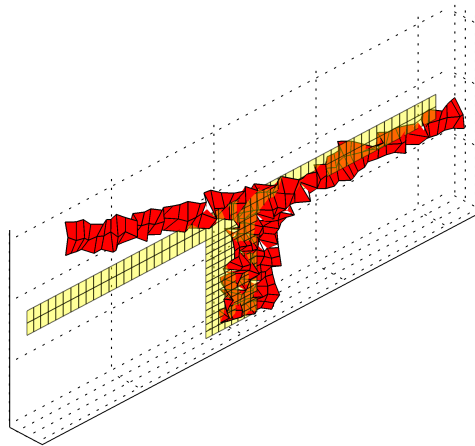
Figure 5.2: Shape which was linearly dependent on preceding shapes after orthogonalisation. Scaling factor: $64 \cdot 10^{12}$

shape function each. For some waves, the imaginary part is linearly dependent on the real part. For others the components of the wave travelling in the positive x-direction is linearly dependent on the corresponding wave travelling in the negative x-direction.

The problem of the procedure presented in the previous section is that it is not robust when more than one linear dependent shape is contained in the set of shapes. Due to the limited precision of calculation the first linear dependent shape will be chunked down to something very close to but not exactly zero. It will become a very edgy shape which still contains common components with upcoming shapes (see figure 5.2). According to equation (5.1) it will be subtracted from "later" shapes and through that introduce edginess to them. This can be prevented by immediately removing a shape which was found to be linearly dependent from the processed set. Listing 5.1 has to be modified as shown in listing 5.2.

An alternative to the presented algorithm is using a QR-decomposition[4] of the matrix of unit deflection shapes $[\Psi]$. When a vector is linearly dependent on his predecessors the corresponding entry on the diagonal of the matrix $[R]$ is very small.

---

[4]QR-decomposition (or QR-factorsation) is a decomposition of a matrix $[A]$ into a product $[A] = [Q][R]$ of an orthogonal matrix $[Q]$ and an upper triangular matrix $[R]$ where $[A]$ is $m \times n$, $[Q]$ is $m \times n$ and $[R]$ is $m \times m$.

Listing 5.2: MATLAB-Code for the orthogonalisation loop modified for dynamic mode shapes.

```matlab
del = 0; % number of removed shapes
for i=2:size(modeset,2)
  cont = modeset'*A*modeset;
  for j=1:i-1
    modeset(:,i-del) = modeset(:,i-del)-cont(j,i-del)/cont(j,j)*modeset(:,j);
  end
  size = mean(abs(modeset(:,i-del)),1);
  if size < 1e-7
    modeset(:,i-del) = [];
    del = del+1;
    bad(del) = i;
  end
end
```
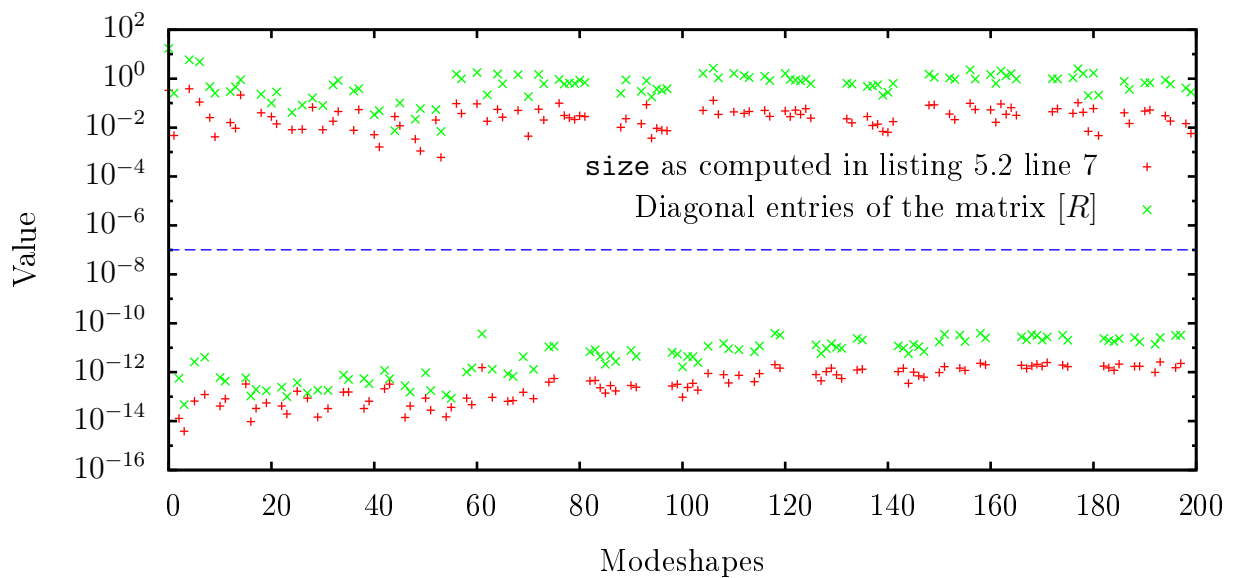

Figure 5.3: Deciding values for a set of 200 dynamic mode shapes.

Figure 5.3 shows the crucial values for both methods: the variable `size` as computed in listing 5.2 line 7 and the corresponding main diagonal entry in the matrix $[R]$ of the QR-decomposition. One can see that both methods separate clearly the "usable" shapes from the linear dependent. The results of the two coincide qualitatively. A good choice for a deciding threshold for both methods seems to be $1 \cdot 10^{-7}$. Shapes with smaller values are deleted, others are used for the pending analysis.

For the QR-decomposition sophisticated algorithms and e.g. an intrinsic MATLAB function
`qr(A)` exists. Consequently, the computational efficiency is much higher for this method and
thus it is chosen as standard approach.

5.3 Processing

5.3.1 Element Matrices and Load Vectors

The beam element stiffness matrices and load vectors are gained by performing a volume
integral for the virtual work inside the beam domain using the deflection shapes both as
ansatz and test functions. The inner virtual work integral is able to include an arbitrary
three dimensional material law. The chosen way is to fill out the domain of a beam element
with volume elements in a preliminary step using standard non-conforming hexahedral Finite
Elements according to Appendix A.2 such that transverse shear locking does not occur.
Afterwards, the stiffness matrix of this volume system $[K]_{\text{bricks}}$ is transformed to the domain
of the participation factors of the front and end node of the beam element by a simple matrix
multiplication

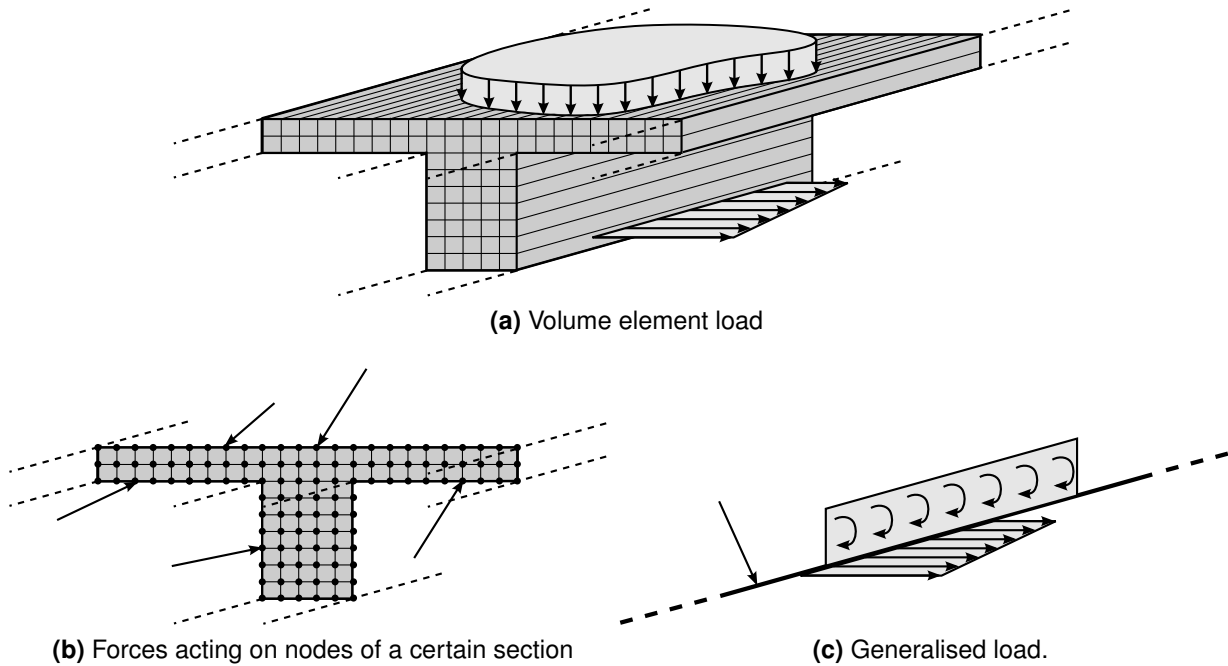$$[\underline{K}]_{\text{elem}} = [N]^T \cdot [K]_{\text{bricks}} \cdot [N] \,. \tag{5.7}$$

with

$$[N] = \begin{bmatrix} \boldsymbol{\psi}_1 & \mathbf{0} & \boldsymbol{\psi}_2 & \mathbf{0} & \cdots & \boldsymbol{\psi}_{n_{\text{modes}}} & \mathbf{0} \\ \mathbf{0} & \boldsymbol{\psi}_1 & \mathbf{0} & \boldsymbol{\psi}_2 & \cdots & \mathbf{0} & \boldsymbol{\psi}_{n_{\text{modes}}} \end{bmatrix} \,. \tag{5.8}$$

The beam element mass matrix can be found in a similar way

$$[\underline{M}]_{\text{elem}} = [N]^T \cdot [M]_{\text{bricks}} \cdot [N] \,. \tag{5.9}$$

The beam element load vector $\big[\underline{p}\big]_{\text{elem}}$ can be derived from a nodal load vector $[p]_{\text{bricks}}$ from
loads as illustrated in figure 5.4a:

$$\big[\underline{p}\big]_{\text{elem}} = [N]^T \cdot [p]_{\text{bricks}} \,. \tag{5.10}$$

(a) Volume element load

(b) Forces acting on nodes of a certain section   **(c)** Generalised load.

Figure 5.4: Different types of possible load applications.

All element wise quantities denoted with $[\ ]_{\mathrm{elem}}$ are afterwards assembled into a corresponding global quantity $[\ ]$ by standard Finite Element procedures.

Additionally, components of the generalised load vector $\left[\underline{p}\right]$ can be determined on a beam nodal basis. Forces $[p]_{\mathrm{secnod}}$ acting at nodes of a certain section as illustrated in figure 5.4b can be transformed into the domain of the generalised parameters $\underline{v}$ by multiplying them with the matrix of unit deflection shapes

$$\left[\underline{p}\right] = [\boldsymbol{\Phi}] \cdot [p]_{\mathrm{secnod}} \,. \tag{5.11}$$

Finally, loads can be detached directly to the generalised degrees of freedom $\underline{v}$ which practically means a certain value is added to an entry in $\left[\underline{p}\right]$. This makes it possible to easily apply line loads if the DOFs of rigid body deflection are addressed or moments in case of rigid body rotations. This type of load application is illustrated in figure 5.4c. It has to be noted that by this procedure the actual distribution of the applied forces over the cross section is not uniquely defined. By definition, this type of load represents an arbitrary load distribution which performs a certain amount of virtual work on the corresponding unit deflection shape.

5.3.2 Assembling and Solution

The assembling and solution of the system follows standard Finite Element procedures. The application of different types of boundary conditions will be illustrated in section 5.4.

The solution of the system of equations yields the participation factors $\underline{v}$ for all considered unit deflections at all beam nodes. Standard linear solvers such as utilised in the MATLAB function `mldivide` can be used.

5.3.2.1 Static Problem

For the static problem, the following system of equations is solved

$$[\underline{K}]\,[\underline{v}] = [\underline{p}]\,. \tag{5.12}$$

5.3.2.2 Dynamic Eigenvalue Problem

For the dynamic eigenvalue problem, the following system is solved for the eigenvalues ω and the eigenvectors $[\underline{\Psi}]$

$$\left([\underline{K}] - \omega^2\,[\underline{M}]\right)[\underline{\Psi}] = [0]\,. \tag{5.13}$$

5.3.2.3 Dynamic Problem: Harmonic Analysis

For the harmonic steady state problem at a discrete angular frequency Ω, the following system is solved for the deflection amplitudes $[\underline{v}]$

$$\left([\underline{K}] - \Omega^2\,[\underline{M}]\right)[\underline{v}] = [\underline{p}(\Omega)]\,. \tag{5.14}$$

5.4 Application of Boundary Conditions

5.4.1 Generalised Boundary Conditions to Primary Variables $\underline{v}_i(x)$

The unknowns in the global system of equations are the participation factors $\underline{v}_i$ at each beam node. *Dirichlet* boundary conditions can be applied directly to them.

The employed process is standard in FEM technologies. In the system of equations the corresponding row is eliminated. The corresponding column is multiplied with the prescribed value (in most cases 0) and shifted to the right hand side if necessary. As a post-processing step the corresponding entry in the vector of unknowns is set to be the prescribed value.

Provided the set of shape functions is orthogonalised as illustrated in section 5.2.1 this type of boundary condition can act as comprehensive support conditions as they are known from any beam analysis (e.g. a hinged displaceable or undisplaceable support) can be applied to the system. The most common use is to "lock" one or more of the rigid body motions of the cross section. It has to be noted that it is ambiguous e.g. to lock lateral rigid body motions while distortions of the cross section are still enabled.

If e.g. a fork bearing or a fully clamped support is desired, *Dirichlet* boundary conditions have to be applied e.g. to all in-plane degrees of freedom or all degrees of freedom at a beam node, respectively. Also symmetry boundary conditions can be applied by locking all warping degrees of freedom.

5.4.2 Boundary Conditions to Nodal Deflections

It is desirable to apply boundary conditions to local nodes since then arbitrary boundary conditions can be modelled. There are several ways to achieve this feature.

The first possibility is to modify the set of shape functions such that the addressed DOF is zero in all of them or all of them but one. There it is preferably equal to one. To this shape then a boundary condition as described in the previous section is applied. This approach is applicable for cases like in figure 5.5 from [Paolini 2012] where the side conditions can be fulfilled by rigid body modifications of the deflection shapes. It is not applicable for more general cases and the orthogonalisation (see section 5.2.1) is not preserved.

From the mathematical point of view boundary conditions are side conditions to the global solution. Generally, such a side condition reads

$$[\Psi_U]\,[\underline{v}] = [\underline{u}]\,. \tag{5.15}$$

It is of the dimension $n \times m$ where n is the number of boundary conditions and m is the dimension of the global system of unknowns. $[\underline{v}]$ is the global vector of unknown participation

(a) Unmodified

(b) First step: Adapt the deflection such that the left bottom node does not deflect.

(c) Second step: Adapt the rotation (about the left bottom node) such that the right bottom node does not deflect vertically.
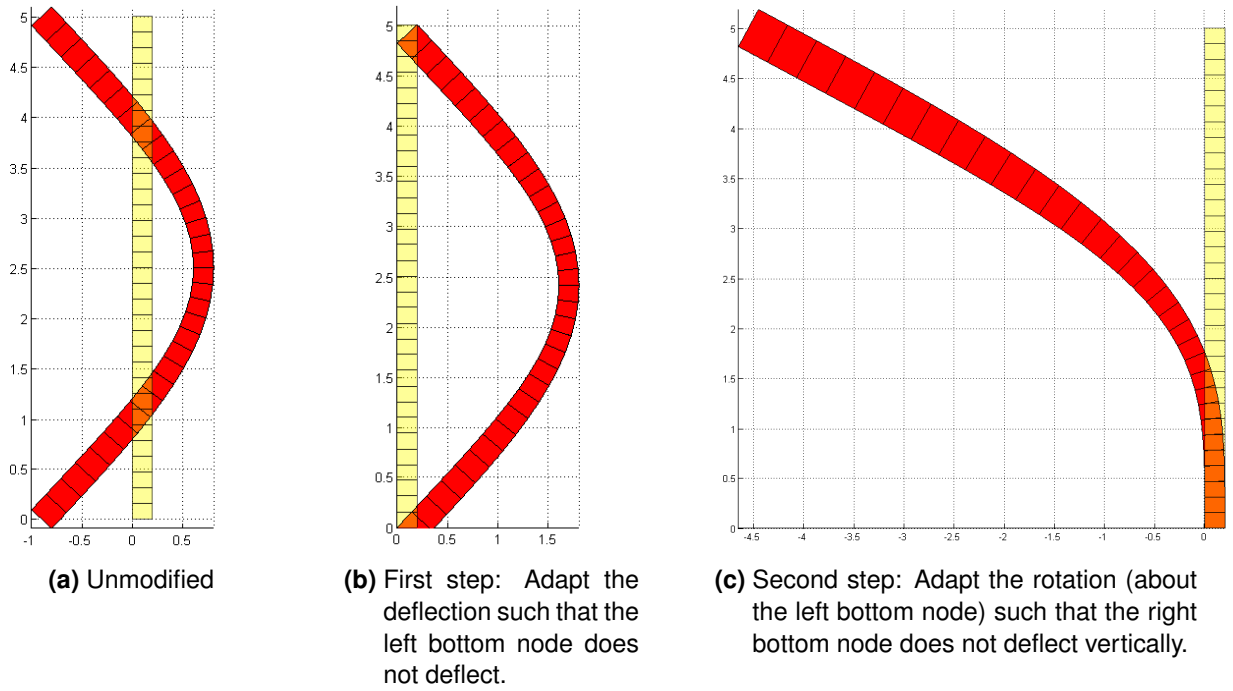
Figure 5.5: Correction of an in-plane deflection shape to fulfil the condition "no deflection of the left bottom node and no vertical deflection of the right bottom node" [from Paolini 2012].

factors. $[u]$ are the prescribed deflection values and a row of $[\Psi_U]$ is of the form

$$\begin{bmatrix} 0 & \ldots & 0 & \ldots & \psi_{1j} & \ldots & \psi_{kj} & 0 & \ldots & 0 \end{bmatrix}. \tag{5.16}$$

ψ_{ij} represents the component of shape i in the direction of the local DOF j and j is the number of DOFs (shapes) at the addressed beam node.

5.4.2.1 Using *Lagrangian* Multipliers

One possibility to introduce the desired boundary condition ("deflection at a particular node equal to a certain value") is utilising the *Lagrangian* multipliers [Bathe 2002].

The boundary conditions (5.15) are introduced to the global potential which then reads

$$\Pi^* \big([\underline{v}], [\lambda]\big) = \frac{1}{2} [\underline{v}]^T [K_{\text{glob}}] [\underline{v}] - [\underline{v}]^T [p] + [\lambda]^T \big[[\Psi_U] [\underline{v}] - [u]\big]. \tag{5.17}$$

$[K_{\text{glob}}]$ and $[p]$ represent the global stiffness matrix and force vector.

For each boundary condition an extra unknown λ is added to the global system of unknowns which then reads

$$
\begin{bmatrix} [K_{\text{glob}}] & [\psi_U]^T \\ [\psi_U] & [0] \end{bmatrix} \begin{bmatrix} [\underline{v}] \\ [\lambda] \end{bmatrix} = \begin{bmatrix} [p] \\ [u] \end{bmatrix}. \tag{5.18}
$$

In this form, without further preconditioning, the band structure of the system is perished. Furthermore, the coefficient matrix is not positive definite but semidefinite. In the scope of this thesis a performance drop by about a factor of two was observed for the solver on systems with *Lagrangian* multipliers compared to a system without. This is illustrated by listing 5.3 (which later has to be compared to listing 5.4). It shows the output of the MATLAB function `mldivide`[5] and indicates that a solver optimised for banded matrices is not used but a more general one.

Listing 5.3: Echo from MATLAB's `mldivide` function for a system with boundary conditions applied with the *Lagrangian* multiplier method [6].

```
sp\: bandwidth = 1629+1+1629.
sp\: is A diagonal? no.
sp\: is band density (0.12) > bandden (0.50) to try banded solver? no.
sp\: is A triangular? no.
sp\: is A morally triangular? no.
sp\: is A a candidate for Cholesky (symmetric, real positive diagonal)? no.
sp\: use Unsymmetric MultiFrontal PACKage with automatic reordering.
sp\: UMFPACK's factorization was successful.
sp\: UMFPACK's solve was successful.
Global BCs and Global solve. Took 0.28038s
```

Remark 1

The bandwidth could be reduced significantly by reordering the system of equations such that the entries corresponding to a certain beam node are located in the region corresponding to that node. [Bathe 2002] nevertheless recommends to leave the entries as indicated in equation (5.18) because the corresponding elements on the main diagonal are zero. Nowadays many different strategies for linear solvers exist. It actually depends on the used solver as to whether or not bandwidth or the position of zeros on the main diagonal play an important

---

[5]Matrix left divide

[6]This output can be obtained by executing `spparms('spumoni',1)` before the `mldivide` call.

role so the consequences of introducing sideconditions as illustrated here cannot be judged concludingly.

Remark 2

When the side condition is introduced as denoted in equation (5.17), the results obtained for $[\lambda]$ are force quantities. This might lead to an ill-conditioned system if the units for forces and deflections are chosen improperly.

5.4.2.2 Using the Penalty Method

Alternatively, the side conditions can be achieved by the penalty method [see also Bathe 2002].

$$\Pi^{**}\big([\underline{v}]\big) = \frac{1}{2}\,[\underline{v}]^T\,[K_{\text{glob}}]\,[\underline{v}] - [\underline{v}]^T\,[p] + \frac{\alpha}{2}\,\big[[\Psi_U]\,[\underline{v}] - [u]\big]^T\big[[\Psi_U]\,[\underline{v}] - [u]\big] \tag{5.19}$$

The penalty number α has to be chosen such that $\alpha \gg \max(k_{\text{glob }ii})$ but also not too big since then numerical errors may occur. An approproate choice is e.g. $\alpha = 1000 \cdot \max(k_{\text{glob }ii})$.

The global system for the minimum of the potential Π^{**} then reads

$$\big[[K_{\text{glob}}] + \alpha\,[\Psi_U]^T\,[\Psi_U]\big]\,[\underline{v}] = [p] + \alpha\,[\Psi_U]^T\,[u]\,. \tag{5.20}$$

Listing 5.4 shows that for a system with side conditions contained as introduced here `mldivide` uses a solver optimised for banded problems which is far more efficient than a general one.

Listing 5.4: Echo from MATLAB's `mldivide` function for a system with boundary conditions applied with the penalty method.

```
sp\: bandwidth = 191+1+191.
sp\: is A diagonal? no.
sp\: is band density (0.75) > bandden (0.50) to try banded solver? yes.
sp\: is LAPACK's banded solver successful? yes.
Global BCs and Global solve. Took 0.101s
```
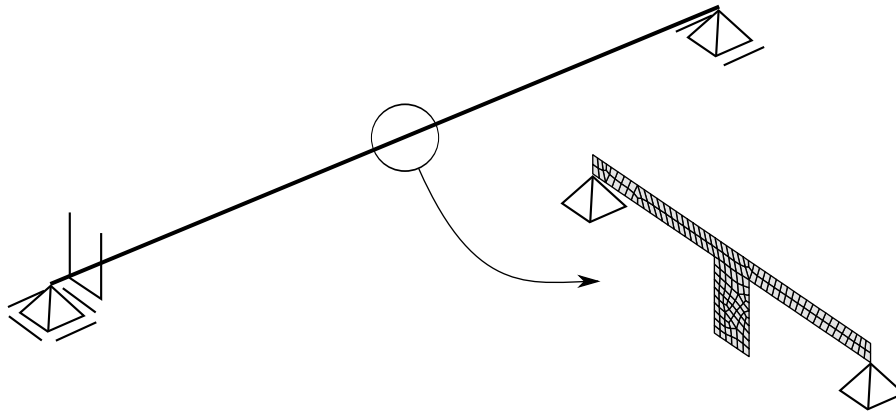
Figure 5.6: Example system for the global and nodal boundary conditions.
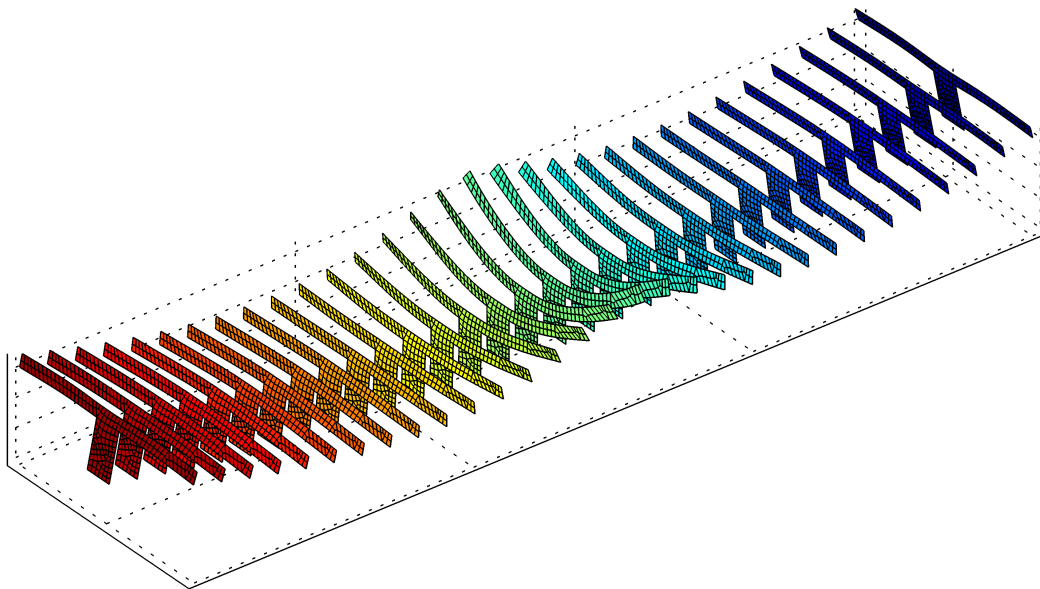
Figure 5.7: Deflected system of the boundary condition example.

Figure 5.6 shows an example application for both the global and the nodal boundary conditions. The t-beam under self weight is supported with boundary conditions to the primary variables (see section 5.4.1) at the first and last beam node. At the section in the middle of the span the bottom nodes at the ends of the plate are supported. The example contains 31 beam nodes and 96 DOFs or shapes at each of them thus 2976 unknown in total. The numbers and calculation times in listings 5.3 and 5.4 also refer to this example. The deflected shape can be seen in figure 5.7.

Remark

As the penalty method introduces stiffness to the system which is order of magnitudes higher than the highest stiffness already contained in the system, it deteriorates the condition of the system of equations. Throughout the calculations made for this thesis this appeared from time to time and the system became close to ill conditioned by introducing side conditions with the penalty method.

As a matter of fact, beam systems generally tend to be more ill conditioned than e.g. volume systems where during mesh generation it is ensured that neighbouring nodes have stiffness values close to each other by limiting the size ratio of neighbouring elements.

5.5 Postprocessing

5.5.1 Deflections

The deflections at the nodes can be obtained by superposition according to equation (1.1). Usually not the full set of shape functions is taken into account for the calculation. This literally means that n_{modes} is smaller than the number of discrete deflections at a section. The superposition then yields only an approximative solution $\hat{\mathbf{u}}$

$$\hat{\mathbf{u}} = \sum_{i=1}^{n_{\mathrm{modes}}} \left(\boldsymbol{\psi}_i \cdot \underline{v}_i \right) = \left[\boldsymbol{\Phi} \right] \left[\underline{v} \right]. \tag{5.21}$$

The presented method enables only discrete deflections at the section at each beam node. Inside the element domain the generalised deflections $\underline{v}$ can be interpolated linearly. High order ansatz functions in the longitudinal direction may allow for a more sophisticated evaluation just as in standard beam analysis. See section 3.1.2 for the method of transmission

matrices and section 3.1.3 for high order ansatz functions (p-version of Finite Elements). The deflection field on the level of the brick elements can be obtained using the utilised shape functions.

5.5.2 Strains and Stresses

The discrete deflections $[u]$ as obtained by superposition in the previous section can be applied to the brick Finite Element system underlying the stiffness matrix $[K]_{\text{bricks}}$ (see section 5.3.1). This yields strains $[\varepsilon]$ inside one beam element applying standard Finite Element procedures.

$$[\varepsilon] = [B] [u] . \tag{5.22}$$

From there stresses $[\sigma]$ can be obtained employing the material matrix $[D]$ from section 2.3

$$[\sigma] = [D] [\varepsilon] . \hspace{2cm} \text{(see equation 2.9)}$$
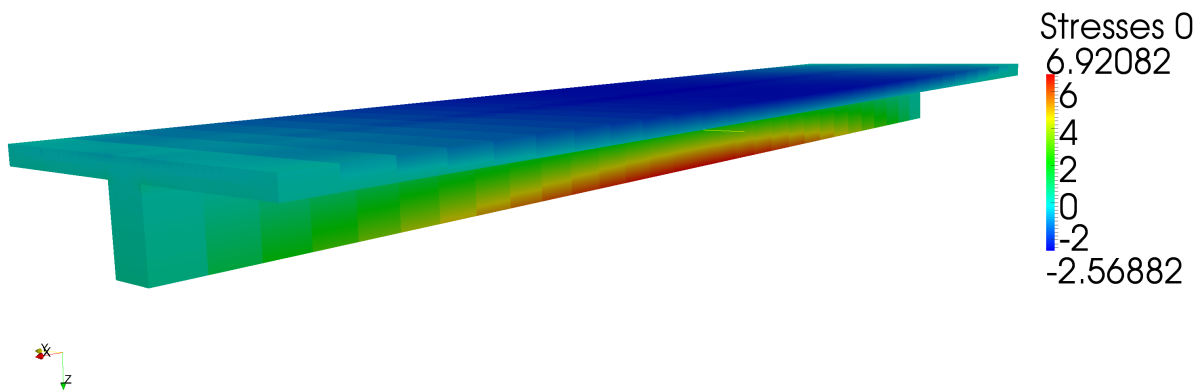
Figure 5.8: Stresses σ_{xx} for a simply supported beam under selfweight visualised using the open source program Paraview employing the VTK file format [VTK 2013].

Remark

The procedure yields the stresses in the *Gauss* integration points. They can be extrapolated to the element nodes by a multiplication with the inverse of the shape function matrix N^{-1}. This yields "stepped" results as they can be observed in figure 5.8. Commercial Finite Element packages perform an averaging at the mesh nodes to obtain smooth results. This is not done here since the size of the jump of the values between elements may also serve as a measure for the inaccuracy of the results in that region.

5.5.3 Support Forces

5.5.3.1 Support Forces at Generalised Supports

Given the orthogonalisation according to section 5.2 has been performed the generalised support forces $\left[\underline{q}\right]_{\text{glob}}$ and moments at generalised support conditions as explained in section 5.4.1 can be estimated by taking them directly from equation (5.12) introducig for $\underline{v}$ both the prescribed and the computed values from the solver

$$\left[\underline{q}\right]_{\text{glob}} = [K]_{\text{glob}} \left[\underline{v}\right] - \left[\underline{p}\right]_{\text{glob}}. \tag{5.23}$$

5.5.3.2 Support Forces at Nodal Supports

At nodal supports according to section 5.4.2 the procedure depends on the method used for the application.

If *Lagrangian* Multipliers according to section 5.4.2.1 are used, the support forces can be taken directly from the solution vector. The entries $[\lambda]$ in those lines corresponding to the introduced side conditions (see equation (5.18)) represent the support forces directly

$$q_{\text{loc}} = -\lambda. \tag{5.24}$$

If alternatively the penalty method according to section 5.4.2.2 is used, the support forces can be obtained from the following equation

$$q_{\text{loc}} = -\alpha \left(\hat{u} - u\right). \tag{5.25}$$

$\hat{u}$ represents the superposed nodal deflection solution according to equation (5.21). α represents the penalty factor and u the prescribed deflection as introduced in section 5.4.2.2.

5.5.4 Sectional Forces Using the Primary Variables $\underline{v}$

Given the orthogonalisation according to section 5.2 has been performed the sectional forces can be estimated according to beam theory, directly with the help of the primary variables $\underline{v}$, their derivatives and certain sectional values.

5.5.4.1 Normal Force, Bending Moments, and the Bimoment

For the sectional values the abbreviation as used in chapter 4.2.1.2 is applied again:

$$EA_{ab} = \int\limits_{(A)} Eab \, dA \qquad \text{and} \qquad EA_a = \int\limits_{(A)} Ea \, dA \tag{5.26}$$

The calculation of the normal force and the moments including the bimoment is still straight forward from the primary deflection and rotation variables $\underline{u}_x, \underline{u}_y, \underline{u}_z, \underline{\varphi}_y, \underline{\varphi}_z$ and the warping $\underline{\Psi}$

$$N = EA \cdot \underline{u}_{x\prime x} + EA_z \cdot \underline{\varphi}_{y\prime x} + EA_y \cdot \underline{\varphi}_{z\prime x} \tag{5.27}$$

$$M_y = EA_z \cdot \underline{u}_{x\prime x} + EA_{zz} \cdot \underline{\varphi}_{y\prime x} - EA_{yz} \cdot \underline{\varphi}_{z\prime x} \tag{5.28}$$

$$M_z = EA_y \cdot \underline{u}_{x\prime x} - EA_{yz} \cdot \underline{\varphi}_{y\prime x} + EA_{yy} \cdot \underline{\varphi}_{z\prime x} \tag{5.29}$$

$$M_B = EA_{\omega\omega} \cdot \underline{\Psi}_{\prime x}. \tag{5.30}$$

The off-diagonal terms may be erased by using the principal axis which intersect in the centre of stiffness. The values $EA_z \; EA_y$ and EA_{yz} become zero then. Furthermore, additional terms occur if the centre of rotation (point of attack of the shear forces) is not chosen in the shear centre.

5.5.4.2 Shear Forces and Torsional Moment

In cases where non-uniform torsion is considered the torsional moment consists of two components

$$M_x = M_{xV} + M_{xS}. \tag{5.31}$$

M_{tV} represents the torsional moment due to uniform (*de St.-Venant*) torsion:

$$M_{xV} = GI_t \cdot \underline{\psi} \tag{5.32a}$$
$$= GI_t \cdot \underline{\varphi}_{x,x}. \qquad \text{(using \textit{Wagner}'s hypothesis)} \tag{5.32b}$$

M_{tS} represents the torsional moment due to non-uniform (warping) torsion (secondary torsional moment). It can be computed by

$$M_{xS} = EI_\omega \cdot \underline{\psi}_{,xx} \tag{5.33a}$$
$$= -EI_\omega \cdot \underline{\varphi}_{x,xxx}. \qquad \text{(using \textit{Wagner}'s hypothesis)} \tag{5.33b}$$

ψ represents the participation factor for the warp shape of primary torsion. It can be seen that to compute M_{tS} with these equations at least the second derivative of a primary variable is needed. This is a big disadvantage since in the presented global approach using the stiffness matrix of a system of brick elements provides only the first derivative (see remark at the end of this section).

Alternatively, if the *Wagner* hypothesis is skipped and shear deformations from warping torsions are allowed for, the secondary torsional moment can be found in analogy to the shear force in *Timoshenko* beam theory (see equation (5.37))

$$M_{xS} = GA_{S\omega} \cdot \underline{\gamma}_\omega \tag{5.34}$$

with

$$\underline{\gamma}_\omega = \underline{\varphi}_{x,x} + \underline{\psi}. \tag{5.35}$$

The shear forces can be obtained from the following equation using the shear stiffnesses calculated in appendix A.5.2 based on the transverse shear warp shapes from section 4.2.1.3.
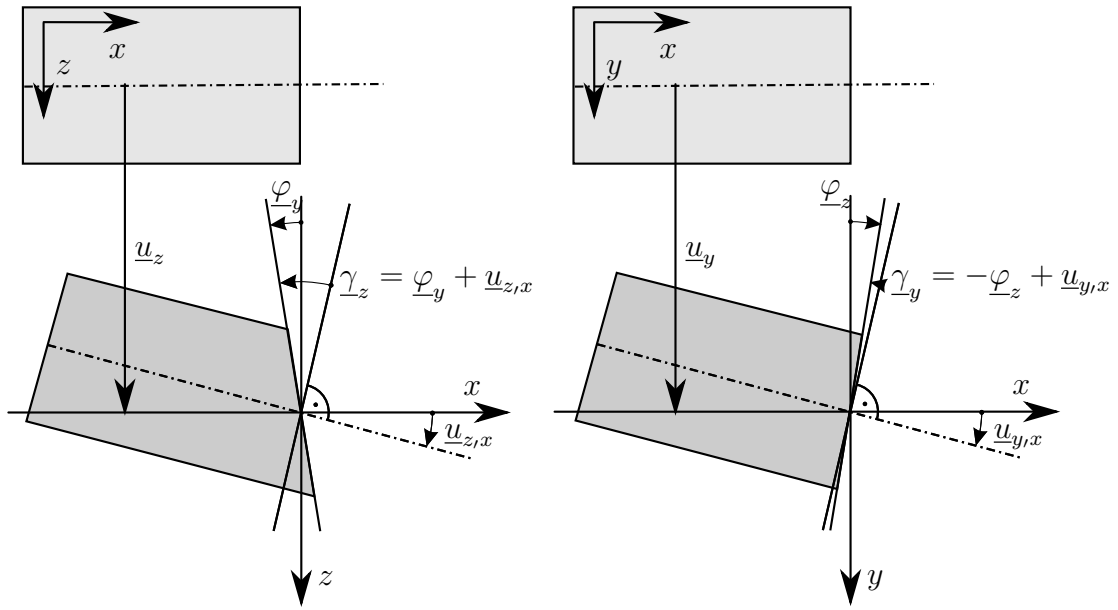
Figure 5.9: Occurring rotation and generalised shear strain values for the *Timoshenko* beam in the deflected position

$$Q_y = GA_{Sy} \cdot \underline{\gamma}_y \tag{5.36a}$$

$$Q_z = GA_{Sz} \cdot \underline{\gamma}_z \tag{5.36b}$$

where the generalised shear strains are computed from

$$\begin{bmatrix} \underline{\gamma}_y \\ \underline{\gamma}_z \end{bmatrix} = \begin{bmatrix} \underline{\varphi}_y + \underline{u}_{z,x} \\ -\underline{\varphi}_z + \underline{u}_{y,x} \end{bmatrix}. \tag{5.37}$$

The values on the right hand side of the latter equation can be obtained from the solution of the system of equations.

As illustrated in appendix A.5 all shear stiffnesses GA_{Si} occurring in this section are coupled and off-diagonal entries exist. In appendix A.5.1 equation (A.5.11) the corresponding flexibility matrix $[GA_{inv}]$ is computed. It can be utilised as follows

$$\begin{bmatrix} Q_y \\ Q_z \\ M_{xS} \end{bmatrix} = [GA_{inv}]^{-1} \cdot \begin{bmatrix} \underline{\gamma}_y \\ \underline{\gamma}_z \\ \underline{\gamma}_\omega \end{bmatrix}. \tag{5.38}$$

5.5.4.3 Remarks

1. The presented approach using the stiffness matrix of a system of brick elements (see section 5.3.1) provides the solution of the primary variables discretely at the beam nodes. That's why it allows only for obtaining the first derivative of the primary variables $\underline{v}$ by

$$\underline{v}_{,x} = \frac{\underline{v}_{\text{end}} - \underline{v}_{\text{start}}}{l_{\text{elem}}}.\tag{5.39}$$

It can be seen that per element only values constant with respect to x can be gained. The second or higher derivatives cannot be obtained at all. Better results can be obtained when either higher order (with respect to x) elements are used (see section 3.1.3) or if the static condensation of the intermediate quadratic DOF (see appendix A.2) is not done on the level of the brick DOFs but on the level of the beam DOFs $\underline{v}$.

2. The relation as depicted in equation (5.38) coincides with sources in literature [e.g. Bogensperger 2000; Katz 2008; Schade 1969]. However, none of the sources evaluated the relations by comparing a beam calculation employing them with a corresponding three dimensional volume or shell model.

3. The examples in the sections 6.1.2 and 6.1.3 show that the values for section forces obtained from this approach of calculation are not reliable once the underlying assumption of the undeformability of the cross section is not fulfilled. Some of the sectional forces seem to be more robust than others. While all quantities related to normal stresses (normal force, bending moments and the bimoment) are estimated comparably well, the quantities related to shear stresses (shear forces and the torsional moments) underlie big vulnerabilities especially at the locations of supports or load applications.

5.5.5 Sectional Forces Using the Stresses

Once the stresses are calculated as illustrated in section 5.5.2 they can be used to calculate the sectional forces by simple surface integrals at each section:

$$N = \int\limits_{(A)} \sigma_x \, dA \tag{5.40a}$$

$$M_y = \int\limits_{(A)} z\sigma_x \, dA \tag{5.40b}$$

$$M_z = - \int\limits_{(A)} y\sigma_x \, dA \tag{5.40c}$$

$$Q_y = \int\limits_{(A)} \tau_{xy} \, dA \tag{5.40d}$$

$$Q_z = \int\limits_{(A)} \tau_{xz} \, dA \tag{5.40e}$$

$$M_x = \int\limits_{(A)} \tau_{xy} \left(z_M - z \right) + \left(y - y_M \right) \tau_{xz} \, dA \tag{5.40f}$$

$$M_B = \int\limits_{(A)} \omega_V \sigma_x \, dA. \tag{5.40g}$$

The evaluations of the integrals of the cross section can be performed efficiently making use of the existing Finite Element mesh. The results are obtained in an intermediate step at the positions of the *Gauss* integration points and have to be extrapolated into the element nodes of the beam element. This leads to slopes which appear to be stepped (see e.g. figures 6.9 and 6.10 and the remark in section 5.5.2).

5.6 Error Estimation

5.6.1 Introduction

As described the presented method is based on modal truncation meaning that the number of actual (generalised) DOFs $\underline{v}$ is smaller than the number of available nodal deflections at all sectional nodes. This truncation induces an error which can be determined straight forward,

if a reference solution is calculated in which all available nodal deflections are considered. Namely, a full 3D analysis with volume elements has to be performed either within the same code or using other, commercial software packages. The actual results can be compared against this reference solution with respect to different quantities. This approach is applied in [Paolini 2012] and briefly explained in section 6.1.1.1. Two drawbacks arise: If generalised support conditions (see section 5.4.1) or generalised loads (see section 5.3.1) are applied it is not always possible to find equivalent boundary conditions for the volume system. Secondly, the computation of a full 3D solution is labour-intensive. The aim of the following approach is to avoid this step.

5.6.2 Derivation

Like for the evaluation of the strains and stresses the deflection field $\mathbf{u}$ can be applied to the underlying brick system forming the elementwise stiffness $[K]_{\mathrm{bricks}}$ (see figure 5.10). By doing so with two elements neighbouring the node of interest i one can obtain the reaction force vector $\mathbf{q}_{\mathrm{re}\,i}$ from the system necessary to enforce this deflection setup around node i

$$\mathbf{q}_{\mathrm{re}\,i} = [K]_{\mathrm{bricks}\,j-1} \cdot \begin{bmatrix} \mathbf{u}_{i-1} \\ \mathbf{u}_i \end{bmatrix} + [K]_{\mathrm{bricks}\,j} \cdot \begin{bmatrix} \mathbf{u}_i \\ \mathbf{u}_{i+1} \end{bmatrix}. \tag{5.41}$$

In the ideal case, these forces are in equilibrium with the load $\mathbf{p}_i$ and support forces $\mathbf{q}_{\mathrm{supp}\,i}$ applied to the system such that

$$\mathbf{q}_{\mathrm{re}\,i} = \mathbf{p}_i + \mathbf{q}_{\mathrm{supp}\,i}. \tag{5.42}$$

Since the presented method aims at a modal truncation this is not the case in general. The error at node i induced by the modal truncation can thus be estimated a posteriori by

$$e_i = \sum_{i=1}^{n_{\mathrm{nodes}}} \left\| \mathbf{q}_{\mathrm{re}\,i} - \mathbf{p}_i - \mathbf{q}_{\mathrm{supp}\,i} \right\|. \tag{5.43}$$

The total error in a beam system can be obtained by summing up over all beam nodes:

$$e_{\mathrm{tot}} = \sum_{i=1}^{n_{\mathrm{nodes}}} \left\| \mathbf{q}_{\mathrm{re}\,i} - \mathbf{p}_i - \mathbf{q}_{\mathrm{supp}\,i} \right\|. \tag{5.44}$$
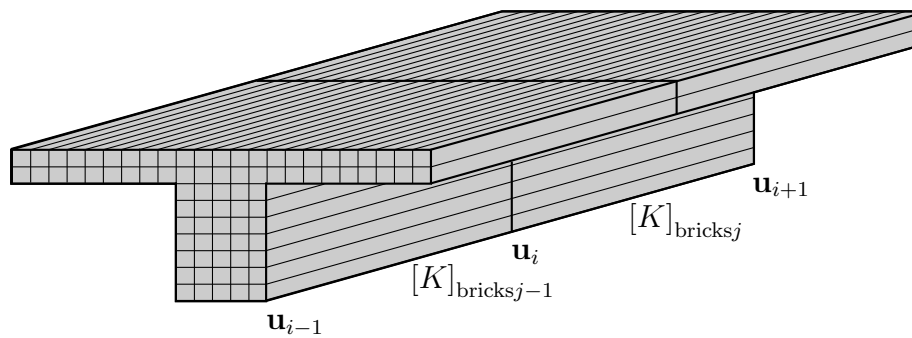
Figure 5.10: Brick system as used for the evaluation of the error forces at node i.

5.6.3 Example

Figure 5.11 shows two plots of these error forces of a system equivalent to the example in section 6.2.1 with a static load. The plots refer to a cross section in a distance of 1m to the clamped support. The two figures 5.11a and 5.11b are scaled equally.

5.11a refers to a configuration which is equivalent to *Timoshenko* beam theory: 3 eigenmodes membrane, 3 eigenmodes bending, 3 shear warp shapes, 6 *Poisson* shapes[7].

5.11b refers to a slightly enriched configuration: 5 eigenmodes membrane, 3 eigenmodes bending, 3 shear warp shapes, 2 high order shear warp shapes, 6 *Poisson* shapes[7].
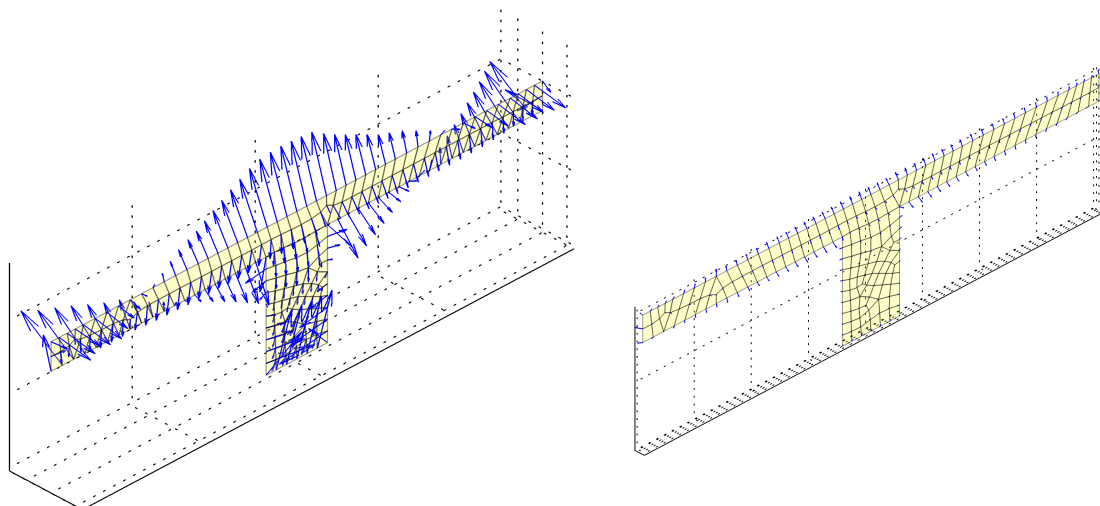
(a) System with 15 DOFs per beam node.

(b) System with 19 DOFs per beam node.

Figure 5.11: Error force plot for different discretisations.

---

[7]The names of the types of unit deflection shapes refer to those in table 5.1 on page 76.

5.6.4 Remarks

1. For the case of a harmonic analysis with the angular frequency Ω, $[K]_{\text{bricks}}$ has to be replaced by the dynamic stiffness matrix $[K]_{\text{dyn bricks}} = [K]_{\text{bricks}} - \Omega^2 \cdot [M]_{\text{bricks}}$.

2. If either generalised loads or generalised support conditions are applied to the beam degrees of freedom $\underline{v}$, a unique, correct nodal load vector cannot be computed. This fact becomes obvious especially for the shear forces. Their corresponding stress distribution over the cross section depends heavily on circumstances such as the fact of whether or not the point of application is allowing for warping deformations.
Consequently, nodes to which either generalised support conditions or generalised loads were applied should remain unconsidered in the summation of equation (5.44).

3. At beamnodes where singularities are applied (point loads or nodal supports) the error may become extremely high and dominate the error of the whole system because singularities are covered only very poorly by the used smooth ansatz functions. Systems with such singularities may even show a higher error if the number of unit deflection shapes is increased.

4. The presented error force does not cover the "internal error" of the employed volume elements. It only contains the part of the error caused by the modal truncation and the limitation of the solution space caused thereby.

5. This error is not relative but absolute meaning that it depends on the absolute stress level inside the system and the size of the system. It is of the unit force [N]. It would be reasonable to make it relative by dividing it by the absolute strain energy in the corresponding part of the system

$$W = \frac{1}{2} \int\limits_{(V)} \boldsymbol{\sigma} \cdot \boldsymbol{\varepsilon} \, dV. \tag{5.45}$$

This strain energy takes into account both the absolute stress level and the size of the system. This division does not lead to a dimensionless quantity because the strain energy is of the unit energy [Nm]. An opportunity to resolve this problem would be to determine a stress and strain state $\boldsymbol{\sigma}_e/\boldsymbol{\varepsilon}_e$ corresponding to the error forces by applying them as a load to the system and perform a direct 3D analysis without the generalised

DOFs. From there a cumulative error can be determined by

$$W_e = \frac{1}{2} \int\limits_{(V)} \boldsymbol{\sigma}_e \cdot \boldsymbol{\varepsilon}_e \; dV \tag{5.46}$$

and the relative error by

$$E = \frac{W_e}{W}. \tag{5.47}$$

The latter step could be done for the whole system which is again labour-intensive and should be avoided. It might be sufficient to perform this step on a small subsystem like e.g. one beam element.

6 Applications and Numerical Examples

6.1 Static Calculations

6.1.1 Comparing Different Types of Mode Shapes

[Kreutz and G. Müller 2012; Paolini 2012]

The presented method gives the opportunity to freely choose the amount and composition of degrees of freedom. The maximum number of linearly independent deflection shapes is for warping degrees of freedom equal to the number of nodes in a cross section. For distortion degrees of freedom it is twice as high. It is clear that when the full extent of the possible and linearly independent deflection shapes is used one will obtain exactly the same result as if one calculated an ordinary volume model. But this is not the aim of the method. The aim of this method is to obtain results preferably close to these with a considerably lower number of degrees of freedom.

In [Paolini 2012] a huge number of examples including conventional beam systems and compact shear walls was calculated for different load situations and with different support conditions. On the basis of these calculations an efficient strategy to choose the types of unit deflection shapes which come to use was determined. The results were integrated into the remarks listed in section 5.1. Here, one example is presented exemplarily. The results represent well those of most of the other examples.

6.1.1.1 Quantities of Validation

The quality of the solution is determined with respect to a Finite Element volume model calculated with the commercial software package SOFiSTiK. Two types of quantification of the quality are used and shall be introduced shortly.

The *Tanimoto* Coefficient T [Willett et al. 1998] is used to compare the nodal values of the discretised stress state $\boldsymbol{\sigma}_{\mathrm{AB}}$ of the complete augmented beam system with the one from the reference model $\boldsymbol{\sigma}_{\mathrm{RM}}$.

$$T(\boldsymbol{\sigma}) = \frac{\boldsymbol{\sigma}_{\mathrm{AB}} \cdot \boldsymbol{\sigma}_{\mathrm{RM}}}{\|\boldsymbol{\sigma}_{\mathrm{AB}}\|^2 + \|\boldsymbol{\sigma}_{\mathrm{RM}}\|^2 - \boldsymbol{\sigma}_{\mathrm{AB}} \cdot \boldsymbol{\sigma}_{\mathrm{RM}}} \tag{6.1}$$

T takes the value one if the two stress states equal exactly. In all other cases it takes values smaller than one.

To cover also the deviations of the peak values which would be overseen by the *Tanimoto* Coefficient additionally the relative deviation of the maximum value of the effective stress $\sigma_{\mathrm{max,AB}}$ is observed. It is calculated by

$$f(\sigma_{\mathrm{max}}) = \frac{\sigma_{\mathrm{max,AB}} - \sigma_{\mathrm{max,RM}}}{\sigma_{\mathrm{max,RM}}} \cdot 100\%. \tag{6.2}$$

It is equal to zero if there is no deviation and can take arbitrary values otherwise.

6.1.1.2 Problem Setup
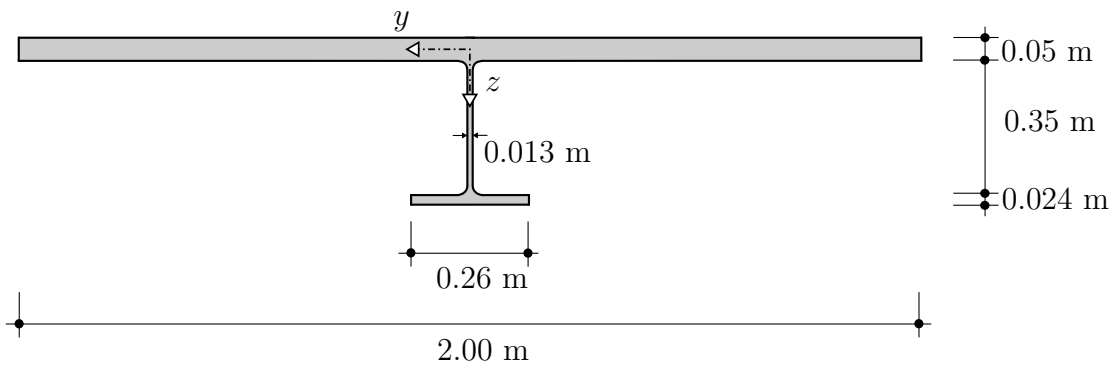
Figure 6.1: Cross section of the beam in the example [Paolini 2012].

The presented example is a two span beam with the cross section given in figure 6.1. Input values for the calculation:

- lengthwise span of the beam: two times 8 m

- elastic modulus: $E = 210000 \ \frac{\mathrm{MN}}{\mathrm{m}^2}$

- *Poisson*-Ratio $\nu = 0.3$
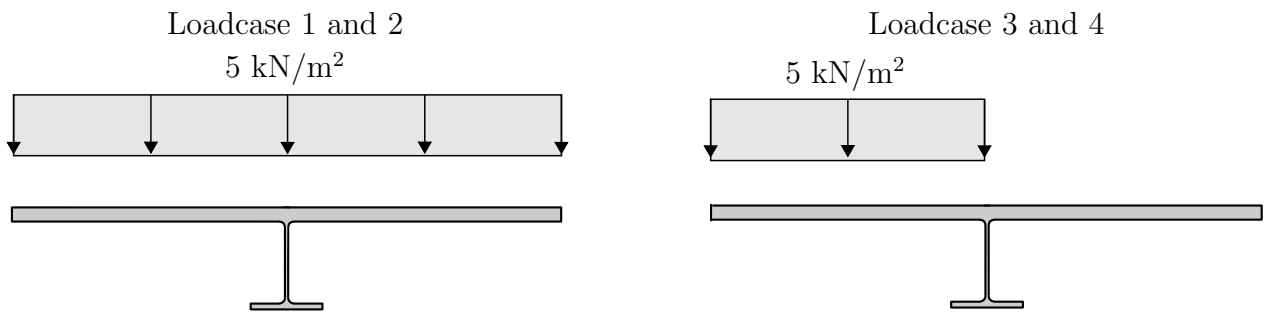
Figure 6.2: Load situations for the example from [Paolini 2012].

Four loadcases are calculated (see figure 6.2):

- loadcase 1: centric load on both spans

- loadcase 2: centric load on one span

- loadcase 3: excentric load on both spans

- loadcase 4: excentric load on one span

The number of degrees of freedom is increased step by step starting from the following initial configuration: three eigenmodes membrane, three eigenmodes bending, no warp shapes and three *Poisson* shapes. This start configuration is chosen such that the solution space is close to standard *Timoshenko* Beam Theory. In a first step the four shear warp shapes corresponding primary torsion, the shear forces and secondary torsion are added. From there the setup is enriched stepwise where in each step the number of considered deflection shapes of the following types is increased by one: eigenmodes membrane, high order warp shapes (corresponding to the eigenmode membrane) and *Poisson* shapes (corresponding to the high order warp shape).

6.1.1.3 Results

Figure 6.3 shows how the validation quantities behave when the number of DOFs is increased as described above. The graphs show two predominant gains of accuracy at four and ten extra DOFs. The first corresponds to the four standard warp shapes as described above. The second is even bigger and corresponds to the deformation of the cross section shown in figure 6.4 and the corresponding *Poisson* shape.
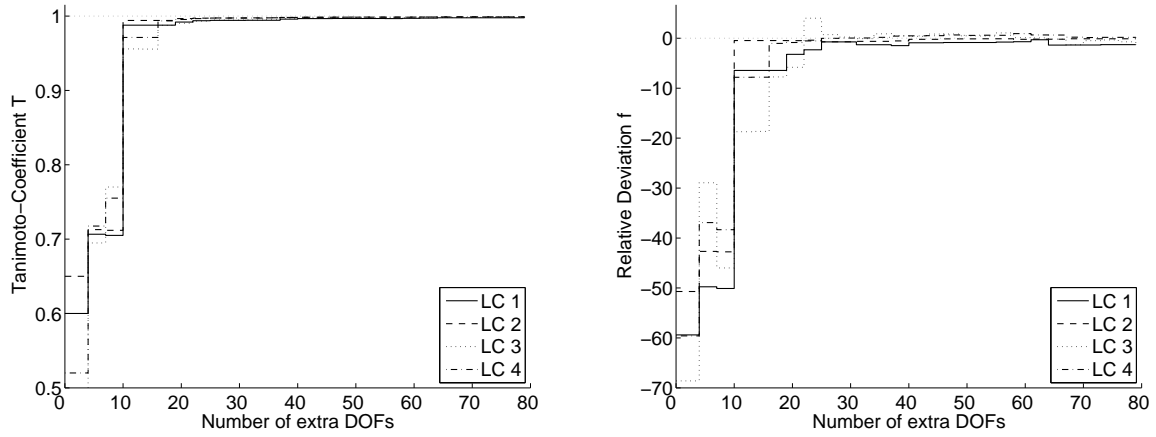
Figure 6.3: Tanimoto Coefficient (left) and relative deviation of the maximum effective stress (right) depending on the additional number of degrees of freedom and the load case.
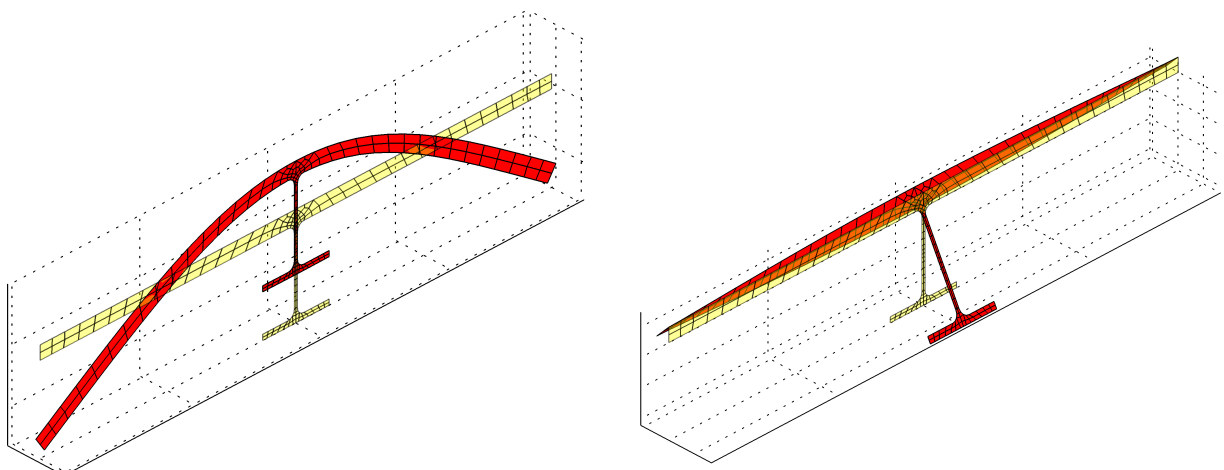
(a) 5. Eigenmode membrane   **(b)** Corresponding high order warp shape

Figure 6.4: Important unit deflection shapes representing the deformation of the cross section.

(a) Fork bearing at $x = 0$ **(b)** Clamped at $x = 0$
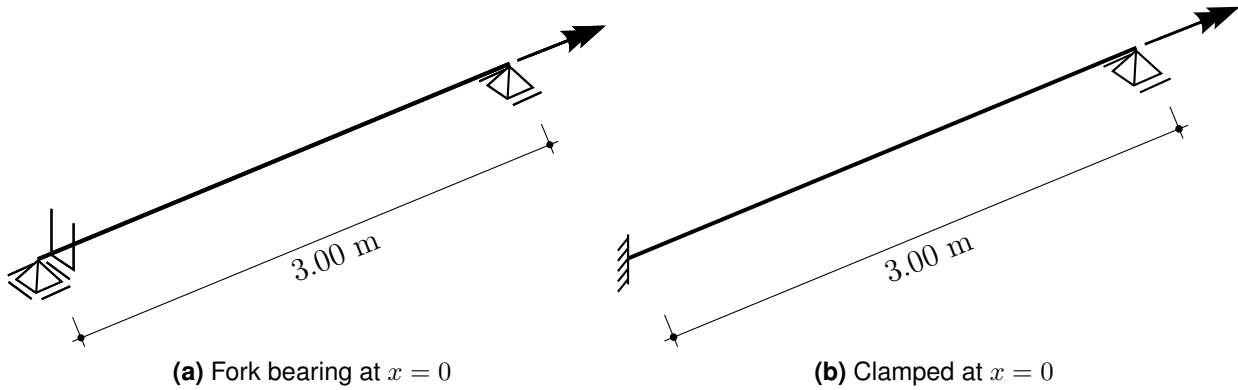
Figure 6.5: Systems for the two torsion examples.

6.1.2 Example: Torsion

This example illustrates the correctness and effectiveness of the warp modes calculated in section 4.2.1 and problems occurring when sectional forces shall be calculated.

6.1.2.1 Setup

The system is a single span beam of 3 m length with different support conditions at $x = 0$ (see figure 6.5). The tip is loaded with a torsional moment of $M_x = 0.08$ MNm. The cross section is an I-beam as drawn in figure 4.22 on page 75. The discretisations of the cross section can be seen in figure 6.6.

The material properties are (isotropic material) $E_x = 210000/1.1 \ \frac{\text{MN}}{\text{m}^2}$ and $\nu = 0.2963$, thus $G = 73636 \ \frac{\text{MN}}{\text{m}^2}$.

6.1.2.2 Results (fork bearing at $x = 0$), Pure *de St.-Venant* Torsion

The torsional resistance can be computed as depicted in appendix A.5.1: $GI_t = 36.7 \cdot 10^{-3}$ MNm^2. Since the ideal case of uniform torsion is fulfilled the exact solution for the rotation at the tip is given by

$$\underline{\varphi}_x = \frac{0.8 \cdot 3.0}{33.33 \cdot 10^{-3}} = 72.0 \text{ mrad.} \tag{6.3}$$

Results for different models can be seen from table 6.1. The number of DOFs refers to a uniform lengthwise division into 20 elements for all models. Of course this number can be
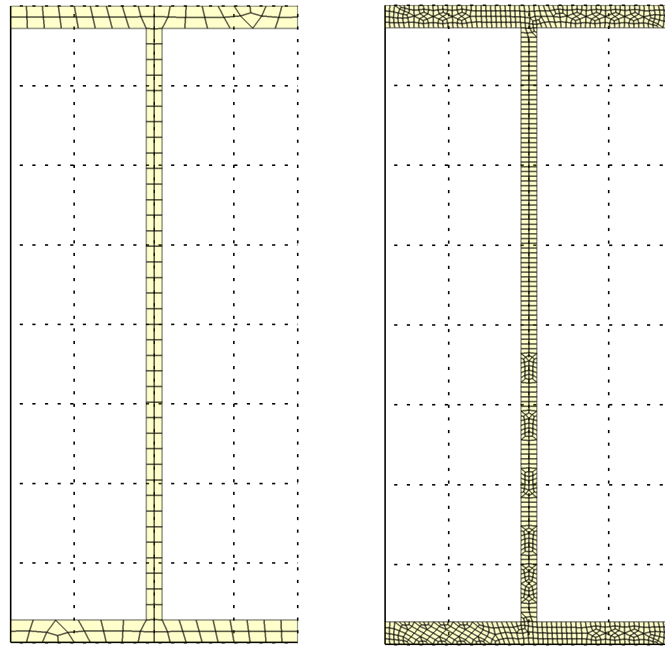
Figure 6.6: Coarse (left) and fine (right) discretisation of the cross section.

Table 6.1: Results for the rotation at the tip $[\mathrm{mrad}]$ for pure *de St.-Venant* torsion

Name	Eigenmodes membrane	Eigenmodes bending	Shearwarp shapes	High order warp shapes	# DOFs (approx.)	φ_x at tip
Beam model (exact)					140	72.0
shell model [Katz 2011]					3600	98.4
volume model					64700	72.2
ab_10_coarse	3	3	4	0	200	70.8
ab_50_coarse	23	3	4	20	1000	70.8
ab_10_fine	3	3	4	0	200	72.2
ab_50_fine	23	3	4	20	1000	72.2
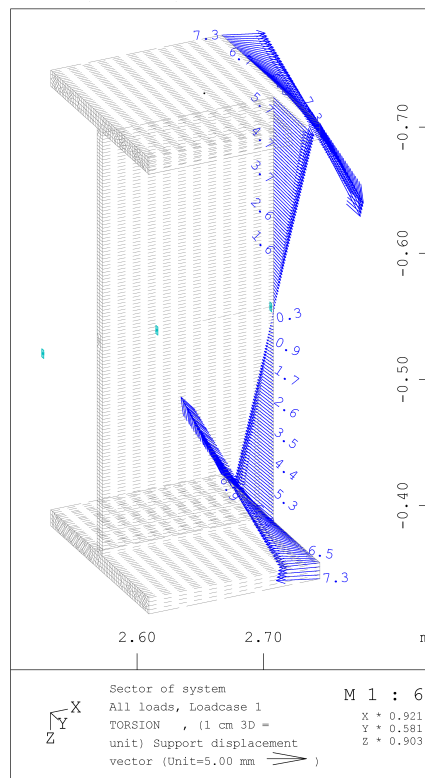
Figure 6.7: Load as a prescribed deflection applied at the tip of the volume model.

reduced significantly for most models if further insights (absense of shear force and warping torsion and reduction of dimension) are made use of.

One can see that all the results fit well with the exact solution except the shell model from [Katz 2011]. The reasons are given in that paper: drill moments are defined differently in plate theory than in beam theory. On thin-walled cross sections for *de St.-Venant* torsion the well known linear shear stress distribution over the thickness of the members only represents half of the torsional moment (force pairs A in figure 6.7). The second half is "stored" in the free ends where the stresses cover a small area but have a big lever arm (force pairs B in figure 6.7). This part is not covered by the common plate theories.

The volume model was computed with the Finite Element package SOFiSTiK. In order to avoid local distortions of the cross section at the load application point, the system was "loaded" with a prescribed deflection (rotation about the centre of rotation at the tip, see figure 6.7). Afterwards, the stresses in the system were integrated to section forces. As expected the system behaves a little softer than the exact solution since non-conforming elements are used.

The results from the augmented beam model coincide very well. One can see that the
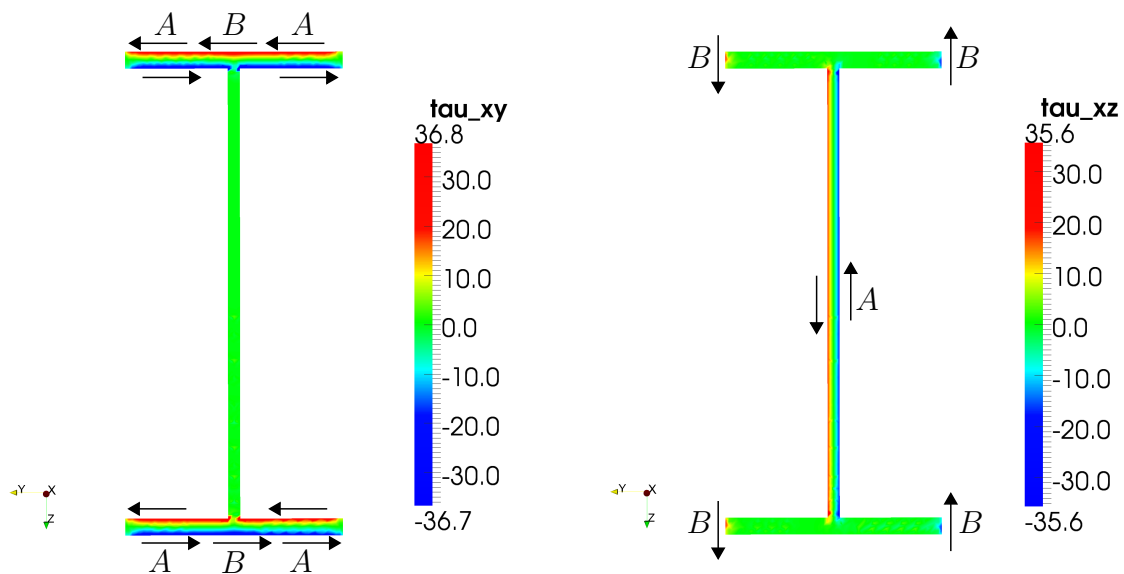
Figure 6.8: Shear stress distribution in $\frac{\text{MN}}{\text{m}^2}$ for pure *de St.-Venant* torsion. The arrows indicate local resultants.

warping degrees of freedom cover the deformation state well and additional unit deflection shapes are not necessary. The models "_coarse" and "_fine" just differ in the discretisation of the cross section (see figure 6.6).

The load was applied as a generalised load but both at the point of load application and on the support all deformations of the cross section except the uniform rotation about the centre of rotation were locked since otherwise additional deformations would occur and the system would behave even softer.

6.1.2.3 Results (clamped at $x = 0$), Warping Torsion

If the support node is not allowing for warping deformations warping torsion occurs which at this type of cross section decays very slowly with respect to x.

The results in table 6.2 show again a good accordance. The beam model is not a real reference solution any more due to the unavoidable presense of stiffening effects due to the *Poisson* ratio near the fixed support in all other models.

The presense of normal stresses makes the corresponding *Poisson* shapes necessary (see section 4.3.1).

One can see that again the deformation state is covered well by the 17 DOFs present in the models ab_17_. Additional shapes contribute only little.

Table 6.2: Results for the rotation at the tip [mrad] for warping torsion.

Name	Eigenmodes membrane	Eigenmodes bending	Shear warp shapes	High order warp shapes	*Poisson* shapes	# DOFs (approx.)	$\underline{\varphi}_x$ at tip
Beam model						140	30.4
shell model [Katz 2011]						3600	37.2
volume model						64700	33.3
ab_17_coarse	3	3	4	0	7	340	33.0
ab_57_coarse	23	3	4	20	7	1140	33.1
ab_17_fine	3	3	4	0	7	340	33.3
ab_57_fine	23	3	4	20	7	1140	33.4
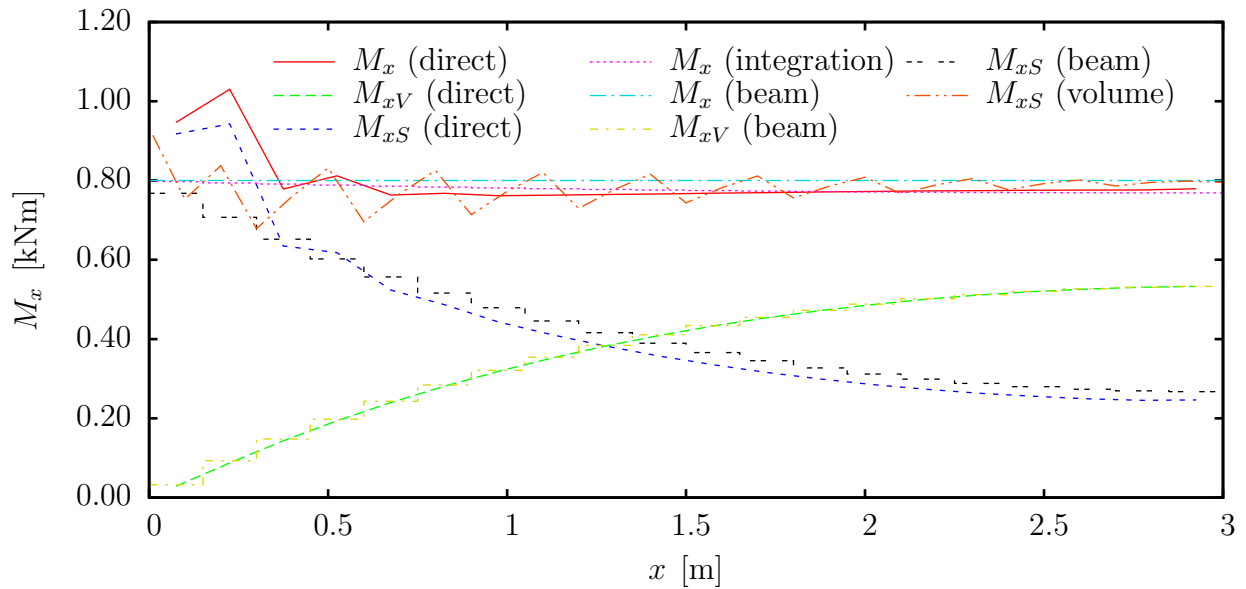
Figure 6.9: Results for the torsional moments of the model ab_57_fine together with reference models. "Direct" refers to the calculation procedure presented in section 5.5.4 using the primary variables $\underline{v}$, "integration" to the procedure performing an integration of stresses as explained in section 5.5.5. "Beam" refers to the standard SOFiSTiK beam model, "volume" to the Finite Element volume model which was evaluated with a spacial integration tool (SIR) which is part of SOFiSTiK.
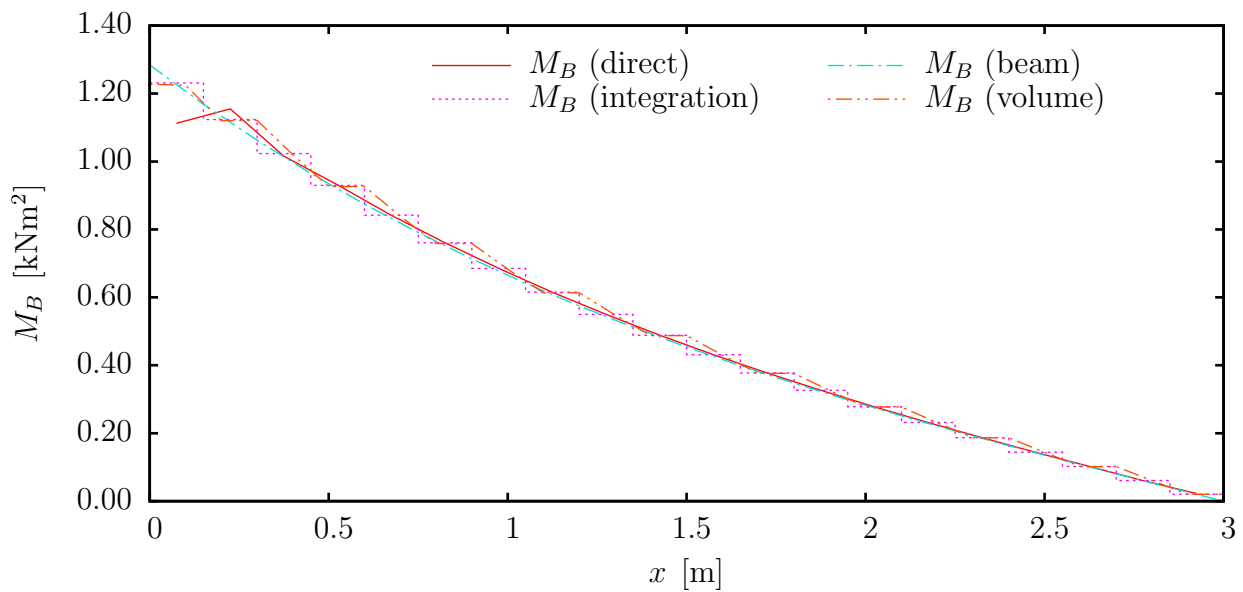
Figure 6.10: Results for the bimoment of the model ab_57_fine together with reference models. The namings correspond to those in figure 6.9.

The graph in figure 6.9 shows different evaluations of the torsional moment M_x for different models. What catches the eye is the fact that except the beam calculation all models have problems to obtain the correct solution. All procedures performing a spatial integration ("volume" and "integration") have accuracy problems. The integration in the augmented beam model benefits from the fact that the stress values are evaluated directly at the *Gauss* points of the underlying volume model. From there, the values for sectional forces are extrapolated to the beam nodes. Integration of stresses does generally not allow for a separation of *de St.-Venant* and secondary torsional moment.

The directly evaluated section forces according to section 5.5.4 show a different degree of accuracy. While the *de St.-Venant* component seems to be evaluated correctly the secondary torsional moment faces severe accuracy problems near the support at $x = 0$. This can be explained with the before mentioned stiffening of the system through *Poisson* effects near the clamped end. This can also be observed in figure 6.10 where the bimoment is plotted.

6.1.3 Example: Thin-Walled Structure

6.1.3.1 Problem Setup

This example treats a thin metal sheet structure. The system is clamped at $x = 0$ m and supported in y-direction at $x = 0.75$ m. Further dimensions and the load can be seen in figure 6.11. The material properties are $E = 210000 \frac{\text{MN}}{\text{m}^2}$ and $\nu = 0.2963$.

The reference model is a usual Finite Element model consisting of shell elements.
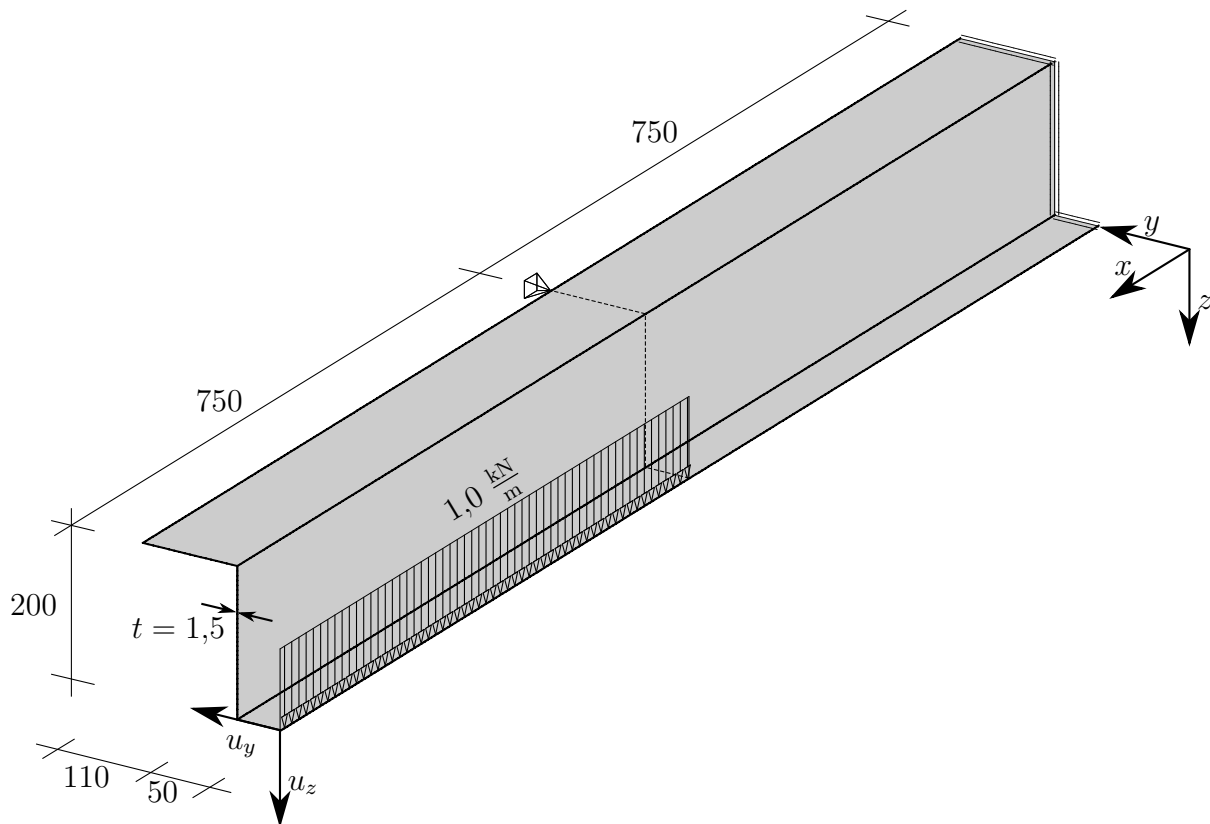
Figure 6.11: Thin-walled system with load

6.1.3.2 Results

The results for the deflection of the bottom front tip in the z- and y- direction can be seen in table 6.3.

The results show a good convergence of both depicted deformation values at the bottom front tip u_y and u_z. One can see that for u_y which is dominated by the rigid body deformations of the cross section (predominantly the rotation) and the stiffness properties at the supports

Table 6.3: Results for the deflection of the bottom front tip. The error in the last column as described in equation (5.44). The node at $x = 0$ is excluded from the error summation.

Name	Eigenm. membrane	Eigen. bending	Shearw. shapes	H. o. warp shapes	*Poisson* shapes	# beam elements	# DOFs (approx.)	u_y at tip [mm]	u_z at tip [mm]	Error [kN $\cdot 10^{-2}$]
shell model (reference)	-	-	-	-	-	-	102600	18.2	9.97	-
ab_17_20	3	3	4	0	7	20	340	17.81	6.65	3.02
ab_37a_20	13	13	4	0	7	20	740	17.9	9.54	9.03
ab_37b_20	13	3	4	10	7	20	740	17.9	9.90	8.46
ab_57b_20	23	3	4	20	7	20	1140	17.9	9.91	8.45
ab_107b_20	33	3	4	30	37	20	2140	17.9	9.93	3.00
ab_107c_20	23	33	4	20	27	20	2140	17.9	9.91	6.73
ab_17_100	3	3	4	0	7	100	1700	17.91	6.69	1.92
ab_37a_100	13	13	4	0	7	100	3700	18.06	9.62	4.18
ab_37b_100	13	3	4	10	7	100	3700	18.03	9.88	3.90
ab_57b_100	23	3	4	20	7	100	5700	18.07	9.89	3.89
ab_107b_100	33	3	4	30	37	100	10700	18.09	9.92	1.43
ab_107c_100	23	33	4	20	27	100	10700	18.08	9.89	3.12
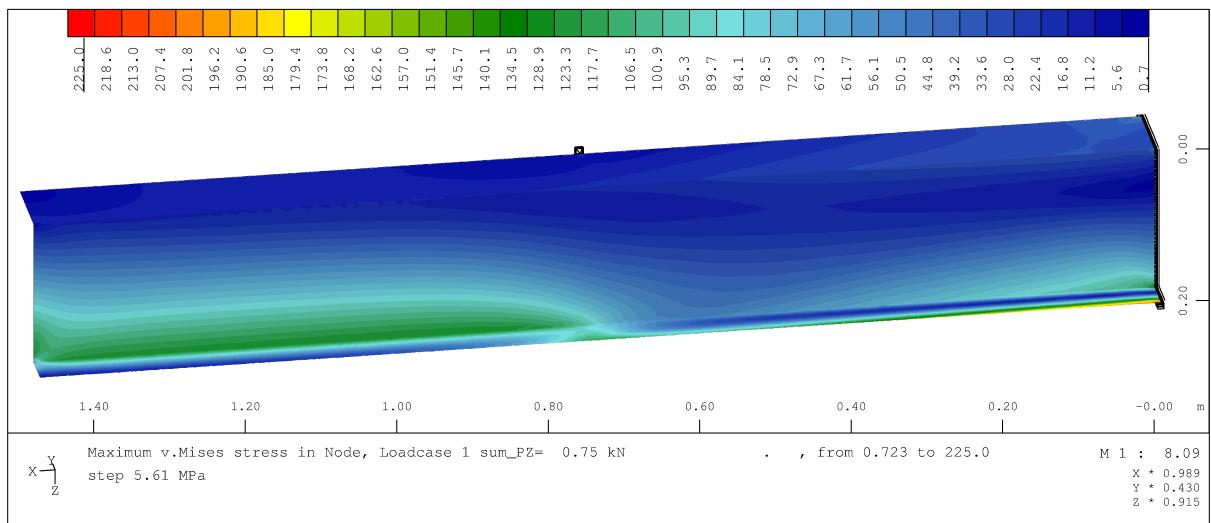
(a) Shell model (SOFiSTiK)
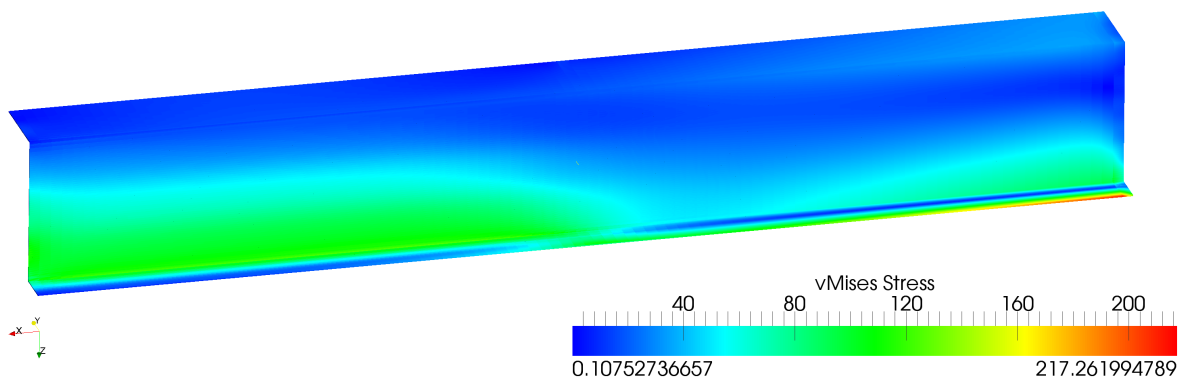
(b) Augmented beam model (ab_37b_100)

Figure 6.12: *Von Mises* stresses in the whole system for the reference model and one of the coarser augmented beam models.

the lengthwise discretisation is of higher importance than the number of additional deflection modes per beamnode. In contrast to that for the vertical deformation at the tip, the additional (distortion) modes play a very important role and the lengthwise discretisation is of subordinate importance.

The error force depicted in the last column of table 6.3 shows no clear convergence. The reason might be that both the load and the support in the middle represent singularities from the view of a cross sectional system.

The comparison of the *von Mises* stresses in the figures 6.12 and 6.13 shows very good accordance between the very fine discretised shell model and the comparably coarse augmented beam model.

(a) Shell model (SOFiSTiK)

(b) Augmented beam model (ab_37b_100)
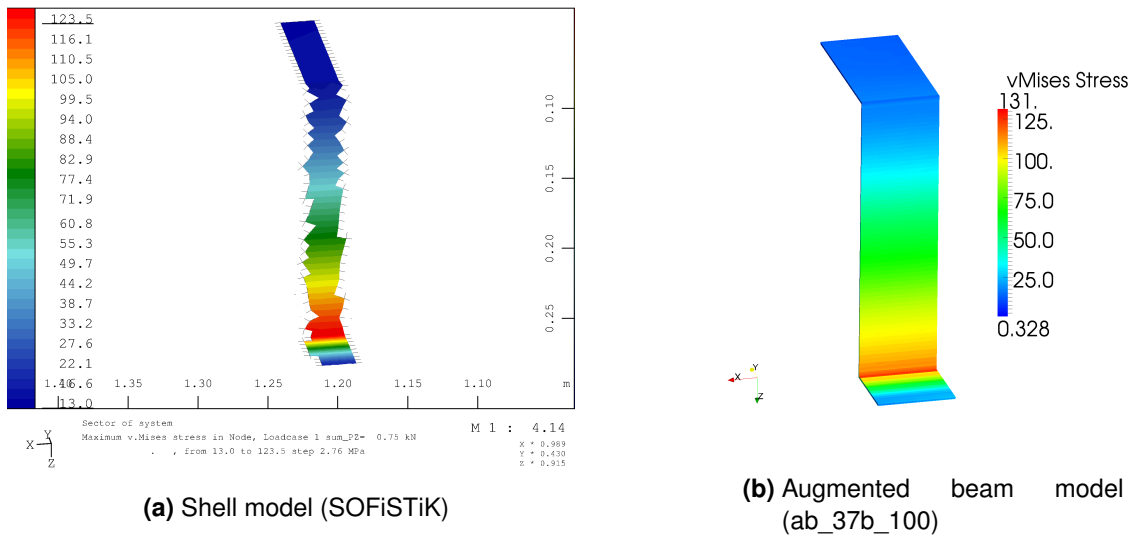
Figure 6.13: *Von Mises* stresses at $x = 1.2$ m for the reference model and one of the coarser augmented beam models.

As described in the remarks in section 5.5.4.3 the sectional forces based on the primary variables $\underline{v}$ yield results which are unfeasable. Especially the transverse forces are vulnerable and yield results ranging up to 1000 kN. In figure 6.14 only those sectional forces are plotted which are gained from the integration of stresses as described in section 5.5.5.
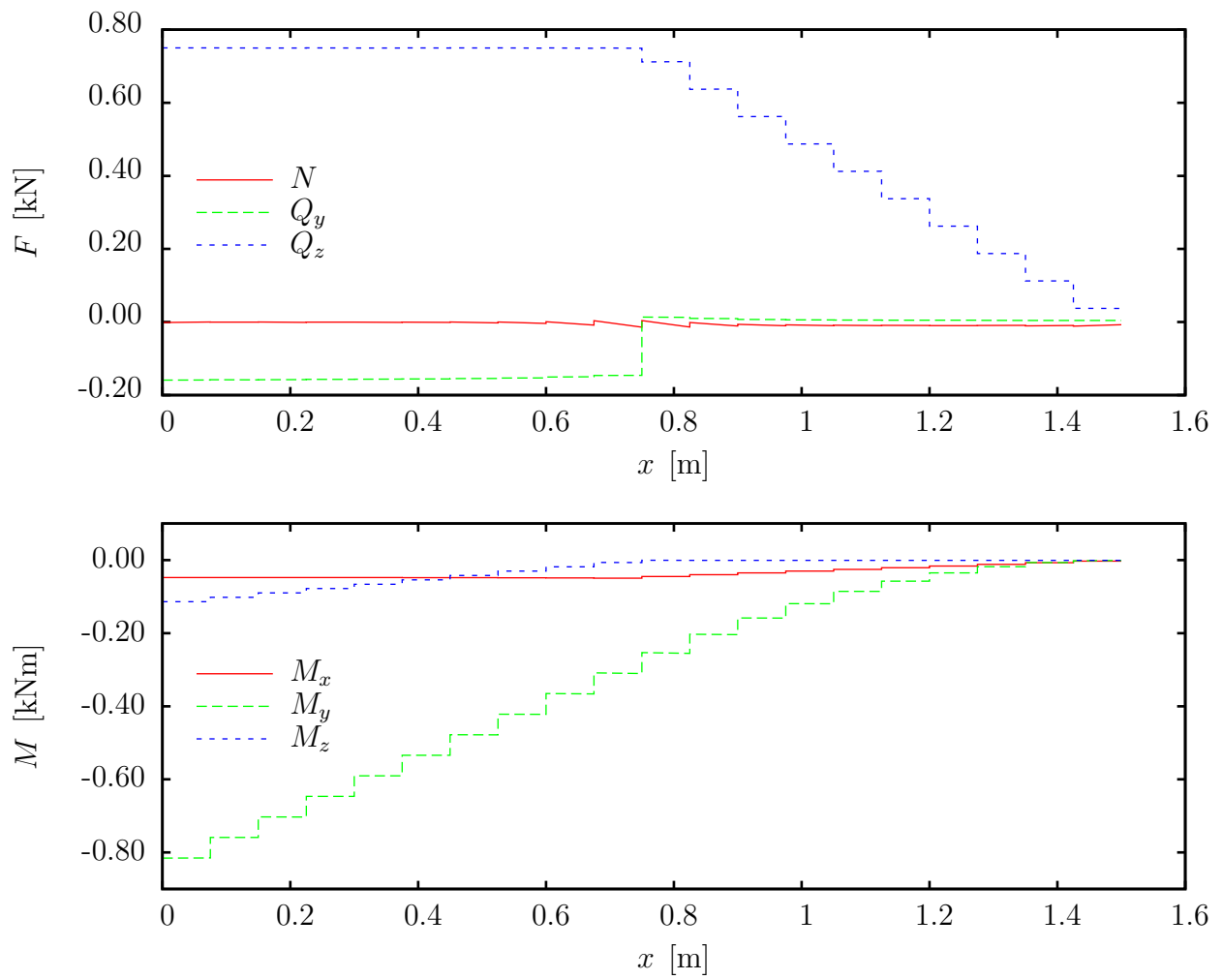
Figure 6.14: Section forces computed by integration (see section 5.5.5) for the model ab_107b_100.

6.2 Dynamic Calculations

6.2.1 Harmonic Analysis

[published in G. Müller and Kreutz 2013]

This example illustrates the properties of the method when it is used to solve dynamic steady state problems (see equation (5.14) on page 86). For this type of analysis also the FT-modes are applicable and are compared to different sets of conventional modes which were used in the previous examples.

6.2.1.1 Setup

The calculated system is a concrete cantilever (clamped at $x = 0$ m) with a line load applied at the tip (see figure 6.15). The dimensions of the cross section can be seen in figure 6.16.

Input values for the calculation:

- span of the beam: 15 m

- elastic modulus: $E = 28300\ \frac{\text{MN}}{\text{m}^2}$, $Poisson$-Ratio: $\nu = 0.2$, density: $\rho = 2500\frac{\text{kg}}{\text{m}^3}$

- load: $1\frac{\text{MN}}{\text{m}}$

The reference volume model is computed with the commercial Finite Element package AN-SYS using eight noded `solid185` elements with `KEYOPT(2)=2` (enhanced strain formulation) [see ANSYS, Inc. 2012].
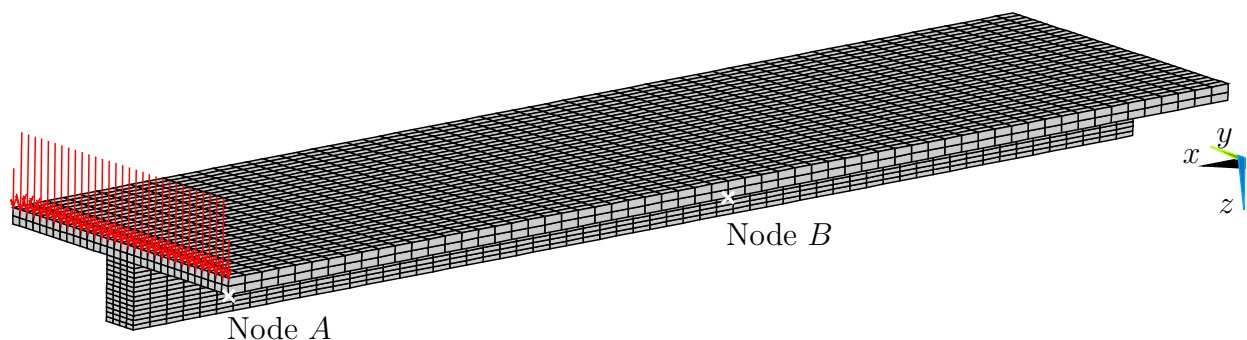
Figure 6.15: FEM model for the harmonic analysis with loading and location of the evaluation nodes A and B.
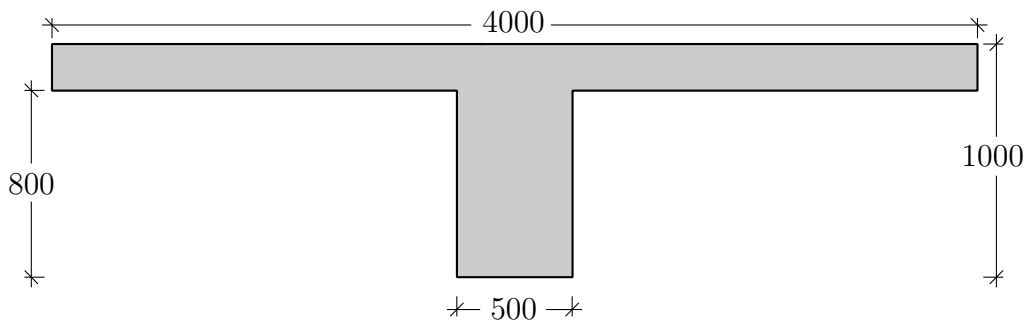
Figure 6.16: Cross section for the harmonic analysis example. Dimensions in mm.

Table 6.4: Configuration of different types of unit deflection shapes for the harmonic analysis.

Config.→	c22	c40	c184	ft22	ft40	ft184
Type						
Eigenmodes membrane	6	12	60	-	-	-
Eigenmodes bending	3	3	3	-	-	-
Shear warp shapes	4	4	4	-	-	-
High order shear warp shapes	3	9	57	-	-	-
Poisson shapes	6	12	60	-	-	-
FT-modes	-	-	-	22	40	184
Total	22	40	184	22	40	184

The frequency steps were chosen very small to be able to resolve the resonance peaks clearly. The beam model and the ANSYS volume model are discretised equally in all three dimensions as indicated in the figures 6.15 and 6.17.

The different combinations of types of unit deflection shapes for the beam model can be seen in table 6.4.

6.2.1.2 Results

Figures 6.18 and 6.19 show the results of the deflection for the different models at the nodes A and B depending on the frequency. The location of the nodes A and B can be seen in figure 6.15. The results for frequencies lower than 100 Hz fit very well and are thus not displayed.

The comparison to the results from ANSYS shows that all beam models behave too soft. This is a matter of the underlying brick element formulation (see section 5.3.1 and appendix A.2) and does not concern the presented method. The finest setup c184 is therefore taken as
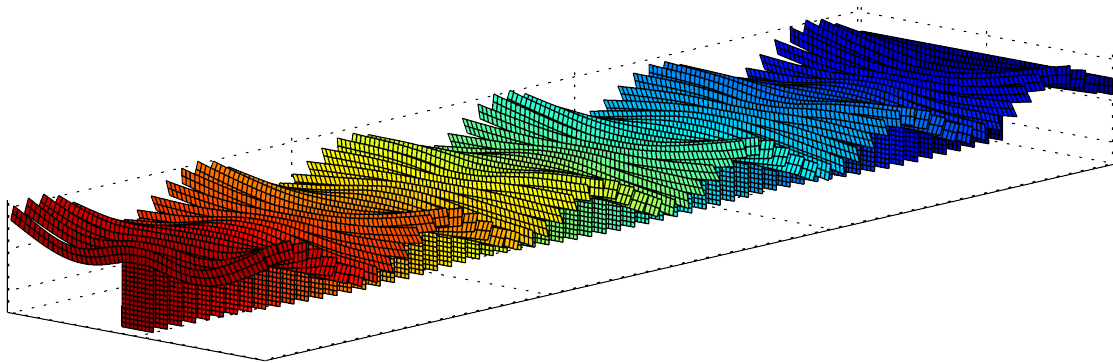
Figure 6.17: Deflection shape of the beam model c184 at $f = 190$ Hz

a reference. It fits very well with the corresponding finest setup using the FT modes ft184. The fact that the ANSYS curve fits apparently well with the results from the coarsest setup using conventional modes c22 is just by chance.

The coarsest setup using FT modes ft22 produces very good results for frequencies below 125 Hz from where on the results become very unstable.

The medium setups ft40 and c40 produce reliable results. Thereby ft40 shows a higher accuracy compared to c40.

The comparison of the figures 6.18 and 6.19 shows that the quality of the results does not depend significantly on the fact of whether or not the observed node is located near the boundary or point of load application as long as the load is not applied to a single section node.

Figure 6.20 shows a dispersion diagram. For every frequency the first 40 k_x eigenvalues are painted together with the information about the phase position $\arg(k_x)$: The x-component of the arrow indicates the relation of real part to the absolute value, the y-component indicates the relation of imaginary part to the absolute value. Multiple instances of k_x may lie on a specific point. It is important to mention that redundant figures are already erased from the set as explained in section 5.2.4. The area of the red semicircle indicates the amplification factor $\underline{v}$ of a real part of an eigenmode, and the green semicircle the amplification factor of the imaginary part. Both are averaged through the whole system (all beam nodes). Before the computation, all modes were normalised such that the maximum deflection equals 1.0. Furthermore, only relative participation factors are shown since the actual magnitude of the deflections may vary especially at resonance peaks (see figures 6.18 and 6.19).
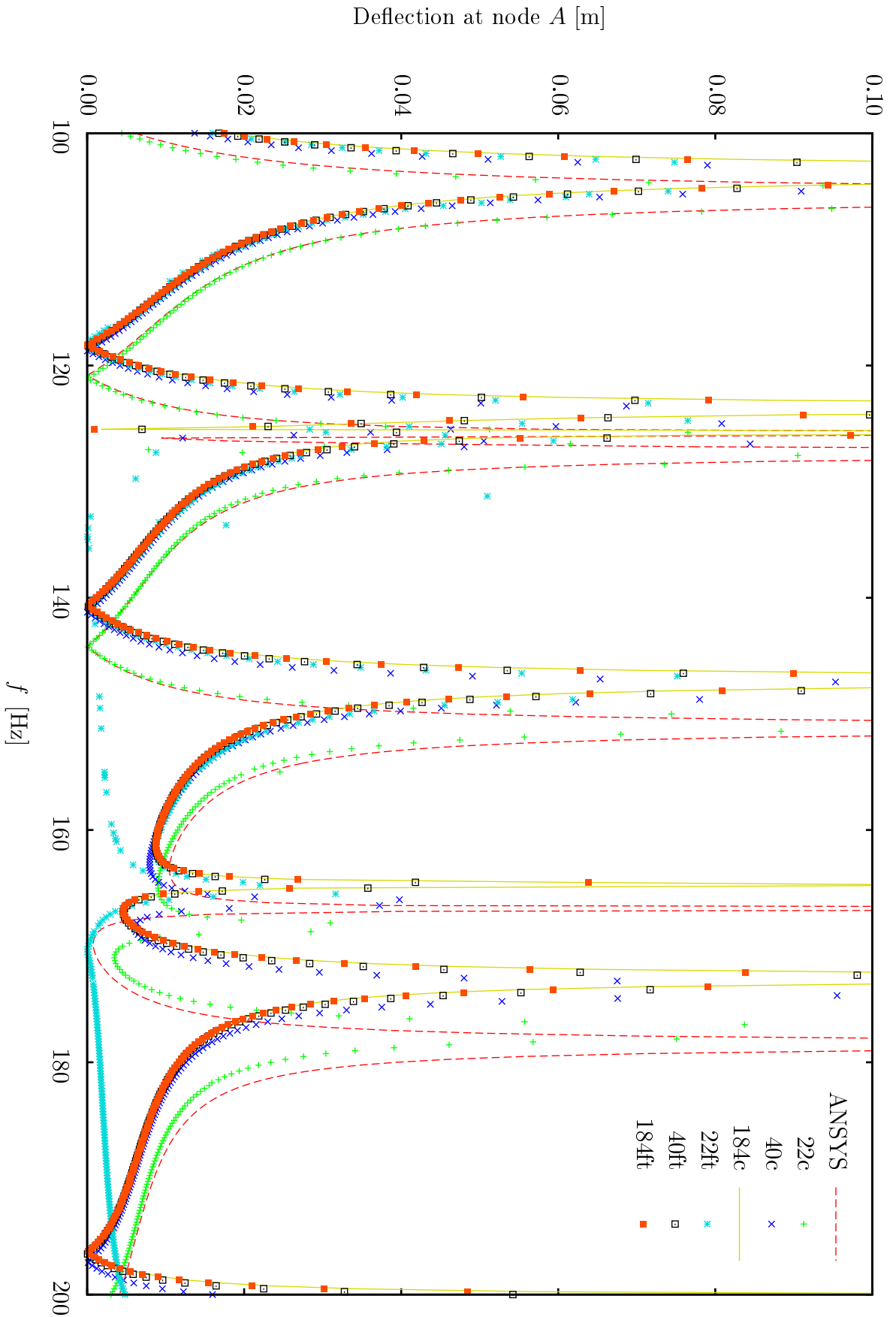
Figure 6.18: Results at node A for the harmonic example for different models.
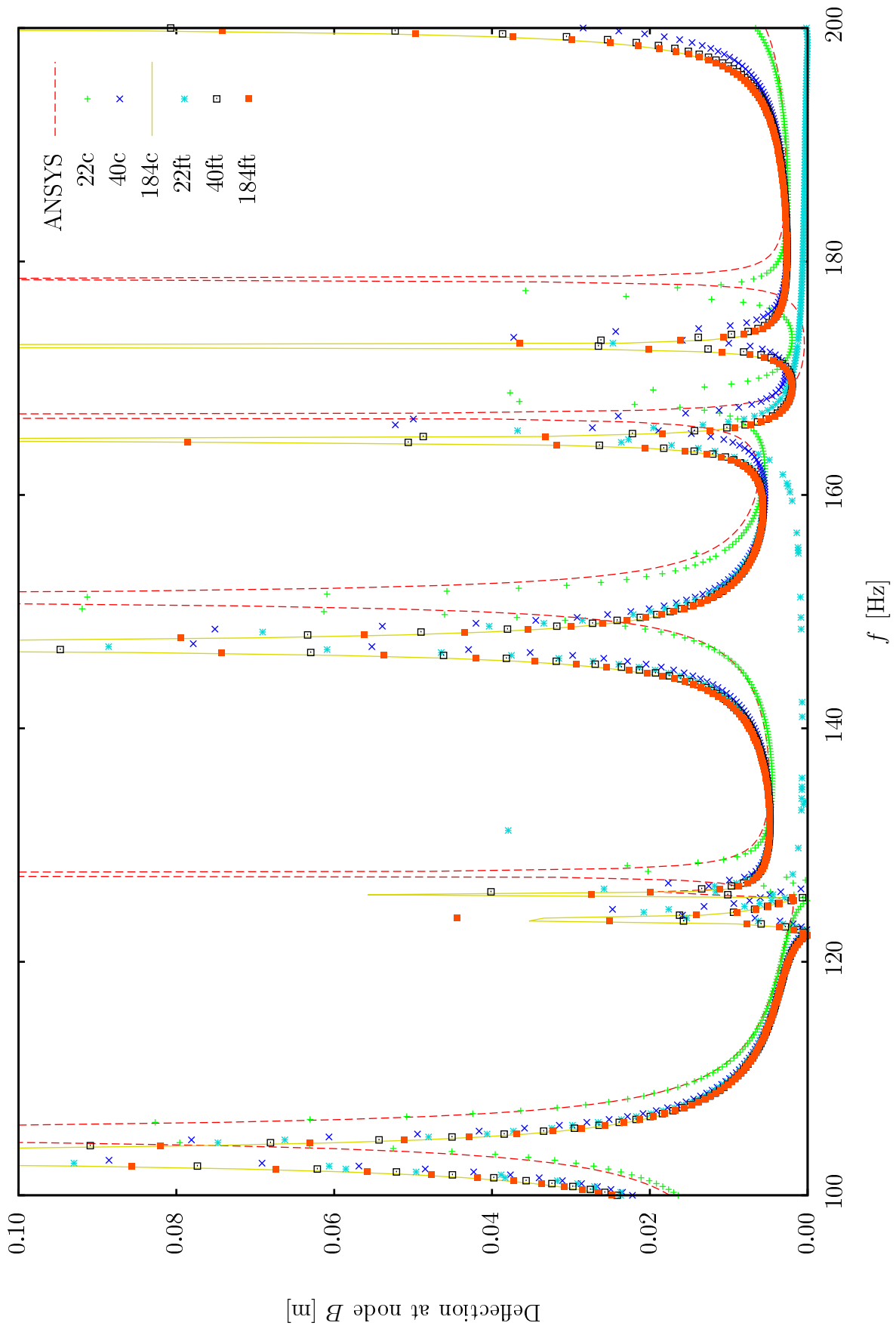
Figure 6.19: Results at node B for the harmonic example for different models.
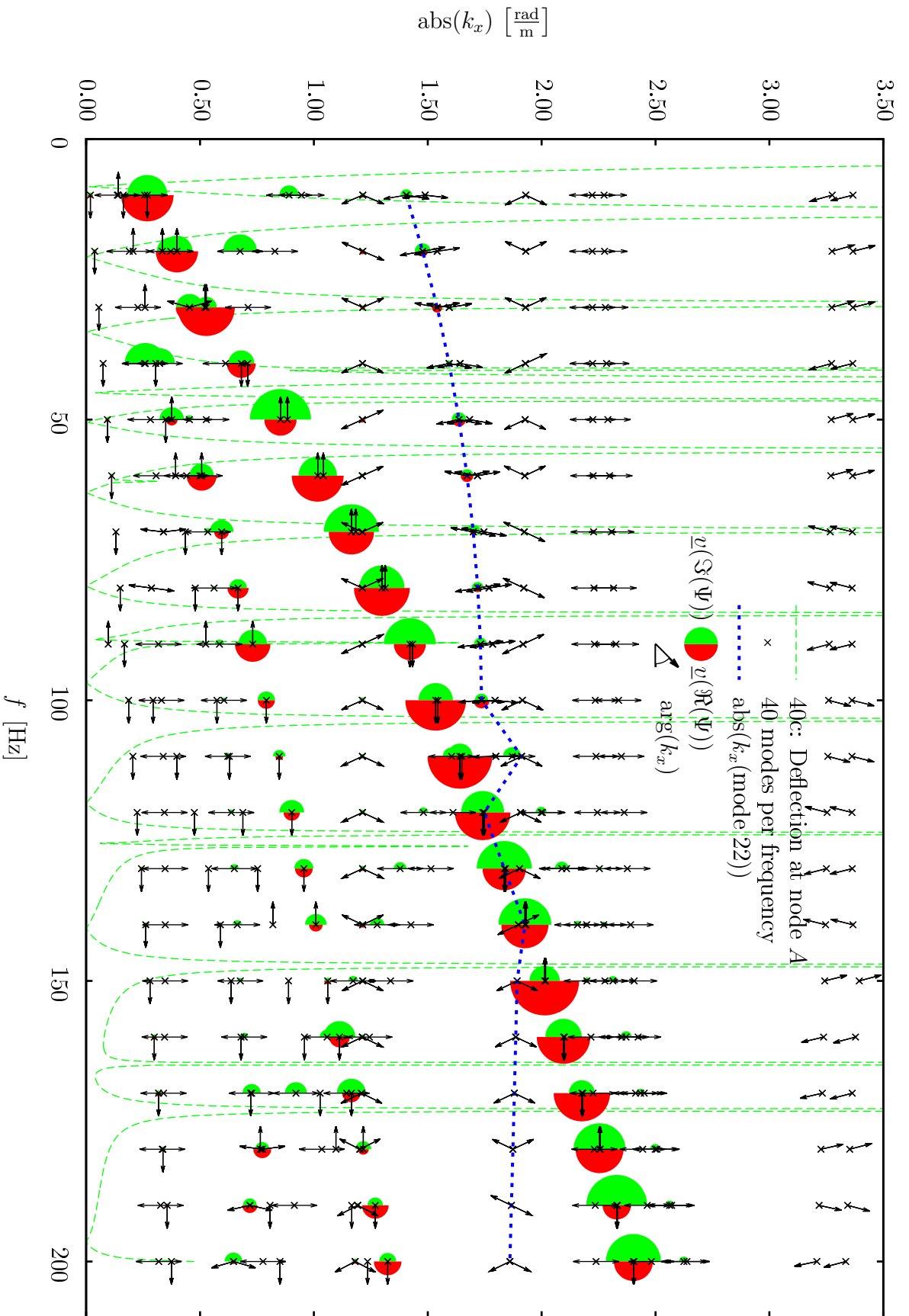
Figure 6.20: Participation factors $\underline{\upsilon}$ for different frequencies. The radius of the circles indicates the size of $\underline{\upsilon}$ for the real part (red) and imaginary part (green) of an eigenmode shape Ψ. The dashed line indicates the wave number k_x of the 22$^{\text{nd}}$ mode shape. The arrows indicate the phase position of k_x (real positive to the right, imaginary positive to the top).

Three important observations can be made from figure 6.20:

1. The reason why the setup ft22 from about 120 Hz on starts to produce defective results is that the dominant modeshape (big semicircles) at this frequency starts to exceed the threshould of the 22nd mode. This means that in ft22 it is not considered anymore. The reason for this "drift" is the fact that as explained in section 4.4.2 with increasing frequency more and more eigenmodes with a small wave number k_x occur. They are actually mode shapes where most of the strain energy is contained in strains deforming the cross section $(\varepsilon_y, \varepsilon_z, \gamma_{xy}, \gamma_{xz}$ and $\gamma_{yz})$.

2. Obviously in the observed range predominantly the modes which correspond to real eigenvalues k_x are of importance (arrows strictly horizontal).

3. One can see that very few shape functions cover the solution (big semicircles). This leads to the perception that the presented method enables for an even more effective description of the system if only those shapes are taken into account which are of importance. The prerequisite is an effective criterion or algorithm to identify these modes before the actual calculation is run.

Figure 6.21 shows some mode shapes $\boldsymbol{\psi}$ corresponding to f/k_x tuples. The red deflection shapes indicate the real part $\Re(\boldsymbol{\psi})$, the green shapes the imaginary part $\Im(\boldsymbol{\psi})$.

1.

$$k_x = 0.3988 - 0i\ \tfrac{\text{rad}}{\text{m}}$$
$$f = 20\ \text{Hz}$$

2.

$$k_x = -0.8112 - 3.2677i\ \tfrac{\text{rad}}{\text{m}}$$
$$f = 20\ \text{Hz}$$

3.

$$k_x = 2.2545 + 0i$$
$$f = 180\ \text{Hz}$$

4.

$$k_x = -0.099 - 0.7672i$$
$$f = 180\ \text{Hz}$$
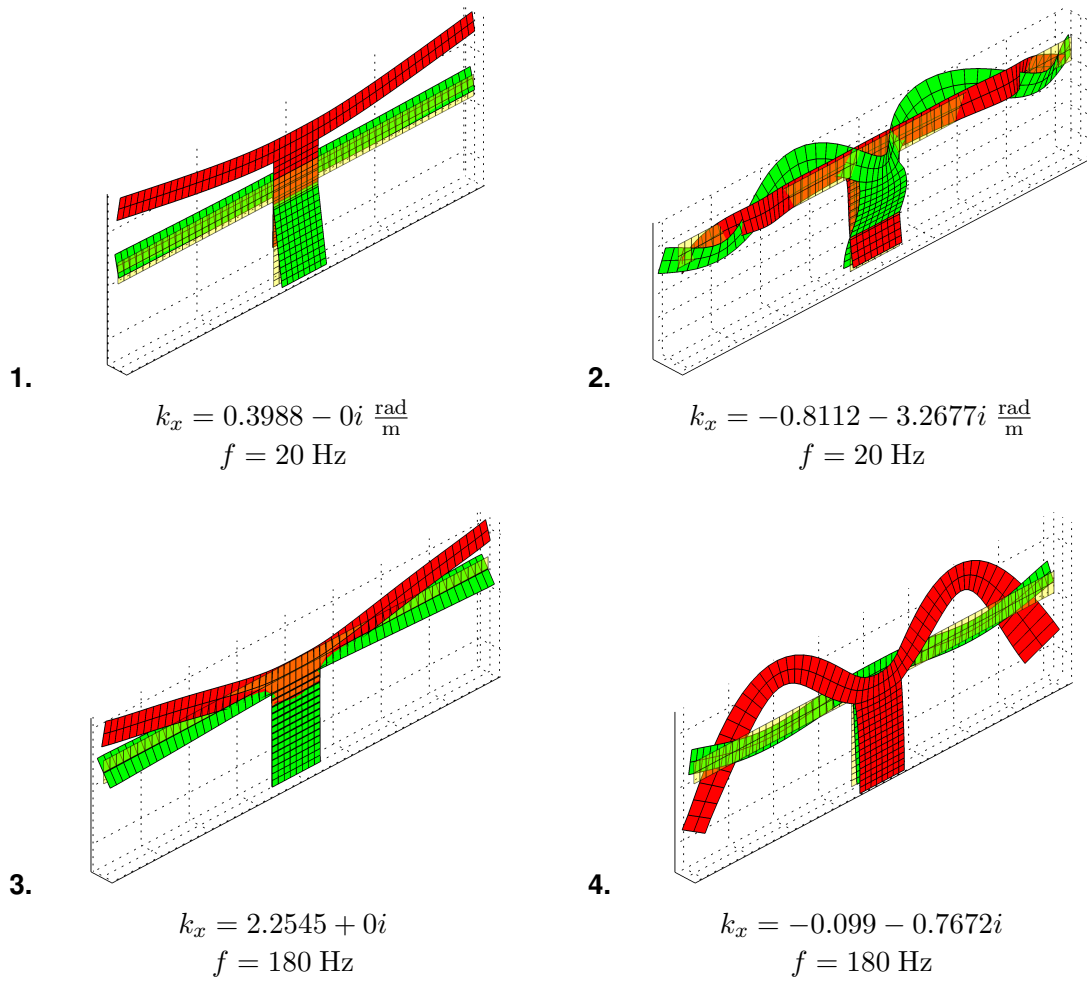
Figure 6.21: Chosen FT mode shapes for different k_x/f pairs. The corresponding participation factor can be seen in figure 6.20.

.

6.2.2 Eigenvalue Analysis

[published in Kreutz and G. Müller 2012]

In this example the presented method is used to calculate dynamic eigenmodes of a single span beam with the same t-beam cross section as in the previous example. Two calculations are run with different numbers of degrees of freedom. Additionally, two reference models were calculated using the commercial Finite Element package SOFiSTiK. One of them consists of standard, non conforming beam elements (see figure 6.22) and the other of volume elements (see figure 6.23).

6.2.2.1 Problem Setup

The material properties and dimensions are chosen equally to the previous example. The support conditions are applied as fork bearings on both ends and can be seen in figure 6.22. The configuration concerning the types of mode shapes can be seen from table 6.5.

Table 6.5: Configuration of different types of mode shapes for the eigenvalue analysis.

Type	Config. 1	Config 2
Eigenmodes membrane	5	30
Eigenmodes bending	3	5
Shearwarp shapes	4	4
High order shear warp shapes	2	27
Poisson shapes	6	30

6.2.2.2 Results

To provide a clear comparison only the eigenmodes for bending in the z-direction are listed.

Table 6.6 shows the results for the eigenfrequencies for a beam model, two different configurations of the presented method and the Finite Element volume model.

Table 6.6: Bending eigenvalues in the z-direction for different discretisations in [Hz]

nDOFs	#	Beam 210	Config. 1 643	Config. 2 2976	FEM 18778
	1	6.45	6.23	6.21	6.24
	2	25.75	21.67	21.28	21.57
	3	57.73	37.02	35.85	36.47
	4	102.09	49.80	47.89	48.54

One can observe that configuration 1 with 643 degrees of freedom improves the result from standard beam elements strongly. As in the preceding example, the reason for the fact that the values for configuration 2 are even lower than the volume model lies in different formulations of the non conforming volume element.

In figure 6.23 one can clearly see a wave pattern of bending and shear waves which could be directly made visible by means of a wave number approach in the longitudinal direction.
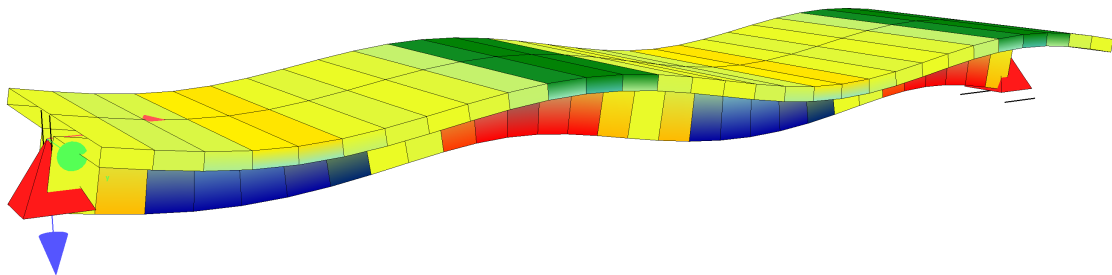
Figure 6.22: Deflection figure of the reference beam modell: 4th bending eigenmode in the z-direction at 102.09 Hz.
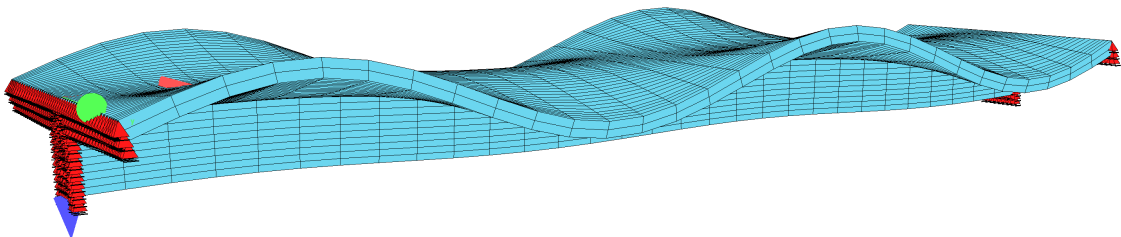
Figure 6.23: Deflection figure of the reference model (FEM): 4th bending eigenmode in the z-direction at 48.54 Hz.

7 Summary and Outlook

7.1 Summary

Beam-shaped structures represent an important field in engineering. Many cases exist still both in static and dynamic analysis where engineers are forced to use strongly simplified beam models due to the limits of computational power and modelling effort.

The presented method provides an efficient way of modelling line shaped structures both for static and dynamic problems. The models can be refined adaptively concerning support conditions and load distributions since both the load and the support conditions can be defined either on a basis of the generalised DOFs (coarse) or on a basis of the volume nodes (fine). In the scope of this thesis the method was restricted to geometrically and material linear, prismatic structures.

Fully three dimensional material laws can be used and thus as results, fully three dimensional stress and strain tensors are obtained. They can be computed efficiently into sectional forces. The shown examples of static problems illustrate that the method is able to produce results with a high accuracy but only needs few global degrees of freedom. It is generally possible to choose the amount of degrees of freedom according to the desired requirements of accuracy and other problem parameters like frequency. Of course the pre- and postprocessing is costly, but these processes are very well suited for parallelisation. The topology of the problem is substructured and leads to a small system of unknowns which can be solved very fast. These properties allow for massive performance gains on current and upcoming processor architectures.

The method might be of special interest for calculations in the field of structural dynamics since there not only the support conditions and the load may lead to the necessity of an enhanced beam model but also the frequency or the wavelength in the structure respectively (see e.g. the example in section 6.2.2).

Also bridge design implies problems where this method yields advantages. Shear lag effects are covered correctly and three dimensional effects like the lateral prestress of the top plate are introduced easily with small modelling effort.

7.2 Outlook

7.2.1 Mechanical Enhancements of the Cross Section and Element Formulation

7.2.1.1 Further Types of Unit Deflection Shapes

As mentioned, the presented choice of types of unit deflection shapes in not universally valid. Further types are conceivable. A specific lack can be identified: The information of the location and amount of load application is not made use of. The same holds for support locations. One could imagine unit deflection shapes which cover especially the deformations occurring at load application points and supports.

Secondly, an efficient adaptive (iterative) procedure could be established by using the error forces derived in section 5.6 for the computation of new deflection shapes. In-plane and warping deflections would have to be considered separately. The global system of equations would have to be solved at least twice.

7.2.1.2 Enhancing the Cross Section

The shown functionalities can be enhanced directly to composite sections and sections containing further types of "features":

- elastic shear gaps as they occur especially in compound timber-concrete structures

- elastic gaps in lateral directions

- singular longitudinal stiffnesses for modelling reinforcement bars.
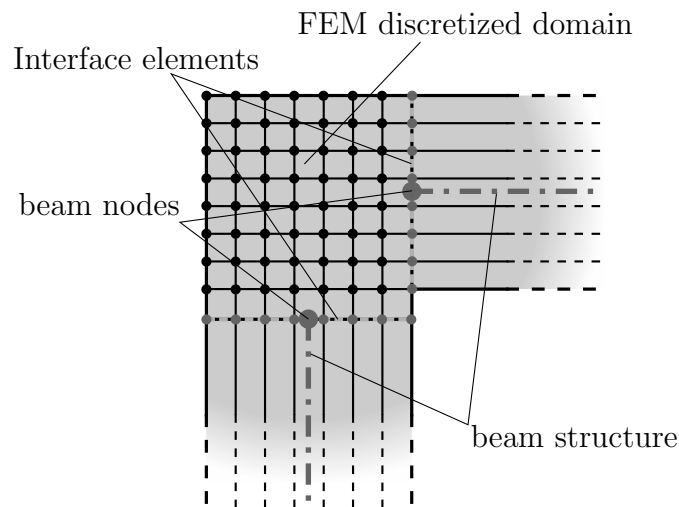
Figure 7.1: FEM discretisation of a joint of two beam elements.

7.2.1.3 Theory of Second Order and Stability Analysis

The presented approach could be extended by the terms of Theory of Second Order on the basis of the implemented volume elements. The obtained implementation would also serve for first order stability analysis (ultimate load analysis with a linear eigenvalue problem).

Implementing theories of higher order would require at least a separate treatment of the rigid body motions of the cross section especially of the rotations [see e.g. Živković et al. 2001]. [Sauer 1998] derives a geometrically nonlinear standard beam finite element for civil engineering purposes where only those rotation terms are included which are necessary in that context. These could be extended as shown in [Živković et al. 2001].

7.2.2 Joints and Interface Elements

The possible deformation figures of the presented approach are so general, that joints with different attached cross sections or corners cannot be modelled simply anymore either. To consider their behaviour correctly it is necessary to set up a volume model of the joint or corner and couple it correctly to the adjacent beams via interface elements as shown in figure 7.1. The "internal" DOFs of the joint can be eliminated by applying a superelement approach (static condensation). By that, only the generalised beam deformation shapes of the adjacent beams remain and the substructure character of the problem is preserved.

7.2.3 Spectral Element

The results from section 6.2.1 showed that the dynamic deflection shapes (FT modes) derived in section 4.4 are effective for describing dynamic waveguides of finite length. The procedure can be optimised making use of another piece of information contained in the eigenvalues k_x: the wavelength. Up to now (and thus also in the examples in section 6.2.1) just linear ansatz functions in longitudinal direction were used (disregarding the additional *Wilson* term, see appendix A.2). The idea of spectral elements is to use the (complex) *e*-functions (actual wave functions) at this point

$$\mathbf{u}(x) = \sum_{j=1}^{n_{\mathrm{modes}}} \left[\boldsymbol{\psi}_j(y,z) \cdot \underline{a}_j \cdot e^{ik_{xj}x} \right] . \tag{7.1}$$

Each "mode" then represents a wave travelling along the beam or a near field deflection shape respectively. The amplification factors corresponding to waves $\underline{a}_j$ need to be transformed into participation factors for deformation shapes at the ends of the beam domanin ($x = 0$ and $x = l$). [Koloušek 1973] and [Friberg 1985] do so. Problems may occur since not the full set of available modes shall be used here and the mentioned transformation may become under-determinate.

Alternatively, a BEM approach might be interesting. The mode shapes $\boldsymbol{\psi}_j(y,z)$ can be used as testing functions. The corresponding test-stresses t^* at the ends of the beam structure can be easily determined by evaluating equation (4.53). By that arbitrary boundary conditions can be applied at the ends and a transformation of the boundary conditions into the wave domain is not necessary.

Furthermore, especially figure 6.20 on page 124 shows that the global deflection shape of a prismatic structure can be covered very effectively by a small number of FT modes. The prerequisite is an significant criterion or algorithm to identify these modes before the actual calculation is run. This could be subject of further investigations. By this, the vulnerability of the FT mode sets arousing through modes with very small wave number occurring at higher frequencies could also be purged.

A Appendix - Further Applications and Theory

A.1 Shifted Eigenvalues

According to [Bathe 2002].

Given is the following eigenvalue problem

$$[K]\,\boldsymbol{\psi} = \lambda\,[M]\,\boldsymbol{\psi}. \tag{A.1.1}$$

By replacing $[K]$ with

$$\left[\hat{K}\right] = [K] - \rho\,[M] \tag{A.1.2}$$

yields a modified eigenvalue problem

$$\left[\hat{K}\right]\boldsymbol{\psi} = \mu\,[M]\,\boldsymbol{\psi}. \tag{A.1.3}$$

with the shifted eigenvalues

$$\mu = \lambda + \rho. \tag{A.1.4}$$

Shifting eigenvalues is often used to quickly find eigenvalues in a certain region. It can also be used when eigenvalues and eigenvectors of systems without supports have to be calculated.

A.2 Non-uniform quadratic extension for quadrilateral and hexahedral elements

[Bathe 2002], originally proposed by [Wilson et al. 1973].

A.2.1 Necessity of extensions

The simplest displacement based Finite Element is the isoparametric one where the deformations are interpolated with the same shape functions as the coordinates of the nodes. The conditions imposed are compatibility and completeness. Completeness means that the elements need to be able to represent a constant stress state as well as stress free rigid body motions. Compatibility means that the deformations must be continuous (not having any gaps) within the elements and across element interfaces. These two conditions are leading to monotonic convergence which means that the accuracy of the solution will always increase as the mesh is refined (subdivided). Isoparametric elements like the four-node quadrilateral fulfil these conditions, and furthermore, their derivation is straight forward. Nevertheless this element is prone to shear locking.

Practice often shows that satisfying results can be obtained from element formulations where the continuity requirements are violated. These elements are called incompatible or nonconforming elements. The elements can penetrate each other and gaps can occur. As a consequence, the calculated potential energy is not necessarily an upper bound to the exact one any more. The completeness condition must not be violated.

A.2.2 Derivation of the Element Stiffness Matrix

The procedure is shown by the example of a 2D quadrilateral plate element. It can be applied accordingly to different problems and also to 3D displacement based hexahedrals.
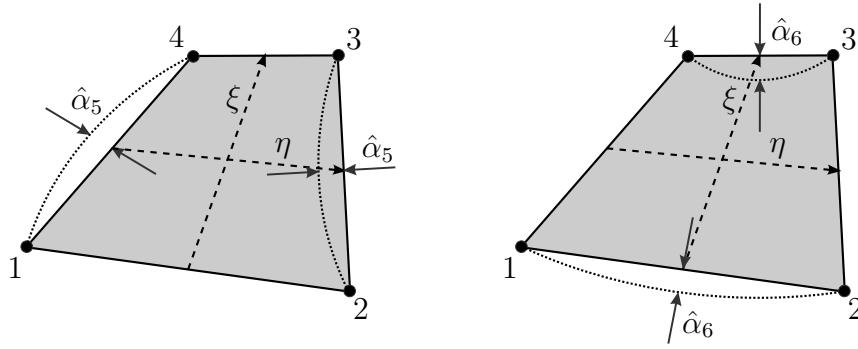
Figure A.1: Quadratic shape functions on the edges

The known shape functions for the corner nodes

$$
\begin{aligned}
N_1 &= \frac{1}{4}(1 - \xi) \cdot (1 - \eta) \\
N_2 &= \frac{1}{4}(1 - \xi) \cdot (1 + \eta) \\
N_3 &= \frac{1}{4}(1 + \xi) \cdot (1 + \eta) \\
N_4 &= \frac{1}{4}(1 + \xi) \cdot (1 - \eta)
\end{aligned}
\tag{A.2.1}
$$

are extended with quadratic functions which have their maximum at the centre of two opposing edges:

$$
\begin{aligned}
N_5 &= 1 - \xi^2 \\
N_6 &= 1 - \eta^2.
\end{aligned}
\tag{A.2.2}
$$

The displacements u_x and u_y are now represented by six shape functions each

$$
\begin{aligned}
u_x &= \sum_{i=1}^{4} N_i u_{xi} + \sum_{i=5}^{6} N_i \alpha_{xi} \\
u_y &= \sum_{i=1}^{4} N_i u_{yi} + \sum_{i=5}^{6} N_i \alpha_{yi}.
\end{aligned}
\tag{A.2.3}
$$

The vector of unknowns on element basis $[\hat{u}]^*$ can thus be written as

$$
[\hat{u}^*] = \begin{bmatrix} [\hat{u}] \\ [\hat{\alpha}] \end{bmatrix}
\tag{A.2.4}
$$

where the nodal deformations

$$[\hat{u}]^T = \begin{bmatrix} u_{x1} & u_{y1} & \dots & u_{x4} & u_{y4} \end{bmatrix} \tag{A.2.5}$$

are separated from the edge deformations

$$[\hat{\alpha}]^T = \begin{bmatrix} \alpha_{x1} & \alpha_{y1} & \alpha_{x2} & \alpha_{y2} \end{bmatrix}. \tag{A.2.6}$$

The strain tensor ε can be obtained through the compound $[B]$-matrix:

$$\varepsilon = \begin{bmatrix} [B] & [B_{\text{IC}}] \end{bmatrix} \begin{bmatrix} [\hat{u}] \\ [\hat{\alpha}] \end{bmatrix} \tag{A.2.7}$$

where the $[B]$-matrices look like

$$\begin{bmatrix} [B] & [B_{\text{IC}}] \end{bmatrix} = \begin{bmatrix} N_{1,x} & 0 & \cdots & N_{6,x} & 0 \\ 0 & N_{1,y} & \cdots & 0 & N_{6,y} \\ N_{1,x} & N_{1,y} & \cdots & N_{6,x} & N_{6,y} \end{bmatrix}. \tag{A.2.8}$$

$[B]$ represents the usual strain-displacement matrix and $[B_{\text{IC}}]$ the contribution of the incompatible modes. The weak equilibrium on element level can be established as

$$\begin{bmatrix} \left[\int\limits_{(V)} [B]^T [D] [B] \, dV \right] & \left[\int\limits_{(V)} [B]^T [D] [B_{\text{IC}}] \, dV \right] \\ \left[\int\limits_{(V)} [B_{\text{IC}}]^T [D] [B] \, dV \right] & \left[\int\limits_{(V)} [B_{\text{IC}}]^T [D] [B_{\text{IC}}] \, dV \right] \end{bmatrix} \begin{bmatrix} [\hat{u}] \\ [\hat{\alpha}] \end{bmatrix} = \begin{bmatrix} [P] \\ [0] \end{bmatrix} \tag{A.2.9}$$

$$[K_{\text{ext}}] [\hat{u}_{\text{ext}}] = \begin{bmatrix} [P] \\ [0] \end{bmatrix}$$

The second condition from above, the completeness, is seen to be indispensable. The reason is that when a Finite Element mesh is refined, the stress and strain state within each of the elements "converge" towards a constant one. Thus, an element has to be able to represent this state in order to enable the whole system to converge towards the exact solution. A benchmark to check for this behaviour is the so-called patch test. An arbitrary assemblage of elements is arranged such that it forms a geometry to which a constant stress condition is

applied externally via nodal loads or prescribed deformations. The stresses at the evaluation points inside each of the elements have to meet this value. Correctly formulated displacement based elements in compatible meshes always pass this test while elements like the one formulated before do not.

At the moment when the nodal deflections are the exact ones $[\hat{u}]^c$ which correspond to a constant stress state $\boldsymbol{\tau}^c$ we can say that

$$\int\limits_{(V)} [B_{IC}]^T [D] [B] \, dV \, [\hat{u}]^c = \int\limits_{(V)} [B_{IC}]^T \boldsymbol{\tau}^c dV. \tag{A.2.10}$$

Forcing the element to fulfil this for an arbitrary stress state $\boldsymbol{\tau}^c$ leads to

$$\int\limits_{(V)} [B_{IC}]^T \, dV \overset{!}{=} [0]. \tag{A.2.11}$$

Applying this to the contributions of the incompatible modes leads to

$$[B_{IC}^{\text{corr}}] = [B_{IC}] - \frac{1}{V} \int\limits_{(V)} [B_{IC}] \, dV. \tag{A.2.12}$$

The improved version of the element stiffness matrix from equation (A.2.9) is then obtained by using $[B_{IC}^{\text{corr}}]$ instead of $[B_{IC}]$.

$$[K_{\text{ext}}] = \begin{bmatrix} \underbrace{\int\limits_{(V)} [B]^T [D] [B] \, dV}_{[K_{uu}]} & \underbrace{\int\limits_{(V)} [B]^T [D] [B_{\text{IC}}^{\text{corr}}] \, dV}_{[K_{u\alpha}]} \\ \underbrace{\int\limits_{(V)} [B_{\text{IC}}^{\text{corr}}]^T [D] [B] \, dV}_{[K_{\alpha u}]} & \underbrace{\int\limits_{(V)} [B_{\text{IC}}^{\text{corr}}]^T [D] [B_{\text{IC}}^{\text{corr}}] \, dV}_{[K_{\alpha\alpha}]} \end{bmatrix} \tag{A.2.13}$$

A.2.2.1 Interpretation

By applying this scheme the element is forced to behave under a constant stress state like the compatible element. Setting $\hat{u} = [\hat{u}]^c$ and $[\hat{\alpha}] = [0]$ produces only forces $[P]$ according to the compatible modes and none according to the incompatible ones. The element in this case behaves as if the incompatible modes were not there.

A.2.2.2 Gaining an Element Stiffness Matrix

From this matrix $[K_{\text{ext}}]$ in equation (A.2.13) the entries corresponding to the extra degrees of freedom $[\hat{\alpha}]$ are removed by static condensation (*Gaussian* elimination). The corresponding entries of the load vector have to stay zero. By that the problem separates into two parts

$$[K_{\text{new}}]\,[\hat{u}] = [P] \tag{A.2.14}$$

$$[\hat{\alpha}] = [Q]\,[\hat{u}] \tag{A.2.15}$$

where the new stiffness matrix $[K_{\text{new}}]$ and the matrix $[Q]$ can be calculated out of the different components of the matrix $[K_{\text{ext}}]$ from equation (A.2.13)

$$[K_{\text{new}}] = [K_{uu}] - [K_{u\alpha}]\,[K_{\alpha\alpha}]^{-1}\,[K_{\alpha u}] \tag{A.2.16}$$

$$[Q] = -\,[K_{\alpha\alpha}]^{-1}\,[K_{\alpha u}]\,. \tag{A.2.17}$$

$[Q]$ is a matrix which is used to calculate the extra degrees of freedom from the nodal ones. It is needed for the postprocessing when strains and stresses are calculated from the deflection field using (A.2.7).

A.2.3 Example

The example is a cantilever with the following values:

- length/height/width: 4 m/1 m/1 m

- elastic modulus: $E = 28300\ \frac{\text{MN}}{\text{m}^2}$ *Poisson* ratio: $\nu = 0.2$

- load at the tip: $P = 1.0$ MN

Table A.1: Different Results for the deformation at the tip [mm].

Analytic result (*Euler-Bernoulli*)	9.046
FEM-system without extension	5.615
FEM-system with extension	9.229

The results can be seen in table A.2. As expected, the results for the system without the here presented extension shows severe locking. The system with extensions behaves weaker than the analytical result for two reasons: The analytical result is based on *Euler-Bernoulli*
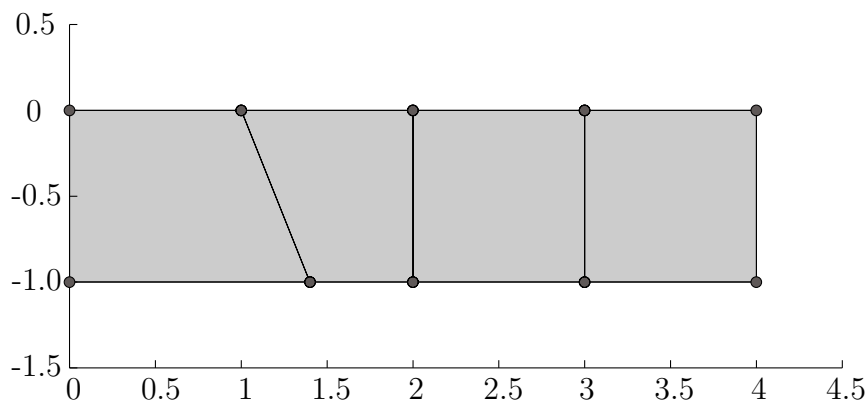
Figure A.2: Finite Element mesh for the cantilever test.

beam theory and does not include shear deformation. Secondly, the extensions made the element non-conforming meaning that the deformations of neighbouring elements do not coincide necessarily. Gaps may occur and the elements might penetrate each other. This sort of elements typically tends to behave "too soft" [Bathe 2002].

A.2.4 Application in this thesis

The derivation shown above was made for a two dimensional quadrilateral element. It can be applied analogously to three dimensional hexahedral elements. Quadrilateral elements were used to calculate the problems in the sections 4.1.1 and 4.3. The hexahedral elements were used to derive the beam element stiffness matrix in section 5.3.1.

A.3 SDOF Oscillator with Complex Stiffness in the Frequency domain

A.3.1 System and Differential Equations

The steady state response of a SDOF system under a harmonically oscillating load is evaluated. Two different systems are observed one with a real spring stiffness k and a damper resistance c the other with a complex spring stiffness

$$k_c = k \left(1 + i \operatorname{sgn}(\Omega) \cdot \eta^D\right) = k_r + i k_i. \tag{A.3.1}$$

η^D represents the damping ratio. The reason for the presence of the $\operatorname{sgn}(\Omega)$ is explained in [G. Müller 1989] and will become clear in the next section.
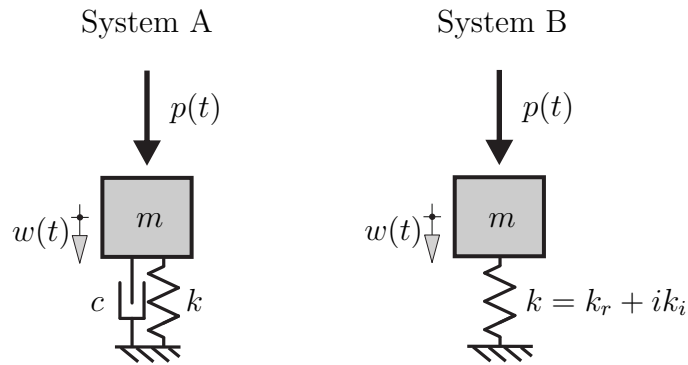
Figure A.3: SDOF Systems

The equation of motion, an ordinary 2nd differential equation (ODE)

$$m\ddot{w}\left(t\right) + c\dot{w}\left(t\right) + k\,w\left(t\right) = p\left(t\right) \quad \text{(System A)} \tag{A.3.2}$$

$$m\ddot{w}\left(t\right) + k_c\,w\left(t\right) = p\left(t\right) \quad \text{(System B)}. \tag{A.3.3}$$

is transformed into the *Fourier* domain and thereby simplified to an algebraic equation (AE)

for $\hat{w}(\Omega)$ [Buchschmid and G. Müller 2012]:

$$-\Omega^2 m\,\hat{w}(\Omega) + i\Omega c\,\hat{w}(\Omega) + k\,\hat{w}(\Omega) = \hat{p}(\Omega)$$
$$\left(-m\Omega^2 + i\Omega\,c + k\right)\hat{w}(\Omega) = \hat{p}(\Omega)$$

(System A)

$$-\Omega^2 m\,\hat{w}(\Omega) + k_c\,\hat{w}(\Omega) = \hat{p}(\Omega)$$
$$\left(-m\Omega^2 + (k_r + ik_i)\right)\hat{w}(\Omega) = \hat{p}(\Omega)$$

(System B).

From these, the solution can be computed as

$$\hat{w}(\Omega) = \frac{\hat{p}(\Omega)}{k - m\Omega^2 + i\Omega\,c} \qquad \text{(System A)} \qquad\qquad (A.3.4)$$

$$\hat{w}(\Omega) = \frac{\hat{p}(\Omega)}{k - m\Omega^2 + ik\,\mathrm{sgn}(\Omega)\cdot\eta^D} \quad \text{(System B).} \qquad (A.3.5)$$

A.3.2 Arbitrary Harmonic Load Case

An arbitrary harmonic load can be defined as

$$p(t) = A\sin(\Omega_0 t) + B\cos(\Omega_0 t). \qquad\qquad (A.3.6)$$

It is assumed that A, B, Ω_0 and t are real numbers. Furthermore, Ω_0 is assumed to be positive.

When equation (A.3.6) is transformed to the frequency domain it reads

$$\hat{p}(\Omega) = \pi\Big(+Ai\delta\left(\Omega + \Omega_0\right) - Ai\delta\left(\Omega - \Omega_0\right) + B\delta\left(\Omega - \Omega_0\right) + B\delta\left(\Omega + \Omega_0\right)\Big). \qquad (A.3.7)$$

A.3.2.1 Solution for System A

Introducing equation (A.3.7) to equation (A.3.4) and applying the IFT leads to

$$w(t) = \frac{\left(-iAk + iAm\Omega_0{}^2 + A\Omega_0 c - Bk + Bm\Omega_0{}^2 - iB\Omega_0 c\right)}{2\left(-k + m\Omega_0{}^2 + i\Omega_0 c\right)\left(k - m\Omega_0{}^2 + i\Omega_0 c\right)}e^{-i\Omega_0 t}$$
$$+ \frac{\left(iAk - iAm\Omega_0{}^2 + A\Omega_0 c - Bk + Bm\Omega_0{}^2 + iB\Omega_0 c\right)}{2\left(-k + m\Omega_0{}^2 + i\Omega_0 c\right)\left(k - m\Omega_0{}^2 + i\Omega_0 c\right)}e^{i\Omega_0 t} \quad (A.3.8)$$

The two expressions are conjugate and thus it follows that $\Im(w(t)) = 0$ and the real part can be reformulated as a term containing sin and cos:

$$w(t) = \underbrace{\frac{\left(Ak - Am\Omega_0{}^2 + B\Omega_0 c\right)}{k^2 - 2km\Omega_0{}^2 + m^2\Omega_0{}^4 + \Omega_0{}^2 c^2}}_{A^*} \sin\left(\Omega_0 t\right)$$

$$+ \underbrace{\frac{\left(Bk - Bm\Omega_0{}^2 - A\Omega_0 c\right)}{k^2 - 2km\Omega_0{}^2 + m^2\Omega_0{}^4 + \Omega_0{}^2 c^2}}_{B^*} \cos\left(\Omega_0 t\right). \quad \text{(A.3.9)}$$

From that, the amplitude $w_{\max}$ value of the oscillation $w(t)$ can be determined by

$$w_{\max} = \sqrt{A^{*2} + B^{*2}} = \sqrt{\frac{A^2 + B^2}{k^2 - 2km\Omega_0^2 + m^2\Omega_0^4 + \Omega_0^2 c^2}}. \quad \text{(A.3.10)}$$

A.3.2.2 Solution for System B

For the solution of system B equation (A.3.7) has to be introduced to equation (A.3.5). After applying the inverse *Fourier* transformation the solution reads

$$w(t) = \frac{\left(-iAk_r + Ak_i + iAm\Omega_0{}^2 - Bk_r - iBk_i + Bm\Omega_0{}^2\right)}{2\left(-k_r + ik_i + m\Omega_0{}^2\right)\left(k_r + ik_i - m\Omega_0{}^2\right)} e^{-i\Omega_0 t}$$

$$+ \frac{2\left(iAk_r + Ak_i - iAm\Omega_0{}^2 - Bk_r + iBk_i + Bm\Omega_0{}^2\right)}{\left(-k_r + ik_i + m\Omega_0{}^2\right)\left(k_r + ik_i - m\Omega_0{}^2\right)} e^{i\Omega_0 t}. \quad \text{(A.3.11)}$$

As above the two expressions are conjugate such that $\Im(w(t)) = 0$ and the real part can be reformulated as a term containing sin and cos

$$w(t) = \underbrace{\frac{\left(Ak_r - Am\Omega_0{}^2 + Bk_i\right)}{k_r{}^2 - 2k_r m\Omega_0{}^2 + m^2\Omega_0{}^4 + k_i{}^2}}_{A^*} \sin\left(\Omega_0 t\right)$$

$$+ \underbrace{\frac{\left(Bk_r - Bm\Omega_0{}^2 - Ak_i\right)}{k_r{}^2 - 2k_r m\Omega_0{}^2 + m^2\Omega_0{}^4 + k_i{}^2}}_{B^*} \cos\left(\Omega_0 t\right). \quad \text{(A.3.12)}$$

The oscillation's amplitude w_{max} can be computed as

$$w_{\mathrm{max}} = \sqrt{\frac{A^2 + B^2}{k_r{}^2 - 2k_r m\Omega_0{}^2 + m^2\Omega_0{}^4 + k_i{}^2}}. \tag{A.3.13}$$

A.4 Validation of the Fourier Transformed FEM Procedure From Section 4.4

A.4.1 Introduction

In this appendix, the program which implements the FEM procedure presented in section 4.4 is validated. The procedure is able to calculate structures of infinite extent in x-direction. The properties of the structure (cross section, material properties and support conditions) have to be stationary along x.

The chosen model is an infinite strip of concrete as depicted in figure A.4. It is loaded at the top with a constant line load $\hat{p} = -1 \cdot 10^{10} i \frac{\text{N}}{\text{m}^2}$ and fixed in all directions at the bottom.
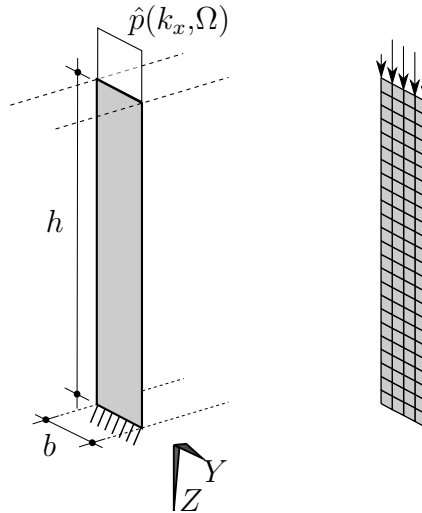
Figure A.4: 2D infinite structure: geometry and load

The wavelength $\lambda = \frac{2\pi}{k_x}$, the width and height of the problem are chosen such that the different directions interact in a measurable way. This is the case when all dimensions (including λ) are chosen within the same order of magnitude. The material constants are chosen as follows:

- $E = 34500 \cdot 10^6 \frac{\text{N}}{\text{m}^2}$ and $\nu = 0.2$

- $\rho = 2500 \frac{\text{kg}}{\text{m}^3}$.

The complex load $\hat{p}(k_x, \Omega)$ represents one *Fourier* coefficient corresponding to the wave number k_x and the angular frequency Ω. The real domain representation can be obtained by

$$p(x,t) = \Re\left(\hat{p}(k_x,\Omega) \cdot e^{ik_x x} \cdot e^{i\Omega t}\right). \tag{A.4.1}$$

The load will act in different directions as the following examples will explain.

A.4.2 Reference Model

The validation is done by comparing the results to those obtained from a prismatic Finite Element volume model with the length λ. λ thereby represents the wavelength or repetition length in the x-direction corresponding to the wave number k_x.
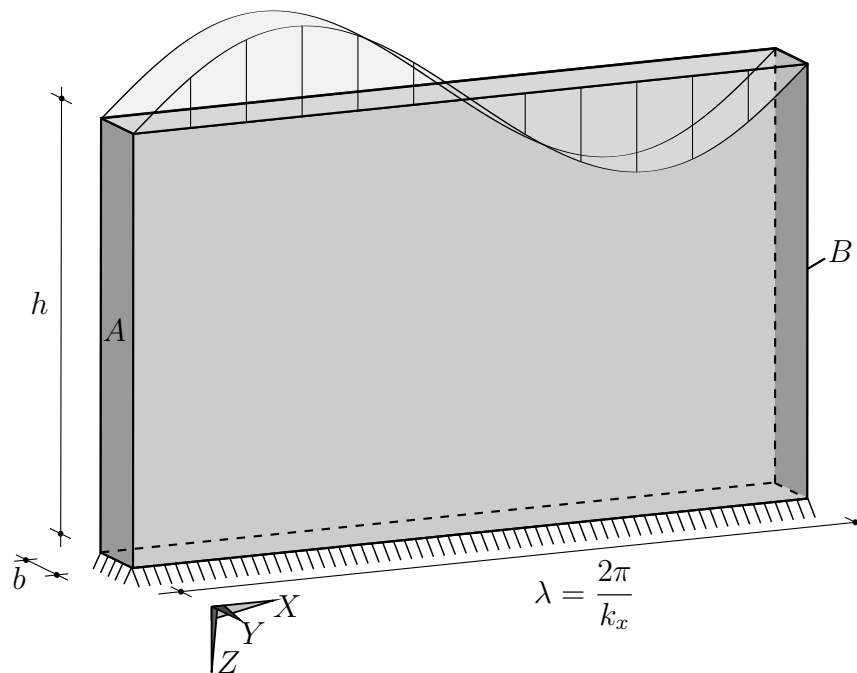
Figure A.5: Volume structure for the FEM calculation of an infinite structure.

The bottom surface is fixed in all directions. The surfaces A and B (see Figure A.5) are coupled such that all displacements on surface A equal those of surface B at the corresponding point.

$$\mathbf{u}_A(y,z) \overset{!}{=} \mathbf{u}_B(y,z). \tag{A.4.2}$$

The reference solution is calculated with the commercial FEM package ANSYS with a sufficient number of volume elements. The coupling of the deflections at the end surfaces is realised by a direct coupling of the nodal degrees of freedom of corresponding nodes.

A.4.3 Static Analysis with Loading in the z-Direction

A.4.3.1 Problem Setup

In the static analysis the angular frequency Ω is set to zero. The observed wave number $k_x = 2\pi \frac{\text{m}}{\text{rad}}$ such that the wavelength $\lambda = 1$ m. The lateral dimensions are $b = 0.1$ m and $h = 0.6$ m. The load will act in the positive z-direction.
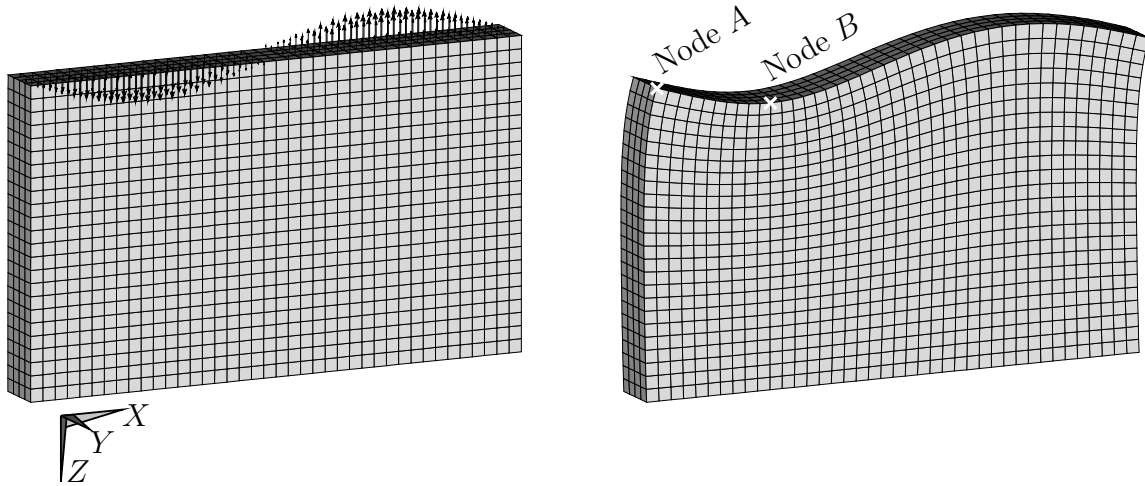
Figure A.6: Finite Element mesh with load graph and deflected structure for a sine load

A.4.3.2 Results

The results of the 2D Finite Element problem contain both real and imaginary parts. They both can be visualised as shown in figure A.7. The real part can be interpreted to represent the deflection at $(x = 0, t = 0)$, the imaginary part the deflection at $(x = \frac{\lambda}{4}, t = 0)$.
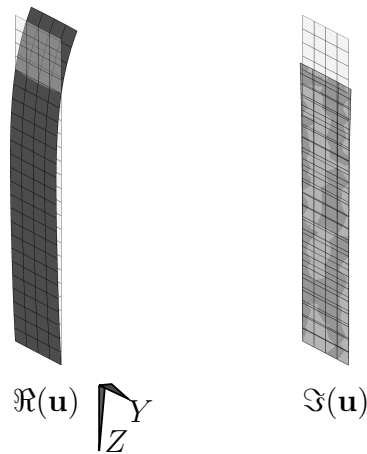
Figure A.7: 2D FEM solution real (left) and imaginary (right) part for $\hat{p}_z = 1 \cdot 10^{10} i \; \frac{\mathrm{N}}{\mathrm{m}^2}$ and $\Omega = 0 \; \frac{\mathrm{rad}}{\mathrm{s}}$.

Table A.2: Deflections $[\mathrm{m}]$ of the static analysis at selected points

Node / DOF	ANSYS	FT FEM
A / u_x	$0.3507 \cdot 10^{-1}$	$0.3494 \cdot 10^{-1}$
B / u_y	$0.5320 \cdot 10^{-2}$	$0.5617 \cdot 10^{-2}$
B / u_z	$0.9108 \cdot 10^{-1}$	$0.9093 \cdot 10^{-1}$

A.4.4 Dynamic Analysis

A.4.4.1 Problem Setup

The method is also capable of computing the particular solution for dynamic load cases. This is validated by the same load shape as depicted in the previous example with an additional time harmonic function (see equation (A.4.1)). The problem is evaluated within a frequency range from 1000 to 10000 Hz.

A.4.4.2 Results

The results can be observed in figure A.8. In general, one can observe a good compliance with the reference solution. In some cases this does not hold for the regions in the vicinity of resonances. This can be explained by the fact that no physical damping was introduced and
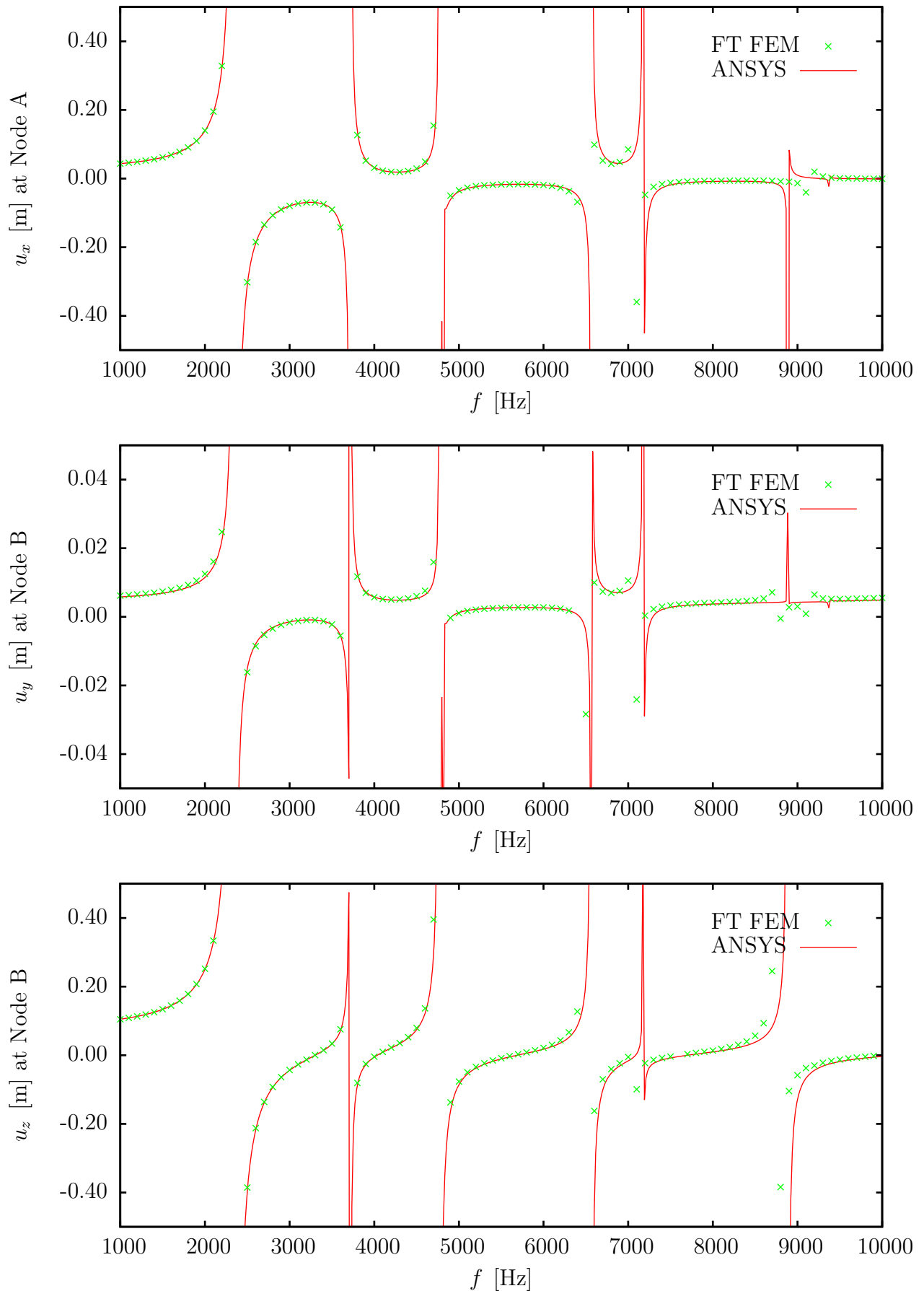
Figure A.8: Results of the frequency sweep for different characteristic directions and locations

thus the systems are very likely to become unstable close to resonances and small differences may cause huge effects.

$\Re(\mathbf{u})$ Y $\Im(\mathbf{u})$
         Z
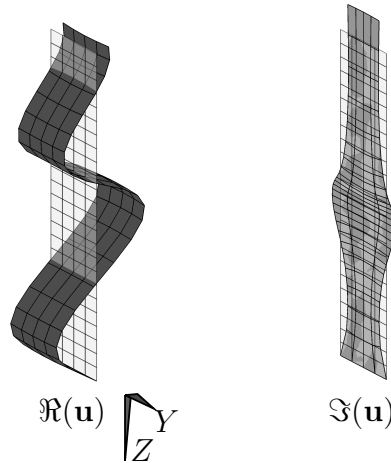
Figure A.9: 2D FEM solution real (left) and imaginary (right) part for $\hat{p}_z = 1 \cdot 10^{10} i \; \frac{\text{N}}{\text{m}^2}$ and $f = 8000$ Hz.

A.4.5 Static Analysis with Loading in the y-Direction

A.4.5.1 Problem Setup

Since the implementation of the observed element is following the isoparametric approach without any extensions or incompatibilities as e.g. shown in section A.2.3 it is conjecturable that the element is prone to shear and volumetric locking.

In order to observe that, the setup from above is modified, such that a slender system is subjected to a bending dominated stress state. The height of the structure is modified to 2 m and the wavelength λ is set to 10 m. The load is pointing in the y-direction.

A.4.5.2 Results

The reference calculation was done with different software packages and discretisations in order to ensure the correctness and illustrate the key issue.

Both the FT FEM element and the used ANSYS SOLID185 with the default `KEYOPT(2)=0` are prone to shear locking. Even the massive mesh refinement only leads to a poor convergence behaviour. The elements using enhanced strain formulations ANSYS SOLID185 with
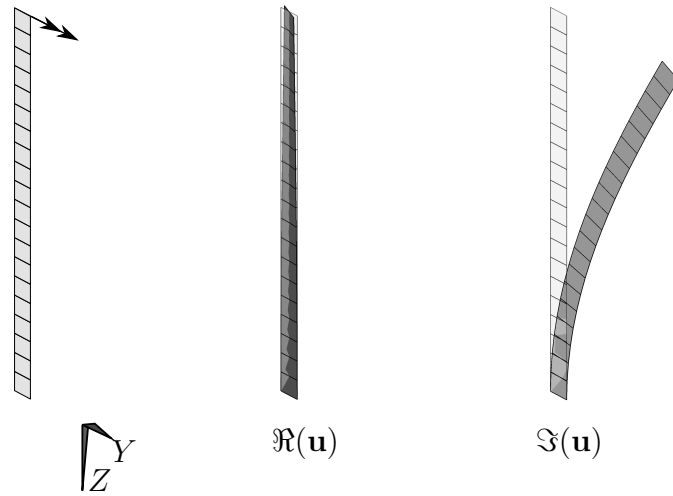
Figure A.10: 2D FEM model and load (left) solution real (middle) and imaginary (right) part for $\hat{p}_y = -1 \cdot 10^{10} i \ \frac{\mathrm{N}}{\mathrm{m}^2}$ and $f = 0$ Hz.

Table A.3: Deflections $[\mathrm{m}]$ of the static analysis at selected points

Software Package	FT FEM	ANSYS	ANSYS	ANSYS	ANSYS	SOFiSTiK
Discretisation $y \times z$	1×20	1×20	4×40	1×20	4×40	1×20
Options[1]	-	0	0	2	2	-
Node A / u_x	-10.549	-10.497	-10.111	-12.887	-12.842	-12.857
Node B / u_y	346.88	344.36	335.06	422.85	424.25	423.06
Node B / u_z	13.295	12.321	13.155	16.177	16.265	16.190

KEYOPT(2)=2 and the SOFiSTiK brick element produce good results also with the coarse mesh of 1×20 elements.

In order to use the validated element in stress states like in this example a different formulation like for example in section A.2 for ordinary shell elements should be implemented.

---

[1]The ANSYS SOLID185 element offers different element formulations which can be chosen with the option KEYOPT(2). KEYOPT(2)=0 is the default setting and leads to full integration with the b-bar method. KEYOPT(2)=2 leads to an enhanced strain formulation [ANSYS, Inc. 2012].

A.5 Calculation of Shear-Related Sectional Values

The warp shapes calculated in section 4.2.1 may be used to calculate the sectional values used in linear beam theory.

A.5.1 Torsional Stiffnesses

A.5.1.1 Torsion Constant

For the torsion constant GI_t different formulas exist using the warp shape ω_V calculated in section 4.2.1.2

$$GI_t = \int\limits_{(A)} G\left(\acute{y}^2 + \acute{z}^2 - {\omega_{V,y}}^2 - {\omega_{V,z}}^2\right)\, dA \qquad \text{[e.g. Katz 1986]} \qquad (A.5.1)$$

$$GI_t = \int\limits_{(A)} G\left((\omega_{V,z} + \acute{y})\,\acute{y} + (-\omega_{V,y} + \acute{z})\,\acute{z}\right)\, dA \qquad \text{[Bogensperger 2000; Kraus 2005]}.$$

$$(A.5.2)$$

$\acute{y} = y - y_M$ and $\acute{z} = z - z_M$ represent the coordinates with reference to the shear centre $(y_M; z_M)$.

Both representations (A.5.1) and (A.5.2) can be shown to be equivalent to a third more general one

$$GI_t = \int\limits_{(A)} \boldsymbol{\gamma}_V^T\, [D_\omega]\, \boldsymbol{\gamma}_V\, dA \qquad (A.5.3)$$

$[D_\omega]$ is explained in section 2.3.2.

$\boldsymbol{\gamma}_V$ represents the shear strain occurring due to torsion as a superposition of the uniform rotation about the centre of rotation and the corresponding warping deformation ω_V

$$\boldsymbol{\gamma}_V = \begin{bmatrix} \gamma_{Vy} \\ \gamma_{Vz} \end{bmatrix} = \begin{bmatrix} -\acute{z} + \omega_{V,y} \\ \acute{y} + \omega_{V,z} \end{bmatrix} \qquad (A.5.4)$$

For an isotropic material $[D_\omega]$ reduces to

$$[D_\omega] = \begin{bmatrix} G & 0 \\ 0 & G \end{bmatrix} \tag{A.5.5}$$

If equation (A.5.5) is introduced to equation (A.5.3) it yields

$$GI_t = \int\limits_{(A)} G\big(\acute{z}^2 - 2\acute{z}\omega_{V,y} + {\omega_{V,y}}^2 + \acute{y}^2 + 2\acute{y}\omega_{V,z} + {\omega_{V,z}}^2\big)\, dA. \tag{A.5.6}$$

It can be transferred into (A.5.2) by once and into (A.5.1) by twice substracting

$$GI_t = \int\limits_{(A)} \underbrace{G\big(-\acute{z}\omega_{V,y} + {\omega_{V,y}}^2\big)}_{\int\limits_{(A)} \tau_{Vy} w^*\, dA} + \underbrace{G\big(+\acute{y}\omega_{V,z} + {\omega_{V,z}}^2\big)}_{\int\limits_{(A)} \tau_{Vz} w^*\, dA}\, dA. \tag{A.5.7}$$

The terms $\int\limits_{(A)} \tau_{Vi} w^*\, dA$ can be seen as the weighted residual of the equlibrium in horizontal / vertical direction weighted with the (arbitrary) test function $w^* = \omega_{V,i}$. Since the shear stresses over the section fulfil this equilibrium the integrals yield zero and they can thus be added or subtracted arbitrarily.

A.5.1.2 Warping Resistance

The calculation of the warping resistance EI_ω or $EA_{\omega\omega}$ is straight forward using the warp shape ω_V calculated in section 4.2.1.2

$$EI_\omega = EA_{\omega\omega} = \int\limits_{(A)} E{\omega_V}^2\, dA. \tag{A.5.8}$$

A.5.2 Shear Stiffnesses and Shear Correction Factors

The stiffnesses for the transverse forces GA_{Sy}, GA_{Sz} needed for *Timoshenko* beam analysis can be calculated together with the shear stiffness for shear deformable warping torsion $GA_{S\omega}$. It is noteworthy that for a general section off-diagonal terms exist for all quantities mentioned here. The existence of the latter is not within the standard knowledge of engineers [Katz 2008].

The calculation concept shall be illustrated using the example of the shear stiffness GA_{Sy}. It is based on the principle of virtual forces stating equality of the virtual work performed by the stresses $([D_\omega] \cdot \boldsymbol{\gamma}(Q_y))$ on the corresponding virtual deflection field $(\boldsymbol{\delta\gamma}(Q_y))$ and the virtual work of the section force (Q_y) on the generalised deflection / rotation $(\frac{\delta Q_y}{GA_{Sy}})$

$$\int_{(A)} \boldsymbol{\delta\gamma}(\delta Q_y)^T \cdot [D_\omega] \cdot \boldsymbol{\gamma}(Q_y) \, dA \overset{!}{=} Q_y \cdot \frac{\delta Q_y}{GA_{Sy}}. \tag{A.5.9}$$

$\boldsymbol{\gamma}_y = \boldsymbol{\gamma}(Q_y = 1.0)$ is the shear strain distribution known directly from the postprocessing of the shear warp figures ω_{Si} calculated in section 4.2.3. $\boldsymbol{\delta\gamma}_y = \boldsymbol{\delta\gamma}(\delta Q_y = 1.0)$ is affine to it. One can thus set $Q_y = 1.0$ and $\delta Q_y = 1.0$ and obtain

$$\int_{(A)} \boldsymbol{\delta\gamma}_y^T \cdot [D_\omega] \cdot \boldsymbol{\gamma}_y \, dA \overset{!}{=} 1.0 \frac{1.0}{GA_{Sy}}. \tag{A.5.10}$$

The integral in equation (A.5.10) thus yields a flexibility instead of a stiffness. They can be transformed into each other by inversion.

As mentioned above the shear stiffnesses are coupled in the general case and so are the flexibilities. Using the shear strains $\boldsymbol{\gamma}_z = \boldsymbol{\gamma}(Q_z = 1.0)$, $\boldsymbol{\gamma}_\omega = \boldsymbol{\gamma}(M_{tS} = 1.0)$ and their virtual correspondants all entries of the flexibility matrix can be computed

$$[GA_{\text{inv}}] = \begin{bmatrix} \int_{(A)} \boldsymbol{\delta\gamma}_y^T \cdot [D_\omega] \cdot \boldsymbol{\gamma}_y \, dA & \int_{(A)} \boldsymbol{\delta\gamma}_y^T \cdot [D_\omega] \cdot \boldsymbol{\gamma}_z \, dA & \int_{(A)} \boldsymbol{\delta\gamma}_y^T \cdot [D_\omega] \cdot \boldsymbol{\gamma}_\omega \, dA \\ \int_{(A)} \boldsymbol{\delta\gamma}_z^T \cdot [D_\omega] \cdot \boldsymbol{\gamma}_y \, dA & \int_{(A)} \boldsymbol{\delta\gamma}_z^T \cdot [D_\omega] \cdot \boldsymbol{\gamma}_z \, dA & \int_{(A)} \boldsymbol{\delta\gamma}_z^T \cdot [D_\omega] \cdot \boldsymbol{\gamma}_\omega \, dA \\ \int_{(A)} \boldsymbol{\delta\gamma}_\omega^T \cdot [D_\omega] \cdot \boldsymbol{\gamma}_y \, dA & \int_{(A)} \boldsymbol{\delta\gamma}_\omega^T \cdot [D_\omega] \cdot \boldsymbol{\gamma}_z \, dA & \int_{(A)} \boldsymbol{\delta\gamma}_\omega^T \cdot [D_\omega] \cdot \boldsymbol{\gamma}_\omega \, dA \end{bmatrix}. \tag{A.5.11}$$

The results from equation (A.5.11) can also be used to calculate the so called shear correction factors for non-composite sections defined as

$$\kappa_i = \frac{GA_{Si}}{G \cdot A}. \tag{A.5.12}$$

B Appendix - Test Implementation

This appendix contains the implementation and application examples of a Finite Element for a cylindrical shell structure. The shell element is implemented using generalised (sinusoidal) ansatz functions for the discretisation in the lateral directions and linear shape functions for the longitudinal direction. The maximum degree (number of waves in circumferential direction) of the sinusoidal functions is variable and can be refined stepwise. By that, this implementation represents a test implementation for the method presented in this work. It shall determine and illustrate whether the idea of smooth generalised extended degrees of freedom is leading to good results. Similar calculations are e.g. done in [Cremer et al. 2010] and [Schardt 1989].

B.1 Derivation

B.1.1 Basics: *Hamilton*'s Principle

The derivation of the element matrices shall be done by making use of *Hamilton*'s principle. It says that from all possible motions of a system always the one really occur for which the difference between kinetic energy E_{kin} and potential Energy E_{pot} has a minimum within a time integral

$$\delta \int_{t_1}^{t_2} \left(E_{\mathrm{kin}} - E_{\mathrm{pot}} \right) dt + \int_{t_1}^{t_2} \delta W \, dt = 0. \tag{B.1.1}$$

W thereby represents the energy fed into the system from outside. By the help of ansatz- or shape functions the scalar quantities E_{kin}, E_{pot} and W are derived as functions of the discrete deflection values. By the help of variational calculus and assumptions or linearisations this principle can be transformed into a linear system of equations where the discrete deflection values are the unknowns.

B.1.2 Definition of the Degrees of Freedom

The continuum of the shell can theoretically perform arbitrary deflection shapes. Some assumptions about the ratio of thickness and radius and further simplifications allow to introduce five deflection quantities of the mid plane which are illustrated in figure B.1b:

η . . .   Deflection in the radial direction

ξ_M . . .   Deflection of the mid plane in the tangential direction

ζ_M . . .   Deflection of the mid plane in longitudinal

φ_ϑ . . .   Rotation about the longitudinal axis

φ_z . . .   Rotation about the tangential axis

(a) coordinates (local and global)   **(b)** deflections / rotations
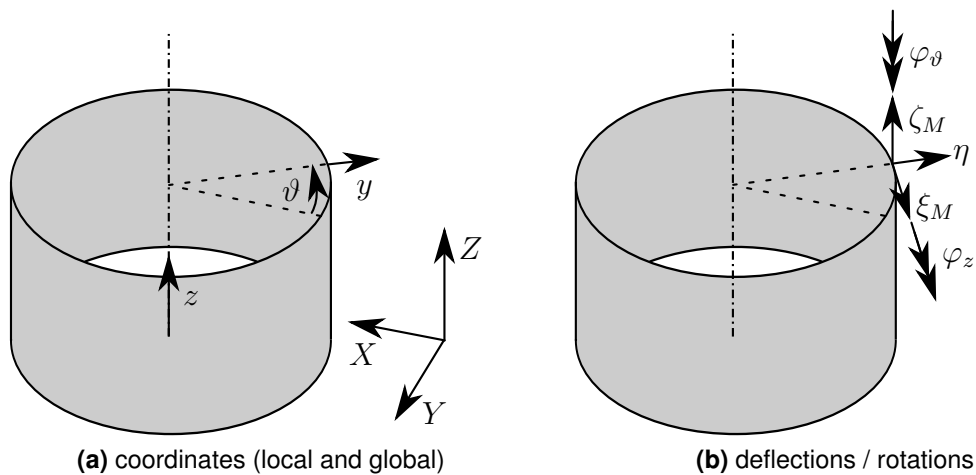
Figure B.1: Sign definitions

From these deflections and rotations and their derivatives with respect to the coordinates in the mid plane of the shell it is possible to derive five strain quantities [Cremer et al. 2010]:

$$\varepsilon_\vartheta = \frac{1}{a}\left(1 - \frac{y}{a}\right)\eta + \frac{1}{a}\frac{\partial \xi_M}{\partial \vartheta} + \frac{y}{a}\frac{\partial \varphi_\vartheta}{\partial \vartheta} \tag{B.1.2a}$$

$$\varepsilon_z = \frac{\partial \zeta_M}{\partial z} + y\frac{\partial \varphi_z}{\partial z} \tag{B.1.2b}$$

$$\gamma_{r\vartheta} = \left(1 - \frac{y}{a}\right)\varphi_\vartheta + \frac{1}{a}\left(1 - \frac{y}{a}\right)\frac{\partial \eta}{\partial \vartheta} \tag{B.1.2c}$$

$$\gamma_{rz} = \varphi_z + \frac{\partial \eta}{\partial z} \tag{B.1.2d}$$

$$\gamma_{z\vartheta} = \left(1 + \frac{y}{a}\right)\frac{\partial \xi_M}{\partial z} + y\frac{\partial \varphi_\vartheta}{\partial z} + \frac{1}{a}\left(1 - \frac{y}{a}\right)\frac{\partial \zeta_M}{\partial \vartheta} + \frac{y}{a}\frac{\partial \varphi_z}{\partial \vartheta}. \tag{B.1.2e}$$

Thereby terms containing y^2 were neglected. Furthermore, the radial derivatives of the quantities ξ_M and ζ_M were set to zero since the deflections of the mid plane are assumed to be constant over the whole thickness of the shell.

B.1.3 Shape Functions

The five deflections η, ξ_M, ζ_M, φ_ϑ and φ_z are interpolated within one element with the help of shape functions. Along the circumferential direction these shape functions shall be sinusoidal functions of variable order P depending on ϑ:

$$N_{\text{harm1}} = \sin(P\vartheta) \qquad \text{(B.1.3a)} \qquad N_{\text{harm2}} = \cos(P\vartheta) \qquad \text{(B.1.3b)}$$
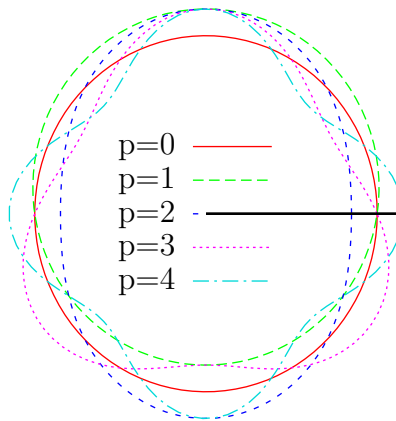
Figure B.2: Cosine shape functions in the circumferential direction for the radial deflection η.

This choice is in analogy to [Cremer et al. 2010] where the approach is used to calculate the sound radiation of an infinitely long cylindrical shell. Because of the fact that this thesis shall treat beam elements, an approach with a finite length is chosen. The shape functions in longitudinal direction shall be linear depending on z

$$N_{\text{lin}1} = 1 - \frac{z}{L} \quad \text{(Node 1)} \qquad \text{(B.1.4a)} \qquad N_{\text{lin}2} = \frac{z}{L} \quad \text{(Node 2).} \qquad \text{(B.1.4b)}$$

Multiplying all harmonic shape functions N_{harm} (for every P) with the linear function N_{lin} yields the two dimensional shape functions on the mid plane of the shell. The interpolated representation of every degree of freedom looks like the following

$$u(\vartheta, z) = \sum_{i=1}^{2} \sum_{j=1}^{2} \sum_{P=0}^{p} \Big(N_{\text{lin}i}(z) N_{\text{harm}j}(\vartheta \cdot P) \cdot \underline{u}_{ijP} \Big). \qquad \text{(B.1.5)}$$

u represents the variables η, ξ_M, ζ_M, φ_ϑ or φ_z. $\underline{u}_{ijP}$ are the discrete degrees of freedom of the system.

Figure B.3 exemplarily shows the shape functions of the deflection degrees of freedom at the "upper edge" of the element for $P = 1$ which means one sine or cosine wave in circumferential direction.

(a) ξ: tangential deflection   **(b)** η: radial deflection   **(c)** ζ: axial deflection
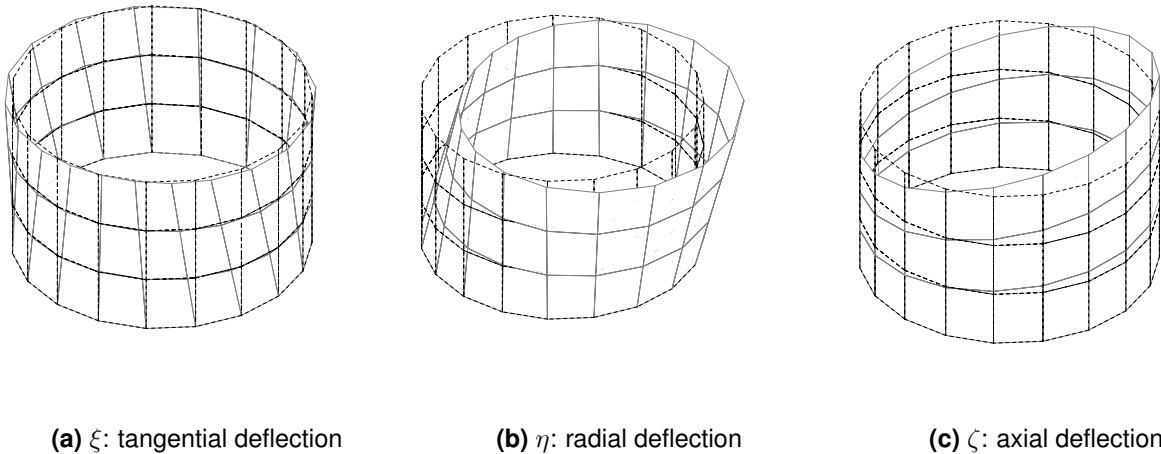
Figure B.3: Three DOFs of a cylindrical shell element for $P = 1$: The dashed lines show the undeformed geometry, the deformed geometry is outlined in grey.

If several of these elements are coupled in terms of the FEM then arbitrary, straight and prismatic pipes can be computed with increasing accuracy. If in the circumferential direction

enough sine and cosine shape functions are used then depending on the shape of the load a satisfying degree of accuracy is achieved.

B.1.4 Stiffness Matrix

The strains in the equations (B.1.2) allow to formulate the potential energy of the internal stresses of an element

$$
\begin{aligned}
E_{\text{pot}} &= \frac{1}{2} \int\limits_{(V)} \left(\boldsymbol{\sigma} \cdot \boldsymbol{\varepsilon} + \boldsymbol{\gamma} \cdot \boldsymbol{\tau} \right) dV \\
&= \frac{1}{2} \int\limits_{0}^{2\pi} \int\limits_{-h/2}^{h/2} \int\limits_{0}^{L} \left[\frac{E}{1-\mu^2} \left(\varepsilon_\vartheta{}^2 + \varepsilon_z{}^2 + 2\mu\varepsilon_\vartheta\varepsilon_z \right) + G \left(\gamma_{r\vartheta}{}^2 + \gamma_{rz}{}^2 + \gamma_{z\vartheta}{}^2 \right) \right] a \; d\vartheta \; dy \; dz
\end{aligned}
$$

$$\tag{B.1.6}$$

with

- L: length of the element
- h: thickness of the wall
- a: radius of the cylinder (with respect to the mid plane of the wall).

If for that the strain equation according to (B.1.2) and the shape functions according to (B.1.5) are used one obtains an expression for E_{pot} which depends on the discrete degrees of freedom $\underline{u}$ of the element. From that, the entries of the stiffness matrix $[K]$ can be computed by

$$
[K]_{ij} = \frac{\partial^2 E_{\text{pot}}}{\partial \underline{u}_i \partial \underline{u}_j}. \tag{B.1.7}
$$

$\underline{u}_i$ and $\underline{u}_j$ represent the discrete degrees of freedom. The application of this formula calls for the fact that the system of equations is linear. This is the case here.

The resulting matrix is (as typical for an element matrix) singular and the system is only solvable after introducing the boundary conditions. Additionally, one has to note that the shape function N_{harm1} for $P = 0$ is always equal to 0 ($\sin(\vartheta \cdot 0)$). The consequence is that the potential energy of this degree of freedom is 0 as well as consequently its stiffness. This means that the corresponding degree of freedom has to be eliminated since otherwise the system of equations will be singular even after introducing the boundary conditions. In contrast,

N_{harm2} with $P = 0$ has to be considered well since it represents a in the circumferential direction constant shape of the corresponding degree of freedom.

B.1.5 Load Vector

The load vector is obtained from the expression W in equation (B.1.1). W is in a first step expressed by the discrete degrees of freedom

$$W = \int\limits_{(V)} (\mathbf{u} * \mathbf{p})\, dV. \tag{B.1.8}$$

$\mathbf{p}$ is a general, spatially distributed and oriented load. The load vector for the linear system of equations is obtained by deriving W with respect to the discrete degrees of freedom. The emerging expression equals the one resulting from the principle of virtual work when the acting load is multiplied with the virtual deflection at the point of load application. The entries of the load vector are obtained by

$$[p]_i = \frac{\partial W}{\partial \underline{u}_i}. \tag{B.1.9}$$

B.1.6 Mass Matrix

For dynamic calculations, the mass matrix is also needed. It can be derived from the kinetic energy. It does not contain the derivatives of the deflections with respect to the coordinates but with respect to time thus the velocities

$$E_{\mathrm{kin}} = \frac{1}{2} \int\limits_{(V)} (\rho \dot{\mathbf{u}})\, dV$$

$$= \frac{\rho h}{2} \int\limits_0^{2\pi} \int\limits_0^L \left[\dot{\xi}_M^2 + \dot{\eta}^2 + \dot{\zeta}_M^2 + \frac{h^2}{12} \left(\dot{\varphi}_\vartheta^2 + \dot{\varphi}_z^2 + \frac{2}{a} \dot{\xi}_M \dot{\varphi}_\vartheta \right) \right] a\, dy\, dz \tag{B.1.10}$$

with

L: length of the element
h: thickness of the wall
a: radius of the cylinder (with respect to the mid plane of the wall).

Like in equation (B.1.6) for E_{pot}, with the help of the shape functions according to the equations (B.1.5) one can get to an expression for E_{kin} which now depends on the derivatives with respect to time of all discrete degrees of freedom $\underline{\dot{u}}$. This can be used to calculate the entries of the stiffness matrix $[M]$

$$[M_{ij}] = \frac{\partial^2 E_{\text{kin}}}{\partial \underline{\dot{u}}_i \partial \underline{\dot{u}}_j}. \qquad\qquad\qquad\qquad\text{(B.1.11)}$$

B.2 Applications

The element derived in the previous sections shall be used to calculate some examples and validate the method of extended beam elements. A Finite Element model with a very fine mesh with 1200 shell elements (see figure B.4) shall serve as reference.

B.2.1 Problem Configuration

The calculated geometry represents a lever arm with a length of three metres and a diameter of one metre. At the support all degrees of freedom are fixed. The thickness of the wall is three centimetres. The material parameters shall be those of a concrete with elastic modulus $E = 28309 \frac{\text{MN}}{\text{m}^2}$ and *Poisson* number $\nu = 0.2$.
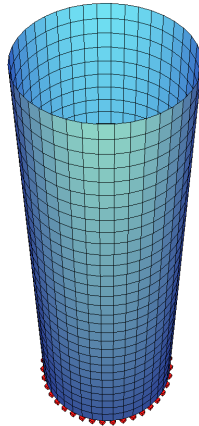
Figure B.4: Finite Element model.

B.2.2 Static Analysis

B.2.2.1 Load

In this example, the lever arm shall be loaded with a point load of 1.0MN in the radial direction at the free end (see figure B.5).
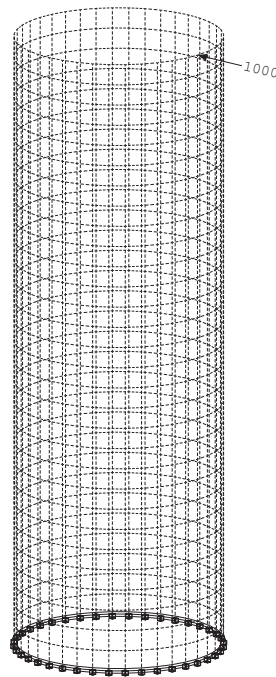
Figure B.5: Load case for the static analysis

B.2.2.2 Results

Figure B.6 shows the deformed system both for the FEM and the pipe element model in an isometric view. The plots in figure B.7 on page 163 show the deflections in axial lines (ϑ = const.) at the angular coordinate where the single load is applied.

The results converge very well except for the point where the single load is applied. Since shell or plate theory is underlying this point is singular which means that both moment and shear force become infinitely large. Furthermore, the smooth shapes of the sine and cosine functions in the circumferential direction are not able to approximate the deflection of the applied load very well.

At points which are not close to the load, the deflection is approximated very well already for low orders p and refinement levels n. As indicated in figure B.7a even the lowest order $p = 1$ produces better results than the classical *Euler-Bernoulli* beam theory.

From figure B.7 one can see that both the h-refinement (using smaller elements) and the p-refinement (elevating the used order of the shape functions) increase in small steps the accuracy close to the singularity. The two types of refinement affect different (spacial) directions thus both are necessary to cope with the singularity which "spreads" in both directions.
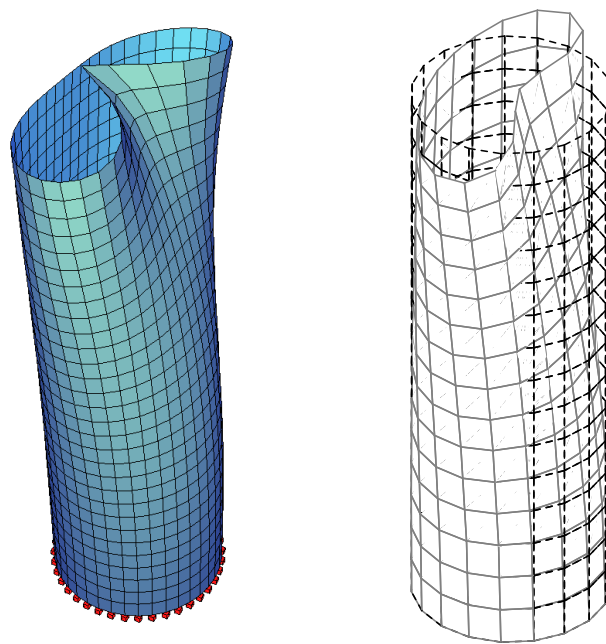
Figure B.6: Isometric view of the deflections of the static analysis: FEM model and $n = 5$ cylindrical shell elements of degree $p = 4$

B.2.3 Dynamic Analysis

B.2.3.1 Computation

The method shall be used to solve the homogeneous part of the solution. This means the eigen frequencies and eigenmode shapes of the system are computed.
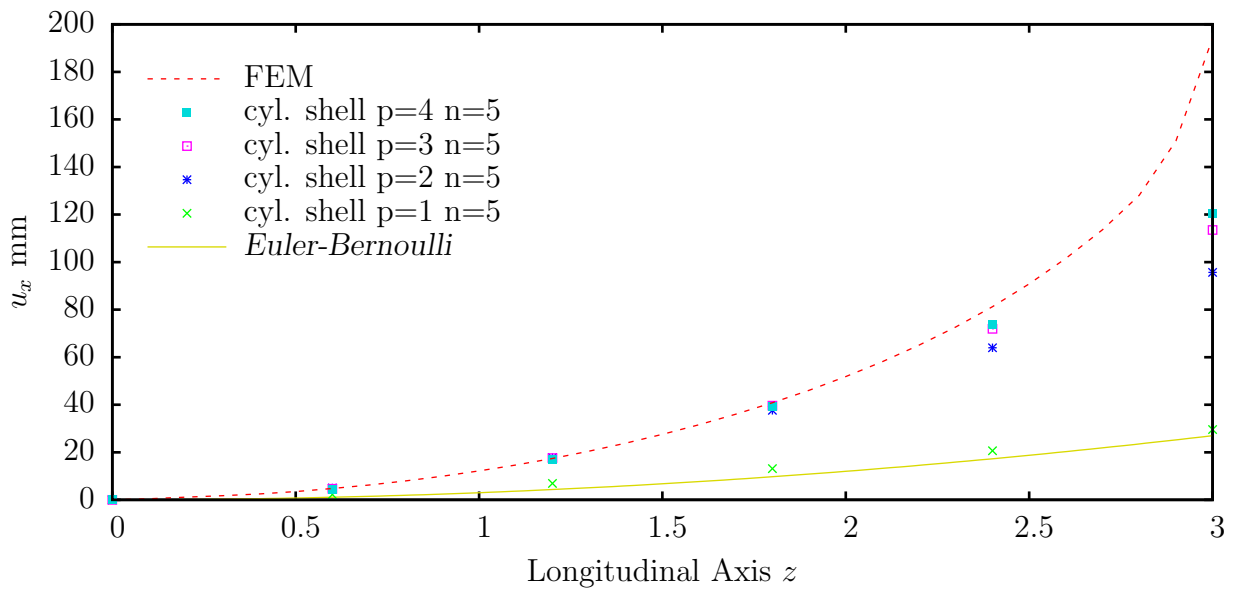
(a) Deflection u_x at $\vartheta = 0$ for 5 elements with different order p
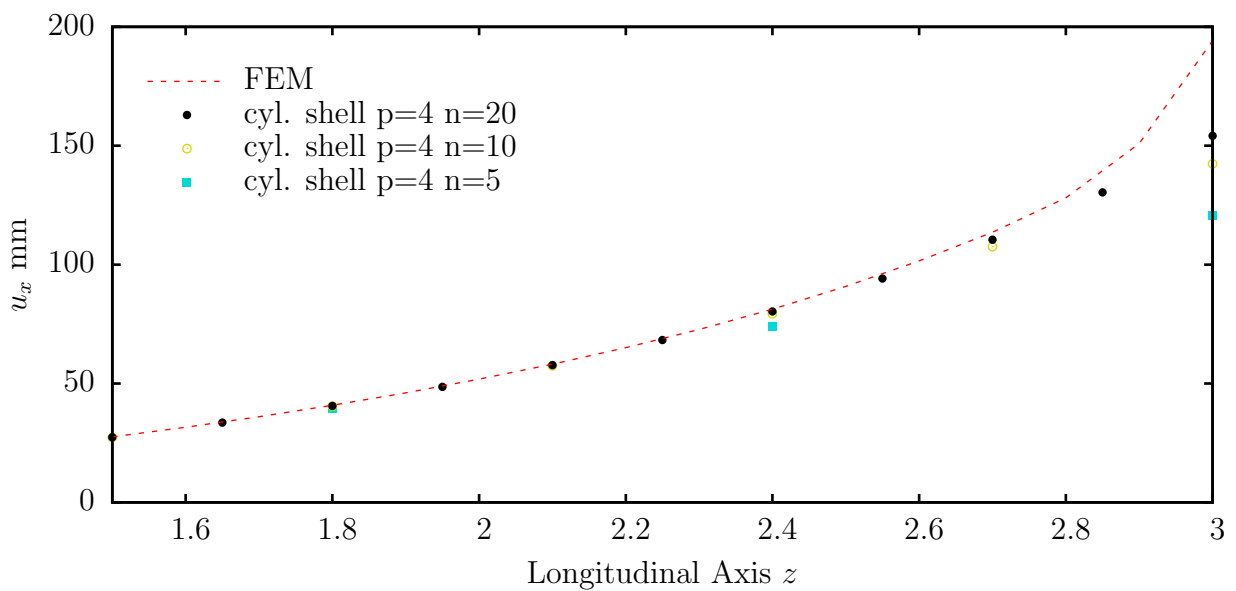
(b) Deflection u_x at $\vartheta = 0$ for different numbers of elements with order $p = 4$

Figure B.7: Deflections from the static analysis for different types of discretisation

B.2.3.2 Results

Table B.1 on page 165 shows the calculated natural frequencies for different types of discretisation and the reference computation using classical shell Finite Elements. One can see that depending on the discretisation some frequencies are missing.
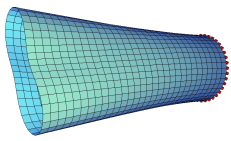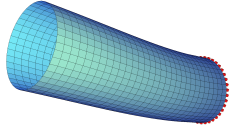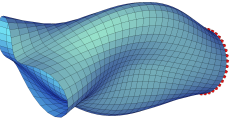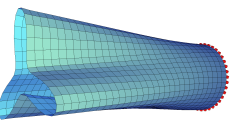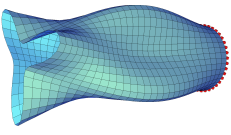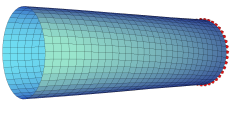
That is due to the fact that only such shapes can occur which can be built by the superposition of the shape functions. Some high frequencies such as the torsional mode but also the longitudinal tension/compression mode are already found by the coarsest models. Comparing the number of DOFs one can say that compared to the FEM the method is highly efficient. On the other hand, one has to admit that the stiffness matrix has a much wider band structure than for the FEM model which reduces some of the gains when it comes to solving the system.

B.2.4 Conclusion

These examples show that extending the classical degrees of freedom of a beam with shape functions on a macro (sub-global) level can be a very efficient procedure. This is especially the case if the underlying shape functions fit well with the expected deflection shape. Like in these examples, the sub-global shape functions are likely to be smooth and thus will have problems to accurately represent deflection shapes in the vicinity of huge discrete loads.

For dynamic applications like the determination of natural frequencies and eigenmode shapes the procedure is even better suited since jumps or discrete loads don't occur in this scenario. One has to admit that the used sine shaped ansatz functions fit very well with the shapes of the eigenmode shapes of the system. The restriction to prismatic, straight and ringlike structures is representing a very special case where this approach is elegant but which does not have a huge practical range of application. Nevertheless it can be seen that once the shape functions at the section fit well with the actual deflection shape the method just like beam methods produces very accurate results with few degrees of freedom and modelling effort.

Table B.1: Results from the dynamic analysis Hz

	nDOF	1./2	3./4.	5./6.	7./8.	9./10.	11.
FEM	7200	56.4	63.2	130.8	144.1	163.1	181.0
$n = 5$							
$p = 0$	50	-	-	-	-	-	181.8
$p = 1$	100	61.0	67.5	-	-	-	181.8
$p = 2$	150	61.0	67.5	199.8	-	-	181.8
$p = 3$	200	61.0	67.5	199.8	146.0	224.1	181.8
$p = 4$	250	57.6	64.7	151.8	144.61	181.5	181.2
$n = 10$							
$p = 0$	100	-	-	-	-	-	181.2
$p = 1$	200	-	64.7	-	-	-	181.2
$p = 2$	300	57.6	64.7	151.8	-	-	181.2
$p = 3$	400	57.6	66.7	151.8	144.6	181.5	181.2
$p = 4$	500	57.6	64.7	151.8	144.6	181.5	181.2
Name:		Oval. 2;1	Bend. 1	Oval. 2;2	Oval. 3;1	Oval. 3;2	Tors. 1
Picture:							

List of Figures

Listings

Bibliography

[Afolabi 1987]   Afolabi, D. "Linearization of the Quadratic Eigenvalue Problem". In: *Computers Structures* 26 (1987), pp. 1039–1040 (cit. on p. 64).

[Anderson et al. 1999]   Anderson, E., Z. Bai, C. H. Bischof, S. Blackford, J. W. Demmel, J. Dongarra, J. D. Croz, A. Greenbaum, S. J. Hammarling, A. McKenney, and D. Sorensen. *LAPACK Users' Guide.* 3rd ed. Society for Industrial and Applied Mathematics (SIAM), 1999 (cit. on p. 64).

[ANSYS, Inc. 2012]   ANSYS, Inc. *Documentation for ANSYS 14.* Users Manual. 2012 (cit. on pp. 119, 150).

[Athanasiadis 1982]   Athanasiadis, G. *Die Integralgleichungsmethode in der Elastizitätstheorie und ihre Anwendung am Beispiel des Torsionsproblems.* VDI-Verlag GmbH Düsseldorf, 1982 (cit. on p. 38).

[Babuska et al. 1981]   Babuska, I., B. A. Szabó, and I. N. Katz. "The p-Version of the Finite Element Method". In: *SIAM Journal of Numerical Analysis* 12 (1981), pp. 515–545 (cit. on p. 19).

[Bai and Su 2005]   Bai, Z. and Y. Su. "SOAR: A Second-Order Arnoldi Method for the Solution of the Quadratic Eigenvalue Problem". In: *SIAM Journal on Matrix Analysis and Applications* 26.3 (2005), pp. 640–659 (cit. on p. 64).

[Bathe 2002]   Bathe, K.-J. *Finite-Elemente-Methoden.* Trans. by P. Zimmermann. 2nd ed. Springer Verlag, 2002 (cit. on pp. 9, 36, 88–90, 133, 134, 139).

[Bathe and Dvorkin 1985]   Bathe, K.-J. and E. Dvorkin. "Short communication: a four-node plate bending element based on Mindlin=Reissner plate theory and a mixed interpolation". In: *International Journal for Numerical Methods in Engineering* 21 (1985), 367–383 (cit. on p. 36).

[Benner et al. 2007]   Benner, P., H. Faßbender, and M. Stoll. *Solving Large-Scale Quadratic Eigenvalue Problems with Hamiltonian Eigenstructure Using a Structure-Preserving Krylov Subspace Method.* Tech. rep. 2007 (cit. on p. 64).

[Bhimaraddi and Chandrashekhara 1993]   Bhimaraddi, A. and K. Chandrashekhara. "Observations on Higher-order Beam Theory". In: *Journal of Aerospace Engineering* 6 (1993), pp. 408–413 (cit. on p. 4).

[Bickford 1982]   Bickford, W. "A Consistent Higher Order Beam Theory". In: *Developments in Theoretical and Applied Mechanics SECTAM.* Vol. 11. 1982, pp. 137–150 (cit. on pp. 4, 23, 24).

[Bogensperger 2000]   Bogensperger, T. "Erweiterte Stabtheorie und der gevoutete Träger im Brückenbau". PhD thesis. Technische Universität Graz, 2000 (cit. on pp. 16, 23, 26, 77, 98, 151).

[Bornscheuer 1952]   Bornscheuer, F. W. "Systematische Darstellung des Biege und Verdrehvorgangs unter besonderer Berücksichtigung der Wölbkrafttorsion". In: *Der Stahlbau* 21 (1952), pp. 1–9 (cit. on p. 3).

[Brigham 1987]   Brigham, E. O. *FFT Schnelle Fourier-Transformation.* München: Oldenbourg Verlag, 1987 (cit. on p. 57).

[Bronstein et al. 2005]   Bronstein, I. N., K. A. Semendjajew, G. Musiol, and H. Mühlig. *Taschenbuch der Mathematik.* Frankfurt am Main: Verlag Harri Deutsch, 2005 (cit. on p. 58).

[Buchschmid and G. Müller 2012]   Buchschmid, M. and G. Müller. "Integral Transform Methods - Theory and Application". Lecture Notes, Unpublished. 2012 (cit. on p. 141).

[Camotim and Basaglia 2012]   Camotim, D. and C. Basaglia. "GBT-Based Local and Global Post-Buckling Analysis of Roorda's Frame". In: European Congress on Computational Methods in Applied Sciences and Engineering (ECCOMAS 2012). 2012 (cit. on pp. 3, 28, 29).

[Chen and Huang 2003]   Chen, Y.-H. and Y.-H. Huang. "Dynamic Characteristics of Infinite and Finite Railways to Moving Loads". In: *Journal of Engineering Mechanics* 129 (2003), pp. 987–995 (cit. on p. 5).

[Cowper 1966]   Cowper, G. R. "The Shear Coefficient in Timoshenko's Beam Theory". In: *Journal of Applied Mechanics* 33/2 (1966), pp. 335–340 (cit. on p. 2).

[Cremer et al. 2010]   Cremer, L., M. Heckl, M. Möser, and W. Kropp. *Körperschall - Physikalische Grundlagen und technische Anwendungen.* 3rd ed. Springer Verlag Berlin Heidelberg, 2010 (cit. on pp. 154, 155, 157).

[Deville et al. 2002]   Deville, M. O., P. F. Fischer, and E. H. Mund. *High-Order Methods for Incompressible Fluid Flow.* Cambridge University Press, 2002 (cit. on p. 21).

[Düster 2007]   Düster, A. *High-Order Finite Element Method (Lecture Notes).* TU München, Lehrstuhl für Bauinformatik, 2007 (cit. on p. 19).

[Düster et al. 2001]   Düster, A., H. Bröker, and E. Rank. "The p-version of the finite element method for three-dimensional curved thin walled structures". In: *International Journal for Numerical Methods in Engineering* 52.7 (2001), pp. 673–703. ISSN: 1097-0207. DOI: 10.1002/nme.222. URL: http://dx.doi.org/10.1002/nme.222 (cit. on pp. 19, 22).

[Ferradi et al. 2013]   Ferradi, M. K., X. Cespedes, and M. Arquier. "A higher order beam finite element with warping eigenmodes". In: *Engineering Structures* 46 (2013), pp. 748–762 (cit. on pp. 5, 23, 47).

[Finnveden 2004]   Finnveden, S. "Evaluation of modal density and groupvelocity by a finite element method". In: *Journal of Sound and Vibration* 273 (2004), pp. 51–75 (cit. on pp. 5, 6, 57).

[Friberg 1985]   Friberg, P. O. "Beam Element Matrices Derived from Vlasov's Theory of Open Thin-Walled Elastic Beams". In: *International Journal for Numerical Methods in Engineering* 21 (1985), pp. 1205–1228 (cit. on pp. 6, 73, 132).

[Gollwitzer 2007]   Gollwitzer, T. "Finite Stabelemente für mehrteilige nachgiebige Verbundquerschnitte zur Berechnung von Verbundrippenschalen". PhD thesis. Universität der Bundeswehr München, 2007 (cit. on p. 5).

[Gonçalves and Camotim 2011]   Gonçalves, R. and D. Camotim. "Generalised Beam Theory-Based Finite Elements for Elastoplastic Thin-Walled Metal Members". In: *Thin-Walled Structures* 49 (2011), pp. 1237–1245 (cit. on pp. 23, 28).

[Gonçalves and Camotim 2012]   Gonçalves, R. and D. Camotim. "Geometrically Non-Linear Generalised Beam Theory for Elastoplastic Thin-Walled Metal Members". In: *Thin-Walled Structures* 51 (2012), pp. 121–129 (cit. on pp. 3, 23, 29).

[Gonçalves, Dinis, et al. 2009]   Gonçalves, R., P. Dinis, and D. Camotim. "GBT Formulation to Analyse the First-Order and Buckling Behaviour of Thin-Walled Members with Arbitrary Cross-Sections". In: *Thin-Walled Structures* 47 (2009), pp. 583–600 (cit. on pp. 27, 28).

[Gonçalves, Ritto-Corrêa, et al. 2010]   Gonçalves, R., M. Ritto-Corrêa, and D. Camotim. "A Large Displacement and Finite Rotation Thin-Walled Beam Formulation Including Cross-Section Deformation". In: *Computer Methods in Applied Mechanics and Engineering* 199 (2010), pp. 1627–1643 (cit. on p. 23).

[Gruttmann and Wagner 2001]   Gruttmann, F. and W. Wagner. "Ein Weggrößenverfahren zur Berechnung von Querkraftschubspannungen in dünnwandigen Querschnitten". In: *Bauingenieur* 76 (2001), pp. 474–480 (cit. on p. 38).

[Gruttmann et al. 1998a]   Gruttmann, F., W. Wagner, and R. Sauer. "Zur Berechnung der Schubspannungen aus Querkräften in Querschnitten prismatischer Stäbe mit der Methode der finiten Elemente". In: *Bauingenieur* 73 (1998), pp. 485–490 (cit. on p. 38).

[Gruttmann et al. 1998b]   Gruttmann, F., W. Wagner, and R. Sauer. "Zur Berechnung von Wölbfunktion und Torsionskennwerten beliebiger Stabquerschnitte mit der Methode der finiten Elemente". In: *Bauingenieur* 73 (1998), pp. 138–143 (cit. on p. 38).

[Haberl and Och 1974]   Haberl, G. and F. Och. "Eine Finite-Element-Lösung für die Torsionssteifigkeit und den Schubmittelpunkt beliebiger Querschnitte". In: *Zeitschrift für Flugwissenschaften und Weltraumforschung* 22 (1974), pp. 115–119 (cit. on p. 38).

[Hackenberg 2010]   Hackenberg, M. "Umsetzung der Finiten Elemente Methode im Wellenzahlbereich und Kopplung mit der Integraltransformationsmethode". MA thesis. Lehrstuhl für Baumechanik TU München, 2010 (cit. on p. 57).

[Hartmann and Katz 2007]   Hartmann, F. and C. Katz. *Structural Analysis With Finite Elements*. 2nd ed. Engineering Online Library. Springer, 2007 (cit. on pp. 22, 23, 81).

[Herrmann 1965]   Herrmann, L. R. "Elastic torsional analysis of irregular shapes". In: *Journal of the Engineering Mechanics Division ASCE* 91 (1965), pp. 11–19 (cit. on p. 38).

[Hinke et al. 2004]   Hinke, L., B. R. Mace, and M. Brennan. *Finite Element Analysis of Waveguides*. Tech. rep. University of Southampton, 2004 (cit. on p. 6).

[Hofmann 1992]   Hofmann, T. J. "Beitrag zur verfeinerten Balkentheorie". PhD thesis. Institut für Baustatik der Universität Stuttgart, 1992 (cit. on pp. 4, 5, 23, 24, 47).

[Katz 1986]   Katz, C. "Self-Adaptive Boundary Elements for the Shear Stress in Beams". In: *Betech 86*. Massachusetts Institute of Technology, USA, June 1986. Computational Mechanics Publications, 1986, pp. 759–769 (cit. on pp. 38, 151).

[Katz 2008]   Katz, C. "FE Substructures for Sectional Analysis". In: *IABSE Conference on Information and Communication Technology for Bridges, Buildings and Construction Practice*. Helsinki, 2008 (cit. on pp. 1, 98, 152).

[Katz 2011]   Katz, C. "Einfluss der Modellbildung bei der Berechnung am Gesamtmodell". In: *Neue Normen und EDV-gestützte Berechnungen*. Bayerische Ingenieurekammer mit der Vereinigung der Prüfingenieure für Baustatik in Bayern e.V. 2011 (cit. on pp. 109, 110, 112).

[Kiener 1988]   Kiener, G. "Übertragungsmatrizen, Lastvektoren, Steifikeitsmatrizen und Volleinspannschnittgrößen einer Gruppe konischer Stäbe mit linear veränderlichen Querschnittsabmessungen". In: *Bauingenieur* 63 (1988), pp. 567–574 (cit. on p. 16).

[Koloušek 1973]   Koloušek, V. *Dynamics in Engineering Structures*. Butterworths, 1973 (cit. on p. 132).

[Krahula and Lauterbach 1969]   Krahula, J. and G. L. Lauterbach. "A finite element solution for Saint-Venant Torsion". In: *AIAA Journal* 7 (1969), pp. 2000–2203 (cit. on p. 38).

[Kraus 2005]   Kraus, M. "Computerorientierte Berechnungsmethoden für beliebige Stabquerschnitte des Stahlbaus". PhD thesis. Ruhr-Universität Bochum, 2005 (cit. on pp. 38, 151).

[Kraus 2007a]   Kraus, M. "Finite-Elemente-Methode für die genaue Berechnung von Querschnittswerten und Spannungen - Beispiele". In: *Bauingenieur* 82.6 (2007), pp. 299–303 (cit. on p. 38).

[Kraus 2007b]   Kraus, M. "Finite-Elemente-Methode für die genaue Berechnung von Querschnittswerten und Spannungen - Theorie". In: *Bauingenieur* 82.2 (2007), pp. 85–94 (cit. on p. 38).

[Kreutz and G. Müller 2012]   Kreutz, J. and G. Müller. "Proposal for an Advanced Wave Guide Element". In: *European Congress on Computational Methods in Applied Sciences and Engineering (ECCOMAS 2012)*. Ed. by J. Eberhardsteiner. Vienna, Austria, 2012 (cit. on pp. 104, 127).

[Kreuzinger 1974]   Kreuzinger, H. "Der Einftuß der Querverformung auf die Berechnung gerader dünnwandiger Stäbe". In: *Der Stahlbau* 2 (1974), pp. 46–52 (cit. on pp. 3, 23–25).

[Levinson 1985]   Levinson, M. "On Bickford's Consistent Higher Order Beam Theory". In: *Mechanics Research Communications* 12 (1985), pp. 1–9 (cit. on pp. 4, 23, 24).

[Li 1990]   Li, L. "Discretization of the Timoshenko Beam Problem by the p and the h-p Versions of the Finite Element Method". In: *Numerische Mathematik* 57 (1990), pp. 413–420 (cit. on p. 19).

[Meerbergen 2001]   Meerbergen, K. "Locking and Restarting Quadratic Eigenvalue Solvers". In: *SIAM Journal on Scientific Computing* 22.5 (2001), pp. 1814–1839 (cit. on p. 64).

[Meerbergen 2008]   Meerbergen, K. "The Quadratic Arnoldi Method for the Solution of the Quadratic Eigenvalue Problem". In: *SIAM Journal on Matrix Analysis and Applications* 30.4 (2008), pp. 1463–1482 (cit. on p. 64).

[Möller 1982]   Möller, R. "Zur Berechnung prismatischer Strukturen mit beliebigem nicht formtreuen Querschnitt". PhD thesis. Technische Hochschule Darmstadt, 1982 (cit. on pp. 23, 25, 28).

[Moore 1965]   Moore, G. E. "Cramming more components onto integrated circuits". In: *Electronics Magazine* 38.8 (Apr. 1965) (cit. on p. 1).

[G. Müller 1989]   Müller, G. "Ein Verfahren zur Erfassung der Fundament-Boden Wechselwirkung unter Einwirkung periodischer Lasten". PhD thesis. TU München, 1989 (cit. on p. 140).

[G. Müller 2012]   Müller, G. "Continuum Mechanics and Tensor Analysis - Lecture Notes". 2012 (cit. on p. 13).

[G. Müller and Buchschmid 2011]   Müller, G. and M. Buchschmid, eds. *Untersuchungen zum Schwingungsverhalten leichter Verbunddeckensysteme.* Aachen: Shaker Verlag, 2011 (cit. on p. 1).

[G. Müller and Kreutz 2013]   Müller, G. and J. Kreutz. "An Augmented Beam Element for Structural Dynamics Using Unit Deflection Shapes Gained on a 2D Finite Element Mesh of the Cross Section". In: *Proceedings in Applied Mathematics and Mechanics* tba (2013), tba–tba (cit. on p. 119).

[K. Müller 2007]   Müller, K. "Dreidimensionale dynamische Tunnel-Halbraum-Interaktion". PhD thesis. Technische Universität München, 2007 (cit. on pp. 5, 57, 59).

[Okur 1971]   Okur, H. "Eine statische Methode zur Lösung von nichtlinearen Differentialgleichungssystemen 4. O. mit ihrer hauptsächlichen Anwendung auf die Untersuchung der Stabilität von prismatischen Faltwerken und Schalen". PhD thesis. TU Darmstadt, 1971 (cit. on pp. 23, 26).

[Orrenius and Finnveden 1996]   Orrenius, U. and S. Finnveden. "Calculation of Wave Propagation in Rib-Stiffened Plate Structures". In: *Journal of Sound and Vibration* 198 (1996), pp. 203–224 (cit. on pp. 6, 23, 63).

[Paolini 2012]   Paolini, A. "Balkenelemente unter Verwendung zusätzlicher Verformungsansätze". Masterthesis supervised by Johannes Kreutz. TU München Lehrstuhl für Baumechanik, 2012 (cit. on pp. 77, 87, 88, 100, 104–106).

[Petersen 1996]   Petersen, C. *Dynamik der Baukonstruktionen.* 1st ed. Braunschweig / Wiesbaden: Vieweg & Sohn Verlagsgesellschaft, 1996 (cit. on p. 70).

[Petersen 1966]   Petersen, C. "Das Verfahren der Übertragungsmatrizen für gekrümmte Träger". In: *Bauingenieur* 41 (1966), pp. 98–102 (cit. on p. 23).

[Rank et al. 1983]   Rank, E., C. Katz, and H. Werner. "On the Importance of the Discrete Maximum Principle in Transient Analysis Using Finite Element Methods". In: *International Journal for Numerical Methods in Engineering* 19 (1983), pp. 1771–1782 (cit. on p. 22).

[Roik and Sedlacek 1970]   Roik, K. and G. Sedlacek. "Erweiterung der technischen Biege- und Verdrehtheorie unter Berücksichtigung von Schubverformungen". In: *Bautechnik* (1970), pp. 20–32 (cit. on pp. 5, 23, 25, 26, 80).

[Sauer 1998]   Sauer, R. "Eine einheitliche Finite-Element-Formulierung für Stab- und Schalentragwerke mit endlichen Rotationen". Dissertation. Institut für Baustatik, Karlsruher Institut für Technologie, 1998 (cit. on p. 131).

[Sayyad 2011]   Sayyad, A. S. "Comparison of various refined beam theories for the bending and free vibration analysis of thick beams". In: *Applied and Computational Mechanics* 5 (2011), pp. 217–230 (cit. on pp. 4, 24).

[Schade 1969]   Schade, D. "Wölbkrafttorsion von Stäben mit dünnwandigem Querschnitt". In: *Ingenieurarchiv* 38.1 (1969), pp. 25–34 (cit. on p. 98).

[Schardt 1989]   Schardt, R. *Verallgemeinerte Technische Biegelehre*. Springer Verlag, 1989 (cit. on pp. 3, 23–26, 28, 154).

[Schneider 2008]   Schneider, K.-J., ed. *Bautabellen für Ingenieure*. 18th ed. Köln: Werner Verlag, 2008 (cit. on p. 70).

[SOFiSTiK AG 2013a]   SOFiSTiK AG. *Handbuch AQUA - Materialien und Querschnitte*. SOFiSTiK AG. Bruckmannring 38, 85764 Oberschleißheim, 2013 (cit. on p. 38).

[SOFiSTiK AG 2013b]   SOFiSTiK AG. *Handbuch STAR2 - Statik der Stabtragwerke Theorie II. Ordnung*. SOFiSTiK AG. Bruckmannring 38, 85764 Oberschleißheim, 2013 (cit. on pp. 16, 17).

[Sprague and Geers 2007]   Sprague, M. A. and T. L. Geers. "Legendre spectral finite elements for structural dynamics analysis". In: *Communications in Numerical Methods in Engineering* 24.12 (2007), pp. 1953–1965 (cit. on pp. 19, 21, 22).

[Sutter 2005]   Sutter, H. "The Free Lunch Is Over: A Fundamental Turn Toward Concurrency in Software". In: *Dr. Dobb's Journal* 30.3 (2005). [Online; Retrieved May 20 2013]. URL: http://www.gotw.ca/publications/concurrency-ddj.htm (cit. on p. 1).

[Szabó et al. 2004]   Szabó, B., A. Düster, and E. Rank. "The p-Version of the Finite Element Method". In: ed. by E. Stein, R. de Borst, and T. J. Hughes. Vol. 1. Wiley Online Library, 2004. Chap. 5, pp. 119–139 (cit. on p. 19).

[Tisseur and Meerbergen 2001]   Tisseur, F. and K. Meerbergen. "The Quadratic Eigenvalue Problem". In: *SIAM Review* 2001.2 (2001), pp. 235–286 (cit. on pp. 63, 64).

[Unterweger 2008]   Unterweger, D. D. H. "Straßenbrücken mit gevoutetem Kastenquerschnitt - ungewöhnliches Torsionstragverhalten und Auswirkungen auf die Bemessungspraxis". In: *Bauingenieur* 83 (2008), pp. 263–276 (cit. on p. 23).

[Unterweger 2001]   Unterweger, D. D. H. "Globale Systemberechnung von Stahl- und Verbundbrücken - Leistungsfähigkeit einfacher Stabmodelle". Habilitation Treatise. Technische Universität Graz, 2001 (cit. on p. 23).

[VTK 2013]   VTK. *File Formats for VTK Version 4.2*. Visualization Toolkit (VTK). Apr. 2013. URL: www.vtk.org/VTK/img/file-formats.pdf (cit. on p. 93).

[Waki et al. 2009]   Waki, Y., B. R. Mace, and M. J. Brennan. "Numerical issues concerning the wave and finite element method for free and forced vibrations of waveguides". In: *Journal of Sound and Vibration* 327 (2009), pp. 92–108 (cit. on p. 6).

[Willett et al. 1998]   Willett, P., J. M. Barnard, and G. M. Downs. "Chemical Similarity Searching". In: *J. Chem. Inf. Comput. Sci.* 38 (1998), pp. 983–996 (cit. on p. 105).

[Wilson et al. 1973]   Wilson, E. L., R. L. Taylor, W. P. Doherty, and J. Ghaboussi. "Numerical and Computer Methods in Structural Mechanics". In: ed. by S. J. Fenves, N. Perrone, A. R. Robinson, and W. C. Schnobrich. Academic Press, New York, 1973. Chap. Incompatible Displacement Models, pp. 43–57 (cit. on pp. 9, 134).

[Wlassow 1958]   Wlassow, W. S. *Allgemeine Schalentheorie und ihre Anwendung in der Technik*. Akademie-Verlag Berlin, 1958 (cit. on pp. 3, 25).

[Wlassow 1964]   Wlassow, W. S. *Dünnwandige elastische Stäbe. Band 1*. German. 2nd ed. VEB Verlag für Bauwesen Berlin, 1964 (cit. on pp. 3, 16, 23, 28).

[Wlassow 1965]   Wlassow, W. S. *Dünnwandige elastische Stäbe. Band 2*. German. 2nd ed. VEB Verlag für Bauwesen Berlin, 1965 (cit. on pp. 3, 16, 25).

[Wunderlich and Kiener 2004]   Wunderlich, W. and G. Kiener. *Statik der Stabtragwerke*. 1st ed. Stuttgart Leipzig Wiesbaden: Teubner, 2004 (cit. on pp. 15, 16, 38).

[Zeller 1979]   Zeller, C. "Eine Finite-Element-Methode zur Berechnung der Verwölbungen und Profilverformungen von Stäben mit beliebiger Querschnittsform". PhD thesis. Ruhr-Universität Bochum, 1979 (cit. on pp. 8, 23, 25, 26, 29, 47, 54, 55, 77).

[Zeller 1982]   Zeller, C. "Querschnittsverformungen von Stäben". In: *Ingenieurarchiv* 52 (1982), pp. 17–37 (cit. on pp. 5, 29, 54).

[Zienkiewicz and Taylor 2005]   Zienkiewicz, O. C. and R. L. Taylor. *The Finite Element Method for Solid and Structural Mechanics*. 6th ed. Vol. 2. Elsevier, 2005 (cit. on pp. 3, 6).

[Živković et al. 2001]   Živković, M., M. Kojić, R. Slavković, and N. Grujović. "A General Beam Finite Element with Deformable Cross-section". In: *Computer Methods in Applied Mechanics and Engineering* 190 (2001), pp. 2651–2680 (cit. on pp. 5, 131).